European Transactions on Telecommunications

EUREL Publication and related technologies

Vol. 6, No. 1, January-February 1995

Special Issue on Spread Spectrum Techniques
Guest Editors: S.G. Glisic, E.S. Sousa

AEI

Published by AEI in co - operation with AEE, AIM, ASN - CPEF, KIWI, ODE, OVE, SER, SEV - ASE, SRBE - KBVE, VDE with the support of the Commission of the European Communities (CEC)

European Transactions on Telecommunications

and related technologies

Aims and Scope

European Transactions on Telecommunications and related technologies (ETT) originates from the well known magazines «Alta Frequenza» International Journal (AEI, Italy) and «ntzArchiv» (VDE, Germany) and aims for two ambitious goals:

- to become the focus in Europe of outstanding contributions from researchers and engineers working in the field of information technology;
- to concentrate papers on the various applications of telecommunications:
  - *Communication Theory*
  - *Telecommunication Systems*
  - *Information Processing*
  - *Signal Processing*
  - *Communication Networks*
  - *Optical Communications*
  - *Computer Communications and Protocols*

In order to improve the quality and the number of the papers, a staff of seven Telecommunication Editors has been settled. Their main tasks are:

- *to encourage paper submission*
- *to propose special issues and focuses*
- *to invite tutorials and critical reviews*

ETT welcomes open contributions from every country in the world. It publishes:

- *invited papers (tutorial or critical reviews)*
- *regular papers (original scientific contributions)*
- *letters (short contributions and scientific correspondences)*

ETT 1995 SUBSCRIPTION CONDITIONS	Italian Lire
Subscription fee	440.000
Member of EUREL societies	350.000
Member of Eurel cooperating Societies	150.000
Postage by airmail	50.000

ETT is published by

AEI	I	Associazione Elettrotecnica ed Elettronica italiana
		in cooperation with
AEE	E	Asociación Electrotécnica Española
AIM	B	Association des Ingénieurs Electriciens sortis de l'Institut Montefiore (Université de Liège)
ASN CPEF	SF	Aatteellisten sähköinsinöörijärjestöjen neuvottelukunta The Consulting Committee of the Professional Electroengineers' Organizations in Finland
KIVI	NL	Koninklijk Instituut van Ingenieurs Afd. elektrotechniek
ODE	P	Ordem Dos Engenheiros
ÖVE	A	Österreichischer Verband für Elektrotechnik
SER	S	Sveriges Elektro-och Dataingenjörers Riksförening
SEV ASE	CH	Schweizerischer Elektrotechnischer Verein Association Suisse des Electriciens
SRBE KBVE	B	Société Royale Belge des Electriciens Koninklijke Belgische Vereniging der Elektrotechnici
VDE	D	Verband Deutscher Elektrotechniker

with the support of the
Commission of the European Communities

EUREL Publication

European Transactions on Telecommunications

and related technologies

Vol. 6, No. 1, January-February 1995

Published by AEI (Italy) in cooperation with: AEE (Spain), AIM (Belgium), ASN/CPEF (Finland), KIVI (Netherlands), ODE (Portugal), ÖVE (Austria), SER (Sweden), SEV/ASE (Switzerland), SRBE/KBVE (Belgium), VDE (Germany). With the support of CEC

Contents

Proprietà ed Editrice: AEI - Associazione Elettrotecnica ed Elettronica Italiana - Viale Monza 259 - 20126 Milano
Direttore responsabile: G. Lucchini

European Transactions on Telecommunications and related technologies è pubblicata col concorso del Consiglio Nazionale delle Ricerche e della Fondazione Ugo Bordoni
Spedizione in abbonamento postale gruppo IV. *La pubblicità non supera il 70% della superficie totale della rivista*

Associati all'USPI - Unione Stampa Periodica Italiana

European Journals

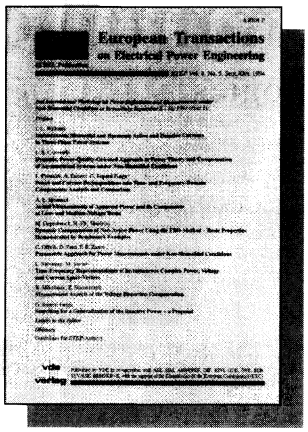

ETEP • European Transactions on Electrical Power Engineering

ETEP is an international forum for research and development in electrical power engineering and automation. Professional researchers in the industry, research centres and universities are contributing outstanding results of latest developments; thus ETEP is essential for all scientists and engineers to keep up with the innovation in electrical power engineering technology. The scope of the journal covers:

• Basic disciplines applied to electrical power engineering • Electrical power systems for generation, transmission, distribution and application of electrical energy • Electrical power components • Electromechanical and electrical energy conversion • Safety and electromagnetic compatibility • Materials for electrical power components

Frequency: bimonthly

Published by VDE (D), AEI (I), AIM (B), ASN/CPEF (SF), DIF (DK), KIVI (NL), ODE (P), ÖVE (A), SER (S), SEV/ASE (CH), SRBE/KBVE (B)

ETEP 1995 Subscription conditions	DM
Normal price	409.20
Members of EUREL societies *please note your membership serial	327.60*
Members of ETEP signatory societies	304.20
Postage by airmail	+ 43.20

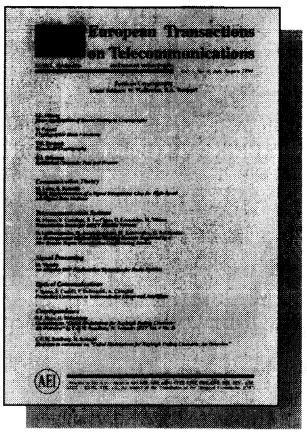

ETT • European Transactions on Telecommunications and Related Technologies

ETT is an international forum for research and development in telecommunications and related fields; it publishes scientific papers of high standard after a peer review. The scope of the journal covers:

• Telecommunication networks and systems • Devices and circuits • Systems • Networks • Transmission • Propagation and radar • Communication theory • Telecommunication systems • Information processing • Signal processing • Communication networks • Optical communications • Computer communications and protocols

Frequency: bimonthly

Published by AEI (I), AEE (E), AIM (B), ASN/ CPEF (SF), KIVI (NL), ÖVE (A), SEV/ASE (CH), SRBE/BKBVE (B), VDE (D)

ETT 1995 Subscription conditions	Italian Lire
Normal price	440 000
Members of EUREL societies *please note your membership serial	350 000*
Members of ETT signatory societies	150 000
Postage by airmail	+ 50 000

With the support of the Commission of the European Communities.

Order form

Please enter my subscription to **ETEP** for 1995

☐ as of now ☐ as of .....date

☐ until cancelled ☐ up to ..... date

☐ Please send me a free sample copy of **ETEP**

Name First Name

Company

Street / P.O. Box

Postal Code City

Country

Date Signature

Mail to:

VDE-VERLAG GmbH
Bismarckstraße 33
D-10625 Berlin / Germany
Phone: +49/ 30/ 348001-0
Fax: +49/ 30/ 3417093

Werb-Nr. 941106 cs

Order form

Please enter my subscription to **ETT** for 1995

☐ as of now ☐ as of .....date

☐ until cancelled ☐ up to ..... date

☐ Please send me a free sample copy of **ETT**

Name First Name

Company

Street / P.O. Box

Postal Code City

Country

Date Signature

Mail to:

AEI/ETT
secretariat
Viale Monza 259
I-20126 Milano/ Italy
Phone/Fax +39227002395

CALL FOR PAPERS

European Transactions on Telecommunications and Related Technologies (ETT)

Focus on

SYNCHRONIZATION OF DIGITAL NETWORKS

Since the first advent of digital telecommunications, network synchronization has a determining influence on the performance and the quality of most services offered by the network operator to his customers. Nowadays, as the introduction of transmission systems based on SDH (*Synchronous Digital Hierarchy*) in the public networks is drawing near, the need for adequate network synchronization facilities becomes more and more stringent in order to fully exploit SDH capabilities. For these reasons, all the major network operators have set up, or are now planning, nationwide synchronisation networks, and the whole subject is at present very debated both in Academia and in the relevant standard bodies. The ETT Journal announces a forthcoming issue on *Synchronization of Digital Networks*, that will include (but will not be limited to) the following topics:

- clock stability characterization
- time and frequency measurement techniques
- phase and frequency noise modelling
- precision frequency sources for telecommunications
- network synchronization techniques
- simulation and analysis of slave clocks systems
- synchronization network architecture
- impact of network synchronization on telecommunications services
- field trials
- test beds

Prospective authors should send five (5) copies of their papers to one of the Guest Editors listed below. The following deadlines will apply

- Submission of manuscripts:	April 30, 1995
- Notification of acceptance:	July 30, 1995
- Submission of final manuscript:	November 15, 1995
- Publication date:	January-February, No. 1, 1996

Guest Editors

Ing. Stefano Bregni
CEFRIEL
Via Emanueli, 15
I-20126 Milano, Italy
Ph.: + 39-2-66100083, Fax: +39-2-66100448
e-mail: bregni@ mailer·cefriel·it

Dr. Erhard P. Graf
OSA - OSCILLOQUARTZ S.A.
CH-2002 Neuchâtel 2
Switzerland
Ph.: +41-38-258501, Fax: +41-38-258508

Note: Papers will be accepted for the focus only when subject to at most minor revision. In case of acceptance with major revision, the paper will be considered as a regular contribution for other ETT issues.

CALL FOR PAPERS

European Transactions on Telecommunications and Related Technologies (ETT)

Special Issue on

ATM FIELD TRIALS AND EXPERIMENTS

During the last 10 years, the Asynchronous Transfer Mode (ATM) technique has received attention in research, standardization and system development worldwide as the key principle for the Broadband Integrated Services Digital Network (B-ISDN). The standardization process within ITU-T and the ATM Forum is in the final phase. Research activities on ATM have been supported within the RACE I and II programmes since 1988. Currently, a number of experimental testbeds, platforms and field trials are in progress to test the new technology, to show the interoperability of various types of equipment, to demonstrate new applications and to validate specific traffic control algorithms, traffic models and Quality of Service (QoS) management procedures. The first ATM equipment is commercially available and becomes operational within local area environments.
Experiments with the new technology play an important role to achieve a well-understood and stable high speed network infrastructure for new services and applications such as multimedia, video on demand or LAN interconnection. Despite considerable progress there remains a number of problems, which need further study such as traffic control, resource management, signalling, QoS management, and traffic validations by measurements and tests under realistic conditions. The result of such experiments are of wide interest for research, standardization, system developlent and operation. The Special Issue aims at the presentation of the state of the art in ATM networking and applications. Contributions are expected especially on the following subjects, which must have a direct relation to experiments:

- Broadband Testbeds and ATM Pilot Experiments
- Signalling in ATM Networks
- Usage Parameter Control (UPC)
- Measurement of Real Broadband Traffic
- Traffic Descriptors and Traffic Model Validations
- Generator/Analyzer Test Equipment
- Advanced Applications
- Interoperability
- Connection Acceptance Control (CAC)
- Quality of Service
- Resource Management
- Dimensioning, Planning and Operation.

The following deadlines will apply

– Submission of Proposal (1 page Abstract):	June 1st, 1995
– Notification of Full Paper proposal:	July 15, 1995
– Submission of Full Papers:	October 1st, 1995
– Notification of Acceptance:	January 1st, 1996
– Submission of final version for publication:	March 1st, 1996
– Publication Date:	July-August, No. 4, 1996

Contributions could be directed to either one of the Guest Editors listed below.

Guest Editors

Professor Dr. A. Danthine
Université de Liège
Institut d'Electricité Montefiore
Sart Tilman B 28
B-4000 Liège, Belgium

Tel.: +32-41-66 26 91
Fax: +32-41-66 29 89
e-mail: danthine@vml.ulg.ac.be

Professor Dr. P.J. Kühn
University of Stuttgart
Inst. of Commun. Switching
and Data Technics (IND)
Seidenstr. 38
D-70174 Stuttgart
Tel.: +49-711-121 2479
Fax: +49-711-121 2477
e-mail: kuehn@ind.uni-stuttgart.d400.de

Dr. J.W. Roberts
France Télécom - CNET
PAA/ATR/GTR
38-40, rue du Général Leclerc
F-92131 Issy-les-Moulineaux

Tel.: +33-1-4529 5701
Fax: +33-1-4529 6069
e-mail:robert@issy.cnet.fr

Note: Papers will be accepted for the special issue only when subject to at most minor revision. In case of acceptance with major revision, the paper will be considered as a regular contribution for other ETT issues.

Workshop Announcement and Call for contributions

ATM Hot Topics on Traffic and Performance: from RACE To ACTS

14-15 June 1995 Italtel

Settimo Milanese (Italy)

Organized by:
BRAVE Project -R2118
Broadband Access Verification Experiments

on behalf of:
RACE PL8 Special Interest Group on Traffic Control and ATM Performance

ATM has experienced great progress during the last few years. The first ATM products are available now and a number of field trials, pilot networks and even some commercial services are currently in operation all over the world. However, although the basic ATM technology has rather matured, many interesting problems remain to be solved, in particular in the field of traffic control.
Moreover, new traffic related problems are induced from one side by the introduction in the ATM network of signaling and IN related capabilities, and from the other side from new applications such as Video on Demand (VoD) and ATM Virtual Private Network (AVPN).
All these items will be subject of investigations and experiments in the context of the forthcoming ACTS programme.
This workshop is therefore aimed at:

- define and update the state of the art in ATM traffic control by open participation of RACE projects;
- contributing in building up a bridge between RACE and ACTS programmes, identifying focal and still open problems by invited speeches mainly coming from the ATM Forum, COST242, DAVIC, ITU-T/ETSI, RCO, TINA organizations.

Presentations are encouraged in, but not limited to, the following topics:

- Traffic Control functions (support of Available Bit Rate Services, Traffic Shaping, Cell Scheduling algorithms, Fast Resource Management, ...)
- Statistical Multiplexing (use of large buffers, use of Sustainable Cell Rate, ...)
- User Applications (traffic management for ATM Virtual Private Networks, Video on Demand, ...)
- Experiments on Traffic and Performance, including QoS and Reliability issues
- Tariffs and billing strategies

Technical Committee

Chairmen:	P. de Sousa	Commission of the European Communities, DG XIII/B
	G. Gallassi	Italtel, Milan
	P. Kuehn	University of Stuttgart, ITC-IAC Chairman
Members:	M. Griffith	Commission of the European Communities, DG XIII/B
	M. Potts	Association Swiss PTT/ASCOM, Basel
	S. Rao	ASCOM, Bern
	G. Stassinopoulos	National Technical University of Athens
	L. Verri	Italtel, Milan
	E. Wallmeier	Siemens, Munich

The workshop will be held in the Italtel premises of Settimo Milanese, few kilometers away from Milan. Attendance will be limited to 60 participants. Registration is recommended by April 1st, 1995. For info send E-mail to *verri@settimo.italtel.it or gallassi@settimo.italtel.it*

Deadlines

April	1st,	1995	Two pages Abstract and Registration form
April	15th,	1995	Acceptance notification
May	15th,	1995	Camera ready copy of the full paper

Contact point

G. Gallassi
Italtel, Central R&D Labs. - CLTB
I-20019 Settimo Milanese (MI) - ITALY
Fax: +39.2.4388.7989
Email: gallassi@settimo.italtel.it

GUEST EDITORIAL

Prof. Savo G. Glisic
University of Oulu
Dept. of Electrical Engineering
Linnanmaa 51
90570 Oulu - Finland

Prof. Elvino S. Sousa
University of Toronto
Dept. of Electrical Engineering
Toronto
Ontario M5S 14A - Canada

The spread spectrum modulation technique has undergone a long evolution since its inception approximately one half a century ago. The initial application was for interference suppression in a military environment, more commonly referred to as anti-jam communications. However, current commercial applications of its use as a multiplexing scheme were also foreseen early on. Research in spread spectrum was mostly of a classified nature until the early seventies. From an implementation perspective the implementation of spread spectrum receivers was difficult due to the requirement of complex synchronization algorithms (acquisition and tracking) and the limitations of the available technology at a reasonable cost. In the last few years all of this has changed and we are now seeing a proliferation of applications of spread spectrum ranging from the traditional military application, to wireless LANs, operation in bands allocated by blanket licences, and cellular networks.

The defining principle of spread spectrum is that the ratio of the transmitted signal bandwidth to the information data rate should be large (processing gain). Along with this property we get a number of benefits such as anti-jam (anti-interference) capability, anti-multipath, low probability of intercept, multiple access capability with a high degree of flexibility of transmission by the different users, and the most recent, efficient frequency re-use as required in cellular-type networks.

Spread spectrum techniques come in various forms such as direct sequence, frequency hopping, and various hybrids. Mathematically all of these share common properties although they are quite different from an implementation standpoint. Also their relative performance depends on the type of interference; e.g. frequency hopping is quite effective against partial band interference, and direct sequence is advantageous for multiple access as long as the powers of the different users are in the same range. Direct sequence multiple access suffers from the so called near/far problem and requires tight power control. Frequency hopping is typically less efficient spectrally but suffers less from the near/far effect.

With recent advances in VLSI it is now not only practical to solve the old problems with implementation of synchronization schemes, but it is also becoming practical to implement various types of complex receiver algorithms which improve the performance of spread spectrum in multiple access channels with multi-path fading. The most common of these is the Rake receiver which consists of a set of correlators that track individual multi-path signal components. The number of multi-path components depends on the chip rate relative to the channel delay spread. Systems such as IS-95 employ in the order of 3-4 correlators. The other types af advanced receivers are the so-called multi-user detectors which come in various forms: maximum likelihood, feedback type receivers, and decorrelators. Another feature of spread spectrum modulation is the prevalent requirement for the use of forward error correction coding. With advances in VSLI it is now possible to implement many coding schemes involving, convolutional codes, orthogonal codes with the corresponding Fast Hadamard Transform based decoders, Reed-Solomon codes, and various concatenated coding schemes involving these basic codes.

An important characteristic of a modulation scheme in current wireless systems is its suitability for spectral re-use and its co-existence with other systems, along with a flexibility to adapt to changes in transmission rate with changes in interference level in the channel. In this area it appears that spread spectrum may ultimately have fundamental advantages over traditional narrow band modulation schemes.

The current issue contains eight papers on the spread spectrum theme.

The first five papers focus on receiver algorithms and their performance evaluation. The other three involve the evaluation of system performance.

The first paper considers a scheme with an interference canceller receiver coupled with error control. The motivation behind this scheme is the improvement of the performance of the multiple access scheme. In the second paper an asynchronous CDMA system with adaptive both transmitter and receiver is analysed. In this scheme better multiple access interference suppression is achieved relative to the systems with adaptive receivers only. The concept of the adaptive transmitter is based on feedback information from the corresponding receiver. The third paper considers a decorrelator multiuser receiver. This receiver has the advantages that its complexity is linear with the number of users and it does not require the estimation of the signal strengths of the various users, hence it is suitable for fading channels.

The fourth paper deals with the analysis of the Rake receiver combined with coding whereas the fifth paper unifies various diversity combining schemes for frequency hopped systems. In the sixth paper authors analyse the outage probability for a DS/CDMA receiver. The difference between this and previously published work is that error correction coding is included. The seventh paper deals with performance evaluation of multicell DS microcellular system. They develop a new analytical model to evaluate the uplink performance which accounts for the user's spatial distribution, the chip waveform, power control and macro selection diversity.

Finally the eighth paper deals with optimal policy for CDMA code allocation to voice and multipriority data traffic. The optimal policy is obtained by minimizing a cost function consisting of the weighted sum of the rejection rates of voice and high priority data traffic subject to performance requirements (bit error rates) on all traffic types.

We have received over 40 submissions for this issue. Unfortunately it was not possible to include all of the good papers. Some of these will be included in future issues.

We would like to thank the various authors who submitted their work to this issue and the numerous reviewers for their very important roles in supporting the publication process.

It was a pleasure to work with all of them.

Elvino S. Sousa was born in Graciosa, Azores, (Portugal) on December 28, 1956. He received the B.A.Sc. degree in engineering science, and the M.A.Sc. degree in electrical engineering from the University of Toronto in 1980 and 1982 respectively, and the Ph.D. degree in electrical engineering from the University of Southern California in 1985. Since 1986 he has been with the department of Electrical and Computer Engineering at the University of Toronto where he is presently an Associate Professor.
Since 1986 he has been a Natural Sciences and Engineering Research Council of Canada (NSERC) University Research Fellow.
He has performed research in the areas of packet radio networks, spread spectrum systems, mobile communications, and indoor wireless communications.
At the University of Toronto he has taught graduate courses in error-correcting codes and mobile communications.
He has given various lectures and short courses in mobile communications.
He is the Technical Program Chairman for the Sixth International Symposium on Personal Indoor and Mobile Radio Communications (PIMRC95).

Savo G. Glisic is professor of Telecommunications at University of Oulu, Finland. He is also Chairman of the Board of Directors of Globalcomm ltd Finland and Associate staff of the Consultare Technology Group Inc. Maryland, USA.
He was visiting scientist at Cranfield Institute of Technology Cranfield, England (1976, 77) and University of California at San Diego, USA (1986, 87).
He has been active in the field of Spread Spectrum for 15 years and has published a number of paper and three books. He is doing consulting in this field in Europe, USA and Australia.
He was Technical Program Chairman of The Third IEEE International Symposium on Spread Spectrum Techniques and Applcations-ISSSTA'94 and will be Technical Program Chairman of The Eight IEEE International Symposium on Personal Indoor and Mobile Radio Communications-PIMRC'97.
Dr Glisic is Senior Member IEEE and Member of The New York Academy of Science.

Integrated Receiver Structure of Staged Decoder and CCI Canceller for CDMA with Multilevel Coded Modulation

Ahmed Saifuddin, Ryuji Kohno
Div. of Elec. and Comp. Eng., Yokohama National University
156 Tokiwadai, Hodogaya-ku, Yokohama-240 - Japan.
Hideki Imai
Institute of Industrial Science, University of Tokyo
7-22-1 Roppongi, Minato-ku,
Tokyo-106, Japan.

Abstract. This work presents a direct sequence spread-spectrum multiaccess (DS/CDMA) receiver that employs integrated structure of staged decoder and CCI (co-channel interference) canceller, when multilevel coded modulation is used and the system undergoes fading channel. We exploit the attractive multistage decoding method of multilevel coding. Each stage decoding is jointly done with the data estimation process and thus replicas of CCI can be formed with high precision, which ultimately results in performance improvement without any additional decoding delay or circuit complexity. We have chosen appropriate multilevel 8-PSK coded modulation schemes for the integrated receiver of staged decoder and CCI canceller in fading channels. Computer simulation results show the significant coding gain that can be achieved by the proposed scheme in comparison with the conventional scheme. The effect of estimation error as well as unequal power is also investigated.

1. INTRODUCTION

There has been increased interest in CDMA where multiple users transmit over a common communication channel, typically using the direct sequence (DS) spread spectrum techniques. In asynchronous CDMA, simultaneous accessing users can transmit and receive data without synchronization between them, i.e., with random access. In DS/CDMA the entire channel bandwidth is available to all users of the system at all times, therefore the signature sequences which are assigned to individual users for spreading the information band must have low cross-correlation properties in order to achieve low level of mutual interference among the users. The traditional method of coherently demodulating DS/CDMA signals is to synchronize a local sequence generator and oscillator to the signal of interest and then to make decisions on the received signal as if the desired signal is the only one present. The received signal usually consists of the desired signal, a multiuser interference which is also called the co-channel interference (CCI), thermal/shot noise and may be further degraded by dispersion.

The two limiting factors of the performance of conventional receiver are CCI and near-far problem. A major improvement over the traditional receiver can be achieved by viewing the CCI not as random noise, but instead as a structured interferer. Because all of the signals making up the CCI in the CDMA network are generally of the same structure as the signal of interest, and because their signature sequences are generally known, it is possible to augment standard receiver structure and exploit the knowledge of CCI by estimating it and attempting to cancel it, or by jointly estimating the entire message. The augmentation required consists of additional synchronization circuitry to lock into some or all of the interfering signals, and then to use these additional statistics to estimate the CCI. There are three options for using this information to regenerate an estimate of the interference for cancelling the actual received interference in the desired channel; these are

i) Precorrelation (reconstruction of the original waveforms)
ii) Postcorrelation (reconstruction of the postcorrelation noise in each Digital Matched Filter (DMF))

iii) Tap manipulation (DMF receiver matching to suppress CCI).

i) and ii) have relative complexity associated with their implementation. In the case of postcorrelation cancellation, it is necessary to regenerate a different CCF (cross correlation function) pairing for each interfering subscriber in the channel to be enhanced. However, the precorrelation noise for each channel need only be regenerated once to be cancelled from any of the desired channels. This has greater implications in the implementation of cascaded successive cancellation stages, which relies on the enhancement of all interference and desired channels. Precorrelation cancellation circuitry has been suggested by Kohno et.al. [1]. In multiuser receivers, the decision of all user's data is an interdependent process. This class of receivers have been proposed by Verdu [2], Xie et.al. [3], and Varanasi et.al. [4]. Cascaded cancellation scheme has been proposed in [5-6]. In [7] a multistage multiuser receiver has been proposed which is based on trellis structure.

Ungerboeck [8] proposed a combined modulation/coding approach for information transmission with bandwidth and power efficiencies. Based on [9] we earlier proposed [10] an cascade of integrated equalization decoding scheme where equalization and decoding operations were carried out at each stage. One draw back of this scheme is the decoding delay involved in each decoding stages. For a remedy to this problem we propose a scheme for CDMA which involves coded modulation and at the receiver, interference cancellation is done in the demodulation process. Not so many works have been done regarding coded modulation applied to CDMA. The first work of this kind was done by Boudreau et.al. [11], where they compared the performance of trellis codes with convolutional codes for CDMA in AWGN channel. It has been shown that convolutional code yields superior performance than a trellis code and it was pointed out that greater distance properties of the lower rate convolutional code is responsible for the better performance. A similar work has been done by Rahman et.al. [12], where they considered block coded modulation instead of trellis codes. Block coded modulation in the form of multilevel code is now an interesting topic for both AWGN and fading channels because of its simple structure, flexibility of construction and mostly because of suboptimum multistage decoding process. In the case of Rayleigh fading which is an important phenomenon for mobile communication, multilevel codes is proved to be quite effective. Recently Seshadri and Sundberg [13] also Wu and Lin [14] proposed multilevel coded modulation for the Rayleigh fading channels which perform better than the codes proposed by Schlegel and Costello [15] using Ungerboeck type codes. We propose a multilevel coded modulation scheme for spread spectrum multiaccess system where CCI cancellation is done in conjunction with each stage decoding of the multistage decoding process resulting BER improvement without additional circuit complexity or decoding delay.

In section 2 we describe the system model. In section 3 multilevel coding is discussed in brief. section 4 depicts receiver architecture. In section 5 theoretical analysis of performance is described. In section 6 some simulation results are illustrated. Finally a conclusion is drawn in section 7.

2. SYSTEM MODEL

The general architecture of the system that we consider is illustrated in Fig. 1, which has been studied previously in different literatures of asynchronous CDMA. The system consists of K simultaneous users. The signal transmitted by the k-th user $S^k(t)$ is assumed to be delayed increasingly according to the user number.

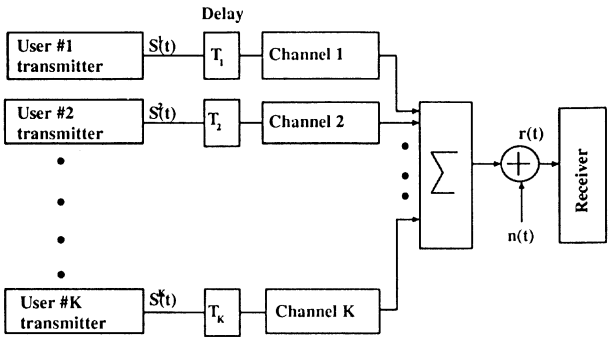

Fig. 1 - General asynchronous CDMA structure.

2.1. *Transmitter model*

The transmitter system model for Multilevel CDMA is illustrated in Fig. 2. This architecture is based on multilevel codes proposed by Imai and Hirakawa [16]. Each user's data stream is converted to l parallel branches for l level modulation scheme by a serial to parallel converter. Data bits of each parallel branches are encoded by the component codes and M-ary baseband signal is formed as shown in Fig. 2. The inphase and quadrature components of the baseband signal are spread by two spreading sequences. After chip shaping filter and local oscillator RF signal is formed and is transmitted.

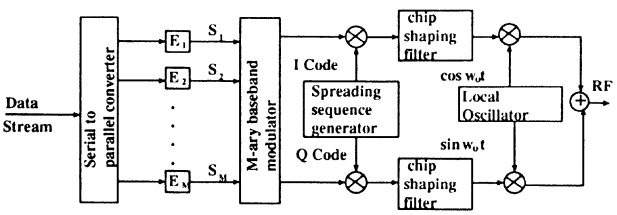

Fig. 2 - Transmitter structure of a particular user using multilevel codes.

The complex baseband symbol of the k-th user during the n-th symbol period is defined by

$$x_n^k = b_n^k \exp\left[j\,\theta_n^k\right] \tag{1}$$

where b_n^k and θ_n^k are the amplitude and phase of the complex baseband output respectively. We define

$$x_n^{kI} = b_n^k \cos\theta_n^k \tag{2}$$

and

$$x_n^{kQ} = b_n^k \sin\theta_n^k \tag{3}$$

The k-th user's complex baseband information signal can be represented by

$$X^k(t) = X_I^k(t) + j\,X_Q^k(t) = \sum_{n=-\infty}^{\infty} x_n^{kI}\,P_T(t-nT) + j\sum_{n=-\infty}^{\infty} x_n^{kQ}\,P_T(t-nT) \tag{4}$$

T is the symbol duration. The DS spreading chip waveform is given by

$$a^k(t) = \sum_{n=-\infty}^{\infty} a_n^k\,P_{T_c}(t-nT_c) \tag{5}$$

where, $T = NT_c$, N is the processing gain and

$$P_T(t) = \begin{cases} 1 & \text{if } 0 \le t \le T \\ 0 & \text{otherwise} \end{cases} \tag{6}$$

The resulting transmitted signal of the k-th user is thus given by

$$S^k(t) = S_I^k(t) + j\,S_Q^k(t) \tag{7}$$

where,

$$S_I^k(t) = \sqrt{2P_k}\,X_I^k(t-T_k)\,a^{2k}(t-T_k)\cdot \cos\left[\omega_c(t-T_k)+\psi_k\right] \tag{8}$$

$$S_Q^k(t) = \sqrt{2P_k}\,X_Q^k(t-T_k)\,a^{2k-1}(t-T_k)\cdot \sin\left[\omega_c(t-T_k)+\psi_k\right] \tag{9}$$

We assume that the offset between the inphase and quadrature components of the signal is zero. As in Pursley [17], we chose the spreading sequence of the quadrature sequence the reverse sequence of the inphase spreading code with the property of having the same aperiodic autocorrelation function. T_k is the k-th user's transmitter time delay and ψ_k is the phase offset relative to those of user 1.

2.2. *Channel model*

We consider the channel model which follows Kavehard [18]. The k-th user's link has the impulse response which takes on the form

$$h_k(t) = \sum_{\lambda=1}^{L_k} \beta_{k,\lambda}\,\delta\left(t-t_{k,\lambda}\right)e^{j\theta_{k,\lambda}} \tag{10}$$

Each path's delay $t_{k,\lambda}$ is organized in order of increasing magnitude with λ. For urban environment following Turin [19] we choose the maximum excess path delay to be $7\mu s$. $\beta_{k\lambda}$ is the λ-th path gain and path phase $\theta_{k,\lambda}$, is uniformly distributed over the interval [0, 2π). The probability density function of β is given by

$$p(\beta) = \begin{cases} 2\beta e^{-\beta^2} & \beta \ge 0 \\ 0 & \text{elsewhere} \end{cases} \tag{11}$$

Moreover $\{t_{k,\lambda}\},\{\beta_{k,\lambda}\}$ $\{\theta_{k,\lambda}\}$ are considered to be mutually independent random process. Also the parameters of the fading channel are considered to be invariant over several bit durations.

3. MULTILEVEL ENCODING AND TIME DIVERSITY

In order to design trellis coded modulation schemes with asymptotically optimal error probability for an independently fading Rayleigh channel, we need to maximize the minimum Hamming distance [13]. Multilevel coding approach with multistage decoding is a better way of achieving this goal than by using the single encoder and single mapper approach used by Ungerboeck. Fig. 2 shows the basic block diagram of a transmitter using ideal coherent phase shift keying modulation. Let us

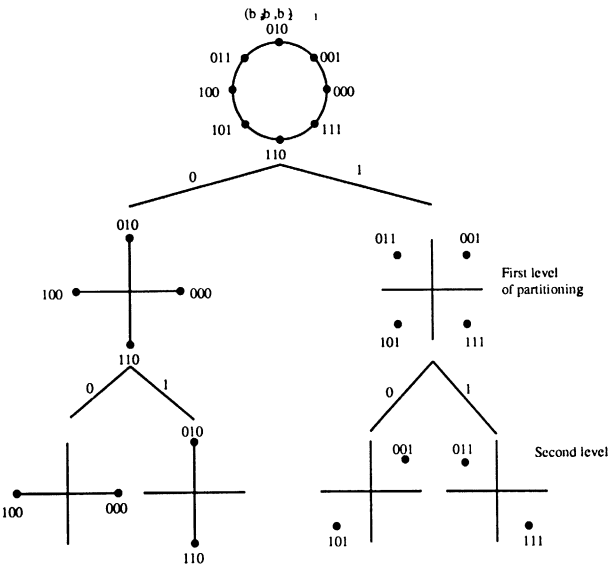

Fig. 3 - 8-PSK signal constellation and its set partitions.

consider the 8PSK signal constellation with the labeling of each point in the signal space just like Ungerboeck codes [8] as shown in Fig. 3. In multilevel construction each digit is now independently addressed by the output of a binary convolutional code or block code. In general for l levels, let the minimum Hamming distance (free distance) for each of the component binary codes be d_{Hi}, for $i = 1, 2, \ldots, l$. Then, the minimum Hamming distance between any two transmitted code sequences is

$$d_H = \min\left(d_{H1}, d_{H2}, \ldots, d_{Hl}\right) \tag{12}$$

This result follows from the signal construction. This is key equation in achieving maximum time diversity systems at a given complexity level. We achieve this time diversity out of coding. Hamming distance grows very quickly with the number of states for binary codes, yielding good time diversity for the multilevel system. In addition to the time diversity, a certain symbol rate should be achieved. Let the total number of information bits into each encoder be k_i and the overall code length be n. Code rate is given by,

$$\frac{\sum_{i=1}^{l} k_i}{n} = R \quad \text{(bits/symbol)}$$

The code design problem is to achieve as large diversity gain as possible at a given transmission rate and decoding complexity.

4. RECEIVER ARCHITECTURE

The receiver structure is shown in Fig. 4. The receiver of any arbitrary i-th signal consists of a pair correlation receiver. The received signal is coherently down-converted to baseband. The resulting $I - Q$ component output, sampled once per chip, is despread by the local replica code sequence and then summed over N chips. $I - Q$ components are fed to signal correlator. The signal correlator correlates the complex signal with each of the possible signal points of the partitioned signal constellation. To improve *BER* performance we adopt interference suppression in the form of multiuser interference estimation and successive cancellation. Several such schemes have been proposed earlier [5, 6, 10]. A previous paper [10] used a cascade of integrated equalization and decoding which had the disadvantage of decoding delays in each stage. To avoid these delays, a scheme using coded modulation and interference cancellation is presented. We exploit here the attractive multistage decoding feature of multilevel code. It has been shown [13, 20] that multistage decoding gives almost the same performance as maximum likelihood decoding at high *SNR* with much less circuit complexity. We utilize decoded information of each stage to form replica with more precesion. In multilevel coding method the least significant bit (LSB) is the most vulnerable one because of the least Euclidean distance separation and component codes are chosen such that the most powerful component code can be assigned for encoding LSB satisfying the rate requirement. As the most vulnerable bit of the multilevel signal is decoded first and is protected by the powerful error correcting code, the probability of error propagation is relatively less. In this manner *BER* performance is improved. In multistage decoding, second and subsequent subset decoding process has to wait till the previous decoding stages are complete and so is in our case. Therefore, it does not require any additional time delay. Moreover, unlike [10] here the decoding stages are carried out only once, hence the proposed scheme does not involve any additional circuit complexity compared to the one where decoding is done at the end as [11]. Multiuser interference estimation and component wise decoding process is illustrated clearly in Fig. 4. Multiuser interference estimation is carried out independently for inphase and quadrature components. For each component interference estimation process, baseband signals of each users are passed through a bank of transversal filters which emulate the channel of the users. The filters consist of taps equal to the number of multipaths and weighted by the gain coefficients. With correct channel and data estimate, each user's received signal component can be recreated. By adding all the recreated signal components except that of desired user a replica of the desired user's CCI component can be formed [28]. In Fig. 4 after signal correlator the terms D^i_{n1}, D^i_{n2}, ..., D^i_{nl} represent the 1, 2, ..., l bit levels of the n-th symbol of user i, and Δ_1 is the decoding delay associated with first level bit decoding. Baseband signal $'i'_1$ etc. are baseband signals formed when the st stage decoding has been accomplished.

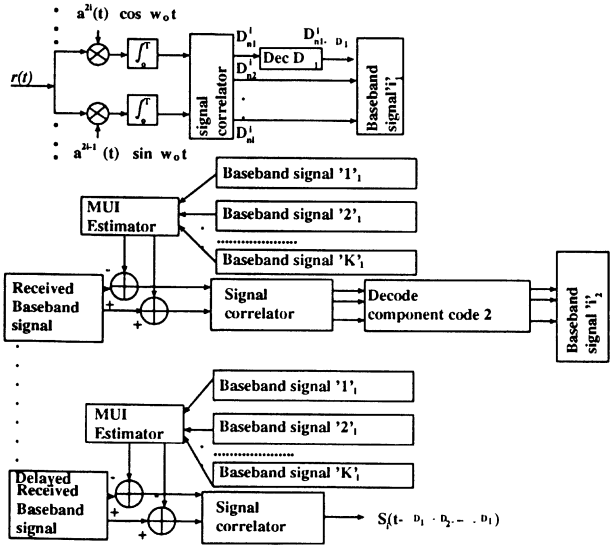

Fig. 4 - Integrated receiver structure.

The received signal can be represented by

$$r(t) = \sum_{k=1}^{K} \int_{-\infty}^{\infty} h_k(\tau)\, S^k(t-\tau)\, \mathrm{d}\tau + n(t) \tag{13}$$

where $n(t)$ is a white zero-mean Gaussian process with two sided power spectral density $N_o/2$. The received signal can be further rewritten into,

$$r(t) = \sum_{k=1}^{K} \sum_{\lambda=1}^{L_k} \sqrt{2P_k} \left\{ X_I^k \left(t - \tau_{k,\lambda}\right) a^{2k} \left(t - \tau_{k,\lambda}\right) \right\} \cdot \cos\left(\omega_c t + \phi_{k,\lambda}\right) + j\, X_Q^k \left(t - \tau_{k,\lambda}\right) a^{2k-1} \left(t - \tau_{k,\lambda}\right) \cdot \sin\left(\omega_c t + \phi_{k,\lambda}\right) \Big\} + n(t) = r_I^t + r_Q^t + n(t) \quad (14)$$

P_k is the received signal power of the k-th user. The symbol energy is defined by

$$E_s = \int_0^T \left[S^k(t)\right]^2 \mathrm{d}\, t$$

The DS/CDMA scheme transmits a pair of phase modulated PN sequences, the phase and amplitude of which are determined by signal point. In eq. (14) $\tau_{k,\lambda} = T_k + t_{k,\lambda}$ and $\phi_{k,\lambda} = (\psi_k + \theta_{k,\lambda} - \omega_c \tau_{k,\lambda}) \bmod 2\pi$. Assuming without loss of generality that $\tau_{i,1}$ and $\phi_{i,1}$ are 0. The correlators are alligned with the signal arriving on the first path. Equivalent lowpass output of the i-th user in the n-th baud interval can be represented by

$$Y_n^i = \int_{(n-1)T}^{nT} r(t)\, a^{2i}(t) \cos\omega_c t \,\mathrm{d}\, t + \int_{(n-1)T}^{nT} r(t) \cdot a^{2i-1}(t) \sin\omega_c t \,\mathrm{d}\, t = Y_n^{iI} + j\, Y_n^{iQ} \quad (15)$$

The superscripts refer to the user under consideration whereas the subscripts denote the time interval under consideration. Now the above equation can be written into,

$$Y_n^i = D_n^{i(I+Q)} + F_n^{i(I+Q)} + I_n^{i(I+Q)} + \eta_n^{i(I+Q)} \quad (16)$$

where D, F, I and η terms represent component due to desired signal, component due to ISI terms, component due to multiuser interference and component due to noise, respectively. Let us define some terms to write the component terms of Y_n^i in compact forms. For $1 \le i \le K$, $1 \le k \le K$ and for $1 \le \lambda \le L_k$ we define

$$G_I(i, k; \lambda) = \beta_{k,\lambda} \cos\phi_{k,\lambda} \quad (17)$$

and

$$G_Q(i, k; \lambda) = \beta_{k,\lambda} \sin\phi_{k,\lambda} \quad (18)$$

where G_I and G_Q represent the inphase and quadrature fading components. The full cross-correlation between user k and user i's spreading signal is defined by

$$f_I(i, k; \lambda, n) = G_I(i, k; \lambda) = \left[X_{n-1}^{kI}\, R_{k,i}^I \left(\tau_{k,\lambda}\right) + X_n^{kI}\, \hat{R}_{k,i}^I \left(\tau_{k,\lambda}\right) \right] \quad (19)$$

$$f_Q(i, k; \lambda, n) = G_Q(i, k; \lambda) \left[X_{n-1}^{kQ}\, R_{k,i}^Q \left(\tau_{k,\lambda}\right) + X_n^{kQ}\, \hat{R}_{k,i}^Q \left(\tau_{k,\lambda}\right) \right] \quad (20)$$

where following [21],

$$R_{k,i}^I \left(\tau_{k,\lambda}\right) = \int_0^{\tau_{k,\lambda}} a^{2k} \left(t - \tau_{k,\lambda}\right) a^{2i}(t) \,\mathrm{d}\, t \quad (21)$$

$$R_{k,i}^Q \left(\tau_{k,\lambda}\right) = \int_0^{\tau_{k,\lambda}} a^{2k-1} \left(t - \tau_{k,\lambda}\right) a^{2i-1}(t) \,\mathrm{d}\, t \quad (22)$$

$$\hat{R}_{k,i}^I \left(\tau_{k,\lambda}\right) = \int_{\tau_{k,\lambda}}^{T} a^{2k} \left(t - \tau_{k,\lambda}\right) a^{2i}(t) \,\mathrm{d}\, t \quad (23)$$

$$\hat{R}_{k,i}^Q \left(\tau_{k,\lambda}\right) = \int_{\tau_{k,\lambda}}^{T} a^{2k-1} \left(t - \tau_{k,\lambda}\right) a^{2i-1}(t) \,\mathrm{d}\, t \quad (24)$$

We assume the chip waveform is a rectangular pulse. With these definitions we can write the followings,

$$D_n^{iI} = \sqrt{P_i/2}\, G_I(i, i, 1)\, X_n^{iI}\, T \quad (25)$$

$$D_n^{iQ} = \sqrt{P_i/2}\, G_Q(i, i, 1)\, X_n^{iQ}\, T \quad (26)$$

$$F_n^{iI} = \sqrt{P_i/2} \sum_{\lambda=2}^{L_i} f_I(i, i; \lambda, n) \quad (27)$$

$$F_n^{iQ} = \sqrt{P_i/2} \sum_{\lambda=2}^{L_i} f_Q(i, i; \lambda, n) \quad (28)$$

$$I_n^{iI} = \sum_{\substack{k=1 \\ k \ne i}}^{K} \sqrt{P_k/2} \sum_{\lambda=1}^{L_k} f_I(i, k; \lambda, n) \quad (29)$$

$$I_n^{iQ} = \sum_{\substack{k=1 \\ k \ne i}}^{K} \sqrt{P_k/2} \sum_{\lambda=1}^{L_k} f_Q(i, k; \lambda, n) \quad (30)$$

$$\eta_n^{iI} = \int_{(n-1)T}^{nT} \eta(t)\, a^{2i}(t) \cos\omega_c t \,\mathrm{d}\, t \quad (31)$$

$$\eta_n^{iQ} = \int_{(n-1)T}^{nT} \eta(t)\, a^{2i-1}(t) \sin\omega_c t \,\mathrm{d}\, t \quad (32)$$

First the inphase and quadrature components of Y_n^i, i.e., Y_n^{iI} and Y_n^{iQ} are fed to the signal correlator where correlation with each of the possible signal points is done and first stage decoding of the most vulnerable bit

is accomplished in the staged decoding process. First estimated baseband signal is formed which are then used for CCI calculation.

5. THEORETICAL ANALYSIS

The exact bit error probability for the case of multistage decoding is very difficult to achieve. Some bound may be ascertained. Using the conditional error probability of each stage, decoding error probability of the array can be obtained [20]. However, no mathematical expression of such conditional probability has been achieved so far. Numerical techniques may be employed. For l level MPSK ($M = 2^l$) there are $(l-1)$ stages of multiuser interference formation and cancellation. Multiuser interference in this case is a function of cross correlation properties of the spreading sequences and the signal constellation. Cancellation of the $I-Q$ components are done on the previous correlator output. For instance for the v-th cancellation stage cancellation is done corresponding to $l = n - v$-th symbol interval. In general for v-th stage cancellation the cancelled correlator $I-Q$ components at the l-th baud interval can be written for I component as,

$$Y_l^{iI}(v) = D_l^{iI} + \tilde{F}_l^{iI}(v) + \tilde{I}_l^{iI}(v) + \eta_l^{iI} \tag{33}$$

The ISI and CCI terms at the v-th stage now becomes,

$$\tilde{F}_l^{iI}(v) = \sqrt{P_i/2} \sum_{\lambda=2}^{L_i} \tilde{f}_I(i, i; \lambda, l, v) = F_l^{iI} - F_l^{iI}(v) \tag{34}$$

$$\tilde{I}_n^{iI}(v) = \sum_{\substack{k=1 \\ k\neq i}}^{K} \sqrt{P_k/2} \sum_{\lambda=1}^{L_k} \tilde{f}_I(i, k; \lambda, l, v) = I_l^{iI} - I_l^{iI}(v) \tag{35}$$

where,

$$\tilde{f}_I(i, k; \lambda, l, v) = f_I(i, k; \lambda, l) - \hat{f}_I(i, k; \lambda, l, v) \tag{36}$$

Similar terms can be obtained for quadrature components by simply replacing I by Q. Replica of full cross correlation for the I component becomes

$$\hat{f}_I(i, k; \lambda, l, v) = \hat{G}_I(i, k; \lambda)\left[X_{l-1}^{kI}(v-1) R_{k,i}^I(\tau_{k,\lambda}) + X_l^{kI}(v-1) \hat{R}_{k,i}^I(\tau_{k,\lambda})\right] \tag{37}$$

and

$$\hat{f}_Q(i, k; \lambda, l, v) = \hat{G}_Q(i, k; \lambda)\left[X_{l-1}^{kQ}(v-1) R_{k,i}^Q(\tau_{k,\lambda}) + X_l^{kQ}(v-1) \hat{R}_{k,i}^Q(\tau_{k,\lambda})\right] \tag{38}$$

where

$$\hat{G}_I(i, k; \lambda) = \hat{\beta}_{k,\lambda} \cos(\phi_{k,\lambda}) \tag{39}$$

and

$$\hat{G}_Q(i, k; \lambda) = \hat{\beta}_{k,\lambda} \sin(\hat{\phi}_{k,\lambda}) \tag{40}$$

We define

$$\tilde{X}_l^{kI}(v) = X_l^{kI} - X_L^{kI}(v) \tag{41}$$

and

$$\tilde{X}_l^{kQ}(v) = X_l^{kQ} - X_L^{kQ}(v) \tag{42}$$

$X_{l-1}^{kI}(v)$ is the improved inphase component of $l-1$-th symbol of user k after v stage cancellation. Moreover, the estimates are obtained essentially in the same way as in [5]. The initial bit error rate at the decoder input of first stage can be approximated by calculating the inphase and quadrature signal to noise ratio, which can be obtained by expected signal strength together with variance of intersymbol interference and CCI. For inphase component

$$E\left[\left(D_n^{iI}\right)^2\right] = \frac{P_i}{2} E\left[G_I(i, i; 1)\right] E\left[\left(X_n^{iI}\right)^2\right] T^2 \tag{43}$$

$$\mathrm{Var}\left[F_n^{iI}\right] = \frac{P_i}{2}(L_i - 1) E\left[\left(X_n^{iI}\right)^2\right] \cdot \mathrm{Var}\left[f_I(i, i; \lambda, n)\right] \tag{44}$$

$$\mathrm{Var}\left[I_n^{iI}\right] = \sum_{\substack{k=1 \\ k\neq i}}^{K} \frac{P_k}{2} L_k E\left[\left(X_n^{kI}\right)^2\right] \cdot \mathrm{Var}\left[f_I(i, k; \lambda, n)\right] \tag{45}$$

The variance of full cross correlation is given by,

$$\mathrm{Var}\left[f_I(i, k; \lambda, n)\right] = E\left[G_I^2(i, k; \lambda)\right] \cdot E\left[\left(R_{k,i}^I(\tau_{k,\lambda})\right)^2 + \left(\hat{R}_{k,i}^I(\tau_{k,\lambda})\right)^2\right] \tag{46}$$

$$\mathrm{Var}\left[\eta_n^{iI}\right] = \frac{N_o T}{4} \tag{47}$$

$$SNR_n^{iI} = \frac{E\left[\left(D_n^{iI}\right)^2\right]}{\mathrm{Var}\left[F_n^{iI}\right] + \mathrm{Var}\left[I_n^{iI}\right] + \mathrm{Var}\left[\eta_n^{iI}\right]} \tag{48}$$

Similar terms can be obtained for Q component and similarly SNR_n^{iQ} can be computed. There are several ways of bit error rate approximation. By using moment statistics, evaluating the characteristic function of the

decision statistics, approximation of the average probability of bit error may be obtained as is done in [26, 27]. This method requires large amount of computation. On the other hand when the variance of the multipath is small, bit error rate can be approximated by calculating *SNR* [5, 23, 25]. Variance are calculated in the same way as in [5]. Following [22] and [23] the approximate bit error rate at the decoder input of first stage can be given by

$$P_b(0)=\frac{1}{\log_2 M}\left[Q\left(2\sin^2(\pi/M)\log_2 M\cdot SNR_n^{iI}\right)+ Q\left(2\sin^2(\pi/M)\log_2 M\cdot SNR_n^{iQ}\right)\right] \tag{49}$$

for M-PSK signal constellation. After decoding the first level code let the probability of error be $P_{b1}(0)$ which can be approximated by [14],

$$P_{b1}(0)\le\sum\sum_{\hat{x},x\in C} b(\hat{x},x)\,p(x)\,P(x\to\hat{x}) \tag{50}$$

for convolutional code, where $b(\hat{x}, x)$ is the number of bit errors that occur when x is transmitted and $\hat{x}$ is chosen by the decoder, $p(x)$ is the a priori probability of transmitting x and C is the set of all coded sequences. And,

$$P_{b1}(0)\simeq\sum_{i=t+1}^{d}\frac{d}{n}\binom{n}{i}P_b(0)^i\left(1-P_b(0)\right)^{n-i}+ \sum_{i=d+1}^{n}\binom{n-1}{i-1}P_b(0)^i\left(1-P_b(0)\right)^{n-i} \tag{51}$$

for block codes. Next using the decoded information multiuser interference, is estimated and upon cancellation improved *BER* is obtained. The *BER* obtained from *SNR* in this case is the *BER* conditioned that the first stage has been correctly decoded. The information of the decoded data is automatically taken into account in the course of *SNR* calculation. In general the notation $P_{bl}(v)$ expresses the bit error probability after l-th level decoding and v stage cancellation. This also represents the conditional bit error rate provided all the first v bit levels are correctly decoded.

For calculating *SNR* after any arbitrary v-th cancellation stage, the variance due to ISI and CCI are represented as follows.

$$\mathrm{Var}\left[\tilde{F}_l^{iI}(v)\right]=\frac{P_i}{2}(L_i-1)\,E\left[\left(X_l^{iI}(v)\right)^2\right]\cdot \mathrm{Var}\left[\tilde{f}_I(i,i;\lambda,l,v)\right] \tag{52}$$

and

$$\mathrm{Var}\left[\tilde{I}_l^{iI}(v)\right]=\sum_{\substack{k=1\\k\neq i}}^{K}\frac{P_k}{2}L_k\,E\left[\left(X_l^{kI}(v)\right)^2\right]\cdot \mathrm{Var}\left[\tilde{f}_I(i,k;\lambda,l,v)\right] \tag{53}$$

For perfect channel estimates,

$$\mathrm{Var}\left[\tilde{f}_I(i,k;\lambda,l,v)\right]=E\left[G_I^2(i,k;\lambda)\right]\cdot E\left[\left(\tilde{X}_l^{kI}(v-1)\right)^2\right]E\left[\left(R_{k,i}(\tau_{k,\lambda})\right)^2+\left(\hat{R}_{k,i}(\tau_{k,\lambda})\right)^2\right] \tag{54}$$

Similarly variances for Q component can be found and thus the equivalent *SNR* can be estimated. *BER* can be obtained there after.

6. SIMULATED SYSTEM PERFORMANCE

It is very tedious and even time consuming to compute the bound of BER theoretically. Instead, we simulated the system performance. As code construction is not our main interest, we use some of the good multilevel codes for Rayleigh fading channel [13, 14]. We assumed no channel state information (CSI) is available since it is difficult to obtain CSI in most cases. We considered 3 level 8-PSK modulation. In fading channel better performance can be achieved by using long code sequence [24]. In the simulation process each user was assigned spreading sequence from a set of balanced Gold sequence of length 127. These were created from two m sequences, with generating polynomials 211E and 217E in octal notations which forms a preferred pair. We considered all the received powers equal assuming perfect power control. On an average we considered two multipaths for each user and $E[\beta^2] = 1$.

Example 1: As a first example we take 3 level 8-PSK code [14] with the component code as follows. C_1 is a 4-state rate-1/2 convolutional code with generator matrix [5, 7], C_2 and C_3 are the (2N, 2N − 1, 2) single parity check code. The resulting multilevel code has minimum symbol distance 2, minimum product distance 4, and information rate (5N − 2)/2N bit/symbol. We choose N = 4. Although the minimum Hamming distance 2 is small in this case, but we are contend with this choice because performance degradation due to multistage decoding becomes more severe as the minimum Hamming distance of component codes increase. Fig. 5 represents the simulated performance for a total 20 simultaneous users. Performance of uncoded QPSK, conventional and proposed scheme using the component codes listed above is shown in the figure. We consider coded modulation [11, 12] when combined in cascade with multistage interference cancellation [5] (having the same l − 1 stages as the proposed scheme) as the conventional scheme. This gives us

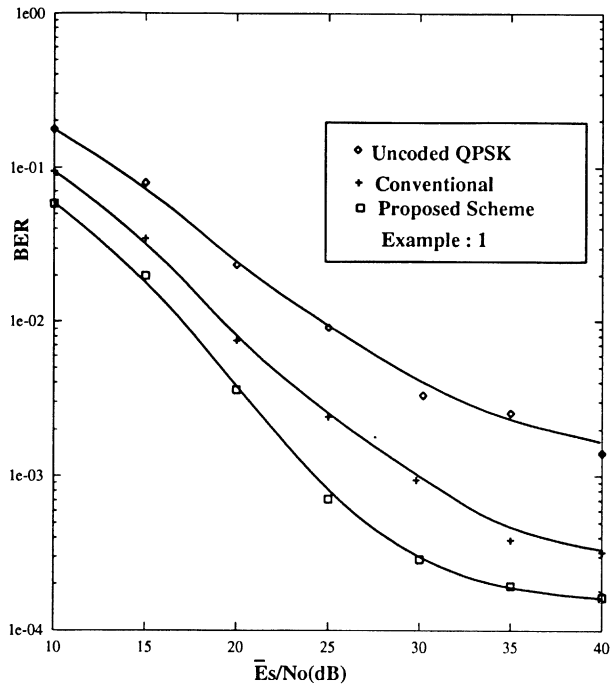

Fig. 5 - Simulated *BER* performance for a total 20 users.

the scope of fair comparison. The performance difference between uncoded QPSK and the conventional scheme is the gain achieved due to coded modulation plus interference cancellation, when they are carried out separately. The additional gain obtained by the proposed scheme is due to joint operation of cancellation and decoding. CCI replica formation of each stage using the precise data estimate of each stage decoding yields the additional gain. It is clear that using the proposed joint scheme significant coding gain can be obtained. Even at *BER* of 10^{-3} about 5 dB coding gain can be achieved compared to the conventional scheme. Notice that in this case we assumed that perfect channel estimation is available. We note that the error probability saturates at high symbol to noise ratio $\bar{E}_s/N_o$ [24]. In this case the system performance is apparently limited by interference. Fig. 6 represents the *BER* performance versus the number of simultaneous users at $\bar{E}_s/N_o$ = 22 dB, for a number of simultaneous users ranging from 5 to 35. The figure clearly exhibit the

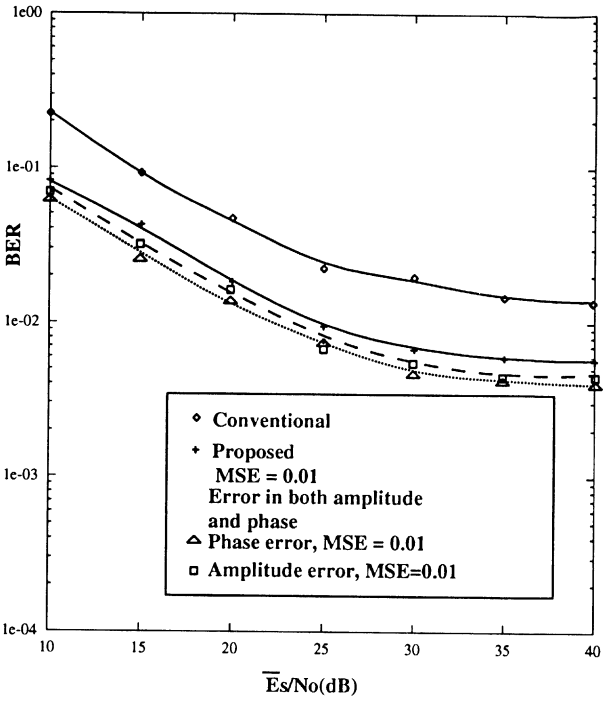

Fig. 7 - Simulated *BER* performance for a total 20 users, MSE = 0.01.

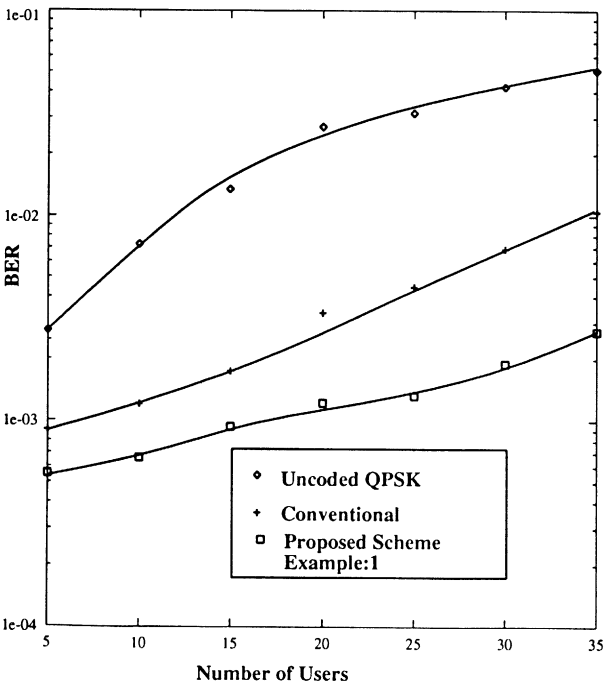

Fig. 6 - Simulated *BER* versus No. of users $\bar{E}_s/N_o$ = 22 dB.

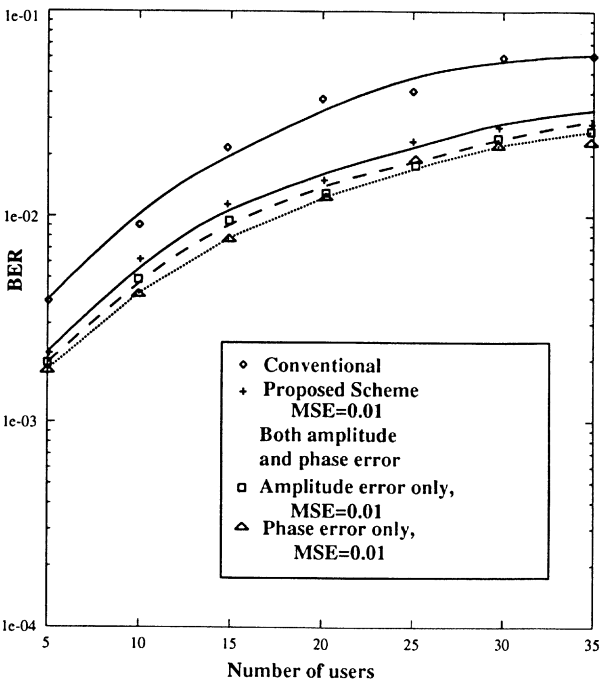

Fig. 8 - Simulated *BER* versus No. of users $\bar{E}_s/N_o$ = 22 dB, MSE = 0.01.

superior performance of the proposed scheme. Next we checked the performance in the presence of estimation error. We set the variance of error in symbol (amplitude and phase) as normalized mean square error. Fig. 7 represents the *BER* performance as a function of $\bar{E}_s/N_o$ for a total number of 20 users and symbol MSE = 0.01, with this same code combination. Performance with phase error only and amplitude error only is also depicted in the same figure. Fig. 8 shows *BER* versus number of users with $\bar{E}_s/N_o$ = 22 dB, with MSE = 0.01. From the figures it is clear that estimation error severely degrades the performance. The results of [5, 25] show large performance gains are possible only if the channel parametes are known to the receiver. However, the extent to which these gains are achieved in practical communication system depends on the accuracy with which the receiver can estimate the channel parameters. Our result also follows the observation. We also simulated the system performance under the condition of unequal powers of the users, which is very common in mobile communication environment and the cause of *near – far* problem. Fig. 9 shows the performance for a total 20 users for equal power case and when the interfering user's power are 2 dB and 3 dB relative to the desired user. We observe that at a *BER* of 10^{-3} the performance difference between equal power case and W_j/W_1 = 2 dB case is only 0.7 dB and for W_j/W_1 = 3 dB case the difference is 1.5 dB. We can conclude that although this scheme is not perfectly *near – far* resistant like decorrelator detector [29], it is *near – far* resistant to some extent.

Example 2: We consider another 3 level 8-PSK code [13] where the first level C_1 code is rate 1/2, M = 4

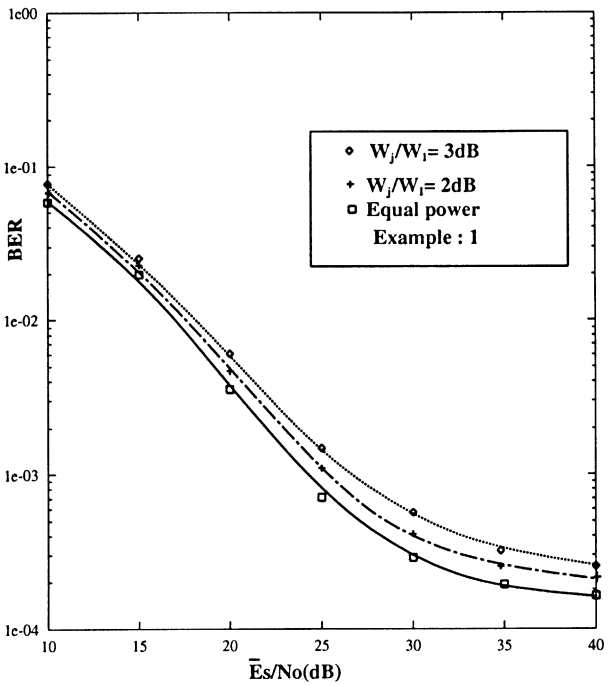

Fig. 9 - Simulated *BER* versus for 20 users with unequal powers. (Example: 1).

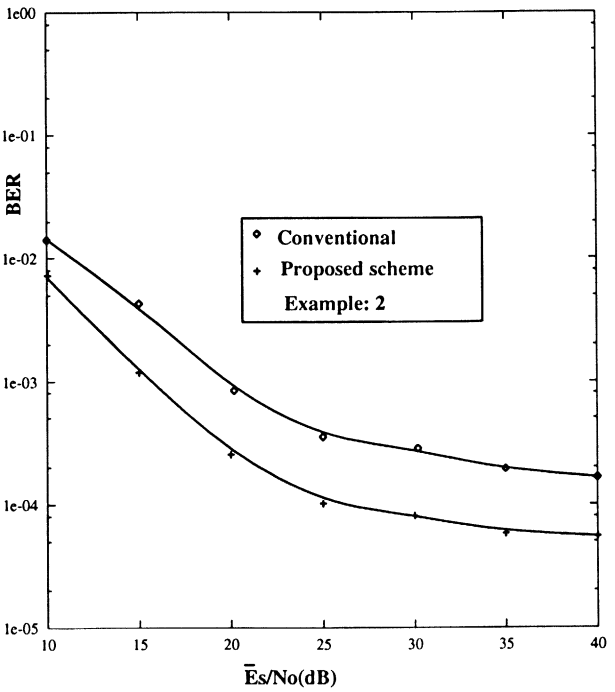

Fig. 10 - Simulated *BER* performance for a total 20 users (Example: 2).

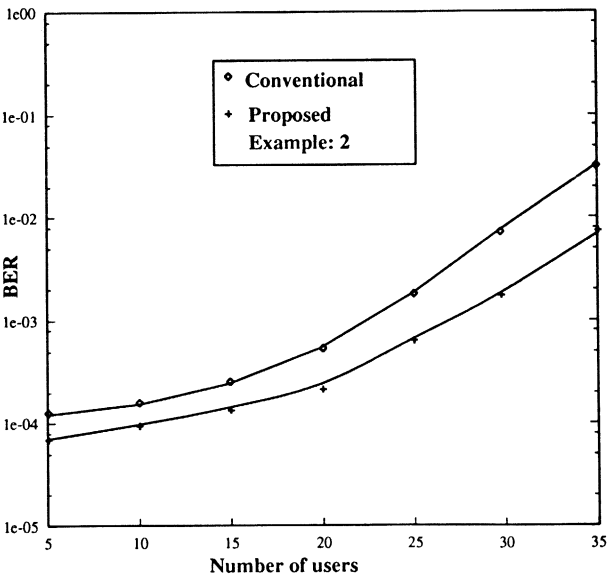

Fig. 11 - Simulated *BER* versus No. of users for $\bar{E}_s/N_o$ = 22 dB, (Example: 2).

code with d_{free} = 7. Codes C_2 and C_3 are rate 2/3 convolutional code with M = 4 and d_{free} = 4. The overall code rate is 1.83 bit/symbol. With these component codes we simulated the performance for a total 20 simultaneous users. The result is shown in Fig. 10. In this case also we observe that the proposed scheme performs better than the conventional scheme. It is noted that the bit error probability saturates at much lower $\bar{E}_s/N_o$ value. Performance in this case is better than example 1, because of the lower spectral efficiency. Fig. 11 illustrates the *BER* versus number of users for both proposed

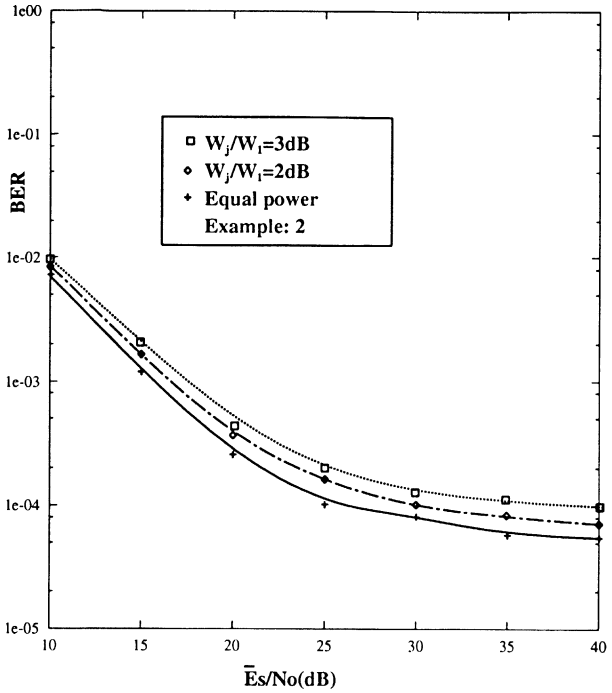

Fig. 12 - Simulated *BER* versus of 20 users with unequal power case (Example: 2).

and conventional (defined previously) scheme. It clearly exhibits the superior performance that can be obtained by the proposed scheme compared to the conventional one. Finally Fig. 12 depicts the result when unequal power case is considered. The figure shows that the scheme is near-far resistant to some extent.

7. CONCLUSION

In this paper, we have shown an integrated structure of staged decoder and CCI canceller for DS/CDMA, when multilevel coding scheme is employed in fading channel. In earlier works of coded modulation for CDMA, conventional methods have been used. We suggested joint interference suppression-decoding method which results in performance improvement without any additional decoding delay or circuit complexity. We have shown the performance improvement of the scheme through computer simulation. We also investigated the performance of the scheme under unequal power condition.

Acknowledgment

The authors would like to express their appreciation to the anonymous reviewers for valuable comments and constructive criticism.

Manuscript received on May 5, 1994.

REFERENCES

[1] R. Kohno, H. Imai, M. Hatori, S. Pasupathy: *An adaptive canceller of cochannel interference for spread-spectrum multiple-access communication networks in a power line.* "IEEE JSAC", Vol. 8, No. 4, May 1990, p. 691-699.

[2] S. Verdu: *Minimum probability of error for asynchoronous Gaussian multiple access channels.* "IEEE Trans. Inform. Theory", Vol.IT-32, Jan.1986, p. 85-96.

[3] Z. Xie, R. T. Short, C. T. Rushforth: *A family of suboptimum detectors for coherent multiuser communications.* "IEEE J. Select. Areas Commun.", Vol. 8, May 1990, p. 683-690.

[4] M. K. Varanasi, B. Aazhang: *Multistage detection in asynchronous code-division multiple-access communications.* "IEEE Trans. Commun.", Vol. 38, Apr. 1990, p. 509-519.

[5] Young C. Yoon, R. Kohno, H. Imai: *A spread-spectrum multiaccess system with cochannel interference cancellation for multipath fading channels.* "IEEE JSAC", Vol. 11, No. 7, Sept 1993, p. 1067-1075.

[6] Pulin R. Patel, Jack M. Holtzman: *Analysis of a DS/CDMA successive interference cancellion scheme using correlations.* Globecom 93.

[7] T. R. Giallorenzi, S. G. Wilson: *Multistage decision feedback and trellis-based multiuser receivers for convolutionally coded CDMA systems.* SEAS report No. UVA/538341/EE93/102, 1993.

[8] G. Ungerboeck: *Channel coding with multilevel/phase signals.* "IEEE Trans. Inform. Theory", Vol. IT-28, Jan. 1982, p. 55-67.

[9] R. Kohno, S. Pasupathy, H. Imai, M. Hatori: *Combination of cancelling intersymbol interference and decoding of error correcting code.* "IEEE Proceedings", Vol. 133, No. 3, June 1986, p. 224-231.

[10] A. Saifuddin, R. Kohno, H. Imai: *Cascaded combination of cancelling co-channel Interference and decoding of error-correcting codes for CDMA.* Proceedings of IEEE ISSSTA'94, Oulu, Finland.

[11] G. D. Boudreau, D. D. Falconer, S. A. Mahmoud: *A comparison of trellis coded versus convolutionally coded spread-spectrum multiple-access systems.* "IEEE JSAC", Vol. 8, No. 4, May 1990.

[12] M. A. Rahman, K. M. S. Murthy, Tho Le-Ngoc, A. K. Elhakeem: *A concatenated coded modulation scheme for spread spectrum multiple access system.* Submitted to Journal of Wireless comm, Kluwer academic press.

[13] N. Seshadri, C. W. Sundberg: *Multilevel trellis coded modulations for the rayleigh fading channel.* "IEEE Trans. Comm", Vol. 41, No. 9, Sept 1993.

[14] J. Wu, Shu Lin: *Multilevel trellis MPSK modulation codes for the rayleigh fading channel.* "IEEE Trans. Comm.", Vol. 41, No. 9, Sept 1993.

[15] C. Schlegel, D. J. Costello: *Bandwidth efficient coding for fading channels: code construction and performance analysis.* "IEEE JSAC", Vol. 7, No. 9, Dec 1989.

[16] H. Imai, S. Hirakawa: *A new multilevel coding method using error correcting codes.* "IEEE Trans. Inform. Theory", Vol. IT-23, May 1977, p. 371-376.

[17] M. B. Pursley: *Spread spectrum multiple access communications.* In Multi-User Communications, (G. Longo, Ed.), Vienna and New York: Springer-Verlag, 1981, p. 139-199.

[18] M. Kavehrad: *Performance of nondiversity receivers for spread spectrum in indoor wireless communications.* "ATT Tech. J.", Vol. 64, No. 6, Part 1, Aug. 1985, p. 181-210.

[19] G. L. Turin: *Introduction to spread spectrum antimultipath techniques and their application to urban digital radio.* "Proc. IEEE", Vol. 68, Mar. 1980, p. 328-353.

[20] S. Sayegh: *A class of optimum block codes in signal space.* "IEEE Trans. Commun.", Vol. COM-34, Oct. 1986, p. 1043-1045.

[21] M. B. Pursley: *Performance evaluation for phase-coded spread-spectrum multiple-access communication - Part I: System analysis.* "IEEE Trans. Commun.". Vol. COM-25, Aug. 1977, p. 795-799.

[22] J. G. Proakis: *Digital Communication*. New York: McGraw-Hill, 1989, 2nd ed.

[23] D. Laforgia, A. Luvison, V. Zingarelli: *Bit error rate evaluation for spread-spectrum multiple-access systems*. "IEEE Trans. Commun.", Vol. COM-32, No. 6, June 1984.

[24] C. S. Gardner, J. A. Orr: *Fading effects on the performance of a spread spectrum multiple access communication system*. "IEEE Trans Commun", Vol. COM-27, No. 1, Jan 1979.

[25] J. S. Lehnert, M. B. Pursley: *Multipath diversity reception of spread-spectrum multiple-access communications*. "IEEE Trans. Commun.", Vol. COM-35, No. 11, Nov. 1987.

[26] E. A. Geraniotis, M. B. Pursley: *Error probability for direct-sequence spread-spectrum multiple-access communications-Part II: Approximations*. "IEEE Trans. Commun.", Vol. COM-30, No. 5, May 1982.

[27] E. A. Geraniotis, M. B. Pursley: *Performance of coherent direct-sequence spread-spectrum communications over specular multipath fading channels*. "IEEE Trans. Commun.", Vol. COM-33, No. 6, June 1985.

[28] A. Saifuddin, R. Kohno, H. Imai: *Integrated co-channel interference cancellation and decoding scheme over fading multipath channel for CDMA*. "Trans. IEICE BII", November, 1994.

[29] R. Lupas, S. Verdu: *Near-far resistance of multiuser detectors in asynchronous channels*. "IEEE Trans. Commun.", Vol. 38, No. 4, April 1990, p. 497-507.

A. Saifuddin, R. Kohno, H. Imai: **Integrated Receiver Structure of Staged Decoder and CCI canceller for CDMA with Multilevel Coded Modulation..**

ETT, Vol. 6 - No. 1 January - February 1995, p. 9 - 19

Linear Adaptive Transmitter-Receiver Structures for Asynchronous CDMA Systems

Predrag B. Rapajic, Branka S. Vucetic
Department of Electrical Engineering the University of Sydney
Sydney, NSW 2006, Australia

Abstract. An asynchronous code-division multiple access (CDMA) system with adaptive transmitters and receivers is considered. It is assumed that the adaptive receiver and transmitter have no knowledge of the signature waveforms and timing of other users. The concept of adaptive transmitter is based on feedback information from the corresponding receiver. The information obtained from the receiver is used to calculate the optimum transmitter signature. The signatures are adaptively adjusted according to the MSE criterion during the training period as well as during data transmission. CDMA systems employing the adaptive transmitters in the presence of multiple access interference achieve the matched filter bound with no interference. The proposed CDMA system are tested by simulation over a channel with multiple access interference and additive white gaussian noise.

1. INTRODUCTION

To reduce the effects of multiuser interference on the performance of code division multiple access (CDMA) systems, various interference cancellation techniques can be used.

A significant improvement in multiple access interference MAI cancellation is obtained in systems where MAI is demodulated and subtracted from the received signal prior to the user of interest signal detection. This method of MAI detection and cancellation is combined with an adaptive array antena in [1]. The concept is critically dependent on successful MAI demodulation.

In all previous methods for MAI cancellation, ideal signal parameter estimation is assumed. An adaptive linear single user receiver which consists of a linear minimum mean square error (MMSE) filter and a decision device [2] does not rely on such assumption. The linear MMSE filter eliminates MAI without the need for timing, signatures and carrier phase information from other users. An adaptive filter is necessary to handle time varying system parameters. Another important feature of these adaptive receivers is the use of a fractionally spaced filter which is insensitive to time differences in the signal arrival times of various users. The receiver timing recovery is highly simplified, (if necessary at all) [3]. The receiver is "near-far resistant" and therefore, does not require strict power control. It achieves a significant improvement in the number of users in a CDMA system relative to the system with conventional matched filter receiver where MAI is treated as AWGN. The complexity of the adaptive linear receiver is independent of the number of users and is slightly higher than the complexity of the matched filter receiver. Also, it is demonstrated that the adaptive linear receiver is effective against narrow-band interference.

In this paper we analyse an asynchronous CDMA systems with adaptive transmitters and receivers. In CDMA systems with adaptive transmitters better MAI suppression is achieved and consequently a larger number of independent users accomodated per a unit of bandwidth relative to the systems with adaptive receivers only. Distinctive property of the CDMA system with an adaptive transmitter is that the matched filter bound in the absence of MAI is practicaly achieved in the presence of MAI.

The concept of the adaptive transmitter is based on feedback information from the corresponding receiver. Recently proposed CDMA schemes [4] sugest usage of the same bandwidth for forward link and reverse link. This concept of communication allows the transmitter in forward link to 'know' in advance conditions of propagation and channel parametars based on information received in reverse link. The information obtained from the receiver is used to calculate the optimum signature for the respective transmitter. The signatures are adaptively adjusted according to the MSE criterion of optimality during the training period as well as during the data transmission.

The rest of the paper is organized as follows. The system model is defined in section 2. In section 3 the proposed model is analyzed and the optimum solution for

the adaptive linear receiver and the transmitter is found, while the simulation results are presented in section 4.

2. SYSTEM MODEL

The general architecture of a direct sequence (DS) CDMA system thet will be analysed is illustrated in Fig. 1. The system consists of K users transmitting asyncronously. We will refer to the *users*, as those subscribers actively engaged in transmission. Each user generates a sequence of symbols $\boldsymbol{a}_k = a_k\ (-N),..,a_k(n),..,a_k(N)$, where $k = 1, 2,.., K$, $(2N + 1)$ is the number of symbols in a transmitted sequence.

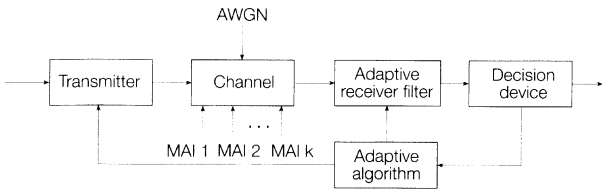

Fig. 1 - Block diagram of a CDMA transmission system with the adaptive receiver and transmitter.

Each user transmits using a different spreading sequence, denoted by $\boldsymbol{s}_k$

$$\boldsymbol{s}_k = (s_k(1), s_k(2),\ldots, s_k(J))^T$$

where J is the signature length, $(\cdot)^T$ denotes the matrix transpose and $k = 1, 2,\ldots, K$. The user signatures are generated by oversampling and filtering the spreading sequence.

The output signals $p_1(t),\ldots, p_k(t),\ldots, p_K(t)$ are sharing the same channel. The transmitted signals are assumed to be delayed randomly by a delay of τ_k. However, the symbol intervals for all transmitters are considered to be the same.

Each receiver consists of a linear adaptive fractionally spaced filter followed by a decision device. A linear filter receiver is specified by its coefficient sequence $\boldsymbol{c}_k = (c_k(-M),\ldots, c_k(M))^T$, $k = 1, 2,\ldots K$ where $2M + 1$ is the total number of filter coefficients.

The adaptive filter receiver optimizes its coefficient set for a given set of user signatures $\boldsymbol{s}_k$ and the channel by minimizing the mean square error between the received and desired signal. The initial values of the coefficients are determined during the training period and are adaptively adjusted during data transmission.

The receiver transmits the information about the optimum coefficient set to the transmitter via a feedback link. This sequence is used in the transmitter to calculate the optimum transmitted signature.

2.1. *Transmitter model*

The transmitter model is illustrated in Fig. 2. The

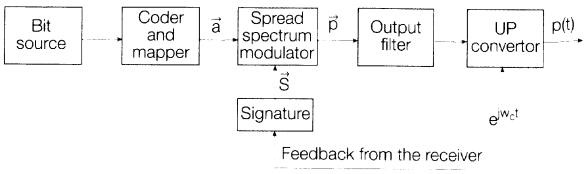

Fig. 2 - Block diagram of a single user CDMA transmitter.

data source generates a binary sequence at the data rate of $r_b = 1/T_b$, where T_b is a bit period. The binary stream is encoded by a $(b - 1)/b$ rate convolutional code. The signal mapper maps a group of b coded symbols to a signal from a 2^b modulation signal set. The symbol interval is $T = bT_b$. Each modulated symbol is then multiplied in the spread spectrum modulator by a repeative signature.

In this paper the emphasis is on signature design. It will be shown that the system performance can be improved relative to a CDMA system with adaptive linear receivers and time invariant sequences [5] by using time variant sequences. We propose to use adaptive transmitter signatures adjusted by feedback information obtained from the receiver. The initial signatures are obtained from binary Gold sequences. The signatures are adaptively adjusted according to the MSE criterion during the training period as well as during the data transmission. By that the optimum signatures that adaptively follow the channel parameter variations caused by MAI are produced.

The baseband signal bandwidth is $B = 1/T$. The spread spectrum modulator expands the signal bandwidth to $B_c = 1/T_c$, where Tc is the duration of the chip pulse. The spreading gain denoted by S_g, is defined as

$$S_g = \frac{B_c}{B}$$

The output filter limits the signal bandwidth to B_c and the up-convertor translates the spread spectrum signal by the carrier frequency.

The transmitted signal of the k-th user can be represented as

$$p_k(t) = \sum_{i=-N}^{N} a_k(i)\, s_k\left(t - iT - \tau_k\right) e^{j\left((\omega_c + \omega_k)t + \varphi_k\right)} \qquad (1)$$

where f_c is a constant nominal carrier frequency for all users, $\omega_c = 2\pi f_c$ and $s_k(t - iT - \tau_k)$ is a time variable signature waveform where τ_k is the time delay of the k-th user. The signature varies at a slow rate compared to the symbol rate. Each transmitter has independent time constant carrier frequency and phase shifts, ξ_k and φ_k, respectively, where $\omega_k = 2\pi\xi_k$.

2.2. *Channel model*

The channel model is shown in Fig. 3. The transmitted signal is corrupted by MA interference and additive white gaussian noise (AWGN).

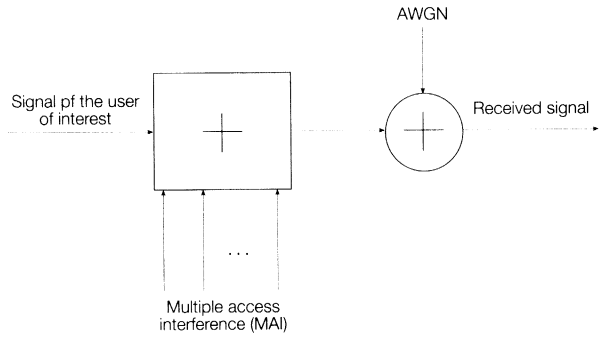

Fig. 3 - Channel model.

The signal at the channel output is given by

$$r(t) = G(t, \boldsymbol{A}) + n(t) \tag{2}$$

where $n(t)$ is a zero mean stationary additive gaussian noise with variance σ^2. $G(t, \boldsymbol{A})$ is the MA signal coming from K independent users given by

$$G(t, \boldsymbol{A}) = \sum_{i=-N}^{N} \sum_{k=1}^{K} a_k(i) f_k(t - iT - \tau_k) e^{j((\omega_c + \omega_k)t + \varphi_k)} \tag{3}$$

where $f_k(t)$ is its received signature waveform. The received signature $f_k(t)$ is different from the transmitted signature waveform $s_k(t)$ due to channel distortions. The distortion can be compensated by an adaptive algorithm [5].

The *symbol matrix*, denoted by $\boldsymbol{A}$, as a matrix consisting of all transmitted symbols by K users and it is defined as

$$\boldsymbol{A} = [\boldsymbol{a}_1, \boldsymbol{a}_2, \ldots, \boldsymbol{a}_k, \ldots, \boldsymbol{a}_K] \tag{4}$$

where $\boldsymbol{a}_k = (a_k(-N), \ldots, a_k(n), \ldots, a_k(N)$ is the k-th user symbol sequence.

2.3. *Receiver model*

The receiver model is shown in Fig. 4. The receiver input signal is shifted to the baseband and filtered by a filter with the bandwidth of B_s, the signal is sampled every T_f seconds, where $B_s = 1/2\ T_f$. The fractionally spaced receiver structure simplifies the system timing recovery to a great extent [3].

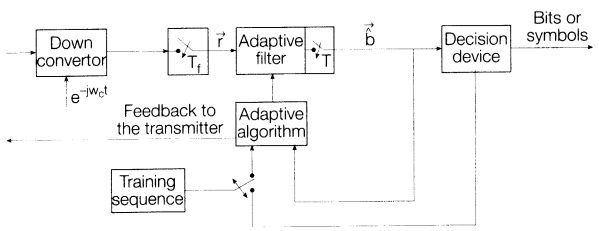

Fig. 4 - Block diagram of and adaptive receiver for the CDMA system.

It is convenient to assume that the user of interest is the user number 1. The signal at the input of the receiver, at instant m is given by

$$r_1(mT_f) = \sum_{i=-N}^{N} \sum_{k=1}^{K} a_k(i) f_k \cdot (mT_f - iT - \tau_k) e^{j\omega_k mT_f + j\varphi_k} + v_1(mT_f) \tag{5}$$

where $v_1(mT_f)$ is a sample of the additive gaussian noise for receiver 1. The sampled signal is fed to the adaptive FIR filter with the time span of $(2M + 1)$ sample intervals.

The filter output, at the n-th symbol interval, calculated every symbol interval, is given by

$$\hat{a}_1(nT) = \sum_{m=-M}^{M} c_1^*(m) r_1(nT - mT_f) \tag{6}$$

where $c_1(m)$ are the complex filter coefficients of the first user and $(\cdot)^*$ denotes the complex conjugate.

The symbol estimate, $\hat{a}_1(nT)$, is further applied to the decision device.

3. SYSTEM ANALYSIS

In this Section the optimum MSE receiver and the optimum MSE transmiter are defined.

3.1. *The optimum adaptive receiver coefficients*

The user number 1, as the user of interest, is considered and for simplicity the subscript for user 1 are omitted. The mean squared receiver error (MSE) at time instant n is given by

$$\varepsilon = E(e(n)^2) = E(|\hat{a}(nT) - a(n)|^2) \tag{7}$$

By substituting $\hat{a}(nT)$ from (6) we get

$$\varepsilon = E(|\boldsymbol{c}^H \boldsymbol{r} - a(n)|^2) \tag{8}$$

where $\boldsymbol{c}$ is the linear filter coefficient sequence, $(\cdot)^H$ is the matrix transpose and conjugate while $\boldsymbol{r}$ is the received signal sample sequence given by

$$\boldsymbol{r} = (r(nT + MT_f), \ldots, r(nT), \ldots r(nT - MT_f))^T \tag{9}$$

The mean squared error (8), achieves its minimum value when the coefficient sequence $\boldsymbol{c}_{\text{opt}}$ is chosen to satisfy [5]

$$\boldsymbol{F}\, \boldsymbol{c}_{\text{opt}} = \boldsymbol{z} \tag{10}$$

and the minimum MSE is then

$$\varepsilon_{\text{opt}} = \sigma_a^2 - \boldsymbol{z}^H \boldsymbol{c}_{\text{opt}} \tag{11}$$

where

$$\boldsymbol{F} = E(\boldsymbol{r}\boldsymbol{r}^H) \tag{12}$$

and

$$z = E(a^*(i)\,\boldsymbol{r}) \tag{13}$$

Eqs. (10), and (11) define the optimum coefficient sequences and the MSE for a general adaptive receiver structure under the condition that matrix $\boldsymbol{F}$ is time invariant and consequently all signatures, time invariant vectors.

This solution is near-far resistant if number of CDMA users does not exceed, so called, critical number of users where user signatures become heavily correlated. The critical number of users is defined as the number of users where at which an increase in the input *SNR* will not cause an increase in the output *SNR* [5].

3.2. *Adaptive algorithm*

The most common adaptive control algorithm is the LMS algorithm [6]. The coefficient adjustment algorithm can be described by the following equations

$$\boldsymbol{c}_{n+1} = \boldsymbol{c}_n - \alpha\, e(n)\, \boldsymbol{r}_n \qquad n = 0, 1, 2, \ldots, \tag{14}$$

where $\boldsymbol{c}_n$ is the filter coefficient sequence at the n-th iteration and α is the step size. The step size determines the adaptive algorithm convergence rate and amplitude fluctuations around the minimum attainable MSE. The algorithm is updated once every symbol interval. Convergence properties of the LMS and RLS algorithm are analyzed in [6]. The specifics of the LMS algorithm application related to the CDMA system in [5].

3.3. *Optimum transmitter signature*

We should recall that the optimum MSE (11) is obtained under the condition of constant transmitter signatures where the receiver is optimized, only. The assumption used to derive eqs. (10), and (11) is that signatures $\boldsymbol{s}$ on the transmitter side, and consequently signatures z, are time invariable sequences independent of the channel parameters or MAI.

In the sequel we will show that ε_{opt} can be further reduced if the transmitter signatures are optimized by adopting the receiver coefficient vector $\boldsymbol{c}_{\text{opt}}$ as a new signature for user No 1 instead of the original signature z. It is not surprising that the optimum receiver coefficient vector is a better choice for the transmitter signature then the original one. The receiver coefficient vector contains the information concerning MAI and produces lower crosscorrelation with other MAI signatures.

The iterative procedure in finding the transmitter signature for the given MAI conditions consists of the following steps.

Step 1. Find the optimum coefficient set $\boldsymbol{c}_{\text{opt}}$ by using eq. (10) with the initial signature value $z^{(0)} = z$. We used Gold sequences as the initial signatures $z^{(0)}$. Then we set $z^{(1)} = \boldsymbol{c}_{\text{opt}}$ with condition that $(z^{(1)})^H z^{(1)} = (z^{(0)})^H z^{(0)}$.

Step 2. Replace signature z by $z^{(1)}$ and calculate a new matrix $\boldsymbol{F}^{(1)}$ by using eq. (12)

Step 3. Repeat the procedure iteratively in the l-th iteration

$$z^{(l+1)} = \frac{\left[\boldsymbol{F}^{(l)}\right]^{-1} z^{(l)}}{\left[\left(\left[\boldsymbol{F}^{(l)}\right]^{-1} z^{(l)}\right)^H \left[\boldsymbol{F}^{(l)}\right]^{-1} z^{(l)}\right]^{\frac{1}{2}}} \qquad l = 1, 2 \ldots \tag{15}$$

where matrix $\boldsymbol{F}^{(l)}$ corresponds to $z^{(l)}$.

Step 4. Calculate the MSE as

$$\varepsilon^{(l+1)} = \sigma_a^2 - \left[z^{(l)}\right]^H \left[\boldsymbol{F}^{(l)}\right]^{-1} z^{(l)} \qquad l \doteq 1, 2 \ldots \tag{16}$$

If the MSE is less then a specified threshold stop the procedure. Set $\boldsymbol{s} = z^{(l)}$ where l is the time iteration number.

The value of MSE shows the transmitter signature convergence rate to its optimum value. The convergence of the algoritm is proved in Apendix 1.

In the section with simulation results it is shown that untill critical number of users is reached, the transmitter signature converges in a few iterations to the sequence which is orthogonal to the signatures of MAI. The orthogonality of the transmitter signature to the MAI signatures guaranties that the output *SNR* achieves the single user matched filter bound.

4. SIMULATION RESULTS

Adaptive receivers and transmitters remove MAI to a great extent. However, when the number of users reaches a certain number, correlation among the user signatures becomes significant resulting in excessive values of the output signal MSE [8]. The performance of CDMA systems employing adaptive receivers is measured by the output signal MSE in terms of the number of users with the input *SNR* as a parameter.

The output *SNR* directly depends on the MSE and it determines the bit error rate of the system. The output *SNR*, in dB, is given by

$$SNR_{\text{out}} = 10 \log \frac{\sigma_a^2}{\varepsilon_{\text{opt}}(K)} \tag{17}$$

The input *SNR* is given by

$$SNR_{\text{in}} = 10 \log \frac{\sigma_a^2}{\sigma^2} \tag{18}$$

Dashed curves in Fig. 5 show the output *SNR* as a function of the number of users for an adaptive linear

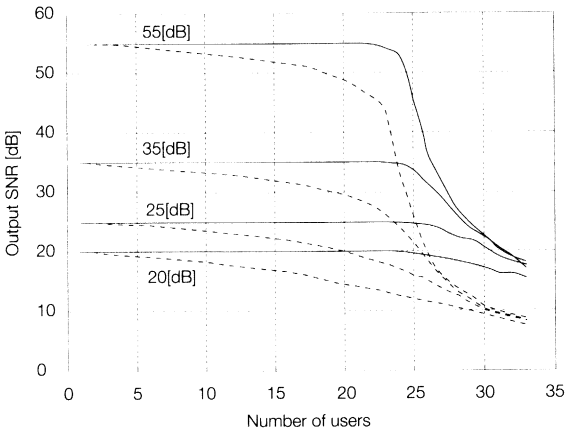

Fig. 5 - The output *SNR* in terms of the number of users with the input *SNR* as a parametar and with T_s = 31 T_c, T = 15 T_c, K_s = 33. Solid - adaptive receiver and transmitter. Dash - adaptive linear receiver.

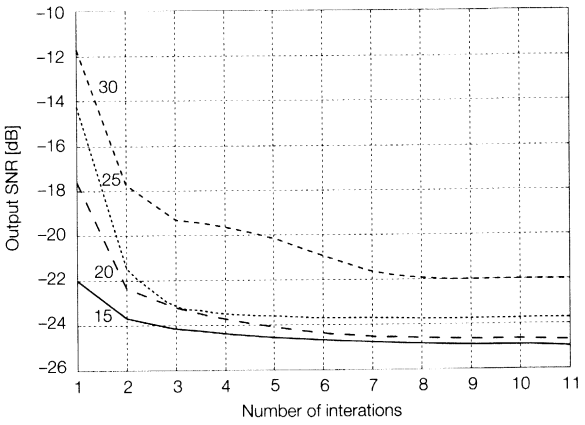

Fig. 6 - The output *SNR* in terms of the number of iterations with the input *SNR* = 25 dB and the number of users as a parameter.

receiver [5]. Transmission in this example is performed for the channel model with AWGN and MAI only. Spreading gain S_g for all users is 31 and all users have the same power. The output *SNR* is averaged over all possible combinations of signatures and all possible values of uniformly distributed time delays τ_k.

The *nominal number of users* (NNU) in a CDMA system is equal to the spreading gain S_g. This number of users is equal to the number of users that can be accomodated by equivalent TDMA of FDMA systems occupying the same bandwidth as the CDMA system. Due to imperfect cancellation of MAI, a rapid decrease in SNR_{out} occurs when the number of users reaches a threshold which is less then NNU. The *critical number of users* (CNU) is defined as the number of users at which an increase in the input *SNR* will not cause an increase in the output *SNR*. The CNU for this particular case is about 24 which is 77% of the NNU.

Solid curves in Fig. 5 show the output *SNR* in terms of the number of users for CDMA systems employing adaptive receiver-transmitter. Distinctive property of the adaptive receiver-transmiter concept is that the output *SNR* is equal to the matched filter output *SNR* until the number of users reaches the critical number of users. The critical number of users is increased in systems with the adaptive transmitter relative to the systems with the adaptive receiver only.

The convergence rate of the adaptive algorithm which is used in designing the optimum transmitter signatures is illustrated in Fig. 6. Optimum MSE is calculated in terms of number of iterations with the number of users as a parameter. The input *SNR* is 25 dB. It is visible in Fig. 6 that the convergence is achieved after just a few iterations for all numbers of users. For the number of users less then the CNU the MSE is determined by the input *SNR* (matched filter bound) and the MSE does not depend on the number of users.

Near-far resistance of the CDMA system with adaptive linear receiver and transmitter is demonstrated in Fig. 7. The curve set depicts the output *SNR* for the user of interest as a function of the number of users. Each MAI signal is 40 dB stronger compared to the user of interest. Until the critical number of users is reached there is negligible loss in the output *SNR* compared to the input *SNR*. A more rapid decrease in the output *SNR* is observed when the number of users exceeds the critical number, since the system can not generate transmitter signatures which are orthogonal to the MAI signatures.

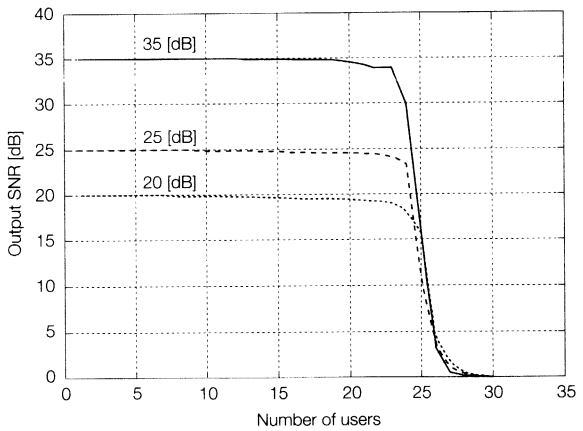

Fig. 7 - Adaptive linear transmitter-receiver with S/MAI level of – 40 dB per a single interferer. The output *SNR* in terms of the number of users with the input *SNR* as a parametar and with T_s = 31 T_c, T = 31 T_c, K_s = 33.

5. CONCLUSIONS

In this paper an adaptive receiver and transmitter structure for asynchronous CDMA systems is considered. A general solution for the optimum filter coefficient sequence is derived.

It is known that the simple receiver structure, referred to as the adaptive linear receiver, is capable of removing interference from other users to a great extent. Its distinguishing property is that timing, signatures and

carrier phase information from other users are not needed. The receiver is "near-far resistant" and hence does not require accurate power control. It achieves a significant improvement in the number of users in a CDMA system relative to the conventional single user receiver. The complexity of the adaptive linear receiver is independent of the number of users and is slightly higher than the complexity of the conventional receiver.

A more complex transmitter-receiver structure has the same properties in terms of timing recovery, "near-far" resistance as the adaptive linear receiver, whereas MAI cancellation is significantly improved. Consequently, a larger number of users can simultaneously share the channel bandwidth relative to a system with the adaptive linear receiver, only. The adaptive transmitter-receiver CDMA system achieves matched filter bound in the presence of MAI if the number od users does not exceed the critical number of users which is 70% – 80% of the CDMA system spreading gain.

The need for additional communication channel, if it is not already part of the system, from the receiver to the adaptive transmitter adds to the complexity of the adaptive receiver-transmitter structure.

Appendix 1

Note that in the further text time iterations in the algorithm are denoted by subscripts rather then superscripts.

In this Appendix we prove the convergence of the iterative procedure used in finding the transmitter signatures. To prove the convergence it is enough to prove that

$$\varepsilon_{i+1} \le \varepsilon_i \qquad i = 1, 2, .. \tag{19}$$

Initial autocorrelation matrix $\boldsymbol{F}$ is denoted as $\boldsymbol{F}_0$ while the initial signature is denoted by z_0. The correlation matrix in the next time iteration is denoted by $\boldsymbol{F}_1$ and the transmitter signature at the same time instant by z_1. The autocorrelation matrices $\boldsymbol{F}_0$ and $\boldsymbol{F}_1$ can be expressed as

$$\boldsymbol{F}_0 = \boldsymbol{B} + z_0 z_0^H$$

$$\boldsymbol{F}_1 = \boldsymbol{B} + z_1 z_1^H$$

where matrix $\boldsymbol{B}$ is a time invariant part of the autocorrelation matrix $\boldsymbol{F}$ and it does not depend on the time variable transmitter signatures $z_0, z_1, z_2, \ldots$. Matrix $\boldsymbol{B}$ is Hermitian which means that $\boldsymbol{B} = \boldsymbol{B}^H$, [5].

It is convenient to normalize the signature power by assuming that $z_0^H z_0 = 1$ and to make sure that we have normalized signal power in the next iteration we will assume that $z_1^H z_1 = 1$.

z_1 is the normalized transmitter signature at time instant $t = 1$. At the same time it is the optimum receiver coefficient sequence when z_0 was used as a transmitter signature. We express that in the mathematical form as:

$$z_1 = \frac{\boldsymbol{F}_0^{-1} z_0}{\left[\left(\boldsymbol{F}_0^{-1} z_0\right)^H \boldsymbol{F}_0^{-1} z_0\right]^{\frac{1}{2}}} \tag{20}$$

For the initial step, the MSE is

$$\varepsilon_0 = \sigma_a^2 - z_0^H \boldsymbol{F}_0^{-1} z_0$$

Without loss of generality we can assume that the symbol power is normalized to one $\sigma_a^2 = 1$ Then we can write equations for MSE in time instants 0 and 1 as:

$$\varepsilon_0 = 1 - z_0^H \boldsymbol{F}_0^{-1} z_0 \tag{21}$$

$$\varepsilon_1 = 1 - z_1^H \boldsymbol{F}_1^{-1} z_1 \tag{22}$$

To prove (19) we will prove that

$$\varepsilon_1 \le \varepsilon_0 \tag{23}$$

By using the matrix inversion lemma

$$\boldsymbol{F}_0^{-1} = \boldsymbol{B}^{-1} - \frac{\boldsymbol{B}^{-1} z_0 z_0^H \boldsymbol{B}^{-1}}{1 + z_0^H \boldsymbol{B}^{-1} z_0} \tag{24}$$

Eq. (21) can be written as

$$\varepsilon_0 = 1 - z_0^H \boldsymbol{B}^{-1} z_0 + \frac{z_0^H \boldsymbol{B}^{-1} z_0 z_0^H \boldsymbol{B}^{-1} z_0}{1 + z_0^H \boldsymbol{B}^{-1} z_0}$$

or after a simplification as

$$\varepsilon_0 = \frac{1}{1 + z_0^H \boldsymbol{B}^{-1} z_0} \tag{25}$$

Following the same procedure, Eq. (22) becomes

$$\varepsilon_1 = \frac{1}{1 + z_1^H B^{-1} z_1} \tag{26}$$

From (25) and (26) it is evident that $\varepsilon_1 \le \varepsilon_0$ if and only if

$$z_0^H \boldsymbol{B}^{-1} z_0 \le z_1^H \boldsymbol{B}^{-1} z_1 \tag{27}$$

If z_1 is substituted by (20) then (27) becomes

$$z_0^H \boldsymbol{B}^{-1} z_0 \le \frac{\left(\boldsymbol{F}_0^{-1} z_0\right)^H \boldsymbol{B}^{-1} \boldsymbol{F}_0^{-1} z_0}{\left(\boldsymbol{F}_0^{-1} z_0\right)^{\mathrm{H}} \boldsymbol{F}_0^{-1} z_0} \tag{28}$$

Term $\boldsymbol{F}_0^{-1} z_0$ can be further simplified by using Eq. (24)

$$\boldsymbol{F}_0^{-1} z_0 = \frac{\boldsymbol{B}^{-1} z_0}{1 + z_0^H \boldsymbol{B}^{-1} z_0} \tag{29}$$

By replacing (29) in (28) and bearing on mind that $(\boldsymbol{B}^{-1})^H = \boldsymbol{B}^{-1}$ we get

$$z_0^H \boldsymbol{B}^{-1} z_0 \, z_0^H \boldsymbol{B}^{-2} z_0 \le z_0^H \boldsymbol{B}^{-3} z_0 \tag{30}$$

Hermitian matrix $\boldsymbol{B}^{-1}$ can be expressed as

$$\boldsymbol{B}^{-1} = \boldsymbol{Q}^H \boldsymbol{\Lambda} \boldsymbol{Q}$$

where $\boldsymbol{Q}$ is a unitary matrix with property $\boldsymbol{Q}^H \boldsymbol{Q} = \boldsymbol{I}$ and $\boldsymbol{\Lambda}$ is diagonal eigenvalue matrix of $\boldsymbol{B}$ with real elements. Inequality (30) can be further simplified to

$$\alpha^H \boldsymbol{\Lambda} \alpha \, \alpha^H \boldsymbol{\Lambda}^2 \alpha \le \alpha^H \boldsymbol{\Lambda}^3 \alpha \tag{31}$$

where $\alpha = \boldsymbol{Q} z_0$. Note that $\alpha^H \alpha = 1$. In order to prove (31) we will prove two lemmas.

Lemma 1

$$\alpha^H \boldsymbol{\Lambda} \alpha \, \alpha^H \boldsymbol{\Lambda} \alpha \le \alpha^H \boldsymbol{\Lambda}^2 \alpha \, \alpha^H \alpha \tag{32}$$

If we denote $\boldsymbol{\Lambda} \alpha = \boldsymbol{x}$ and $\alpha = \boldsymbol{y}$, then (32) transforms into well known Cauchy-Schwartz inequality

$$\boldsymbol{x}^H \boldsymbol{y} \boldsymbol{y}^H \boldsymbol{x} \le \boldsymbol{x}^H \boldsymbol{x} \boldsymbol{y}^H \boldsymbol{y}$$

Lemma 2

$$\alpha^H \boldsymbol{\Lambda}^2 \alpha \, \alpha^H \boldsymbol{\Lambda}^2 \alpha \le \alpha^H \boldsymbol{\Lambda}^3 \alpha \, \alpha^H \boldsymbol{\Lambda} \alpha \tag{33}$$

Now it is enough to denote $\boldsymbol{\Lambda}^{3/2} \alpha = \boldsymbol{x}$ and $\boldsymbol{\Lambda}^{1/2} \alpha = \boldsymbol{y}$ then (33) becomes

$$\boldsymbol{x}^H \boldsymbol{y} \boldsymbol{y}^H \boldsymbol{x} \le \boldsymbol{x}^H \boldsymbol{x} \boldsymbol{y}^H \boldsymbol{y}$$

which is again Cauchy-Schwartz inequality.

By combining (32) and (33) we can write

$$\begin{aligned} &\alpha^H \boldsymbol{\Lambda} \alpha \, \alpha^H \boldsymbol{\Lambda} \alpha \, \alpha^H \boldsymbol{\Lambda}^2 \alpha \le \alpha^H \cdot \\ &\boldsymbol{\Lambda}^2 \alpha \, \alpha^H \boldsymbol{\Lambda}^2 \alpha \le \alpha^H \boldsymbol{\Lambda}^3 \alpha \, \alpha^H \boldsymbol{\Lambda} \alpha \end{aligned} \tag{34}$$

With $\alpha^H \alpha = 1$ finally we can state

$$\alpha^H \boldsymbol{\Lambda} \alpha \, \alpha^H \boldsymbol{\Lambda}^2 \alpha \le \alpha^H \boldsymbol{\Lambda}^3 \alpha$$

which proves (23) and (19).

Manuscript received on May 15, 1994.

REFERENCES

[1] R. Kohno, H. Imai, M. Hatori, S. Pasupathy: *Combination of an adaptive array antenna and a Canceller of interference for direct-sequence spread-spectrum multiple-sccess system.* "IEEE J. Select. Areas Commun.", Vol. SAC-8, No. 4, May 1990, p. 691-699.

[2] P. Rapajic, B. Vucetic: *Adaptive single user receiver for asynchronous CDMA systems in the narrowband interference environment.* Proc. of the Second International Workshop on Mobile and Personal Communication Systems, Adelaide, Australia, Nov. 12-13, 1992, p. 143-148.

[3] R. D. Gitlin, H. C. Meadors, Jr.: *Center-tap tracking algorithms for timing recovery.* "Bell Syst. Tech. J.", Vol. 66, No. 6, Nov. 1987, p. 73-78.

[4] R. Esmailzadeh, M. Nakagawa: *Time division duplex method of transmission of direct sequence spread spectrum signals for power control implementation.* "IEICE Trans. Commun.", Vol. E76-B, No. 8, Aug. 1993, p. 1030-1038.

[5] P. Rapajic, B. Vucetic: *Adaptive receiver structures for asynchronous CDMA systems.* "IEEE J. Select. Areas Commun.", Vol. 12, No. 4, May. 1994, p. 685-697.

[6] S. Haykin: *Adaptive filter theory.* Prentice Hall, 1991.

[7] J. G. Proakis: *Digital communications.* J. Wiley and Sons, 1989.

[8] P. Rapajic, B. Vucetic: *A linear adaptive fractionally spaced single user receiver for asynchronous CDMA systems.* "Proc. IEEE International Symposium on Information Theory", San Antonio, Texas, USA, Jan. 17-22, 1993, p. 45.

Predrag B. Rapajic, Branka S. Vucetic: **Linear Adaptive Transmitter-Receiver Structures for Asynchronous CDMA Systems**

ETT, Vol. 6 - No. 1 January - February 1995, p. 21 - 27

Decorrelators for Multi-Sensor Systems in CDMA Networks (1)

Srinivas Kandala, Elvino S. Sousa, Subbarayan Pasupathy
Department of Electrical and Computer Engineering
University of Toronto, Toronto, M5S 1A4, Canada

Abstract. In this paper we consider a multi-sensor detection problem in both additive white Gaussian noise (AWGN) and fading channels with the users using the channel based on a code division multiple access (CDMA) scheme. Several multi-sensor detectors that have been studied previously do offer good performance; however, these detectors require the knowledge of the signal energies and these have to be estimated. Such an estimation might not be feasible in fading and time-varying channels. We show how the linear optimal detector can then be simplified to obtain a decorrelating detector which does not require the knowledge of the users' signals. We show that this decorrelating detector performs almost as well as the linear optimal detector in an AWGN channel. We further investigate its performance in single-path and frequency-selective slowly fading channels. In a slowly fading channel when there is multi-user interference, the conventional detector reaches a saturation point beyond which no improvement in performance can be obtained. We show that the performance of the decorrelating detector does not depend on the other users' energies and hence on the other users' fading characteristics. We further show that a decorrelating detector can be used to obtain a Rake type of receiver in frequency-selective fading channels.

1. INTRODUCTION

Multi-user multi-sensor detectors have been examined for additive white Gaussian noise (AWGN) channels in [1, 2] based on the principles of multi-user detection and diversity. In systems like cellular networks and Personal Communication Networks (PCN), the performance can be improved without much increase in complexity by using the above principles. This improvement is based on tracking of the signal by more than one base station (sensor) [3, 4, 5], computing the sufficient statistic at each base station, and then sending the sufficient statistic to the switch where a decision is made on the combined statistics (Fig. 1). In the detectors studied in [1, 2], the combining is performed by using the maximal-ratio combing rule. A maximal-ratio combining receiver requires the values of the energies so that the received signals can be combined efficiently. This means that the energies of the signals from each user have to be estimated. While some sort of estimation is typically done in cellular networks to make sure that the signal does not fade below a certain level, it might not be easy to obtain accurate estimates even when they do not vary rapidly. The situation in rapidly fading channels is even worse.

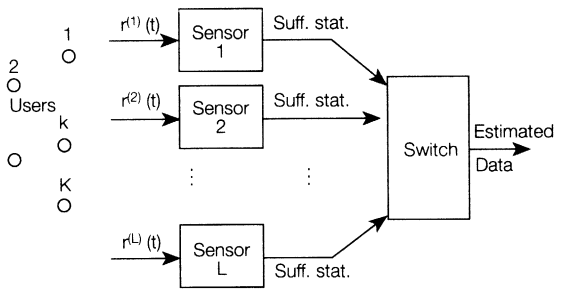

Fig. 1 - The multi-sensor system; suff. stat. = sufficient statistics.

In section 2, we develop and study the performance of a decorrelator detector for a single sensor in AWGN channels (first described in [6, 7, 8] and also studied in [9, 10]) which does not require knowledge of the energies of the signals. In section 3, we extend the detector described in section 2 to multiple sensors.

In a multi-path fading channel and a multi-user environment, the performance of a matched filter detector (also referred to as conventional detector) cannot be improved beyond a certain point irrespective of the energies of the user signals. We are thus motivated to study the decorrelator in single-path Rayleigh fading channels for both the cases of a single sensor as well as multiple sensors in sec-

(1) This research was supported by a grant from the Information Technology Research Centre, a Centre of Excellence, funded by the province of Ontario, Canada.

tion 4. Then, based on the observations made in section 4, we suggest a Rake type receiver for the multi-path Rayleigh fading channels. Section 5 concludes the paper.

2. DECORRELATOR FOR A SINGLE SENSOR

When multiple copies of a signal are available, it makes sense to combine them to increase the signal to noise ratio (*SNR*) and hence decrease the error probability. However, even for a single user detector, there are various ways of combining the signal. While the maximal ratio combining rule gives the optimum performance, it may be preferable to use other types of combining due to the dependence of the optimal detectors on the signal strengths. One of the combining schemes that does not require knowledge of the signal energies is the equal-gain combining (EGC) scheme. When all the signals have almost equal energy (for non-fading channels), the performance of this detector will be close to that of maximal-ratio combining. Unfortunately, equality of energies can not always be assured and there will be deterioration in performance relative to the maximal ratio scheme. This motivates us to develop an EGC-like scheme, but with better performance and where the estimation of energies can be avoided.

In [1, 2] three different detectors for multi-sensor systems have been studied: conventional, decision-based, and linear. A conventional receiver, for a single sensor, does not use the estimates of the energies; hence it is the simplest to implement. However, the performance of a conventional receiver is very poor even when the maximal-combining rule is used. In a decision-based detector, we estimate the interference and subtract it from the received signal (at the output of the matched filter). To make a reasonable estimate of the interference, we need to have at least some approximations of the signal strengths. Hence the situation does not improve much even if we were to use an equal gain combining rule. An optimal (in the MMSE sense) linear detector too requires the knowledge of signal energies [1, 2]. However, with simple changes to the MMSE detector, we will now show how one can obtain a detector which does not depend on the estimation of the users' signal energies.

2.1. *System model*

Suppose there are K users on the channel with one sensor (denote it by l) tracking the signals. The baseband version of the received signal at the front end of this l-th sensor (receiver) is

$$r^{(l)}(t) = S^{(l)}(t; \boldsymbol{b}, C^{(l)}) + n^{(l)}(t) \qquad -\infty \le t \le \infty \qquad (1)$$

where

$$S^{(l)}\left(t;\boldsymbol{b},C^{(l)}\right) = \sum_{i=-M}^{M}\sum_{k=1}^{K} b_k(i)\,c_k^{(l)}(i)\,s_k\left(t - iT - \tau_k^{(l)}\right)$$

and $n^{(l)}(t)$ is a complex white Gaussian noise process with two-sided power spectral density equal to σ_l^2, T is the symbol interval, $s_k(t)$ is the complex representation of the k-th user's signature sequence, $c_k^{(l)}(i)$ is the channel attenuation, and $b_k(i)$ is the data symbol associated with the k-th user during the i-th symbol interval. We assume that $s_k(t)$ is zero for $t \notin [0, T]$ and has unit energy, $\tau_k^{(l)}$ is the delay (symbol epoch) associated with the k-th user (without loss of generality, we assume $0 \le \tau_k^{(l)} < T$), and $NT = (2M + 1)\,T$ is the observation interval. We let $\boldsymbol{b} = [\boldsymbol{b}^T(-M), \ldots, \boldsymbol{b}^T(0), \ldots \boldsymbol{b}^T(M)]^T$, where $\boldsymbol{b}(i) = [b_1(i), \ldots, b_K(i)]^T$ and $\boldsymbol{b}(-M-1) = \boldsymbol{b}(M+1) = 0$ where T denotes the matrix transpose.

Let $\boldsymbol{y}^{(l)} = [\boldsymbol{y}^{(l)T}(-M) \ldots \boldsymbol{y}^{(l)T}(M)]^T$, with $\boldsymbol{y}^{(l)T}(i)$ being a vector of outputs of the bank of matched filters, each matched to the respective signature sequence $s_k(t - iT - \tau_k^{(l)})$ and sampled at $iT + T + \tau_k$. Then,

$$\boldsymbol{y}^{(l)} = \mathcal{R}^{(l)}\,C^{(l)}\,\boldsymbol{b} + \boldsymbol{n}^{(l)} \qquad (2)$$

where

$$\mathcal{R}^{(l)} = \begin{bmatrix} \boldsymbol{R}^{(l)}(0) & \boldsymbol{R}^{(l)}(-1) & \boldsymbol{0} & \cdots & \boldsymbol{0} \\ \boldsymbol{R}^{(l)}(1) & \boldsymbol{R}^{(l)}(0) & \boldsymbol{R}^{(l)}(-1) & & \vdots \\ \boldsymbol{0} & \boldsymbol{R}^{(l)}(1) & \boldsymbol{R}^{(l)}(0) & \ddots & \boldsymbol{0} \\ \vdots & & \ddots & \ddots & \boldsymbol{R}^{(l)}(1) \\ \boldsymbol{0} & \cdots & \boldsymbol{0} & \boldsymbol{R}^{(l)}(1) & \boldsymbol{R}^{(l)}(0) \end{bmatrix}$$

$C^{(l)}$ is the channel attenuation matrix given by diag $([\boldsymbol{C}^{(l)}(-M), \ldots, \boldsymbol{C}^{(l)}(M)])$, with $\boldsymbol{C}^{(l)}(i) = \text{diag}\,([c_1^{(l)}(i), \ldots, c_K^{(l)}(i)])$ and $\boldsymbol{n}^{(l)}$ is the corresponding noise vector due to the additive white Gaussian noise whose covariance matrix is $\sigma_l^2\,\mathcal{R}^{(l)}$. The (k, j)-th element of the cross-correlation matrix of the signals at the l-th sensor, $\boldsymbol{R}^{(l)}(i)$, is given by

$$R_{kj}^{(l)}(i) = \int_{-\infty}^{\infty} s_k\left(t - \tau_k^{(l)}\right) s_j^*\left(t + iT - \tau_j^1\right) \mathrm{d}t = \begin{cases} 0 & \text{if } |i| > 1 \\ R_{jk}^{(l)^*}(-i) & \text{if } i = 0, \pm 1 \end{cases} \qquad (3)$$

where * denotes the complex conjugate. The optimum linear transformation $G^{(l)}$ in the MMSE sense (or the operation to be performed by a linear detector) is then given by [1, 2],

$$G^{(l)} = \mathcal{H}^{(l)H}\left(\mathcal{H}^{(l)}\,\mathcal{H}^{(l)H} + \sigma_l^2\,\mathcal{R}^{(l)}\right)^{-1} \qquad (4)$$

where H denotes the Hermitian transpose of a matrix, and $\mathcal{H}^{(l)} = \mathcal{R}^{(l)}\,C^{(l)}$. Here we assume that the matrix ex-

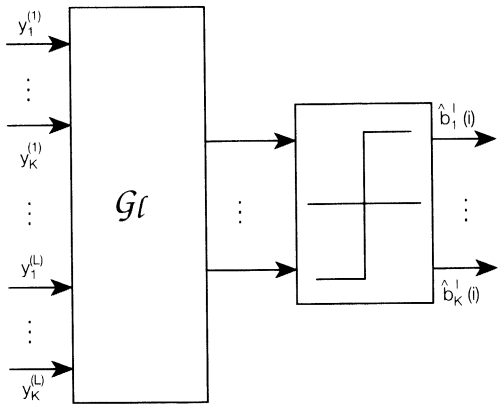

Fig. 2 - Linear detector for synchronous systems.

ists ($\mathcal{R}^{(l)}$ being positive definite is a sufficient condition to assure this). If the inverse does not exist, the following argument still follows with the regular matrix inverse being replaced by the generalized inverse matrix. The structure of this detector is given in Fig. 2.

Now suppose that the signals are being transmitted in a high *SNR* environment where the amount of Gaussian noise is insignificant. In other words, we let $\sigma_l \to 0$. Then, $\mathcal{G}^{(l)} \to \mathcal{G}_l^{(l)}$ where

$$\mathcal{G}_l^{(l)} = \mathcal{H}^{(l)H} (\mathcal{H}^{(l)} \mathcal{H}^{(l)H})^{-1} = \mathcal{H}^{(l)-1} = C^{(l)-1} \mathcal{R}^{(l)-1} \tag{5}$$

The transformed input vector to the decision making device is then (for a single sensor, l, Fig. 2)

$$\begin{aligned} \hat{\boldsymbol{b}} &= \mathcal{G}_l \boldsymbol{y}^{(l)} = C^{(l)-1} \mathcal{R}^{(l)-1} (\mathcal{R}^{(l)} C^{(l)} \boldsymbol{b} + \boldsymbol{n}^{(l)}) \\ &= \boldsymbol{b} + C^{(l)-1} \mathcal{R}^{(l)-1} \boldsymbol{n}^{(l)} \end{aligned} \tag{6}$$

It can be seen from (6) that with this linear transformation the desired signal is free of other users' signals. However, the additive noise term is now dependent on the signaling waveform (as well as the channel attenuation) and is not white. The covariance matrix of the noise term is

$$\begin{aligned} Q^l &= \boldsymbol{E} [C^{(l)-1} \mathcal{R}^{(l)-1} \boldsymbol{n}^{(l)} \boldsymbol{n}^{(l)H} (C^{(l)-1} \mathcal{R}^{-1})^H] \\ &= \sigma_l^2 C^{(l)-1} (\mathcal{R}^{(l)-1})^H (C^{(l)-1})^* \end{aligned} \tag{7}$$

where $\boldsymbol{E}$ denotes expectation. The error probability for this detector for $b_k(i)$ is then

$$P_{d,k}(\text{error}) = \frac{1}{2} \text{erfc} \left(\sqrt{\frac{\left| c_k^{(l)}(i) \right|^2}{2\sigma_l^2 \left(\mathcal{D}^{(l)} \right)_{k,k}}} \right) \tag{8}$$

where $(\mathcal{D}^{(l)})_{k,k}$ is the (k, k-th element of $\mathcal{D}^{(l)} = \mathcal{R}^{(l)-1}$.

From (4) we note that the above detector requires knowledge of the received signal energies. Now, observe the argument of the error function in (8). If we interpret the numerator as the signal strength and the denominator as the variance of the noise $\mathcal{R}^{(l)-1} \boldsymbol{n}^{(l)}$, then we see that we can interpret the linear transformation used in this detector as just $\mathcal{R}^{(l)-1}$ *along with the phase information of the signal.* This implies that we would have obtained the same performance by using the transformation $\mathcal{G}_d^{(l)} = C_p^{(l)*} \mathcal{R}^{(l)-1}$, where $C_p^{(l)}$ is a diagonal matrix each of whose elements is the corresponding element of $C^{(l)}$ divided by its modulus. Note that the transformation $\mathcal{G}_d^{(l)}$ does not require the energies of the users to be known. This detector can be interpreted as a *decorrelator* and has been described in [7, 8] where it has been shown to achieve the same asymptotic user efficiency and near-far resistance as the optimal detector. Even though the output of the decorrelator is free of the other users' energies, the noise terms are correlated and it performs poorly in comparison with the single user detector for the same *SNR*. The above derivation is for an asynchronous system, and a similar detector can be developed for synchronous systems. To evaluate the performance of this detector, we compare it with the MMSE detector and the single user detector (a matched filter detector for detecting a signal transmitted without any interference).

Consider the expression for the error probability of a single user detector which is given below [11]

$$P_1(1) = \frac{1}{2} \text{erfc} \left(\sqrt{\frac{E_1}{2\sigma^2}} \right) \tag{9}$$

where E_1 is the energy of the signal. Comparing (8) with (9), we see that the loss in *SNR* for using the decorrelator when compared to a single user receiver is given by 10 log $(\mathcal{D}^{(l)})_{k,k}$. We compare the decorrelator-detector with the MMSE detector [2], using the following numerical example. Consider a synchronous system having two users with cross-correlation ρ between the two users' signals. Fig. 3, shows the average error probability of user 1, for the MMSE detector, decorrelator, and the single user detector, as a function of its *SNR*, *SNR*1, with the second user's *SNR*, *SNR*2 = 8 dB, and $\rho = 0.5$. This situation can be thought of as a high *SNR* environment. It can be seen that the performance of both

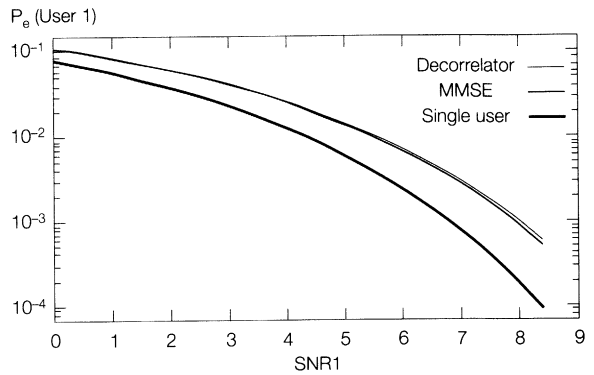

Fig. 3 - Error probability of the user 1 versus *SNR*1 for *SNR*2 = 8 dB, and $\rho = 0.5$.

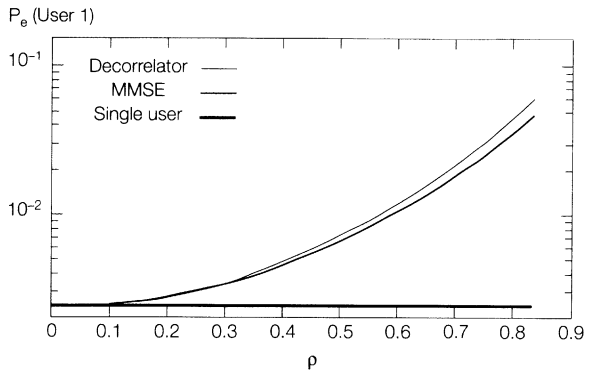

Fig. 4 - Error probability of the user 1 versus ρ for $SNR1$ = 6 dB, and $SNR2$ = 8 dB.

MMSE detector and the decorrelator are almost identical (both are quite inferior compared to the single user detector - but this is to be expected with such a high correlation between the signature sequences). In Fig. 4, the error probability is plotted as a function of ρ for $SNR1$ = 6 dB and $SNR2$ = 8 dB. Again we see that the difference in performance is almost negligible. To study the performance in a low SNR environment, we plot in Fig. 5, the average error probability of user 1 as a function of $SNR1$ for $SNR2$ = 4 dB and ρ = 0.5. We see that the performance of the decorrelator is still close to MMSE even in a low SNR environment. In Fig. 6 we set both $SNR1$ and $SNR2$ to 4 dB and plot the error rate as a function of ρ. It can be seen that as ρ is increased, the performance of the decorrelator becomes worse compared to that of the MMSE detector. Even though the difference in this case is very small, in certain other situations (large number of users) the difference could be quite significant, as we shall see later.

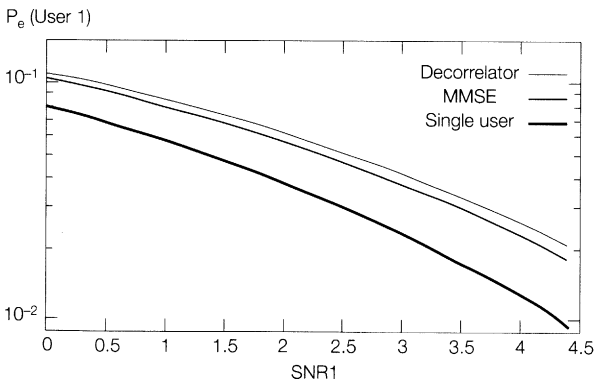

Fig. 5 - Error probability of the user 1 versus $SNR1$ for $SNR2$ = 4 dB, and ρ = 0.5.

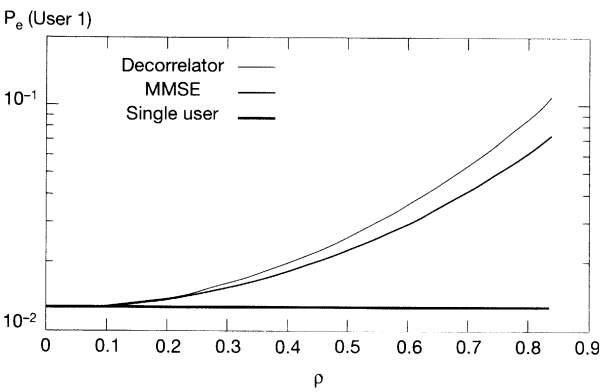

Fig. 6 - Error probability of the user 1 versus $SNR1$ for $SNR1$ = 4 dB, and $SNR2$ = 4 dB.

3. DECORRELATORS FOR MULTI-SENSOR DETECTORS

In this section, we extend the concept of the decorrelator to multi-sensor detectors. Towards this end, we assume that there are K users and L sensors indexed by integers. Let K_l be the number of users tracked by the l-th sensor and the set B_l be the set containing the users tracked by it. As before, the vector $\boldsymbol{y}^{(l)}$, comprising of the outputs of the matched filters for the signals to be detected at that sensor, is given by (2). For the conventional maximum-likelihood ratio combining, the matched filter outputs are combined and then passed through a linear filter. Here, however, we first decorrelate the outputs of the matched filter and then combine, as shown in Fig. 7. The corresponding transformation is $\mathcal{G}_d^{(l)} = \mathcal{C}_p^{(l)*} (\mathcal{R}^{(l)})^{-1}$. Now, when some of the users' signals are not tracked at any given sensor, then the energies as well as the corresponding outputs of the matched filter of these untracked signals can be assumed to be zero. We can exploit this fact by setting the corresponding rows and columns in $(\mathcal{R}^{(l)})^{-1}$ to zero. This will reduce the dimension of the matrix that has to be inverted from NK to NK_l. Denoting such a modified transformation by $\mathcal{G}^{(l)}$, the output vector after performing such a transformation is given by

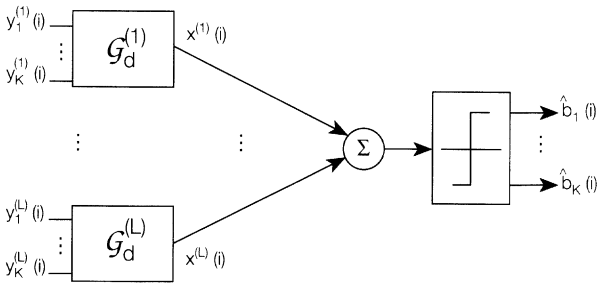

Fig. 7 - Detector using equal gain combining ratio with the decorrelators in eq. (10).

$$x^{(l)} = \mathcal{G}^{(l)} \boldsymbol{y} = \mathcal{C}_a^{(l)} \boldsymbol{b} + \mathcal{G}^{(l)} \boldsymbol{n}^{(l)} \tag{10}$$

where $\mathcal{C}_a^{(l)}$ is the amplitude matrix of the channel. The covariance matrix of the noise term is given by

$$\begin{aligned} Q^{(l)} &= \boldsymbol{E}\left[\mathcal{G}^{(l)} \boldsymbol{n}^{(l)} (\boldsymbol{n}^{(l)})^H (\mathcal{G}^{(l)})^H\right] \\ &= \sigma^2 \mathcal{G}^{(l)} \mathcal{R}^{(l)} (\mathcal{G}^{(l)})^H \end{aligned} \tag{11}$$

Note that, the terms corresponding to $k \notin B_l$ in $Q^{(l)}$ in (11) would be zero. Then the vector of decision variables is ([1])

$$\hat{\boldsymbol{b}} = \operatorname{sgn}\left\{\sum_{l=1}^{L} \boldsymbol{x}^{(l)}\right\} = \left\{\sum_{l=1}^{L}\left[C_a^{(l)}\boldsymbol{b} + \mathcal{G}^{(l)}\boldsymbol{n}^{(l)}\right]\right\} \tag{12}$$

Note that the right hand side of (12) suggests that all the signals of a given user are added directly, as desired. However, more noise terms of noise are involved and are correlated with each other, as was observed for the single sensor case. The average error probability for the k-th user is

$$P_{d,k}(\text{error}) = \frac{1}{2}\operatorname{erfc}\left(\frac{\sum_{l=1}^{L}\left|c_k^{(l)}(i)\right|}{\sigma_l\sqrt{2\sum_{l=1}^{L}\left(Q^{(l)}\right)_{k,k}}}\right) \tag{13}$$

where $(Q^{(l)})_{k,k}$ is the (k, k)-th element of $Q^{(l)}$. Note that the performance of this detector does not depend on the other users' energy at any sensor. Thus it is easier to design a decorrelator based system as compared to a system based on other types of multi-sensor multi-user detectors. However, as in the case of single-sensor, the noise is colored due to the interference of the other signals.

Even though, our discussion has been entirely for asynchronous systems, the detector can be easily modified (with lesser complexity) for synchronous systems in an obvious manner.

3.1. *Numerical results*

To evaluate the decorrelator performance we consider a few numerical examples. First, we consider the 3 user, 2 sensor synchronous system. We shall label the users 1, 2, and 3, and label the sensors as 1 and 2. The first two users are tracked by sensor 1, whereas the last two are tracked by sensor 2 (i.e., all the users are not tracked by all the sensors). Let

$$\boldsymbol{R}^{(1)}(0) = R^{(2)}(0) = \begin{bmatrix} 1 & \rho_1 & 0 \\ \rho_1 & 1 & \rho_2 \\ 0 & \rho_2 & 1 \end{bmatrix}$$

$$\boldsymbol{c}_a^{(1)}(i) = \begin{bmatrix} c_1^{(1)} & 0 & 0 \\ 0 & c_2^{(1)} & 0 \\ 0 & 0 & 0 \end{bmatrix} \quad \boldsymbol{c}_a^{(2)}(i) = \begin{bmatrix} 0 & 0 & 0 \\ 0 & c_2^{(2)} & 0 \\ 0 & 0 & c_3^{(2)} \end{bmatrix}$$

([1]) We assume that the signum function (sgn) operates only on the real part.

and σ_1^2 and σ_2^2 be the two-sided power spectral densities of the noise at the two sensors which we assume to be equal. We are interested in the performance of the detector with respect to user 2. Let $|c_2^{(1)}|^2$ and $|c_2^{(2)}|^2$, the energies of the second user at the two sensors, be equal. Hence, the *SNR* of the second user is the same at both sensors which we denote by *SNR*21. Further, let us assume that $c_2^{(1)} = c_3^{(2)}$ and $\rho_1 = \rho_2 = \rho$. We denote the *SNR* of user 1 at sensor 1 by *SNR*1 and that of user 3 at sensor 2 by *SNR*2. For simplicity we consider only the case when *SNR*1 = *SNR*2.

In Fig. 8 and Fig. 9, we plot the average error probabilities of the decorrelator, MMSE detector, and the single user detector, for user 2, as a function of *SNR*21, for $\rho = 0.5$ and $\rho = 0.7$, with *SNR*1 = 10 dB. It can be seen that the performance of the decorrelator is very close to that of the MMSE detector even though we are using high values of ρ. This is due to the fact that the system is operating at a high *SNR*. This can also be seen in Fig. 10, where we show a similar plot for *SNR*21 = 4 dB. The

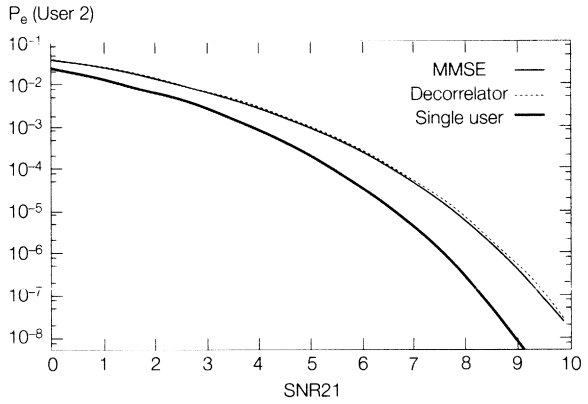

Fig. 8 - Average error probability for three users versus *SNR*21 for *SNR*1 = 10 dB, and $\rho = 0.5$.

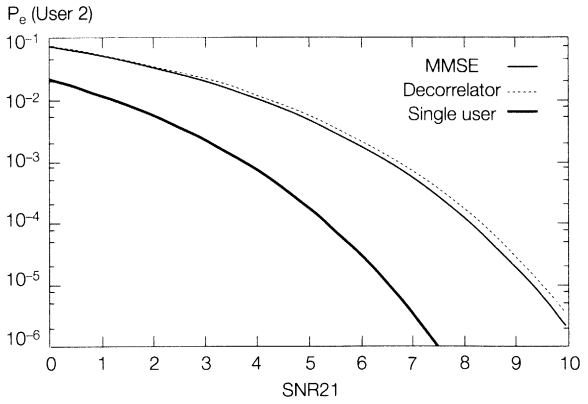

Fig. 9 - Average error probability for three users versus *SNR*21 for *SNR*1 = 10 dB, and $\rho = 0.7$.

MMSE detector does not provide a great advantage in this situation. To see the performance in low *SNR* we plot the average error probability of the second user as a function of SNR21 for $\rho = 0.5$ and $\rho = 0.7$, with *SNR*1 = 5 dB, in Fig. 11 and Fig. 12 respectively, and as a func-

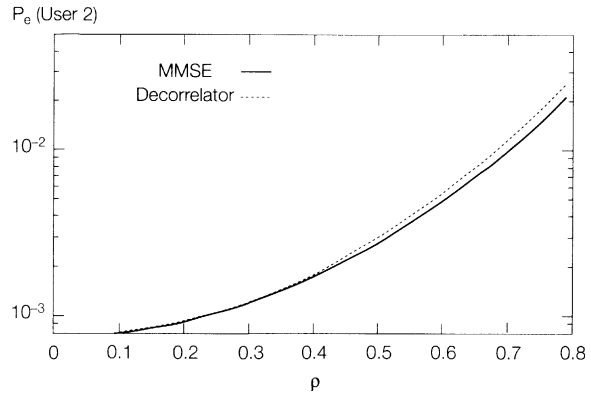

Fig. 10 - Average error probability for three users versus ρ for $SNR1$ = 10 dB, and $SNR21$ = 4 dB.

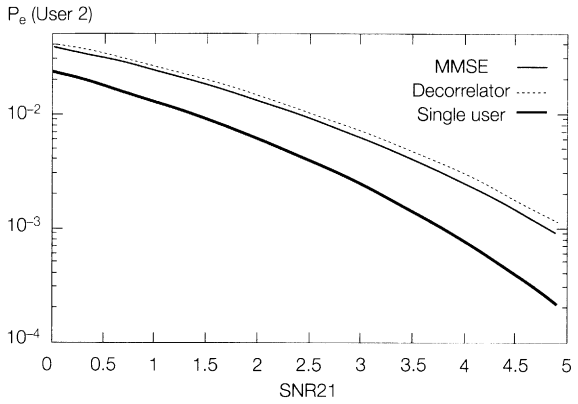

Fig. 11 - Average error probability for three users versus $SNR21$ for $SNR1$ = 5 dB, and ρ = 0.3.

tion of r for $SNR1$ = 5 dB and $SNR21$ = 2 dB in Fig. 13. As the value of ρ is increased, the performance of the decorrelator becomes slightly worse. Note that the MMSE detector performs better than the decorrelator. Even though its performance depends on the other users' signal strengths, an MMSE detector performs better than a decorrelator as it is the optimal linear detector.

As a second example, we consider the 6 user synchronous system with 2 sensors tracking them. We use the sequences described in [12, Table 5.10] as the signature sequences. These sequences are not optimized in any sense and have reasonably high correlations. The correlation matrix is

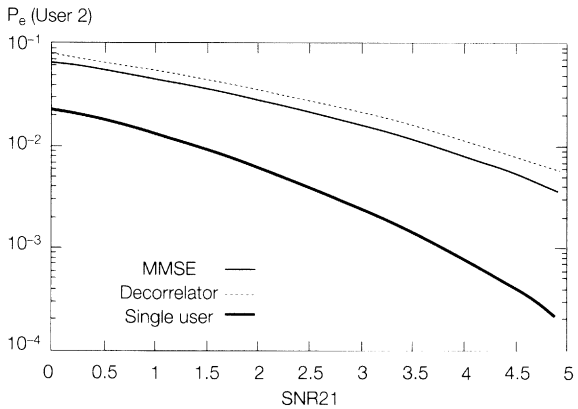

Fig. 12 - Average error probability for three users versus $SNR21$ for $SNR1$ = 5 dB, and ρ = 0.5.

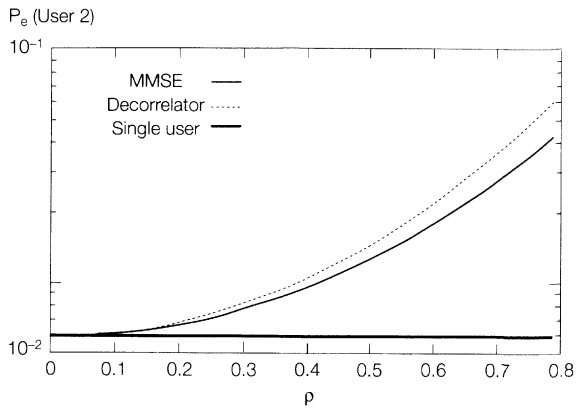

Fig. 13 - Average error probability for three users versus ρ for $SNR1$ = 5 dB, and $SNR21$ = 2 dB.

$$\boldsymbol{R}^{(l)}(0) = \frac{1}{31}\begin{bmatrix} 31 & -9 & -9 & -9 & -9 & 11 \\ -9 & 31 & -9 & 11 & -9 & -9 \\ -9 & -9 & 31 & -9 & 11 & -9 \\ -9 & 11 & -9 & 31 & -9 & -9 \\ -9 & -9 & 11 & -9 & 31 & -9 \\ 11 & -9 & -9 & -9 & -9 & 31 \end{bmatrix} \tag{14}$$

In Table 1, we consider the case when all the users have equal SNR's and are tracked by both sensors. We tabulate the error probabilities P_e for the MMSE detector and the decorrelator with and without diversity. Also tabulated is the effective signal to interference ratio (SIR) that is required to obtain the same error probability if there was no interference; i.e., if the error probability for a given user, utilizing a given detector, is P_e, then we define SIR as the effective SNR of that user, given implicitly by the following equation

$$P_e = \frac{1}{2}\operatorname{erfc}\left(\sqrt{\mathrm{SIR}}\right) \tag{15}$$

SIR is analogous to the signal to interference ratio that is commonly used in spread spectrum systems [12]. Also tabulated is the average signal to interference ratio (ASIR), which we define for a given user as

$$\mathrm{ASIR} = \frac{\{E[d(i)]\}^2}{\mathrm{var}[d(i)]} \tag{16}$$

where var denotes the variance and $d(i)$ is the variable on which the decision is made for that user. For a single user system, in an AWGN environment, the ASIR would be the same as the SNR. Thus the ASIR can be thought of as a generalization to a multi-user environ-

Table 1 - *Error probabilities and the corresponding SIRs for the MMSE detector and the decorrelator for 6 users with equal energies.*

	MMSE				Decorrelator			
SNR	No Diversity		Diversity		No Diversity		Diversity	
	P_e	ASIR	P_e	ASIR	P_e	ASIR	P_e	ASIR
4 dB	3.50×10^{-2}	2.15	6.53×10^{-3}	4.88	4.77×10^{-2}	1.43	9.21×10^{-3}	4.44
5 dB	2.22×10^{-2}	3.05	2.88×10^{-3}	5.81	3.07×10^{-2}	2.43	4.08×10^{-3}	5.44
6 dB	1.28×10^{-2}	3.96	1.05×10^{-3}	6.75	1.79×10^{-2}	3.43	1.50×10^{-3}	6.44
8 dB	2.91×10^{-3}	5.80	6.52×10^{-5}	8.65	4.13×10^{-3}	5.43	9.35×10^{-5}	8.44
10 dB	3.06×10^{-4}	7.69	8.94×10^{-7}	10.57	4.41×10^{-4}	7.43	1.28×10^{-6}	10.44

ment. Note that the numerator would be the same as the total signal energy as we have assumed equi-probable symbols. Hence the ASIR can be interpreted as the ratio of the signal energy of the user of interest to the sum of the variance of the additive white noise and the interference power from all the interfering users at the input of the threshold device. This would be a true measure of the interference if it could be modelled as Gaussian [13]. We note that SIR and ASIR would be identical for a decorrelator since as the total interference is still a Gaussian variable. Also the correlation matrix for this system suggests that every user will have the same amount of interference. From the table, it can be seen that in lower *SNR* environments, the decorrelator suffers a loss of about 0.7 dB with respect to the MMSE detector. As the *SNR* of each of the users is increased, the decorrelator's performance tends to improve and becomes much closer to that of the MMSE detector. Further, it can be seen that the increase in ASIR for the decorrelator is identical to that of the actual increase in the *SNR* in the user's signal. This is to be expected as the decorrelator's performance does not depend on the other user's energies and since the background noise would be the same in all situations, hence the ASIR would be increased by the same amount as the *SNR*. Finally, we note that by using diversity, we always obtain a gain ([1]) of 3 dB, which is the maximum gain that can be obtained by using second order diversity which is not the case for MMSE detector.

Next, we consider the same system, but with users neither having identical energies at both the sensors, nor equal energies at a given sensor. The energies of each of the users at each sensor are tabulated in Table 2. This table illustrates how much performance is lost when a decorrelator is being used. Also tabulated in this table are the ASIR's for both the MMSE detector and the decorrelator with and without diversity at both

Table 2 - *Error probabilities and the corresponding SIRs for the MMSE detector and the decorrelator for 6 users with unequal energies.*

User	*SNR* @1	*SNR* @2	ASIR @ 1		ASIR @ 2		Diversity	
			MMSE	Decor.	MMSE	Decor.	MMSE	Decor.
1	4 dB	8 dB	2.04	1.43	6.22	5.43	7.69	6.67
2	6 dB	2 dB	4.17	3.43	0.09	– 0.57	5.57	4.67
3	2 dB	6 dB	0.03	– 0.57	4.14	3.43	5.63	4.67
4	8 dB	4 dB	6.16	5.43	2.09	1.43	7.58	6.67
5	6 dB	2 dB	4.03	3.43	0.14	– 0.57	5.51	4.67
6	4 dB	4 dB	2.04	1.43	2.22	1.43	5.00	4.44

([1]) The maximum possible gain is 3 dB since the users have the same signal strength at both the sensors.

the sensors. It can be seen that without diversity, the loss in performance for using a decorrelator instead of an MMSE detector is close to 0.7 dB, while with diversity it is about 1 dB. It should be noted that as the number of users increase, this loss will be more and more significant as can be seen by comparing with the 3 user example. However, if all the users are transmitting with reasonably high energy, then a decorrelator can still be used.

In the final example, we will study the case when there are 10 users and 2 sensors in order to understand the behaviour when all users are not tracked by all the sensors. Again, the signature sequence is of length 31. The first six sequences are the auto-optimal m-sequences given in [14, Fig. A1], while the other four have the least side-lobe energy phase with the best odd auto-correlation parameters from [14, Fig. B1]. The correlation matrix for a synchronous system with these sequences is

$$\boldsymbol{R}^{(l)}(0) = \frac{1}{31}\begin{bmatrix} 31 & -1 & -1 & 7 & -1 & -1 & -1 & 7 & 3 & -1 \\ -1 & 31 & -9 & -9 & 7 & -1 & -1 & -1 & -1 & 3 \\ -1 & -9 & 31 & -1 & -1 & -5 & -1 & -1 & 7 & -1 \\ 7 & -9 & -1 & 31 & 7 & 7 & -9 & 7 & -1 & -1 \\ -1 & 7 & -1 & 7 & 31 & 7 & -9 & -1 & -1 & -1 \\ -1 & -1 & -5 & 7 & 7 & 31 & -1 & -9 & -9 & 7 \\ -1 & -1 & -1 & -9 & -9 & -1 & 31 & 7 & 3 & -1 \\ 7 & -1 & -1 & 7 & -1 & -9 & 7 & 31 & 7 & -5 \\ 3 & -1 & 7 & -1 & -1 & -9 & 3 & 7 & 31 & -1 \\ -1 & 3 & -1 & -1 & -1 & 7 & -1 & -5 & -1 & 31 \end{bmatrix} \tag{17}$$

The *SNR*'s of the users at each sensor are given in Table 3. The first seven users are tracked by sensor 1 and the latter seven by sensor 2. Also tabulated are the ASIR's for both the MMSE detector as well as the decorrelator with and without diversity. Several observations are in order here. For the users having all their signal energy at one sensor (users 1, 2 and 3 at sensor 1 and users 8, 9 and 10 at sensor 2), the performance of the decorrelator is the same whether or not diversity is utilized. This observation can also be made from (13), where the denominator in the argument of the complementary error function would have only one term due to the fact that, we define the transformation $\mathcal{G}^{(l)}$ in such a way so that only the rows (and columns) for the users that are tracked are non-zero. However, for the MMSE detector, the performance still improves (albeit not by a great amount) due to the usage of the information about

Table 3 - *Error probabilities and the corresponding SIRs for the MMSE detector and the decorrelator for 10 users with unequal energies.*

User	*SNR* @1	*SNR* @2	ASIR Without Diversity				ASIR With Diversity	
			Sensor 1		Sensor 2			
			MMSE	Decor.	MMSE	Decorr.	MMSE	Decor.
1	8 dB	– 100 dB	7.73 dB	7.69 dB	–	–	7.80 dB	7.69 dB
2	8 dB	– 100 dB	6.86 dB	6.63 dB	–	–	7.14 dB	6.63 dB
3	8 dB	– 100 dB	7.46 dB	7.37 dB	–	–	7.53 dB	7.37 dB
4	8 dB	4 dB	6.65 dB	6.41 dB	2.83 dB	2.57 dB	8.17 dB	7.73 dB
5	2 dB	3 dB	1.03 dB	0.89 dB	2.38 dB	2.27 dB	4.73 dB	4.60 dB
6	3 dB	2 dB	2.52 dB	2.44 dB	0.63 dB	0.39 dB	4.67 dB	4.41 dB
7	4 dB	8 dB	3.39 dB	3.30 dB	7.00 dB	6.71 dB	8.63 dB	8.23 dB
8	– 100 dB	8 dB	–	–	6.83 dB	6.50 dB	7.27 dB	6.51 dB
9	– 100 dB	8 dB	–	–	7.57 dB	7.48 dB	7.68 dB	7.47 dB
10	– 100 dB	8 dB	–	–	7.74 dB	7.66 dB	7.82 dB	7.66 dB

the users that are mutually tracked by both sensors. The decorrelator's performance is quite comparable to that of the MMSE detector in the example as most of the users are operating with a high *SNR*.

4. RAYLEIGH FADING CHANNELS

In this section we extend the ideas regarding the decorrelator to the case of a CDMA network operating in a Rayleigh fading channel. It has been shown in [15, 16] that CDMA systems with conventional receivers operating in the presence of multi-path fading and multi-user interference reach a saturation level below which the error probability can not be reduced regardless of the *SNR* level. It has been concluded that the only way to improve performance is to use long sequences as well as some sort of diversity. Also, in many situations there might not be more than one path available at a given sensor. In this section we circumvent this problem by using multi-sensor decorrelators. First we study the performance in a single-path fading channel and then extend the results to channels with multiple paths.

4.1. *Single sensor*

As before, suppose there are K users on the channel with one sensor (denote it by l) tracking the signals. The baseband version of the received signal is the same as given by (1). Since the channel is Rayleigh faded, $c_k^{(l)}(i)$ is now a complex-valued Gaussian random variable [11]. We assume that the amplitude does not vary rapidly enough and would remain fixed within a given symbol interval and that the associated phase is slow enough to be tracked perfectly. We assume that the amplitudes c_k of different users are mutually independent with the real and imaginary components having zero mean and variance $\alpha_k^{(l)2}$. The decorrelator for this system will be $\mathcal{G}^{(l)} = (\mathcal{R}^{(l)})^{-1}$. Performing this transformation (Fig. 7) we obtain

$$\boldsymbol{x}^{(l)} = \mathcal{G}^{(l)}\,\boldsymbol{y}^{(l)} = \mathcal{C}^{(l)}\,\boldsymbol{b} + \mathcal{G}^{(l)}\,\boldsymbol{n}^{(l)} \tag{18}$$

Again, since $\mathcal{C}^{(l)}$ is a diagonal matrix, the only term that has the required information for the detection of $b_k(i)$ is the $((i-1)K+k)$-th term of $\boldsymbol{x}^{(l)}$ which we denote by $x_k^{(l)}(i)$ and write

$$x_k^{(l)}(i) = c_k^{(l)}(i)\,b_k(i) + w_k^{(l)}(i) \tag{19}$$

where $w_k^{(l)}(i)$ is the $((i-1)K+k)$-th term of the noise vector in (18). The covariance matrix of the noise vector is given by

$$Q^{(l)} = \boldsymbol{E}\left[\mathcal{G}^{(l)}\,\boldsymbol{n}^{(l)}\,(\boldsymbol{n}^{(l)})^*\,(\mathcal{G}^{(l)})^*\right] = \sigma_l^2\,(\mathcal{R}^{(l)-1})^* \tag{20}$$

The only unknown variable for the detection of $b_k(i)$ is $c_k^{(l)}(i)$. However, we have already assumed that the phase variations are slow enough so that they can be estimated perfectly. Then multiplying $x_k^{(l)}(i)$ by $c_k^{(l)*}(i)/\left|c_k^{(l)}(i)\right|$, we obtain

$$z_k^{(l)}(i) = \left|c_k^{(l)}(i)\right| b_k(i) + \frac{c_k^{(l)^*}(i)}{\left|c_k^{(l)}(i)\right|}\,w_k^{(l)}(i) \tag{21}$$

The additive noise term in the above equation is still Gaussian with the variance given by the $((i-1)K+k, (i-1)K+k)$-th element of $Q^{(l)}$ which we denote by $(Q^{(l)})_{k,i}$. Then, given $\left|c_k^{(l)}(i)\right|$, the error probability for the detection of $b_k(i)$ is given by

$$P_{d,k}\left(\text{error}/\left|c_k^{(l)}(i)\right|\right) = \frac{1}{2}\,\text{erfc}\left(\frac{\left|c_k^{(l)}(i)\right|}{\sigma_l\sqrt{2\left(Q^{(l)}\right)_{k,i}}}\right) \tag{22}$$

Since, $c_k^{(l)}(i)$ is a complex Gaussian random variable the $\left|c_k^{(l)}(i)\right|$ has a Rayleigh distribution. Defining the effective *SNR* of user k as

$$\gamma_k^{(l)} = \frac{\left|c_k^{(l)}(i)\right|^2}{2\sigma_l^2\left(Q^{(l)}\right)_{k,i}} \tag{23}$$

(8) can be rewritten as

$$P_{d,k}\left(\text{error}\left|\gamma_k^{(l)}(i)\right.\right) = \frac{1}{2}\,\text{erfc}\left(\sqrt{\gamma_k^{(l)}}\right) \tag{24}$$

Now, $\gamma_k^{(l)}$ is an exponential random variable [17], with density function

$$p\left(\gamma_k^{(l)}\right) = \left(1/\overline{\gamma_k^{(l)}}\right)\exp\left(-\gamma_k^{(l)}/\overline{\gamma_k^{(l)}}\right) \qquad \gamma_k^{(l)} \geq 0 \tag{25}$$

where $\boldsymbol{E}\left[\gamma_k^{(l)}\right] = \overline{\gamma_k^{(l)}} = \alpha_k^{(l)2}/2\,\sigma_l^2\,(Q^{(l)})_{k,i}$ is the average effective *SNR* of user k. The average error probability for the k-th user is then

$$\begin{aligned} P_{d,k}(\text{error}) &= \int_0^\infty P_{d,k}\left(\text{error}\left|\left|c_k^{(l)}(i)\right|\right.\right) p\left(\gamma_k^{(l)}\right)\mathrm{d}\,\gamma_k^{(l)} \\ &= \frac{1}{2}\left[1 - \sqrt{\frac{\overline{\gamma_k^{(l)}}}{1+\overline{\gamma_k^{(l)}}}}\right] \end{aligned} \tag{26}$$

Now, compare (26) with the error probability of a single user receiver [11]

$$P_s(\text{error}) = \frac{1}{2}\left[1 - \sqrt{\frac{\bar{\gamma}}{1+\bar{\gamma}}}\right] \tag{27}$$

where $\bar{\gamma}$ is the average *SNR* of the user. From the defini-

tion of $\overline{\gamma_k^{(l)}}$, it can be seen that the effect of interference is to directly reduce the *SNR* by the degree of cross-correlations. However, the error probability of the decorrelator in a multi-user environment itself decreases with an increase in the *SNR* of the user. Hence, the decorrelator circumvents the problem that arises with the use of a conventional detector and thus is near-far resistant. Further, if the users are operating in a very high *SNR* environment, then, by using the binomial expansion of $(1+x)^{-1/2}$,

$$P_{d,k}\,(\text{error}) \approx 1/(4\,\overline{\gamma_k^{(l)}}) \tag{28}$$

$$P_s\,(\text{error}) \approx 1/(4\,\bar{\gamma}) \tag{29}$$

This approximation suggests that the error probabilities of both the decorrelator and the single user detector decrease at the same rate and are inversely proportional to the average *SNR*.

To understand the effect of the interference, we consider an example with two users. We assume that the system is synchronous. Consider the following correlation matrix

$$\boldsymbol{R} = \begin{bmatrix} 1 & \rho \\ \rho & 1 \end{bmatrix} \tag{30}$$

Without loss of generality, we study the error probabilities associated in detecting the signal from user 1. Using (20), we see that the covariance matrix of the additive noise at the input of the decision making device is given by

$$\boldsymbol{Q} = \frac{1}{1-|\rho|^2}\begin{bmatrix} 1 & \rho^* \\ \rho^* & 1 \end{bmatrix} \tag{31}$$

The error probability is given by

$$P_{d,1} = \frac{1}{2}\left[1 - \sqrt{\frac{\left(1-|\rho|^2\right)\bar{\gamma}_1}{1+\left(1-|\rho|^2\right)\bar{\gamma}_1}}\right] \tag{32}$$

where γ_1 is the average *SNR* of user 1. In Fig. 14, we plot the average error probability for the single user detector as well as the decorrelator for $\rho = 0.7$ as a function of user 1's *SNR*. From the figure, it can be seen that for the decorrelator, the error probability does decrease with an increase in the *SNR* of user 1 and decreases with the same slope as the single user detector; actually the loss in *SNR* remains constant as was the case for AWGN channels. In Fig. 15, we show a similar plot for the *SNR* of user 1 set to 20 dB. It can be seen that the loss in performance is not very significant for large ρ.

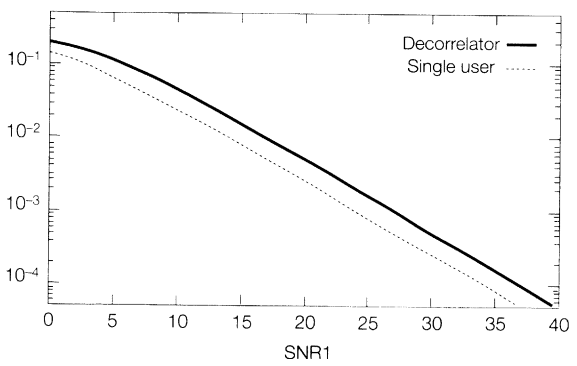

Fig. 14 - Average error probability for two users in a Rayleigh fading channel versus *SNR*1 for $\rho = 0.7$.

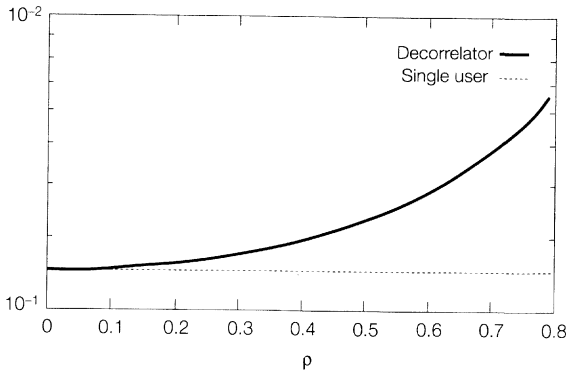

Fig. 15 - Average error probability for two users in a Rayleigh fading channel as a function of ρ for *SNR* = 20 dB.

4.2. *Multiple sensors*

In this section, we study the decorrelator detector for the multiple sensor case. We first assume equal gain combining. As we have done for the AWGN channels, we combine the signals *after* they are decorrelated at each sensor. The decorrelator output $x_k^{(l)}(i)$ given in (19), however, is not free of the random phase. Since the phase information is very important to a phase modulation scheme like BPSK (which we have been considering throughout this paper), and as we assume perfect estimates of the random phase are available, it would be more advantageous to combine them after the random phase has been removed. If it were not so, it would not be possible to remove the random phase after combining the signals, since the random amplitudes are unknown. Thus, we combine $z_k^{(l)}(i)$, given by (21), and then the decision variable is

$$\begin{aligned}\hat{b}_k(i) &= \operatorname{sgn}\left\{\Lambda_k(i)\right\} = \operatorname{sgn}\left\{\sum_{l=1}^{L} z_k^{(l)}(i)\right\} \\ &= \operatorname{sgn}\left\{\sum_{l=1}^{L}\left[\left|c_k^{(l)}(i)\right| b_k(i) + \frac{c_k^{(l)^*}(i)}{\left|c_k^{(l)}(i)\right|} w_k^{(l)}(i)\right]\right\}\end{aligned} \tag{33}$$

Λ_k, for a given set of $\{\,|c_k^{(l)}|\,\}$, is a Gaussian random variable with mean $\sum_{l=1}^{L}|c_k^{(l)}(i)|$ and variance $\sum_{l=1}^{L}(Q^{(l)})_{k,i}$. Hence the error probability for $b_k(i)$ is

$$P_{d,k}\left(\text{error}\,|\,\gamma\right) = \frac{1}{2}\operatorname{erfc}\left(\sqrt{\gamma}\right) \tag{34}$$

where

$$\gamma = \frac{\left\{\sum_{l=1}^{L}\left|c_k^{(l)}(i)\right|\right\}^2}{\sum_{l=1}^{L}\left(Q^{(l)}\right)_{k,k}} \tag{35}$$

To obtain the average error probability we have to average the right hand side of (35). The resulting integral can not be evaluated in closed form. However, observe (19); since $c_k^{(l)}(i)$ can be interpreted as a signal and $x_k^{(l)}(i)$ as its observation variable, it is much easier to estimate it. Once the estimates of $c_k^{(l)}(i)$ are available we can combine $x_k^{(l)}(i)$ using the optimal combining ratio. Then the decision variable would be

$$\begin{aligned}\hat{b}_k(i) &= \operatorname{sgn}\left\{\Lambda_{k,m}(i)\right\} = \operatorname{sgn}\left\{\sum_{l=1}^{L} c_k^{(l)^*}(i)\, x_k^{(l)}(i)\right\} \\ &= \operatorname{sgn}\left\{\sum_{l=1}^{L}\left[\left|c_k^{(l)}(i)\right|^2 b_k(i) + c_k^{(l)}(i)^*\, w_k^{(l)}(i)\right]\right\}\end{aligned} \tag{36}$$

Now, for a known $\{|c_k^{(l)}|\}$, $\Lambda_{k,m}$ is a Gaussian variable with mean $\sum_{l=1}^{L}|c_k^{(l)}(i)|^2$, and variance $\sum_{l=1}^{L}|c_k^{(l)}(i)|^2 (Q^{(l)})_{k,i}$. The error probability is then

$$P_{d,k}(\text{error}) = \int_0^{\infty} P_{d,k}\left(\text{error}\,|\,\lambda = u\right) p_\lambda(u)\,\mathrm{d}u \tag{37}$$

where

$$\lambda = \frac{\sum_{l=1}^{L}\left|c_k^{(l)}(i)\right|^2}{\sum_{l=1}^{L}\left(Q^{(l)}\right)_{k,k}} \tag{38}$$

$p_\lambda(\cdot)$ is the probability density function of λ. Now, since $|c_k^{(l)}(i)|$ are Rayleigh, the characteristic function of λ is ([17]),

$$\psi_\lambda(j\omega) = \prod_{l=1}^{L}\frac{1}{1 - j\omega\theta_l} \tag{39}$$

where

$$\theta_l = \frac{\alpha_k^{(l)2}}{\sum_{l=1}^{L}\left(Q^{(l)}\right)_{k,k}} \tag{40}$$

Under the assumption that the θ_l are distinct, taking the inverse transform we obtain the following density function

$$p(\lambda) = \sum_{l=1}^{L}\beta_l \exp\left(\frac{-\lambda}{\theta_l}\right) \tag{41}$$

where

$$\beta_l = \prod_{j+1, j\neq l}^{L-1}\frac{\theta_l}{\theta_l - \theta_k} \tag{42}$$

Evaluating the integral in (37), we obtain,

$$P_{d,k}(\text{error}) = \sum_{l=1}^{L}\beta_l\left[1 - \sqrt{\frac{\theta_l}{1+\theta_l}}\right] \tag{43}$$

If the θ_l are not distinct it can be shown [11] that

$$P_{d,k}(\text{error}) = \left(\frac{1-\mu}{2}\right)^L \sum_{l=1}^{L}\binom{L-1+k}{k}\left(\frac{1+\mu}{2}\right)^l \tag{45}$$

where

$$\mu = \frac{\theta_l}{1+\theta_l} \tag{45}$$

This detector (shown in Fig. 16) is essentially a Rake receiver where the multiple paths are obtained from different sensors - the error probability is of the same form [11]. By duality, this also suggests the receiver for a single-sensor in a frequency selective multi-path fading channel. The received signal consisting of K signals can be resolved into L paths, with each path containing K components corresponding to each user. Each of these paths can be decorrelated, combined optimally, and input to a decision device.

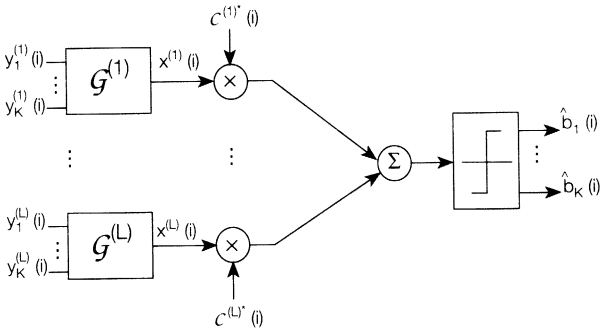

Fig. 16 - Decorrelator for a fading channel: eq. (10).

To study the performance, consider a system with 2 users, each user having 2 resolvable paths (or a 2 sensor, 2 user system) have identical average signal to noise ratio $SNR1$. Then, assuming that the correlation within two users, in both the paths, is given by the matrix in (30), we plot the error probability of the single user detector (which would be a Rake) as well as the detector derived above. In Fig. 17, we plot the error probabilities for user 1, for $\rho = 0.7$ versus $SNR1$. The figure clearly shows that no saturation level exists and further that the error probability of the decorrelator detector decreases at the same rate as that of the single user Rake

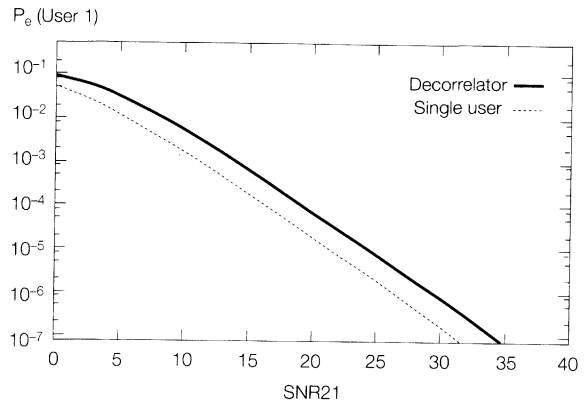

Fig. 17 - Average error probability for two users in a 2-path Rayleigh fading channel as a function of $SNR1$ for $\rho = 0.7$

receiver. In Fig. 18 we give a similar plot for $SNR1 = 10$ dB. Again, we see that the performance of the decorrelator is very good even for high values of ρ.

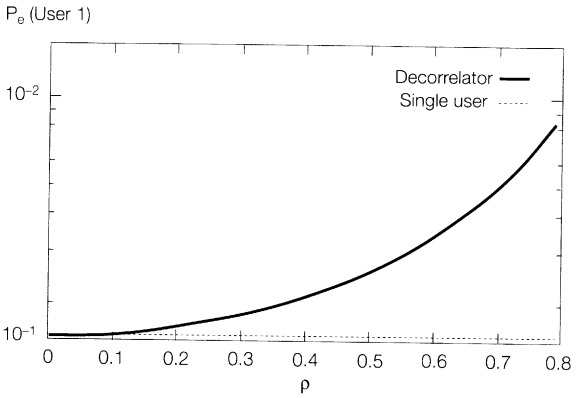

Fig. 18 - Average error probability for two users in a 2-path Rayleigh fading channel as a function of ρ for $SNR = 10$ dB.

5. CONCLUSIONS

In this paper, we have developed a decorrelating detector for CDMA type networks using more than one sensor. These detectors do not require the knowledge of the energies of the users' signals. We have studied this detector in AWGN channels for both single-sensor and multiple sensors. The performance of this detector does not depend on the energies of the interfering users and is not much worse in most situations when compared to the MMSE detector. We also studied the performance of this detector in fading channels. It has been found that this detector does not exhibit the saturation phenomenon which exists in the conventional detector. Further, we have seen that the rate of decrease of the error probabilities is identical to that of the single user detector in this environment. We have also studied this detector in the presence of multipath channels. When this decorrelator is used, it is actually possible to estimate energies and these energies can in turn be used to perform maximal ratio combining. We have also seen that the decorrelator coupled with maximal ratio combining has the structure of the Rake receiver. Since the error probabilities for the decorrelator depend purely on the noise colored by the correlations with the other users' noise and the decorrelator does perform well for significantly high correlations, its performance gives an approximate idea of how high the correlations can be, and such insight could be useful in designing new code waveforms.

Manuscript received on December 19, 1994.

REFERENCES

[1] S. Kandala, E. S. Sousa, S. Pasupathy: *Diversity based detectors in multi-access networks.* "Thirteenth Ann. Allerton Conf. on Commun., Control and Computing", 1992, p. 436-445.

[2] S. Kandala, E. S. Sousa, S. Pasupathy: *Multi-user multi-sensor detectors for CDMA networks.* "IEEE Trans. on Commun.", 1995 (to be published).

[3] L. F. Chang, J. C. I. Chuang: *Diversity selection using coding in a portable radio communications channel with frequency-selective fading.* "IEEE J. Select. Areas. Commun.", Vol. 7, Jan. 1989, p. 89-98.

[4] Qualcomm Inc., CA: *Wideband spread spectrum digital cellular system dual-mode mobile station - base station compatibility standard.* Proposed EIA/TIA interim standard. April 1992.

[5] L. J. Greenstein, et al: *Microcells in personal communications systems.* "IEEE Commun. Mag.", Vol. 30, Dec. 1992, p. 76-88.

[6] Z. Xie, R. T. Short, C. K. Rushforth: *Suboptimum coherent detection of direct sequence multiple access signals.* "Proc. MILCOMM", 1989, p. 0128-0133.

[7] R. Lupas, and S. Verdú: *Near-far resistance of multi-user detectors in asynchronous channels.* "IEEE Trans. Commun.", April 1990, p. 496-508.

[8] R. Lupas and S. Verdú: *Linear multiuser detectors for synchronous code-division multiple-access channels.* "IEEE Trans. Inf. Theory", Jan. 1989, p. 123-136.

[9] A. Duel-Hallen: *Decorrelating decision-feedback multiuser detector for synchronous code-division multiple-access channel.* "Trans. Commun.", Vol. COM-41, Feb. 1993, p. 285-290.

[10] U. Madhow, M. L. Honig: *Minimum mean-squared error interference supression for direct-sequence spread-spectrum code-division multiple access.* International Conf., Universal Personal Commun., Dallas, Texas, Sept. 1992.

[11] J. G. Proakis: *Digital Communications.* New York: McGraw-Hill Book Company, 1989.

[12] M. K. Simon, J. K. Omura, R. A. Scholtz, B. K. Levitt: *Spread spectrum communications.* Rockville, MD: Computer Science Press, Vol. I, 1985.

[13] E. S. Sousa: *Interference modelling in a direct sequence spread spectrum packet radio network.* "IEEE Trans. on Commun.", Vol. 38, No. 9, Sept. 1990, p. 1475-1482.

[14] M. B. Pursley, H. F. A. Roefs: *Numerical evaluation of correlation parameters for optimal phases of binary shift-register sequences.* "IEEE Trans. Commun.", Vol. COM-27, Oct. 1979, p. 1597-1604.

[15] M. Kavehrad: *Performance of nondiversity receivers for spread spectrum in indoor wireless communications.* "AT & T Technical Journal", Vol. 64, July-Aug 1985, p. 1181-1185.

[16] G. L. Turin: *The effects of multipath and fading on the performance of direct sequence CDMA systems.* "IEEE JSAC", July 1984, p. 597-603.

[17] A. Papoulis: *Probability, random variables and stochastic processes.* New York: McGraw-Hill Book Company, 1984.

Performance of Coded Direct-Sequence Systems with Rake Reception in a Multipath Fading Environment

Dennis Goeckel ([1]), **Wayne Stark** ([2])
Univ. of Michigan - EECS
1301 Beal, Ann Arbor, MI 48109-2122 - USA

Abstract. The probability of error is determined for an uncoded coherent direct-sequence spread-spectrum system with rake reception operating in a specular multipath fading environment. Bounds on the probability of error for a convolutionally-coded system are also calculated through the use of the union bound. The model that is utilized contains a large number of paths divided into groups across the signalling interval. The rake is assumed to be locked onto the direct path and one strong path from each of a subset of the other groups. The probability of error is calculated using the characteristic function to determine the effect of various system parameters such as the processing gain and the number of rake branches. Comparisons are made with results obtained through the standard Gaussian assumption. Finally, further analytic results are presented for the rake receiver in the low signal-to-noise ratio limit.

1. INTRODUCTION

Direct-sequence spread spectrum (DS/SS) systems find wide application in mobile communication code-division multiple-access (CDMA) systems. One of the key characteristics of the mobile channel is the multipath fading that occurs due to the many objects existing in the environment that reflect the signal to the receiver. Because the distance the signal must travel as it reflects off of distinct objects is different, a number of copies of the signal arrive at the receiver shifted in time. These delayed signal copies can add constructively or destructively, causing the signal to fade in and out, hence the term "multipath fading". Due to the presence of large objects that create a number of signal paths closely spaced in time, a reasonable model for the time distribution for the signal delays is as a set of paths divided into groups spaced across the bit interval. In mobile communications, these groups often consist of a large number of low amplitude paths with similar delays and one or two large paths in the group [1].

In this work, the error probability of a rake receiver is considered [2] in the aforementioned environment where each branch of the rake is able to "lock" onto the strong signal path in one of the groups. The error probability is derived using the characteristic function method. By using such an approach to directly calculate the error probability given the statistics of the multipath environment, not only are the error probabilities determined, but also under what conditions the Gaussian approximations for the interference that are used in most standard calculations are valid. This work can be viewed as a generalization of a portion of the work in [3] as the standard correlation receiver can be obtained by specializing the above calculation to a rake with one branch matched to the direct path (delay 0).

2. SYSTEM AND CHANNEL MODELS

2.1. *Transmitter*

The transmitter is the standard direct-sequence spread spectrum transmitter with phase-shift-keyed (PSK) modulation. The user's data bit stream (b_l) is modelled as a sequence of mutually independent random variables, each with equal probability of being + 1 or − 1. The data signal $b(t)$ is then given by

$$b(t) = \sum_{l=-\infty}^{\infty} b_l \, p_T (t - l T)$$

([1]) D. L. Goeckel is supported by a National Science Foundation Graduate Fellowship.
([2]) This work was supported in part by the National Science Foundation under grant NCR-9115969.

where

$$p_T(t) = \begin{cases} 1 & 0 \le t < T \\ 0 & \text{otherwise} \end{cases}$$

The signal is then spread by the waveform $x(t)$, given by

$$x(t) = \sum_{i=-\infty}^{\infty} x_i \, p_{T_c}(t - i\,T_c)$$

where x_i is the binary signature sequence assuming values + 1 and – 1, and

$$p_{T_c}(t) = \begin{cases} 1 & 0 \le t < T_c \\ 0 & \text{otherwise} \end{cases}$$

It is assumed that the signature sequence is identical over each data bit and thus has period identical to the ratio of bit duration to chip duration. This period, also known as the processing gain, will be denoted $N = T/T_c$. Because path delays will be constrained to be less than the duration of a data bit, it is not imperative that spreading sequences with a period longer than N be considered. If path delays were allowed to be longer, it would be inadvisable to use the period equal to the length of a data bit as large correlation would then exist between future direct paths and delayed paths with delay near an integer number of data bits.

Denoting the transmitter power P and the phase angle of the PSK modulator θ, the created spread-spectrum signal $u(t)$ can be expressed as

$$u(t) = \sqrt{2P}\, b(t)\, x(t) \exp(j\theta)$$

where $j = \sqrt{-1}$. Thus, with carrier frequency f_c, the transmitted signal for a PSK DS/SS system is given by

$$s(t) = \Re\left[u(t) \exp(j\,2\,\pi\, f_c\, t)\right]$$

where $\Re[x]$ denotes the real part of x.

2.2. *Channel*

In this section, the channel model that will be considered in succeeding sections will be introduced. The channel is assumed to be composed of M groups of paths consisting of L paths each with all paths in a given group having the same distribution of delay. Besides its obvious physical significance, a reason that a discrete path model is used is that it allows us to approximate many models that are used in the literature. For example, the Gaussian Wide-Sense Stationary Uncorrelated Scattering (GWSSUS) model, introduced by Bello [4], can be obtained as the number of paths is allowed to go to infinity [5]. The model also allows the fading amplitude distribution to vary naturally as system parameters change (e.g., an increase or decrease in the spreading factor) instead of being constrained to a given distribution such as Rayleigh or Rician where the only freedom is to adjust the parameters. What is lost in simplicity of calculation will be regained in the flexibility and the intuition into the environment that the model allows.

The output of the channel is then given by

$$y(t) = \sum_{m=1}^{M} \sum_{l=1}^{L} \Re\left\{g_{m,l}\, u\left(t - \tau_{m,l}\right) \cdot \exp\left(j\,2\,\pi\, f_c\left(t - \tau_{m,l}\right)\right)\right\} \tag{1}$$

where the complex gain coefficients are given by

$$g_{m,l} = \alpha_{m,l}\, e^{j\theta_{m,l}}$$

Here, $\alpha_{m,l}$ and $\theta_{m,l}$ represent the attenuation and phase shift incurred from the reflection of the l-th delayed path of the m-th group, respectively, $\tau_{m,l}$ and l-th is the m-th path delay of the group relative to the direct path which has delay 0 ($\tau_{1,1} = 0$).

The variables $\{\theta_{m,l},\ m = 1, \ldots, M,\ l = 1, \ldots, L\}$ will be modelled as a set of mutually independent random variables uniformly distributed between 0 and 2π. The elements of $\{\tau_{m,l},\ m = 1, \ldots, M,\ l = 1, \ldots, L\}$ are modelled as random variables that are mutually independent of each other. The distribution of a given $\tau_{m,l}$ will be taken as uniform between B_m and U_m, where B_m is the lower bound on the delay for paths in the m-th group and U_m is the corresponding upper bound.

It is assumed that for the rake receiver there is one strong path in each group and that this path has a deterministic amplitude. This will be the path that the rake is able to lock onto and will be indexed as the first path in the group (i.e. for the j-th group, the strong path will have amplitude $\alpha_{j,1}$, delay $\tau_{j,1}$, and phase $\theta_{j,1}$). The weak paths, the remaining paths in each group, will also be taken to have a deterministic amplitude with all of the amplitudes of the weak paths in a given group being equal. Note that it is also possible to allow the amplitude of the paths to have a random distribution without significantly raising the complexity of the calculation in many cases (section 3.1).

2.3. *Receiver and basic analysis*

The following analysis aims to calculate the probability of error for a single data bit b_0, which, without loss of generality, can be assumed to be equal to 1. All random path delays will be taken to be less than the length of the signalling interval, thus causing the current bit to interfere only with the succeeding bit on the channel. Due to this intersymbol interference and the nature of the rake, the probability of error calculation will depend on both b_{-1} and b_1. For ease of notation during the following analysis, it will be assumed that b_{-1} and b_1 are given. When numerical results are evaluated, the aver-

age over all four instantiations of these variables is computed. This will change when soft decision decoding is considered and will be explained in that section.

The output of the channel $y(t)$ is combined with additive white Gaussian noise $n(t)$ with power spectral density $N_0/2$ to produce the received signal $r(t)$. For deciding b_0, the j-th branch of the rake receiver, $j = 1, \ldots, J$, locks onto the delay $\tau_{j,1}$ to compute

$$Z_j = \sqrt{\frac{2}{T}} \int_{\tau_{j,1}}^{\tau_{j,1}+T} r(t)\, x\left(t-\tau_{j,1}\right) \cdot \cos\left(2\pi f_c \left(t-\tau_{j,1}\right)+\theta_{j,1}\right) \mathrm{d}t \tag{2}$$

where it has been tacitly assumed (without loss of generality) that the rake locks onto a path in the first J groups. In addition, the phase θ of the transmitted signal is set equal to 0. Substituting the appropriate quantities into (2) and ignoring the double frequency terms yields

$$Z_j = n_j + \sum_{m=1}^{J} \alpha_{m,1} \sqrt{\frac{P}{T}} \cos\left(\phi_{m,1}-\phi_{j,1}\right) \cdot \int_{\tau_{j,1}}^{\tau_{j,1}+T} b\left(t-\tau_{m,1}\right) x\left(t-\tau_{m,1}\right) x\left(t-\tau_{j,1}\right) \mathrm{d}t + \sum_{m=1}^{M} \sum_{l=l_m}^{L} \alpha_{m,l} \sqrt{\frac{P}{T}} \cos\left(\phi_{m,l}-\phi_{j,1}\right) \cdot \int_{\tau_{j,1}}^{\tau_{j,1}+T} b\left(t-\tau_{m,l}\right) x\left(t-\tau_{m,1}\right) x\left(t-\tau_{j,1}\right) \mathrm{d}t$$

where

$$\phi_{m,l} = 2\pi f_c\, \tau_{m,l} - \theta_{m,l}$$

$$l_m = \begin{cases} 2 & m \le J \\ 1 & \text{otherwise} \end{cases}$$

and n_j is a zero mean Gaussian random variable with variance $N_0/2$.

The elements of $\{\phi_{m,l},\ m = 1, \ldots, M,\ l = 1, \ldots, L\}$ will be modelled as uniform random variables over 0 to 2π, where all of the elements of a given set are independent of each other and of elements in the other set. Because f_c is assumed to be large, these random variables are also assumed to be independent of the elements in $\{\tau_{m,l},\ m = 1, \ldots, M,\ l = 1, \ldots, L\}$. Letting

$$R_x(\tau) = \begin{cases} \dfrac{1}{T}\displaystyle\int_0^{\tau} x(t-\tau)\, x(t)\, \mathrm{d}t & \tau \ge 0 \\ 0 & \tau < 0 \end{cases}$$

$$\hat{R}_x(\tau) = R_x(T-\tau)$$

and

$$v(\tau_1,\tau_2) = b_{-1} R_x(\tau_1-\tau_2) + b_0 \hat{R}_x\left(|\tau_1-\tau_2|\right) + b_1 R_x(\tau_2-\tau_1)$$

the following expression is obtained:

$$Z_j = n_j + \sqrt{\frac{P}{T}} \left[\alpha_{j,1} b_0 T + \sum_{m=1,m\ne j}^{J} \alpha_{m,1} \cdot \cos\left(\phi_{m,1}-\phi_{j,1}\right) v\left(\tau_{m,1},\tau_{j,1}\right) T + \sum_{m=1}^{M} \sum_{l=l_m}^{L} \alpha_{m,l} \cdot \cos\left(\phi_{m,l}-\phi_{j,1}\right) v\left(\tau_{m,l},\tau_{j,1}\right) T \right] = n_j + \sqrt{E_b} \cdot \left(\alpha_{j,1} b_0 + \sum_{m=1,m\ne j}^{J} G_m^j + \sum_{m=1}^{M} \sum_{l=l_m}^{L} F_{m,l}^j \right)$$

where

$$G_m^j = \alpha_{m,1} \cos\left(\phi_{m,1}-\phi_{j,1}\right) v\left(\tau_{m,1},\tau_{j,1}\right)$$

$$F_{m,l}^j = \alpha_{m,l} \cos\left(\phi_{m,l}-\phi_{j,1}\right) v\left(\tau_{m,l},\tau_{j,1}\right)$$

and $E_b = PT$ is the transmitted energy per data bit.

The combination of all of the rake branches forms the decision variable Z, defined as

$$Z = \sum_{j=1}^{J} \beta_j Z_j$$

where B_j is the combining factor of the j-th branch (section 2.3). Substituting appropriate expressions for Z_j, $j = 1, \ldots, J$ into the expression for Z results in

$$Z = \eta + \mathcal{A} b_0 + I$$

where

$$\eta = \sum_{j=1}^{J} \beta_j n_j \qquad \mathcal{A} = \sqrt{E_b} \sum_{j=1}^{J} \beta_j \alpha_{j,1}$$

$$I = B + R$$

$$B = \sqrt{E_b} \sum_{j=1}^{J} \sum_{m=1,m\ne j}^{J} \beta_j G_m^j$$

$$R = \sqrt{E_b} \sum_{j=1}^{J} \sum_{m=1}^{M} \sum_{l=l_m}^{L} \beta_j F_{m,l}^j$$

Interpretation of the symbols introduced above is then straightforward: η is the total thermal noise in the decision variable Z; $\mathcal{A}$ is the amplitude of the desired signal component; and B and R are the portions of the interference I that account for the locked paths and the non-locked paths, respectively.

3. AVERAGE PROBABILITY OF ERROR FOR AN UNCODED SYSTEM

3.1. *Calculations*

Using the method in [3], the probability of error given the data bits b_1 and b_{-1} adjacent to b_0 can be written as

$$\overline{P}_e(b_1, b_{-1}) = Q\left(\frac{\mathcal{A}}{\sigma}\right) + \frac{1}{\pi}\int_0^\infty \mathcal{A}\,\mathrm{sinc}(\mathcal{A}u/\pi)\cdot \xi_\eta(u)\left[1-\xi_I(u)\right]\mathrm{d}u \tag{3}$$

where

$$Q(x) = \frac{1}{\sqrt{2\pi}}\int_x^\infty \exp\left(-t^2/2\right)\mathrm{d}t$$

σ^2 is the variance of η, and ξ_η and ξ_I are the respective characteristic functions of η and I. Assuming the noise in the system is dominated by thermal noise in the receiver (and thus implying the independence of the η_j's), the variance of η is given by

$$\sigma^2 = \sum_{j=1}^{J} \beta_j^2 \frac{N_0}{2}$$

Since η is a zero-mean Gaussian random variable, its characteristic function is given by

$$\xi_\eta(u) = \exp\left(-\frac{1}{2}u^2\sigma^2\right)$$

Now the characteristic function of the interference I must be determined. Letting $E[\cdot]$ denote the expectation operator, $\xi_I(u) = E[\exp(juI)]$ where the expectation is over the phases $\{\phi_{m,l}, m = 1, \ldots, M, l = 1, \ldots, L\}$ and the path delays $\{\tau_{m,l}, m = 1, \ldots, M, l = 1, \ldots, L\}$ as defined above. The operation would be greatly simplified if B and R as defined above are independent, but they both depend on the variables in the set $\{\phi_{m,1}, m = 1, \ldots, J\}$ and $\{\tau_{m,1}, m = 1, \ldots, J\}$. The first step taken to alleviate this problem is to fix the path delay $\tau_{j,1}$ of the locked path in the j-th group to the expected value of the delay of that group (i.e. $(B_j + U_j)/2$). This will not affect the probability of error calculation to a great extent if it is assumed that the groups of paths have a separation of at least T_c between them which is usually the case.

The calculation of the characteristic functions is then straightforward although somewhat tedious and therefore is relegated to Appendix A. There the requirement that $\phi_{j,1} = 0, j = 1, \ldots, J$, is added. However, this does not greatly affect the result as discussed in Appendix A. Given these assumptions, ((18) and (19) of Appendix A)

$$\xi_B(u) = \exp\left(ju\sum_{j=1}^{J}\sum_{m=1,m\neq j}^{J}\beta_j\sqrt{E_b}\,\alpha_{m,1}v\left(\tau_{m,1},\tau_{j,1}\right)\right) \tag{4}$$

$$\xi_R(u) = \prod_{m=1}^{M}\prod_{l=l_m}^{L}\left[\frac{1}{(U_m - B_m)}\int_{B_m}^{U_m} J_0\left(u\sqrt{E_b}\,\alpha_{m,l}\sum_{j=1}^{J}\beta_j\,v\left(\tau_{m,l},\tau_{j,1}\right)\right)\mathrm{d}\,\tau_{m,l}\right] \tag{5}$$

where J_0 is the Bessel function of order 0, $\xi_B(u)$ is the characteristic function of B, and $\xi_R(u)$ is the characteristic function of R. Recognizing the independence of B and R given the above assumptions, (3) with $\xi_I(u) = \xi_B(u)\xi_R(u)$ yields the final result which is used to generate the probability of error data in the next section. The above result can be easily modified to include cases where the amplitudes are random with a given density function instead of deterministic as above. Both the Rician and Nakagami-m densities, important models for the mobile cellular environment [6, 7], are capable of being integrated analytically in such a manner [8].

For comparison purposes, the probability of error utilizing the standard Gaussian assumption for the distribution of the interference is calculated in the results section for a number of cases. The following equations were used to generate the results for the Gaussian case:

$$\overline{P}_{e_G}(b_1, b_{-1}) = Q\left(\frac{\mathcal{A}+\bar{I}}{\sigma_G}\right) \tag{6}$$

where

$$\bar{I} = \sum_{j=1}^{J}\sum_{m=1,m\neq j}^{J}\beta_j\sqrt{E_b}\,\alpha_{m,1}\,v\left(\tau_{m,1},\tau_{j,1}\right) \tag{7}$$

$$\sigma_G^2 = \sigma^2 + \frac{1}{2}\sum_{m=1}^{M}\sum_{l=l_m}^{L}E_b\,\alpha_{m,l}^2\frac{1}{(U_m - B_m)}\int_{B_m}^{U_m}\left(\sum_{j=1}^{J}\beta_j\,v\left(\tau_{m,l},\tau_{j,1}\right)\right)^2\mathrm{d}\,\tau_{m,l} \tag{8}$$

3.2. *Combining factors*

One of the design specifications that is considered is the set of combining factors $\{\beta_j, j = 1, \ldots, J\}$ used on the branches of the rake. The simplest case, termed "equal weight combining", is simply to weight each rake branch the same (i.e. $\beta_j = 1, \forall_j$). Given Gaussian statistics and

that the signal has a much larger bandwidth than the coherence bandwidth of the channel, the optimal form of weighting for the diversity receiver when there is a rake branch locked onto each effective multipath is to weight each branch by the amplitude of the signal coming in at that path [9]. The major problem with this approach for the system described in this work is that not all paths are locked onto, only a small subset of them. Thus, combining factors are derived below that are matched to the system and environment described in this work.

To derive these combining factors, the inputs to each branch of the rake are modelled as independent with Gaussian interference (the sum of Gaussian noise and interference has a Gaussian distribution) that is due only to the background noise and the interfering paths in the locked path's group. Note that the Gaussian assumption is not being used for analysis - it is simply being used to specify the combining factors.

Given the above assumptions, it is straightforward to see that the optimal factors are given by

$$\beta_j = \sqrt{E_b}\,\alpha_{j,1}/\sigma_j^2 \tag{9}$$

where σ_j^2 is the variance of the Gaussian-distributed interference in the j-th branch.

What remains to be calculated is σ_j^2. It is easy to show that this can be expressed as

$$\sigma_j^2 = \frac{N_0}{2} + E_b\,\alpha_j^2\,\frac{(L-1)}{2\left(U_j - B_j\right)}\int_{B_j}^{U_j} V^2\left(\tau - \tau_{j,1}\right)\mathrm{d}\,\tau =$$

$$\frac{N_0}{2} + E_b\,\alpha_j^2\,\frac{(L-1)}{2\left(U_j - B_j\right)}\sum_{i=I_B}^{I_U}\int_{iT_c}^{(i+1)T_c} V^2\left(\tau - \tau_{j,1}\right)\mathrm{d}\,\tau$$

where $I_B = (B_j - \tau_{j,1})/T_c$, $I_U = ((\tau_{j,1} - U_j)/T_c) - 1$, α_j equals the common amplitude of the weak paths in the j-th group, and $V(t) = v(t, 0)$. Note that it has been tacitly assumed to save some bookkeeping that $\tau_{j,1}$, B_j and U_j all fall on integer multiples of T_c and that $[\tau_{j,1} - T_c, \tau_{j,1} + T_c] \subset [U_j, B_j]$. The key now is to realize that V is piecewise linear, being linear between iT_c and $(i+1)T_c, \forall\, i$. Letting $a_i = V(iT_c)$,

$$V(x) = a_i\,(1+i) - i\,a_{i+1} + \frac{x\left(a_{i+1} - a_i\right)}{T_c}$$

$$i\,T_c \le x \le (i+1)\,T_c$$

which implies, after a bit of algebra,

$$\sigma_j^2 = \frac{N_0}{2} + E_b\,\alpha_j^2\,\frac{(L-1)\,T_c}{6\left(U_j - B_j\right)} \cdot$$

$$\sum_{i=I_B}^{I_U}\left(a_{i+1}^2 + a_i\,a_{i+1} + a_i^2\right)$$

Assuming random spreading sequences, taking the expectation of the above over a_i, $i = I_B, \ldots, I_U + 1$, and noting

$$E\left(a_i^2\right) = \begin{cases} 1 & i = 0 \\ 1/N & \text{otherwise} \end{cases}$$

the final result is obtained as

$$\sigma_j^2 = \frac{N_0}{2} + E_b\,\alpha_j^2\,\frac{(L-1)\,T_c}{3\left(U_j - B_j\right)}\left(1 + \frac{\left(I_U - I_B\right)}{N}\right) \tag{10}$$

The above is used in conjunction with (9) in the results section to determine the combining factors for what will be denoted "maximum ratio combining". It will also be shown how this compares with the other types of combining discussed above for a given fading environment.

3.3. *Results*

In this section results are presented for uncoded systems using the equations presented in the previous sections. Key tradeoffs are investigated for systems operating over the channel such as the effect of the spreading factor, the number of rake branches, and the type of combining used for the rake branch outputs. As mentioned earlier, the results of this paper are also compared to those made using the Gaussian interference assumption. Due to the nature of the application (mobile cellular), the main concern is performance at fairly low signal-to-noise ratios (*SNR*), and the results will reflect this concentration.

The fading channel model that will be considered for much of this section consists of the following:

L paths: $\tau_{1l} \sim U\left[0, 0.0314\,T\right]$, $\alpha_{1,1} = 1.0$

L paths: $\tau_{2l} \sim U\left[0.0785\,T, 0.1098\,T\right]$, $\alpha_{2,1} = 0.5$

L paths: $\tau_{3l} \sim U\left[0.1569\,T, 0.1882\,T\right]$, $\alpha_{3,1} = 0.5$

L paths: $\tau_{4l} \sim U\left[0.2353\,T, 0.2667\,T\right]$, $\alpha_{4,1} = 0.25$

The spreading factor N, number of locked rake branches J, and the power ratio γ_l, defined to be the ratio of the power in the locked path to the total power of the random paths in the l-th group, complete the specification of the channel and system. The generators for the various spreading sequences that were used in this section were obtained from [10] and [11] and are of the auto-optimal least-sidelobe-energy (AO/LSE) variety. The sequences of length N = 127 were generated by shift register polynomial H = 301 and initial register state 0010010. The sequences of length N = 1023 were generated by shift register polynomial H = 2201 and initial register state 0111011010.

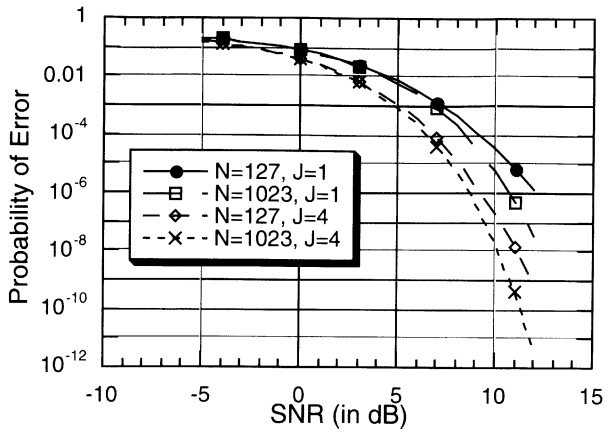

Fig. 1 - Probability of Error as a Function of the Number of Branches and the Processing Gain, $\gamma = 6$ dB, $L = 10$ and Maximum Ratio Combining.

Next the performance of the correlation and rake receivers as a function of bandwidth is compared. This yields Figs. 1 and 2 which show the effect of both the number of rake branches and the bandwidth on the probability of error (note that when simply γ is specified that this implies that all groups have the same "locked-to-random" power ratio). Complexity and performance obviously increase as a function of processing gain and the number of branches, so it is interesting to compare the tradeoff between the two as a function of γ. The environment of 1 is termed "weakly fading" due to the fact that for $J = 1$ and $N = 127$, it requires only $E_b/N_0 =$ 10.5 dB, only approximately 1 dB more than the AWGN case, to obtain $\overline{P_e} = 10^{-5}$, while the environment of 2 is referred to as "strongly fading". For weakly fading environments, the addition of rake branches (the capture of more coherent energy) is more important than an increase in spreading gain (better multipath rejection). For more strongly fading environments, however, Fig. 2 shows that the increase in spreading gain can start to become more useful, especially at the higher signal-to-noise ratios shown. Finally, note that the rake provides greatly increased performance over the correlation receiver in most cases.

The accuracy of the Gaussian approximation is next examined for some of the fading environments discussed above. In advance, one would expect that as the number of paths L goes to infinity that the Gaussian approximation would become tight. What is of interest is to find how close it is when L is fairly small. Figs. 3 and 4 display the applicable curves for this work. Note that at fairly low signal-to-noise ratios that the noise dominates the interference and thus both the Gaussian analysis and the results of this work are very similar, but as higher signal-to-noise ratios are considered, where the interference becomes the predominant factor, the analyses show a great deal of difference. This leads to the conclusion that for work in systems dominated by noise, particularly coded systems where the channel signal-to-noise ratio will be fairly small, the Gaussian approximation is indeed accurate enough. However, for higher signal-to-noise ratios or systems dominated by interference, the Gaussian assumptions may not be accurate.

Finally, "maximum ratio combining" is compared to other types of combining. For the maximum ratio com-

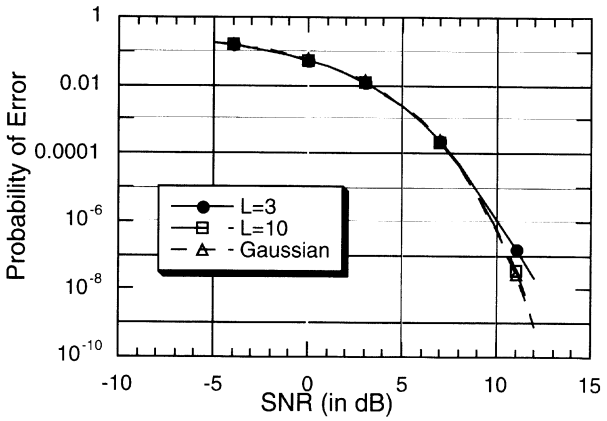

Fig. 3 - Probability of Error as a Function of the Number of Paths, $N = 1023$, $J = 4$, $\gamma = 0$ dB and Equal Weight Combining.

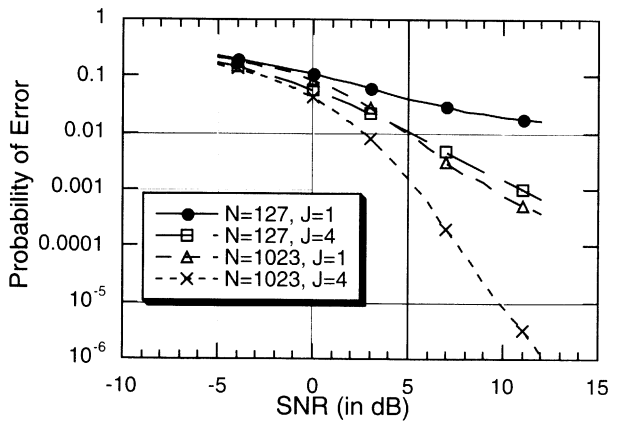

Fig. 2 - Probability of Error as a Function of the Number of Branches and the Processing Gain, $\gamma = -6$ dB, $L = 10$ and Maximum Ratio Combining.

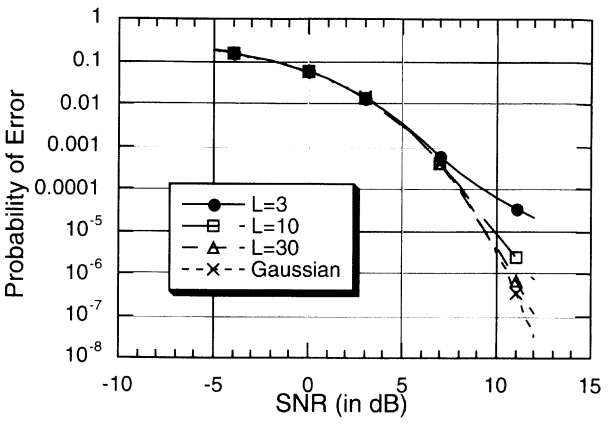

Fig. 4 - Probability of Error as a Function of the Number of Paths, $N = 1023$, $J = 4$, $\gamma = -6$ dB and Equal Weight Combining.

bining, (9) and (10) as derived in section 3.2 are used. Fig. 5 shows the desired probability of error curves for a typical fading environment where γ_l is different for various groups. In this case, $\gamma_1 = \gamma_3 = -6$ dB, $\gamma_2 = \gamma_4 = 0$ dB for the comparison. Note that the "maximum ratio" combining derived in the previous section is superior to equal weight combining where $\beta_j = 1, \forall j$, and "locked" combining where the combination is done with the amplitude of the locked path. For low signal-to-noise ratios, the interfering paths are negligible compared to the noise and thus "locked" combining approaches optimal combining [9]. As the signal-to-noise ratio increases, the interference starts to become the predominant factor, and "locked" combining loses out to the other two types of combining. The near-optimality of the equal weight combining at high signal-to-noise ratios is a function of the fading environment and will not be true in general. Also note that these results are for the real system with AO/LSE sequences and interference between groups. Thus, the assumptions of section 3.2 are violated and the optimality of "maximum ratio" combining is no longer guaranteed.

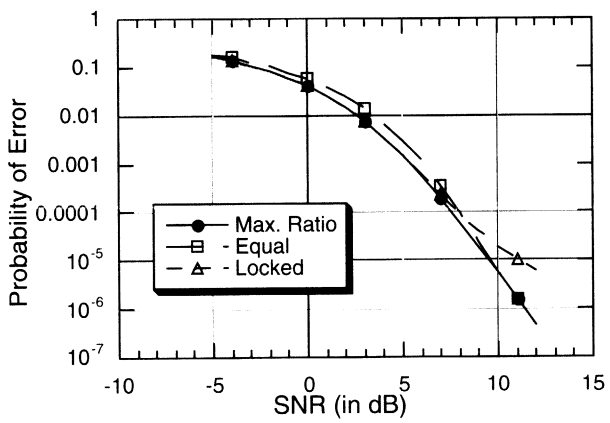

Fig. 5 - Comparison of Various Types of Combining, $N = 1023$, $J = 4$, $L = 10$, γ Varying.

4. BOUNDS ON THE ERROR PROBABILITY FOR CODED SYSTEMS

4.1. *Union-Bhattacharyya bound*

The probability of error using convolutional codes can be bounded by evaluating the appropriate weight enumerator polynomial at the D parameter of the system [12, p. 218] [13, p. 63]. Thus, the need to calculate the D parameter for this fading environment arises. Note that perfect interleaving is assumed so that code symbols are independent. The D parameter for hard decisions is given by

$$D_h = \sqrt{4\,p\,(1-p)} \tag{11}$$

where p is the probability of error calculated in the previous section. For soft decisions, D is approximated by quantizing the decision variable Z into K levels by defining the function W as

$$W = w_k \quad \text{for} \quad a_k \le Z < a_{k+1}, \quad k = 1, 2, \ldots, K$$

where a_k is the lower boundary for quantization level k. Given the above quantization scheme, the D parameter for soft decisions can be approximated by

$$D_s = \sum_{k=1}^{K} \sqrt{p\left(w_k \mid b_0 = +1\right) p\left(w_k \mid b_0 = -1\right)} \tag{12}$$

In an analogous way to the derivation in the previous section of the probability of error for the uncoded system, it is straightforward to show in a manner similar to the derivation of 3 that

$$P\left(a_k \le Z < a_{k+1} \mid b_0 = +1\right) = \Phi\left(\frac{a_{k+1} - \sqrt{r}\mathcal{A}}{\sigma}\right) - \Phi\left(\frac{a_k - \sqrt{r}\mathcal{A}}{\sigma}\right) - \frac{1}{\pi}\int_0^{\infty} \frac{\xi_n(u)}{u}\left(1 - \xi_I(u)\right) g(u)\,\mathrm{d}\,u$$

where

$$g(u) = \sin\left(\left(a_{k+1} - \sqrt{r}\mathcal{A}\right)u\right) - \sin\left(\left(a_k - \sqrt{r}\mathcal{A}\right)u\right)$$

$$\Phi(t) = 1\,Q(t)$$

and r is the rate of the code. By symmetry,

$$p\left(w_k \mid b_0 = -1\right) = p\left(-a_{k+1} < z \le -a_k \mid b_0 = +1\right)$$

4.2. *Union bound*

The Union-Bhattacharyya bounds derived in the previous section are accurate at high signal-to-noise ratios but become quite loose at low signal-to-noise ratios. The bounds can be tightened for both hard and soft decisions by replacing the Union-Bhattacharyya bound with simply the Union Bound, the difference being that the Union-Bhattacharyya Bound upper bounds the pairwise error probability between two codewords that differ in C places, denoted by $P_{e,C}$, by D^C, whereas the Union Bound utilizes the exact pairwise probability of error. Thus, $P^h_{e,C}$ and $P^s_{e,C}$, the pairwise error probabilities between two codewords differing in C places for hard and soft decisions, respectively, are required. Once again, note that perfect interleaving is assumed so that code symbols are independent.

For hard decisions, the result is trivial and can be written for C odd as [9, p. 464]

$$P^h_{e,C} = \sum_{k=\frac{C+1}{2}}^{C} \binom{C}{k} p^k\,(1-p)^{C-k}$$

and for C even as

$$P_{e,C}^{h} = \sum_{k=\frac{C}{2}+1}^{C} \binom{C}{k} p^{k} (1-p)^{C-k} + \frac{1}{2} \cdot \binom{C}{C/2} p^{C/2} (1-p)^{C/2}$$

where p is simply the probability of error for a single bit transmitted across the channel.

For soft decisions, the result is not nearly so obvious but can be obtained using the characteristic function in a straightforward manner. Assuming the all-zero codeword is sent,

$$P_{e,C}^{s} = \Pr\left(\sum_{c=1}^{C} Z^{c} \le 0 \,\middle|\, b_0 = +1 \right)$$

where Z^c is the decision variable for the c-th non-zero bit in the non-zero codeword. The difficulty is that the characteristic function of the interference in the variable Z^c, denoted $\xi_I^C(u)$, is required. Despite the independence of the code symbols, it is incorrect to claim that this is $\xi_I(u)$ derived previously raised to the C-th power. The previously derived $\xi_I(u)$ depended on b_{-1} and b_1. Raising this to the C-th power and then averaging the probability of error over b_1 and b_{-1} would be tacitly implying that the bits occurring around every codesymbol in the codeword are the same which is not what is desired. The solution is to average $\xi_I(u)$ over b_{-1} and b_1 to obtain what is denoted $\bar{\xi}_I(u)$. Raising this quantity to the C-th power will then yield $\xi_I^C(u)$. Given this, the desired error probability is easily obtained as

$$P_{e,C}^{s} = Q\left(\frac{\sqrt{C r \mathcal{A}}}{\sigma} \right) + \frac{1}{\pi} \int_0^{\infty} C\sqrt{r}\mathcal{A} \operatorname{sinc}\left(C\sqrt{r}\mathcal{A} u/\pi \right) \cdot \xi_\eta^C(u) \left[1 - \xi_I^C(u) \right] \mathrm{d}u \tag{13}$$

where

$$\xi_\eta^C(u) = \exp\left(-\frac{1}{2} C \sigma^2 u^2 \right)$$

In the next section, numerical results are given for the Union-Bhattacharyya Bound for soft decisions and the Union Bound for hard decisions for a (2, 1) convolutional code and a (3, 1) convolutional code, each with contraint length 7. The weight enumerators used for these calculations were taken from [14].

4.3. *Results*

In this section results for various coded systems are compared to determine what system parameters have the greatest effect on performance. Note that the coded systems have their spreading factors reduced so as to have the same bandwidth as the uncoded systems (i.e. for the rate 1/2 code with the N = 1023 system, the coded system would only have N = 511). All rake receivers in this section use equal weight combining.

The results for coded sytems where hard decisions are made on each codeword symbol are shown in Fig. 6. The Union Bound, the tighter of the two bounds discussed in the previous section, is shown; it was found that this bound was a factor of five to ten tighter than the Union-Bhattacharyya Bound across the displayed ranges. The upper bound is approximate based on all of the terms in the weight enumerator up through approximately weight 30. The bounds on the coded systems are shown only where the series were converging quickly, leading to the result that the coded system peformance can only be bounded at fairly high signal-to-noise. Although the main interest is in fairly low *SNR* results for the mobile cellular environment, this is not entirely disappointing as for the higher error rates at low *SNR* it is practical to obtain results by simulation. The dotted lines in Fig. 6 display the results of such a simulation for the correlator receiver cases. Analogous results to

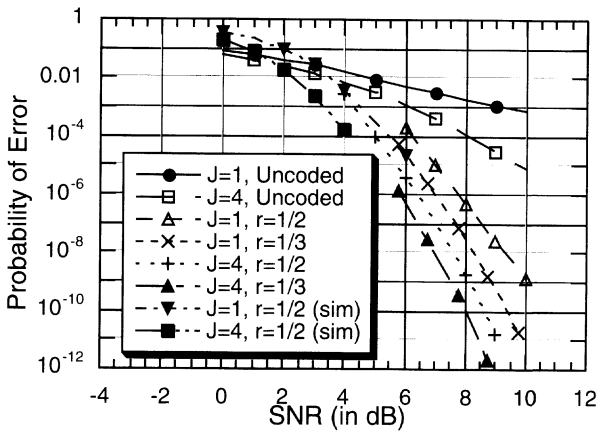

Fig. 6 - Union Bound for Convolutionally-Coded Systems, Hard Decisions, N = 1023, γ = –6 dB, L = 10.

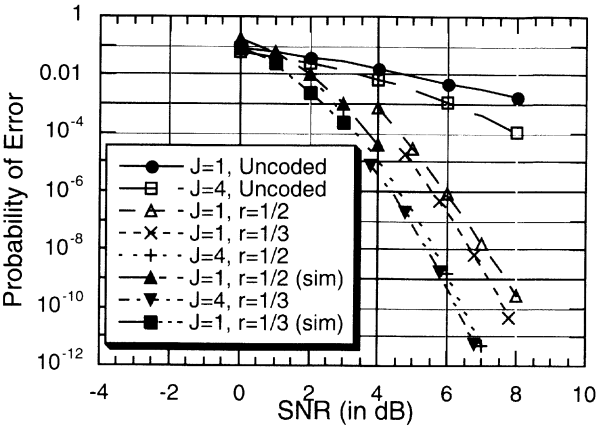

Fig. 7 - Union-Bhattacharyya Bound for Convolutionally-Coded Systems, Soft Decisions, N = 1023, γ = –6 dB, L = 10.

those for the hard decisions are shown for soft decisions in Fig. 7. In this case, the looser of the two bounds, the Union-Bhattacharryya Bound, is displayed.

The most notable observation to be made from these curves is that in general the lower rate codes show better performance, leading to the proposition that perhaps coding is better than spreading given a fixed amount of bandwidth. For this reason, a future research goal is to reduce the spreading rate even further while decreasing the rate of the code (thus keeping the bandwidth constant) and seeing if this pattern continues. Note once again that these are only error bounds and that there is no guarantee that different curves have the same degree of tightness.

5. LOW SNR APPROXIMATIONS

The results thus far have shown that a wideband (N = 1023) system is uniformly better than a narrowband (N = 127) system at moderate to high *SNR*s but that the gap lessens at lower signal-to-noise ratios. This, coupled with the fact that for noncoherent systems the narrowband is better at low *SNR* in certain cases, leads to the question: Which system is better for very low *SNR* for the coherent system? By the convexity of the Q function, the symmetric distribution of the interference, and the fact that the narrowband system on average gives more interference than the wideband system, one would predict that the wideband system will be uniformly superior to the narrowband system. In this section that fact is confirmed, first with the Gaussian approximation and then with an asymptotic low *SNR* calculation using characteristic functions.

The Gaussian approximation is derived by assuming the interference is Gaussian distributed and thus requires only the mean and variance for complete characterization. Given the environment considered in earlier sections with the additional assumptions that random and mutually independent spreading sequences are being used with equal weight combining, the mean of the interference is zero and the variance of the interference is given by

$$\sigma_I^2 = \frac{1}{6}\sum_{m=1}^{J}\sum_{l=l_m}^{L} E_b\,\alpha_{m,l}^2\,\frac{T_c}{(U_m - B_m)}\cdot \left[\frac{2\,J\,(U_m - B_m)}{N\,T_c} + 2 - \frac{2}{N}\right] + \frac{J}{3\,N}\sum_{m=J+1}^{M}\sum_{l=l_m}^{L} E_b\,\alpha_{m,l}^2 \tag{14}$$

where the same method as in section 3.2 has been used to obtain the variance expression. To save bookkeeping, it has been assumed that $\tau_{j,1}, B_m$, and U_m, all fall on integer multiples of T_c, $\forall m$, $\forall j$, and that $[\tau_{j,1} - T_c, \tau_{j,1} + T_c] \subset [B_j, U_j]$, $\forall j$.

The probability of error under the Gaussian assumption is then given by

$$P_{e_G} = Q\left(\frac{\mathcal{A}}{\sqrt{\sigma^2 + \sigma_I^2}}\right)$$

Noting that σ_I^2 is strictly decreasing with increasing N, we conclude that the wideband system is superior to the narrowband system across all signal-to-noise ratios.

Next, a similar analysis using the characteristic function method is conducted. From the previous work in this paper, the error curves approach each other only at low *SNR*, so an attempt is made to determine an approximation for the error probability in this region. This will probably be the only region where the narrowband system has a chance of showing better performance.

To perform the calculation using the characteristic function, the single key step is to write $\xi_I(u)$ in terms of its moments as [15]

$$\xi_I(u) = \sum_{l=0}^{\infty} \frac{\left(-u^2\right)^l \mu_{2l}}{(2\,l)!}$$

where μ_{2l} is the $2\,l$-th central moment of the interference. Note that the odd moments are not present because they will be zero by the symmetry of the interference distribution. Substituting this into (3), interchanging the summation and the integral, and recognizing $\mu_2 = \sigma_I^2$ as given in (14), as $\sigma \to \infty$ [8], yields

$$\bar{P}_e \cong Q(\mathcal{A}/\sigma) + \frac{K\sigma_I^2}{\sigma^3}\exp\left(\frac{-\mathcal{A}^2}{2\,\sigma^2}\right)$$

where K is a constant that does not depend on the spreading factor or the noise variance. Thus, in the limit of low *SNR*, the wideband system is still superior to the narrowband system, which leads to the conjecture that this is true for all signal-to-noise ratios.

6. CONCLUSIONS

In this paper, the effect of various system parameters on the probability of error of a direct-sequence spread-spectrum communication system was examined. The results obtained point to the conclusion that for coherent reception the superior multipath rejection capabilities of the wideband system make it uniformly better than the narrowband system, moreso in environments where the interference is high. The performance of a rake receiver in a specific fading environment has also been investigated, and it has been found that for the uncoded system it may be able to gain back the loss in multipath rejection capabilities in comparison to the wideband system without a rake. Finally, a method of rake branch combining has been introduced that is applicable to this type of fading environment, and it has been shown how it compares to other common combining types.

In addition, the error incurred by making a Gaussian assumption when calculating the probability of error versus the actual calculations that are made in this work was investigated. The Gaussian assumption appears to be very good as long two conditions are satisfied: 1) there are a large number of paths in a given time region and 2) the system does not have a large amount of interference. In a system that is interference limited, it appears that the work in this paper would be much more applicable than Gaussian assumptions, even under the assumption of a fairly large number of paths.

Appendix A
Characteristic Function of the Interference

In this section, the characteristic function of the interference is derived. It would be expedient to claim that B and R as defined in the text are independent, but both depend on the variables in the set $\{\phi_{j,1}, j = 1, \ldots, J\}$. Taking the expectation with respect to the variables in $\{\phi_{m,l}, m = 1, \ldots, M, l = l_m, \ldots, L\}$ and $\{\tau_{m,l}, m = 1, \ldots, M, l = l_m \ldots, L\}$ first, the quantity which depends on B (denoted $\xi_B(u)$) is independent of these variables and thus comes out of the expectation. What remains is $E[\exp(juR)]$ which will be denoted $\xi_R(u)$. The expectations now stand as:

$$\xi_B(u) = \exp\left(j\,u \sum_{j=1}^{J} \sum_{m=1, m\neq j}^{J} \beta_j \sqrt{E_b}\,\alpha_{m,1} \cdot \cos\left(\phi_{m,1} - \phi_{j,1}\right) v\left(\tau_{m,1}, \tau_{j,1}\right)\right) \tag{15}$$

$$\xi_R(u) = E\left[\exp\left(j\,u \sum_{j=1}^{J} \sum_{m=1}^{M} \sum_{l=l_m}^{L} \sqrt{E_b}\,\beta_j F_{m,l}^{j} \right)\right] \tag{16}$$

Moving the sum over j in the latter to the inside and making use of the fact that the elements of $\{\tau_{m,l}, m = 1, \ldots, M, l = l_m, \ldots, L\}$ and $\{\phi_{m,l}, m = 1, \ldots, M, l = l_m, \ldots, L\}$ are independent along with realizing that the elements of $\{\tau_{m,l}, l = l_m, \ldots, L\}$ are identically distributed between B_m and U_m,

$$\xi_R(u) = \prod_{m=1}^{M} \prod_{l=l_m}^{L} \left[\frac{1}{\pi\left(U_m - B_m\right)} \int_{B_m}^{U_m} \int_{0}^{\pi} \cos\left(u\sqrt{E_b}\alpha_{m,l} \cdot \sum_{j=1}^{J} \beta_j \cos\left(\phi_{m,l} - \phi_{j,1}\right) v\left(\tau_{m,l}, \tau_{j,1}\right)\right) \mathrm{d}\,\phi_{m,l}\, d\,\tau_{m,l} \right]$$

Expanding the inner cosine and doing the integration with respect to $\phi_{m,l}$ yields [8]

$$\xi_R(u) = \prod_{m=1}^{M} \prod_{l=l_m}^{L} \left[\frac{1}{\left(U_m - B_m\right)} \int_{B_m}^{U_m} I_0\left(j\,u\,\sqrt{E_b}\alpha_{m,l} \cdot \sqrt{a^2 + b^2}\right) \mathrm{d}\,\tau_{m,l} \right] \tag{17}$$

where, I_0 is modified Bessel function of order 0 and

$$a = \sum_{j=1}^{J} \beta_j \cos\left(\phi_{j,1}\right) v\left(\tau_{m,l}, \tau_{j,1}\right)$$

$$b = \sum_{j=1}^{J} \beta_j \sin\left(\phi_{j,1}\right) v\left(\tau_{m,l}, \tau_{j,1}\right)$$

Now the expectation over the elements of the set $\{\phi_{j,1}, j = 1, \ldots, J\}$ must be taken, which at this point appears to be intractable. The root of this problem is the term $\lambda_{m,l}^{j} = \phi_{m,l} - \phi_{j,1}$ that appears inside the triple summation in R. The calculation would be greatly simplified (proceeding along the same lines as above) if the assumption were made that $\{\lambda_{m,l}^{j}, m = 1, \ldots, M, l = l_m, \ldots, L, j = 1, \ldots, J\}$ is a mutually independent set, but this does not seem to be a valid assumption. Whereas the set is certainly independent in m and l, once $\lambda_{m,l}^{1}$ is known for a given m and l, the remaining variables $\{\lambda_{m,l}^{j}, j = 2, \ldots, J\}$ are uniquely determined given $\{\phi_{j,1}, j = 1, \ldots, J\}$which is constant over m and l (i.e. the phase of each locked path is set). This option was discarded and the following simplification made instead: $\phi_{j,1} = 0, j = 1, \ldots, J$. The translation of this assumption is that the phases of the locked paths relative to each other is exactly 0. As more paths enter into the environment, this assumption should have less of an impact on the overall probability of error as the fixed paths will cause a smaller percentage of the total interference. Sample cases run have shown that this error runs less than two percent of the probability of error for the cases examined, with two percent being the maximum difference as the rake branch angles are varied through all ranges.

The expectation with respect to the elements of $\{\phi_{j,1}, j = 1, \ldots, J\}$ now goes away and the characteristic functions become

$$\xi_B(u) = \exp\left(j\,u \sum_{j=1}^{J} \sum_{m=1, m\neq j}^{J} \beta_j \sqrt{E_b}\,\alpha_{m,1}\, v\left(\tau_{m,1}, \tau_{j,1}\right)\right) \tag{18}$$

$$\xi_R(u) = \prod_{m=1}^{M} \prod_{l_m=1}^{L} \left[\frac{1}{\left(U_m - B_m\right)} \int_{B_m}^{U_m} J_0\left(u\,\sqrt{E_b}\alpha_{m,l} \cdot \sum_{j=1}^{J} \beta_j\, v\left(\tau_{m,l}, \tau_{j,1}\right)\right) \mathrm{d}\,\tau_{m,l} \right] \tag{19}$$

where J_0 is the Bessel function of order 0.

Manuscript received on May 15, 1994.

REFERENCE

[1] D. L. Noneaker, M. B. Pursley: *On the chip rate of CDMA systems with doubly selective fading and rake reception.* "IEEE Journal on Selected Areas in Communications", Vol. 12, June 1994, p. 853-861.

[2] R. Price, P. E. Green: *A communication technique for multipath channels.* "Proceedings IRE", Vol. 46, March 1958, p. 555-570.

[3] E. A. Geraniotis, M. B. Pursley: *Performance of coherent direct-sequence spread-spectrum communications over specular multipath fading channels.* "IEEE Transactions On Communications", Vol. COM-33, June 1985, p. 502-508.

[4] P. A. Bello: *Characterization of randomly time-variant linear channels.* "IEEE Transactions on Communications Systems", Vol. COM-11, December 1963, p. 360-393.

[5] P. Hoeher: *A statistical discrete-time model for the WSSUS multipath channel.* "IEEE Transactions on Vehicular Technology", Vol. 41, November 1992, p. 461-468.

[6] U. Dersch, R. J. Ruegg: *Simulation of the time and frequency selective outdoor mobile radio channel.* "IEEE Transactions on Vehicular Technology", Vol. 42, August 1993, p. 338-344.

[7] U. Dersch, R. J. Ruegg: *A physical mobile radio channel.* "IEEE Transactions on Vehicular Technology", Vol. 40, August 1991, p. 472-482.

[8] I. S. Gradshteyn, I. M. Ryzhik: *Tables of integrals, series, and products.* Academic Press, New York, 1980.

[9] J. G. Proakis: *Digital communications.* McGraw-Hill, New York, 1989.

[10] M. B. Pursley, H. F. A. Roefs: *Numerical evaluation of correlation parameters for optimal phases of binary shift-register sequences.* "IEEE Transactions On Communications", Vol. COM-27, October 1979, p. 1597-1604.

[11] R. Skaug, J. F. Hjelstad: *Spread spectrum in communication.* Peter Peregrinus Ltd., London, UK, 1985, p. 68-77.

[12] R. J. McEliece: *The theory of information and coding.* Addison-Wesley, London, 1977.

[13] A. J. Viterbi, J. K. Omura: *Principles of digital communication and coding.* McGraw-Hill, New York, 1979.

[14] J. Conan: *The weight spectra of some short low-rate convolutional codes.* "IEEE Transactions on Communications", Vol. COM-32, September 1984, p. 1050-1053.

[15] S. O. Rice: *Probability distributions for noise plus several sine waves - The problem of computation.* "IEEE Transactions on Communications", June 1974, p. 851-853.

D. Goeckel, W. Stark: **Performance of Coded Direct-Sequence Systems with Rake Reception in a Multipath Fading Environment.**

ETT, Vol. 6 - No. 1 January - February 1995, p. 41 - 51

The Performance of Diversity Combining for Fast Frequency Hopped NCMFSK in Rayleigh Fading (1)

T. Aaron Gulliver
Department of Systems and Computer Engineering, Carleton University
1125 Colonel By Drive, Ottawa, ON - Canada K1S 5B6
Rolands E. Ezers
SHAPE Technical Centre
P.O. Box 174, 2501 CD The Hague - The Netherlands
E. Barry Felstead
Communications Research Centre
Box 11490, Station H, Ottawa, ON - Canada K2H 8S2
James S. Wight
Department of Electronics, Carleton University
1125 Colonel By Drive, Ottawa, ON - Canada K1S 5B6

Abstract. Frequency hopping (FH) spread spectrum is a well known technique used in communications systems to provide protection against interference such as jamming. With fast FH (FFH) (one or more hops per transmitted data symbol), powerful and robust methods for diversity combining have been developed as an additional jamming countermeasure. These same techniques can be applied to reduce the effects of multiple access interference, and so can be considered for civilian CDMA applications. Although the performance of a FFH communications system can be degraded considerably by fading, few results exist which show the effects of fading on the diversity combining process. In this paper, both analytic and simulation results are presented for several diversity combining methods in a Rayleigh fading channel, which is often considered to be the worst case. The performance of these combining methods in fading is compared with that in AWGN and multitone interference to determine which methods are effective against these degradations.

1. INTRODUCTION

Frequency hopping (FH) spread spectrum modulation is a powerful technique which can be used in communications systems to provide protection against jamming and multiple-access interference, and fading. Increased protection against interference and fading can be obtained through the inherent time and frequency diversity of fast frequency hopping (FFH). The enhancement in performance depends heavily upon the form of diversity combining used at the receiver. To date, such combining methods have been designed to combat intentional jamming. However, the interference created by multiple-access users can also be considered as jamming; therefore the same diversity combining techniques can also be used to improve the performance. The differences are in the assumptions made concerning the signal to interference ratio (*SIR*), the interferer's purpose and intelligence, and the statistics of the interference signals. In this paper, we do not explicitly state specific assumptions for a CDMA environment, but rather use a nominal set of characteristics to predict the FH system performance. These results allow us to make recommendations concerning the use of diversity combining in a FH CDMA system.

Fading is of great concern in mobile and indoor com-

(1) This work was supported in part by the Natural Sciences and Engineering Research Council of Canada.

munications systems. In a FH CDMA system with a large hopping bandwidth, there can be significant variations in the received signal levels. Certain jamming strategies result in the jamming power varying hop to hop. Conversely, fading is manifested as the signal power level varying from hop to hop. Therefore it is not surprising that diversity is able to combat jamming and fading [1, p. 202]. Although the jamming and fading appear to have the same effect, that of a varying SIR, the best combining techniques may not be the same for both jamming and fading. To determine the best overall combining methods, their performance in Rayleigh fading will be compared with that in AWGN and multitone interference.

In this paper, the transmitted signals are noncoherent M-ary frequency shift keyed (MFSK) orthogonal signals which hop over a total spread spectrum bandwidth W_{ss}. The M-ary symbol rate, R_s, is related to the bit rate, R_b, by $R_s = R_b/\log_2 M$. The hop rate is R_h so that the diversity level is

$$L = R_h / R_s \tag{1}$$

With fast frequency hopping (FFH), one M-ary symbol is transmitted on $L \geq 1$ hops. In most practical systems, the hop rate, R_h, is fixed while the symbol rate, R_s, can vary [2, 3], and so a fixed hop rate is considered here. The system model is shown in Fig. 1. A Fourier transform device plus an envelope detector is typically used as the matched filter demodulator. Orthogonal signalling is assumed with the MFSK tone spacing equal to R_h, so that an M-ary channel has a bandwidth equal to MR_h. The symbol duration is $T_h = 1/R_h$.

For L hops, there are LM envelope values per transmitted symbol. The problem is to process these values, which may be impaired by noise, tone interference and fading, to achieve a low bit-error rate (*BER*).

1.1. *Signal and interference description without fading*

The dehopped receiver input in Fig. 1 can consist of a signal tone, plus one or more interfering tones and/or white Gaussian noise. Let z_{mi} be the envelope detector output for the m-th, $m = 1, 2, \ldots, M$, frequency bin during the i-th, $i = 1, 2, \ldots, L$, hop interval. The signal tone is given by

$$\sqrt{2}\, s_{mi} \cos\left(2\pi f_m t + \phi_{mi}\right) \tag{2}$$

where s_{mi} is the rms amplitude,

$$s_{mi} = \begin{cases} \sqrt{E_h/T_h} = \sqrt{P} & \text{in the signal bin;} \\ 0 & \text{in the other } M-1 \text{ bins,} \end{cases} \tag{3}$$

f_m is the frequency, and ϕ_{mi} is a random phase angle uniformly distributed between 0 and 2π. E_h is the hop symbol energy. The interference tone is given by

$$\sqrt{2}\, a_{mi} \cos\left(2\pi f_m t + \theta_{mi}\right) \tag{4}$$

where a_{mi} is the rms amplitude, f_m is the frequency, and θ_{mi} is a random phase angle uniformly distributed between 0 and 2π. ϕ_{mi} and θ_{mi} are statistically independent. The total average jamming power is assumed to be limited to some value J_t. The noise is a white Gaussian random process with zero mean and single-sided noise power spectral density N_O. The sum of these three signals passes through a matched filter and envelope detector.

The envelope detector output, z_{mi}, is the magnitude of a two-dimensional vector, and can be written as a complex number, $\tilde{y}_{mi}$,

$$\tilde{y}_{mi} = y_{mic} + j\, y_{mis} = \tilde{s}_{mi} + \tilde{a}_{mi} + \tilde{n}_{mi} \tag{5}$$

where

$$\tilde{s}_{mi} = s_{mi} \cos\left(\phi_{mi}\right) + j\, s_{mi} \sin\left(\phi_{mi}\right) \tag{6}$$

$$\tilde{a}_{mi} = a_{mi} \cos\left(\theta_{mi}\right) + j\, a_{mi} \sin\left(\theta_{mi}\right) \tag{7}$$

and

$$\tilde{n}_{mi} = n_{mic} + j\, n_{mis} \tag{8}$$

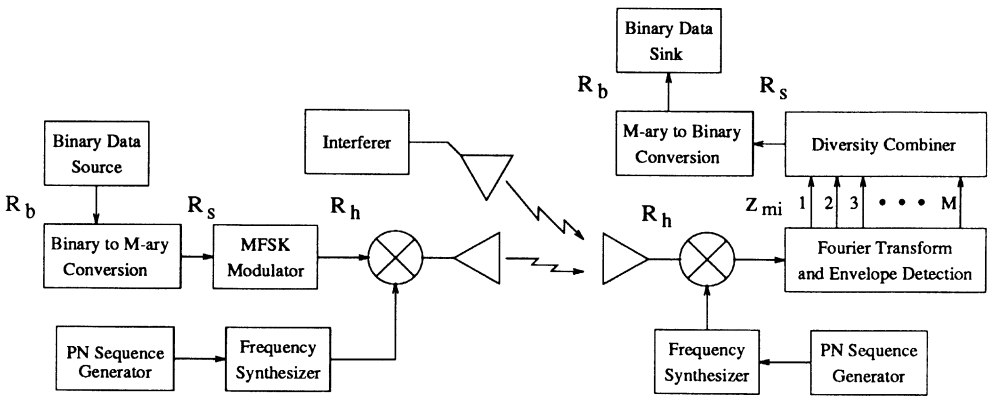

Fig. 1 - Block diagram of a FH/MFSK communication system.

The symbol " ~ " denotes a complex number. With no Gaussian noise jamming present, the noise components, n_{mic} and n_{mis}, are Gaussian random variables with zero mean and variance

$$\sigma_n^2 = N_O / 2\, T_h \tag{9}$$

When noise jamming is present, the variance becomes $\sigma^2 = (N_O + J_O)/2\,T_h$, where J_O is the noise jamming power spectral density defined as $J_O = J_t / W_{ss}$. The effective signal to jammer ratio is then

$$\text{SJR} = E_h / J_O \tag{10}$$

For partial band noise jamming where a fraction, $0 < \rho \le 1$, of W_{ss} is jammed at a density of J_O/ρ, the performance with no diversity ($L = 1$) can be approximated by

$$P_s \approx \frac{\rho}{M} \sum_{j=2}^{M} (-1)^j \binom{M}{j} \exp\left[-\left(\frac{j-1}{j}\right)\frac{E_h}{N_O + J_O/\rho}\right] \tag{11}$$

This equation can be optimised [4, p. 576] to find the worst case fraction, ρ_{wc}.

For multitone interference, let P_j be the power in a single interference tone if one tone were placed in all $N = W_{ss}/R_h$ bins. Thus, $P_j = J_t/N$ and the SJR can be defined as

$$\text{SJR} = \frac{P}{P_j} = \frac{P\,T_h\,W_{ss}}{J_t} \tag{12}$$

For partial band MT jamming, the jammer can cover a fraction, ρ, of W_{ss} with tones of power

$$P_j/\rho = J_t/N\rho \tag{13}$$

If a single jamming tone is located randomly in only one of the M bins of each hop, $\rho = 1/M$ (worst case in Houston's sense [5]), the jamming tone power level is MP_j so that the rms amplitude of this tone is

$$a_{mi} = \begin{cases} \sqrt{MP_j} & \text{in the jammed bin;} \\ 0 & \text{in the other } M-1 \text{ bins,} \end{cases} \tag{14}$$

The performance of MFSK in worst case partial-band Houston multitone jamming without system noise can be found in [4, p. 598].

For illustration purposes, results are given in this paper for interference spread uniformly across the hopping bandwidth. This is of interest because in a multiple access environment, it can be considered similar to a worst case distribution of multi-user tones.

2. SIGNAL AND INTERFERENCE DESCRIPTION WITH FADING

In Rayleigh fading, the signal amplitude, s_{mi}, is a random variable with pdf,

$$f_{s_{mi}}(s_{mi}) = \frac{s_{mi}}{s_0^2} \exp\left(-\frac{s_{mi}^2}{2s_0^2}\right) \quad s_{mi} \ge 0 \tag{15}$$

For $s_{mi} < 0$, $f_{s_{mi}}(s_{mi}) = 0$. The mean power of the signal is $2s_0^2$. The two-dimensional characteristic function of the matched filter output sample is

$$\Phi_{\tilde{y}_{mi}}(\rho) = \exp\left(-\frac{\rho^2\left(\sigma_n^2 + s_0^2\right)}{2}\right) \tag{16}$$

The pdf of the output sample with signal and noise present is

$$f_{sn}(z_{mi}) = \frac{z_{mi}}{\sigma_n^2 + s_0^2} \exp\left(\frac{-z_{mi}^2}{2\left(\sigma_n^2 + s_0^2\right)}\right) \quad z_{mi} \ge 0 \tag{17}$$

For $z_{mi} < 0$, $f_{sn}(z_{mi}) = 0$.

The probability of symbol error with no diversity ($L = 1$), and with combined partial band noise jamming and Rayleigh fading can be approximated by [1, p. 212]

$$P_s \approx \frac{\rho}{M} \sum_{j=2}^{M} (-1)^j \binom{M}{j} \frac{1}{1 + \left(\frac{j-1}{j}\right)\frac{\overline{E_h}}{N_O + J_O/\rho}} \tag{18}$$

where $\overline{E_h} = 2\,T_h s_0^2$ is the average received signal energy. For most values of $\overline{E_h}/J_O$ and M, it can be shown that broadband jamming, $\rho = 1$, is the worst case noise jamming in Rayleigh fading [1, p. 212]. This indicates that fading has a significant impact on performance and so will also affect the choice of a suitable diversity combining method for FFH.

3. DIVERSITY COMBINING METHODS

The algorithms for diversity combining can be classified according to the processing required of the LM values, z_{mi},to produce a decision on the received symbol. This decision is ultimately based on a set of bin metric values, q_m, which are a function of the z_{mi}

$$q_m = f(z_{mi}) \qquad m = 1, 2, \ldots, M \tag{19}$$

$f(\,)$ is usually a nonlinear process, and for most methods q_m has the form

$$q_m = \sum_{i=1}^{L} f(z_{mi}) \qquad m = 1, 2, \ldots, M \tag{20}$$

The largest q_m is chosen as the transmitted symbol for the methods considered here. In some cases, $f(z_{mi})$ processes the values on a hop basis, after which the metric

(20) is evaluated. This is termed hop-processing diversity combining. In other cases they are processed on a bin basis, with either the metric q_m computed directly, or via (20). This is termed bin-processing diversity combining. A survey of combining techniques is given in [6]. The metrics for the combining techniques considered in this paper are presented below.

3.1. *Linear and square-law combining*

These methods require only a sum of the values in each bin

$$q_m = \sum_{i=1}^{L} z_{mi}^{\alpha} \tag{21}$$

and so is the simplest of all combining methods. When $\alpha = 1$, $f(z_{mi})$ in (20) is just z_{mi} and this is termed linear envelope combining. When $\alpha = 2$, (21) is termed square-law or square-law linear combining. This is the optimum combining method in Rayleigh fading and AWGN [7].

As an example of how the performance of such diversity combining can be analysed, consider $\alpha = 1$, $L = M = 2$ and Rayleigh fading. The cdf of q_m can be computed as

$$F_{q_m}(q_m) = \int_0^{q_m} \int_0^{q_m - z_{m1}} \frac{z_{m1}\, z_{m2}}{\sigma^4} \cdot \exp\left(\frac{-z_{m1}^2 - z_{m2}^2}{2\sigma^2}\right) \mathrm{d}z_{m1}\, \mathrm{d}z_{m2} \tag{22}$$

Simplifying,

$$F_{q_m}(q_m) = 1 - \exp\left(\frac{-q_m^2}{2\sigma^2}\right) - \frac{q_m \sqrt{2}}{2\sigma} \cdot \exp\left(\frac{-q_m^2}{4\sigma^2}\right) \operatorname{erf}\left(\frac{q_m}{2\sigma}\right) \quad q_m \geq 0 \tag{23}$$

where

$$\operatorname{erf}(z) = \frac{2}{\sqrt{\pi}} \int_0^z \exp\left(-t^2\right) \mathrm{d}t, \quad q_m \geq 0 \tag{24}$$

The pdf of q_m can be found by differentiating (23). Thus,

$$f_{q_m}(q_m) = \frac{q_m}{2\sigma} \exp\left(\frac{-q_m^2}{2\sigma^2}\right) - \frac{\sqrt{\pi}}{4\sigma^3}\left(q_m^2 + 2\sigma^2\right) \cdot \exp\left(\frac{-q_m^2}{4\sigma^2}\right) \operatorname{erf}\left(\frac{q_m}{2\sigma}\right) \quad q_m \geq 0 \tag{25}$$

The probability of bit error for binary NCFSK must be found numerically by integrating

$$P_b = 1 - \int_0^{\infty} F_n(v)\, f_{sn}(v)\, \mathrm{d}v \tag{26}$$

For square-law diversity combining in Rayleigh fading, the probability of symbol error for M-ary NCFSK with diversity L, is given by [8]

$$P_s = \frac{(M-1)!}{(1+\gamma)^M (L-1)!} \sum_{r=1}^{M-1} \frac{(-1)^{r-1}}{(M-r-1)!(r)!} \cdot \left(\sum_{j=0}^{r(L-1)} \frac{(L+j-1)!}{\left(r + \frac{1}{1+\gamma}\right)^{L+j}} C_{r,j} \right) \tag{27}$$

where

$$C_{r,j} = \sum_{x=j-(L-1)}^{j} C_{r-1,j} \frac{1}{(j-x)!} \delta_x^{0 \leq x \leq (r-1)(M-1)} \tag{28}$$

$\delta_x^{\alpha \leq x \leq \beta} = 1$ for $\alpha \leq x \leq \beta$ and $\delta_x^{\alpha \leq x \leq \beta} = 0$ elsewhere, $C_{0,0} = 1$, $C_{1,j} = 1/j!$, $C_{r,1} = r$, $C_{r,0} = 1$, and $\gamma = E_h/N_O$. For $M = 2$, this result agrees with that in [7].

For $L = M = 2$, the pdf and cdf are given by [9]

$$f_{q_m}(q_m) = \frac{q_m}{4\sigma^4} \exp\left(-\frac{q_m}{2\sigma^2}\right) \quad q_m \geq 0 \tag{29}$$

and

$$F_{q_m}(q_m) = 1 - \left(1 + \frac{q_m}{2\sigma^2}\right) \exp\left(-\frac{q_m}{2\sigma^2}\right) \quad q_m \geq 0 \tag{30}$$

After considerable algebraic manipulation, the probability of bit error is given by

$$P_b = \frac{4 + 3\beta}{8 + 12\beta + 6\beta^2 + \beta^3} \tag{31}$$

where $\beta = SNR = s_0^2/\sigma_0^2$. This result agrees with that in [7].

3.2. *Self-normalised diversity combining*

Self-normalised (SN) diversity combining [6, 10], (also called normalised-envelope detection (NED)) is achieved by dividing the z_{mi} on each hop by the sum of the hop envelope values. This normalises the z_{mi} to

$$\hat{z}_{mi} = \frac{z_{mi}^{\alpha}}{\sum_{m=1}^{M} z_{mi}^{\alpha}} \tag{32}$$

where $\alpha = 1$ or 2. The metric is formed by summing these values,

$$q_m = \sum_{i=1}^{L} \hat{z}_{mi} \tag{33}$$

This is effectively linear diversity combining with adaptive weighting. SN combining has been shown to be effective against both noise and multitone jamming, and in broadband jamming the performance is similar to linear combining [2, 6, 11].

3.3. *Hard decision majority vote*

With hard decision majority vote (HDMV) combining, a decision is made on the symbol received for each hop. If the z_{mi} are ranked according to

$$z_{k_1 i} \le z_{k_2 i} \le \ldots \le z_{k_{M-1} i} \le z_{k_M i}, \quad i = 1, 2, \ldots, L \tag{34}$$

then $z_{k_M i}$ is declared the received symbol on the i-th hop, and the bin with the largest number of $z_{k_M i}$ determines the received symbol. If $f(z_{mi}) = 1$ for the largest z_{mi} on each hop ($z_{k_M i}$), and zero otherwise, then the metric is given by (20). HDMV combining has been shown to be ineffective against jamming [12, 13]. This poor performance is largely a result of rejecting most of the information contained in the $L \times M$ matrix of values.

3.4. *Moments methods diversity combining*

This class of methods uses moments of the values in each bin to produce a metric. It was developed to exploit the combinatorial properties of a tone jammed MFSK signal by subtracting the effects of the interference [13]. Three methods have been developed, the fourth and second moment (4 – 2M) method, with metric

$$q_m = 2\,\eta_{2m}^2 - \eta_{4m} \tag{35}$$

the second-and-first moment (2 – 1M) method, with metric

$$q_m = 2\,\eta_{1m}^2 - \eta_{2m} \tag{36}$$

and the first-and-half moment method (1 – 1/2M), with metric

$$q_m = 2\,\eta_{1_{\frac{1}{2}}m}^2 - \eta_{1m} \tag{37}$$

where the estimate of the k-th moment, η_{km}, is given by

$$\eta_{km} = \frac{1}{L} \sum_{i=1}^{L} z_{mi}^k \tag{38}$$

Unlike most other methods, these metrics require the calculation of the difference of two other metrics. With little or no interference, the result is similar to square-law or linear combining. However, when interference such as multitone jamming is present, this subtraction produces a metric which is small or negative in the non-signal bins, which effectively eliminates the interference.

As an example of performance analysis, consider $L = M = 2$ and Rayleigh fading. The decision metric for the 2 – 1M and 4 – 2M methods becomes

$$q_m = z_{m1}\, z_{m2} \tag{39}$$

Define a variable $v = z_{m2}$. The joint pdf of q_m and v is found from the joint pdf of z_{m1} and z_{m2}. Because of the independence of z_{m1} and z_{m2}, the joint pdf of z_{m1} and z_{m2} is the product of the individual pdfs. Thus, the joint pdf is

$$f_{z_{m1}, z_{m2}}(z_{m1}, z_{m2}) = \frac{z_{m1}\, z_{m2}}{\sigma^4} \cdot \exp\left(\frac{-z_{m1}^2 - z_{m2}^2}{2\,\sigma^2}\right) \quad z_{m1} \ge 0,\ z_{m2} \ge 0 \tag{40}$$

The magnitude of the Jacobian of the transformation from (z_{m1}, z_{m2}) to (q_m, v) is

$$\left| J(z_{m1}, z_{m2}) \right| = v \tag{41}$$

The joint pdf of q_m and v is [14]

$$f_{q_m, v}(q_m, v) = \frac{f_{z_{m1}, z_{m2}}(z_{m1}, z_{m2})}{\left| J(z_{m1}, z_{m2}) \right|} \tag{42}$$

where $z_{m1} = q_m / v$ and $z_{m2} = v$. Thus, substituting (40) and (41) into (42),

$$f_{q_m, v}(q_m, v) = \frac{q_m}{q\,\sigma^4} \exp\left(\frac{-\left(\frac{q_m}{v}\right)^2 - v^2}{2\sigma^2}\right) \quad q_m \ge 0,\ v \ge 0 \tag{43}$$

The pdf of q_m can be found by integrating (43) with respect to v,

$$f_{q_m}(q_m) = \int_0^{\infty} \frac{q_m}{v\,\sigma^4} \exp\left(\frac{-\left(\frac{q_m}{v}\right)^2 - v^2}{2\sigma^2}\right) \mathrm{d}\,v \qquad q_m \ge 0 \tag{44}$$

Simplifying [15],

$$f_{q_m}(q_m) = \frac{q_m}{\sigma^4} K_0\left(\frac{q_m}{\sigma^2}\right) \qquad q_m \ge 0 \tag{45}$$

where $K_0(\,)$ is the zeroth-order modified Bessel function. By integrating (45), the cdf of q_m can be found as

$$F_{q_m}(q_m) = \int_0^{q_m} f_{q_m}(x)\, \mathrm{d}\,x \qquad q_m \ge 0 \tag{46}$$

Simplifying [16],

$$F_{q_m}(q_m) = 1 - \frac{q_m}{\sigma^2} K_1\left(\frac{q_m}{\sigma^2}\right) \qquad q_m \geq 0 \tag{47}$$

where $K_1(\,)$ is first-order modified Bessel function.

The bit-error probability, P_b, for binary NCFSK can be found from

$$P_b = 1 - \int_0^\infty F_n(q)\, f_{sn}(q)\, \mathrm{d}q \tag{48}$$

$$= \int_0^\infty \frac{q^2}{\sigma_n^4 \sigma_T^2} K_0\left(\frac{q}{\sigma_T^2}\right) K_1\left(\frac{q}{\sigma_n^2}\right) \mathrm{d}q \tag{49}$$

$$= \left(\frac{\sigma_n}{\sigma_T}\right)^4 {}_2F_1\left(2, 1; 3; 1 - \left(\frac{\sigma_n}{\sigma_T}\right)^4\right) \tag{50}$$

$$= \left(\frac{\sigma_n}{\sigma_T}\right)^4 \sum_{k=0}^{\infty} \frac{1}{k+2} \left(1 - \left(\frac{\sigma_n}{\sigma_T}\right)^4\right)^k \tag{51}$$

$$= \frac{\left(\frac{\sigma_n}{\sigma_T}\right)^4}{\left(1 - \left(\frac{\sigma_n}{\sigma_T}\right)^4\right)^2} \left(4 \ln\left(\frac{\sigma_T}{\sigma_n}\right) + \left(\frac{\sigma_n}{\sigma_T}\right)^4 - 1\right) \tag{52}$$

where $F_n(\,)$ is the cdf of q_m with only noise present, $f_{sn}(\,)$ is the pdf of q_m with signal plus noise present, and ${}_2F_1(,;;)$ is the Gauss hypergeometric function.

3.5. *Order statistics diversity combining*

The use of order statistics (OS) for diversity combining requires the sorting of the L values in each bin [11]

$$z_{ml_1} \leq z_{ml_2} \leq \ldots \leq z_{ml_{L-1}} \leq z_{ml_L} \qquad m = 1, 2, \ldots, M \tag{53}$$

z_{ml_1} is referred to as the smallest OS of the m-th bin, and is referred to as the largest OS of the m-th bin. The i-th order statistic can be chosen as the decision metric in each bin

$$q_m = z_{ml_i} \tag{54}$$

Median filtering is a special case of (54) where l_i is equal to $\lceil L/2 \rceil$.

As an alternative, a combination of $1 < k < L$ order statistics can be used to determine the decision metric, i.e., the sum of the 1st to k-th ordered values

$$q_m = \sum_{i=1}^{k} z_{ml_i} \tag{55}$$

Note that if $k = L$ the result is just linear combining.

In [11, 17] these order statistic methods were investigated, and the results compared in both noise and multitone jamming with other methods. The results indicated that the largest and smallest of the order statistics should be avoided as unreliable.

3.6. *OS-NED diversity combining*

To improve the multitone jamming performance of NED, a concatenation of OS and NED has been considered. To justify this combination, consider the effect of ordering the values in each bin. Ordering groups the jamming or interference tones together as the largest of the OS values. If these ordered values are then normalised as modified hops, their amplitudes are reduced significantly. If a jammer were to increase the amplitude of the jamming tones by decreasing the number of tones, the performance of OS-NED combining would be improved, so the effectiveness of partial-band jamming or interference is nullified. The lower order statistic hops are emphasized since by definition their values are small. They have a greater role in the metric calculation, but any jamming or interference should be less dominant on these modified hops. Thus the OS and NED methods are complementary.

With this method, OS processing is done first to rank the z_{mi}, (53), then the ranked values are normalised to

$$\hat{z}_{ml_i} = \frac{z_{ml_i}}{\sum_{m=1}^{M} z_{ml_i}} \tag{56}$$

Clearly the more interference that exists on each modified hop, the larger is $\sum_{m=1}^{M} z_{ml_i}$, and therefore the greater is the normalisation achieved, so this method adapts to changes in the interference pattern and levels. The metric is formed by summing these modified values in each bin

$$q_m = \sum_{i=1}^{L} \hat{z}_{ml_i} \tag{57}$$

As a means of improving the performance of HDMV, the OS and HDMV methods can be concatenated to produce OS-HDMV combining. Although this method also reduces the effectiveness of partial-band jamming and interference, and is an improvement over HDMV combining alone, the performance is worse than OS-NED combining.

3.7. *Nonparametric diversity combining*

Rank sum diversity combining is a nonparametric method (as is HDMV). In this case, the LM values are first ranked

$$z_1 \le z_2 \le \ldots \le z_p \le \ldots \le z_{L-1} \le z_{LM} \tag{58}$$

and then simply replaced by their rank values [18]

$$\hat{z}_{mi} = p \tag{59}$$

where p represents the position of z_{mi} in the ranked list (58). The ranks in each of the M bins are then summed to obtain the decision metrics.

A similar method is hop rank sum. In this case, the M values on each hop are ranked

$$z_{k_1 i} \le z_{k_2 i} \le \ldots \le z_{k_p i} \le \ldots \le z_{k_{M-1} i} \le z_{k_M i} \qquad i = 1, 2, \ldots, L \tag{60}$$

Note that this is the same as (34). The z_{mi} are then replaced by their positions in the ranked list (60)

$$\hat{z}_{mi} = (k_p)\, i \tag{61}$$

where $k_p i$ denotes the rank of z_{mi}.

It was shown in [6] that rank type receivers can provide substantial performance improvements in partial-band jamming. However, their performance is poor in fading and AWGN.

4. PERFORMANCE RESULTS

In this section, the performance of the diversity combining methods in noise and multitone jamming is compared with that in Rayleigh fading. Results are given only for higher bit error rates because error correction coding provides a more efficient means of improving performance below a *BER* of $\approx 10^{-3}$ [19]. The purpose of diversity is to reduce the *BER* to a level where standard coding techniques can be effective.

4.1. *AWGN and multitone interference*

To provide a benchmark, the probability of bit error, P_b, given by (11) for $\rho = 1$ and the worst case ρ is plotted in Fig. 2 for $M = 2$, 4, 8 and 16. Note that the relationship between E_h/J_O and P_b is degraded from exponential to linear. Diversity combining has been shown to help improve performance by eliminating the effectiveness of partial band jamming, thus forcing a jammer to resort to broadband jamming [17].

For the following simulations, receiver noise at a level of $E_h/N_O = 13.35$ dB was added, and the data signalling was chosen to be 8-ary FSK. The SJR was set to $E_h/J_O = 0.0$ dB. This very low SJR results in a *BER* of 0.385 without diversity ($L = 1$), which cannot be effectively reduced with standard error correction techniques [20, 21]. To aid in identifying the combining methods, the abbreviations and linestyles used for the methods are given in Table 1.

Table 1 - *Abbreviations for the diversity Combining Methods.*

Abbreviation	Method	Linestyle
4 – 2M	Fourth and second moment	- - - - - - - -
2 – 1M	Second and first moment	————
1 – 1/2M	First and one half moment	- - - - - -
Square-law	Square-law	- - - - - -
Linear	Linear	————
NED	Normalised envelope detection	- - - - - -
Median	Median	- - - - - - - -
HDMV	Hard decision majority vote	————
OS-NED	Order Statistic-NED	- - - - - - - -
RS	Rank-sum	
HRS	Hop rank sum	
OS-HDMV	Order Statistic-HDMV	

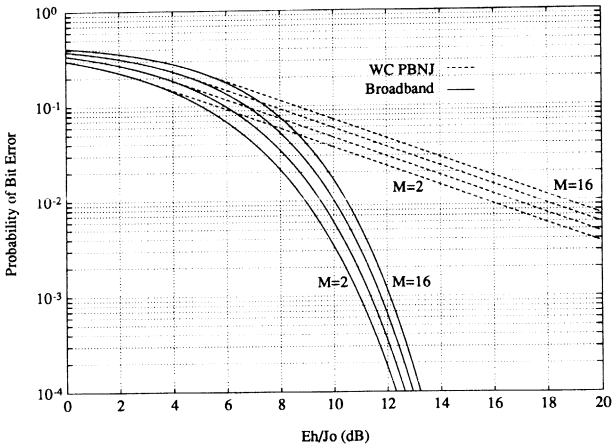

Fig. 2 - Performance of M-ary NCFSK in broadband and worst case partial band noise jamming, $M = 2$, 4, 8 and 16.

The performance of nine combining methods, NED, 4 – 2M, 2 – 1M, 1 – 1/2M, linear, square-law, median, OS-NED and HDMV, in broadband AWGN is given in Fig. 3. As can be seen, all methods except for median have a linear relationship between L and $\log 10(BER)$. Therefore curve fitting with the polynomial

$$aL + b$$

can be used to obtain the performance for any value of L. The coefficients a and b are given in Table 2. The *BER* is then given by the following expression

$$BER = 10^{aL+b} \tag{62}$$

The value for $L = 1$ should be the same in all cases, but

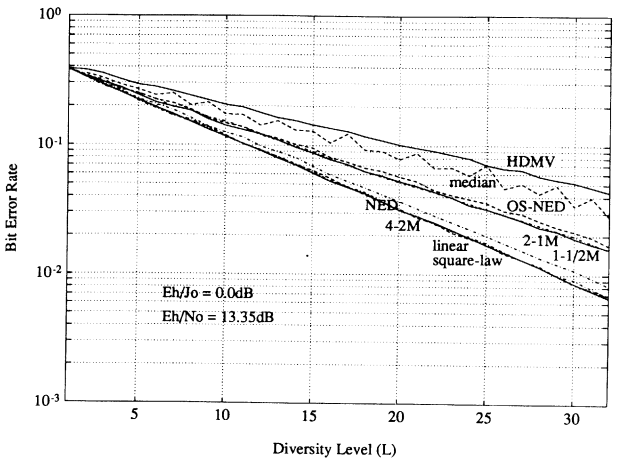

Fig. 3 - Performance of nine diversity combining methods in noise jamming, $E_h/J_O = 0.0$ dB, $E_h/N_O = 13.35$ dB and $M = 8$.

differs slightly because of the statistical variability of the simulations. Analytically, the *BER* at $L = 1$ is 0.385 and $\log_{10}(0.385) = -0.415$. Therefore (62) can be written as

$$BER = 10^{a(L-1)-0.415} \tag{63}$$

Table 2 - *Fitted Curve Coefficients for AWGN Performance.*

Method	*a*	*b*
Linear	−0.0564	−0.367
4−2M	−0.0564	−0.363
Square-law	−0.0559	−0.369
NED	−0.0535	−0.365
OS-HDMV	−0.0505	−0.353
RS	−0.0481	−0.358
1−1/2M	−0.0445	−0.382
2−1M	−0.0443	−0.390
HRS	−0.0430	−0.357
OS-NED	−0.0428	−0.389
Median (even)	−0.0355	−0.398
Median (odd)	−0.0323	−0.394
HDMV	−0.0307	−0.375

The relative performance of the 12 methods can easily be seen from Table 2, which is arranged from best to worst in order of decreasing slope, *b*. The first 4, linear to NED, are very close in performance. NED is sometimes used as a benchmark since it performs well against a variety of interference types. From Fig. 3, it is seen that at $L = 32$, all methods have a $BER < 0.05$, and the best performers a $BER < 0.007$, an impressive achievement considering the *BER* for $L = 1$ is 0.385. HDMV and median combining have the worst performance because they use little of the information contained in the z_{mi}.

The corresponding performance of the nine methods in multitone jamming is given in Fig. 4. In this case, the *BER* performance is much more diverse. HDMV, 4−2M and square-law combining are ineffective and their performance is much worse than NED. Linear is again similar to NED, while median combining is now substantially better. Next are the 2−1M, 1−1/2M and OS-NED methods, respectively.

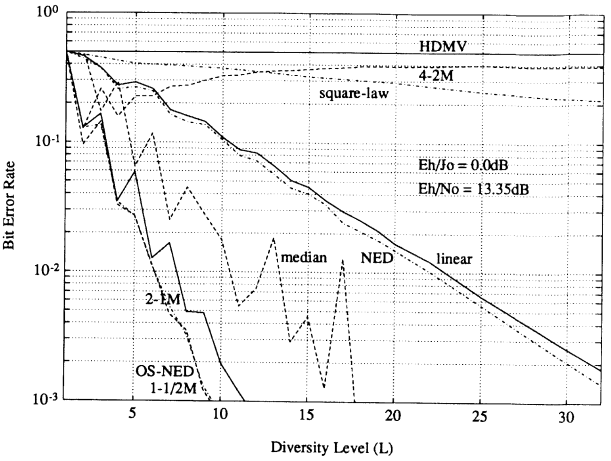

Fig. 4 - Performance of nine diversity combining methods in multitone jamming, $E_h/J_O = 0.0$ dB, $E_h/N_O = 13.35$ dB and $M = 8$.

It should be noted that linear combining may be susceptible to partial-band jamming (and therefore multi-user interference), as are the moment methods to some extent. Therefore the performance of these techniques under changing jammer strategies or interference patterns may be compromised. In view of these results, the best overall, or most robust methods, are NED and RS, followed by linear, 2−1M, 1−1/2M and OS-NED. It should be noted that those methods which perform well against Houston MT jamming can be expected to also be effective against multi-user interference.

4.2. *Performance in Rayleigh fading*

Although diversity combining can be employed to counteract jamming and interference with great success, *M*FSK performance can also be affected by fading, as shown in Fig. 5. This figure shows the performance with Rayleigh fading and worst case partial band noise jamming with no diversity. The relationship between E_h/J_O and P_b is approximately linear, as in Fig. 2, even though the jamming is now broadband. It is now shown that diversity combining can also improve the performance in fading.

For $L = 2$, Figs. 6 and 7 compare the results in Rayleigh fading for $M = 2$ and $M = 8$, respectively. From these, it can be seen that square-law combining is best,

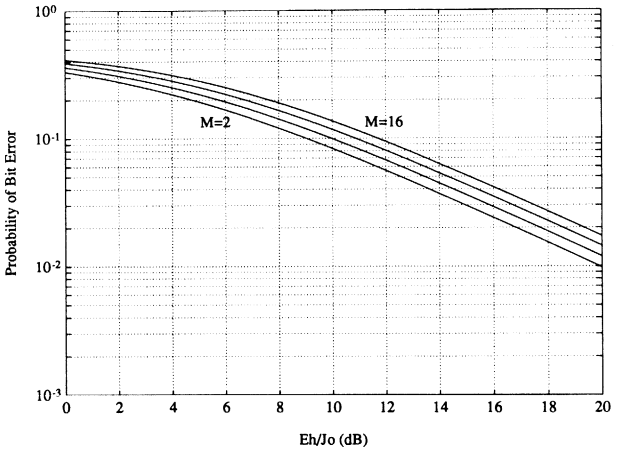

Fig. 5 - Performance of M-ary NCFSK in worst case partial band noise jamming and Reyleigh fading, M = 2, 4, 8 and 16.

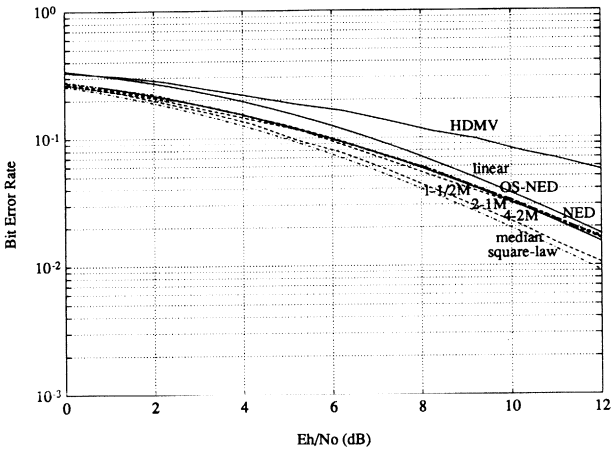

Fig. 6 - Performance of nine diversity combining methods in Rayleigh fading, M = 2 and L = 2.

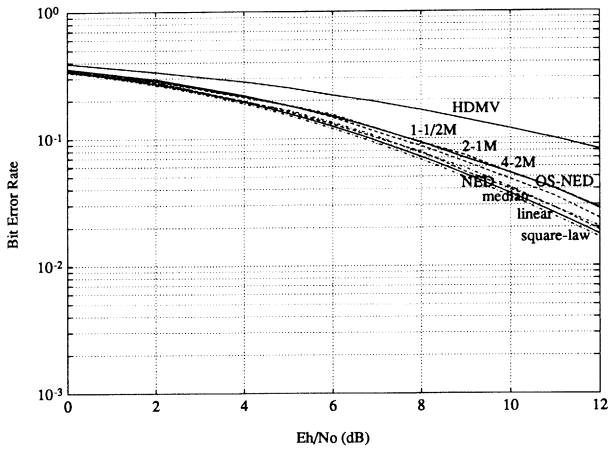

Fig. 7 - Performance of nine diversity combining methods in Rayleigh Fading, M = 8 and L = 2.

as expected since it is the optimum combining method in Rayleigh fading, followed by median. These methods were two of the worst in jamming. For M = 8, linear is the second best method, but for M = 2, it is the next worst after the HDMV. The moment and NED methods provide similar performance for M = 2, which is slightly better than linear, while for M = 8, the NED methods are somewhat better. Although choosing the best methods depends on M, there are no substantial differences when L = 2, except with linear combining.

The results for L = 4 and 8, and M = 8 are shown in Figs. 8 and 9. As L increases, the effectiveness of the 2-1M and 4-2M methods is lost, as was the case in MT jamming for the 4-2M method. Square-law, linear and NED remain the three best methods, respectively, for M = 8. OS-NED is the next best. As L increases, the performance of median combining approaches that of HDMV, and so is poor for large L.

Median combining is good in fading and MT jamming, but very poor in AWGN, while square-law is best in AWGN and fading, but near worst in MT jamming. Therefore, the choice of a combining method requires the determination of the types and severity of the channel impairments. Taking all results into account, both with jamming and fading, the best overall methods are NED, linear, OS-NED, 1-1/2M and median, in that order.

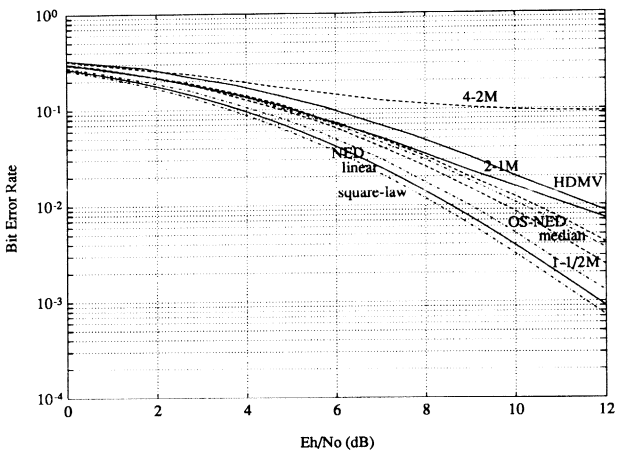

Fig. 8 - Performance of nine diversity combining methods in Rayleigh Fading, M = 8 and L = 4.

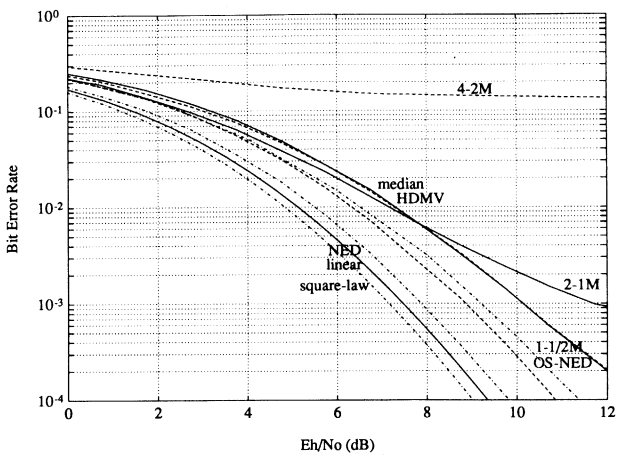

Fig. 9 - Performance of nine diversity combining methods in Rayleigh Fading, M = 8 and L = 8.

5. CONCLUSION

Several diversity combining methods which were developed to improve the jamming performance of fast frequency hopped noncoherent M-ary frequency shift keying have been investigated in Rayleigh fading. This represents a worst case fading environment. Based on performance results, several methods were identified as effective in both jamming and fading. These include linear and $1 - 1/2M$ combining which may not be robust in a changing interference environment. Two robust methods, NED and OS-NED, were also found to provide good performance in jamming and fading. Another method, median combining, achieves robustness at the expense of discarding information, and so is not as effective in AWGN jamming. However, it is a simple method which is very effective in multitone jamming.

While many of the methods presented require processing such as sorting the L values in each M-ary bin, or normalising the M values on each hop, they provide an increased robustness and should not be seriously affected by changing jammer strategies or interference levels.

Manuscript received on May 15, 1994

REFERENCES

[1] M. K. Simon, J. K. Omura, R. A. Scholtz, B. K. Levitt: *Spread spectrum communications*. Vol. II. Computer Science Press, Rockville, MD 1985.

[2] T. A. Gulliver, E. B. Felstead: *Anti-jam by fast FH NCMFSK - myths and realities*. IEEE Military Communications Conference, Boston, MA (USA). Oct. 1993, p. 187-191.

[3] J. K. Omura: *Variable data bit rate with a fixed hop rate noncoherent FH/MFSK system*. International Telemetering Conference, Oct. 1981, p. 1445-1463.

[4] R. E. Ziemer, R. L. Peterson: *Digital communications and spread spectrum systems*. MacMillan, New York 1985.

[5] S. W. Houston: *Modulation techniques for communication, part 1: tone and noise jamming performance of spread spectrum M-ary FSK and 2, 4-ary DPSK waveforms*. IEEE NAECON, 1975, p. 51-58.

[6] T. A. Gulliver, E. B. Felstead, R. E. Ezers, J. S. Wight: *A unified approach to time diversity combining for fast frequency hopped NCMFSK*. IEEE International Symposium on Spread Spectrum Techniques and Applications. Oulu (Finland). July 1994, p. 303-308.

[7] J. N. Pierce: *Theoretical diversity improvement in frequency-shift keying*. "Proceedings of the IRE", Vol. 46, May 1958, p. 903-910.

[8] P. M. Hahn: *Theoretical diversity improvement in multiple frequency-shift keying*. "IRE Transactions on Communications Systems". Vol. COM-10, June 1962, p. 177-184.

[9] J. G. Proakis: *Digital communications*. McGraw-Hill, New York 1983.

[10] K. S. Gong: *Performance of diversity combining techniques for FH/MFSK in worst case partial band and multi-tone jamming*. IEEE Military Communications Conference, Boston, MA (USA). Oct. 1983, p. 17-21.

[11] T. A. Gulliver: *New diversity combining techniques for improving the performance of fast frequency hopping*. International Conference on Advances in Communication and Control Systems, Victoria, BC (Canada). Oct. 1991, p. 72-85.

[12] J. S. Bird, E. B. Felstead: *Antijam performance of fast frequency-hopped M-ary NCFSK - an overview*. "IEEE Journal on Selected Areas in Communications", Vol. SAC-4, Mar. 1986, p. 216-233.

[13] T. A. Gulliver, E. B. Felstead: *Moment methods for diversity combining of fast frequency hopped noncoherent MFSK*. Queen's Symposium, Kingston, ON (Canada), May 1990, p. 12-15.

[14] A. Papoulis: *Probability, random variables, and stochastic processes*. McGraw-Hill, New York 1984.

[15] I. S. Gradshteyn, I. M. Ryzhik: *Table of integrals, series, and products*. Academic Press, San Diego 1980.

[16] M. Abramowitz, I. A. Stegun: *Handbook of mathematical functions*. Dover, New York 1964.

[17] T. A. Gulliver: *Order statistic diversity combining for worst case noise and multitone jamming*. IEEE Military Communications Conference, McLean, VA (USA). Nov. 1991, p. 385-389.

[18] R. Viswanathan, S. C. Gupta: *Nonparametric receiver for FH-MFSK mobile radio*. "IEEE Transactions on Communications". Vol. COM-33, Feb. 1985, p. 178-184.

[19] T. A. Gulliver: *Diversity combining and Reed-Solomon coding for fast frequency hopped noncoherent MFSK*. IEEE Military Communications Conference, Monterey, CA (USA). Sept., Oct. 1990, p. 111-115.

[20] E. B. Felstead, T. A. Gulliver: *Improving the ECCM performance of fast frequency hopping by diversity combining*. AGARD AVP Symposium on ECCM for Avionics Sensors and Communication Systems, Ottobrunn (Germany). Oct. 1990, p. 28.1 - 28.10.

[21] W. E. Stark: *Coding for frequency-hopped spread-spectrum communication with partial-band interference Part II: Coded performance*. "IEEE Transactions on Communications", Vol. COM-33, Oct. 1985, p. 1055-1056.

DS-CDMA Outage Performance Over a Mobile Satellite Channel

B. R. Vojcic, R. L. Pickholtz
Dept. of EECS, George Washington University
Washington, D.C. 20052 - USA
L. B. Milstein
Dept., University of California at San Diego
La Jolla, CA92093 - USA.

Abstract. A DS CDMA satellite uplink with power control error is considered. CDMA system performance is normally interference limited, and, in an additive, white, Gaussian noise channel, with many users, sufficient processing gain, and effective power control, individual users typically experience the average performance over all users. In this case, the other users appear as the equivalent of additional Gaussian noise and each user experiences the same environment. An alternative measure of performance under fading conditions is the probability of outage. For coded signals, the fading must be averaged over all the symbols in the code word. For properly interleaved signals and i.i.d. Rayleigh fade statistics, the average must be performed over a chi-squared variate. The probability of outage, defined as the probability that the decoded bit error rate exceeds a specified threshold, is monotonic with the probability that the chi-squared variate is less than a specified threshold. We derive upper and lower bounds on the outage probability for soft decision decoding.

1. INTRODUCTION

CDMA system performance is normally interference limited, and, in an additive, white, Gaussian noise channel, with many users, sufficient processing gain, and effective power control, individual users experience the average performance over all users. In this case, the other users appear as the equivalent of additional Gaussian noise and each user experiences the same environment. Under fading channel conditions, an alternative measure of performance is the probability of outage. The easiest way to look at this is from the point of view of a user who is experiencing fading (usually accompanied by shadowing loss). This user observes the bit error rate (*BER*) of the decoded signal to vary from epoch to epoch. For the sake of simplicity, suppose the epoch is the duration of a code word. Obviously, the variation is due to both the random sample and the statistics of the fading. If the epoch is sufficiently long, the dominant effect is due to fade statistics. The observed *BER* is then itself the sample of a random variable. The user would like to know the percentage of time (epochs) that the *BER* is larger than some acceptable threshold.

Thus, suppose that the acceptable *BER* with additive, white, Gaussian noise alone is 10^{-3} in a fading condition, one might expect that the decoded *BER* will vary, and the user might be interested in the probability that the *BER* is greater than 10^{-2}. In this paper, we show how to map this problem into an equivalent one by first establishing a monotonic relationship between the above probability and the probability that the combined fade statistic over the epoch is less than some corresponding threshold. For sufficient interleaving, we may assume that the fading is i.i.d. for each coded symbol. Next, since the *BER*, conditioned on the fading, is a monotonic function of the sum of squares of the fade amplitudes, we need only to examine the statistics of this latter variable. We assume that the fading is dominated by a Rayleigh distribution, so that the statistics of the sum of squares is chi-squared.

In this paper, we consider the outage performance of a coded DS CDMA system operating over a mobile satellite channel. In addition to being an alternative performance measure of interest for fading mobile channels, the probability of outage may, in some instances, admit a simpler analytical analysis than the average bit error

rate. Also, it is of interest to compare the probability of outage with the corresponding average probability of error results presented in [1].

The paper is organized as follows. In the next section, the system model for the uplink of a mobile DS CDMA satellite system with power control error is outlined. In section 3, the analysis is given for convolutionally encoded DS CDMA, and upper and lower bounds on the outage are derived for soft decision Viterbi decoding. In section 4, numerical results are presented and compared to the average probability of error performance. Finally, our conclusions are presented in section 5.

2. SYSTEM MODEL

The system and channel models are taken from [1]. A coded DS CDMA system with perfect interleaving and coherent reception is considered. Due to the large propagation delay in a satellite channel, an open loop power control mechanism is assumed. Since the uplink and the downlink operate in different frequency bands, in general, the open loop power control can only track the received power variations due to shadowing. The mobile adjusts its transmit power based on the level of the received power averaged over a sufficient time window to eliminate the effect of fast fading. Assume each spot beam has K simultaneously active users, and there are $J + 1$ spot beams which are simultaneously operating. Then the received signal for the uplink is given by

$$r(t) = \sum_{i=1}^{K} A_i R_i d_i(t-\tau_i) PN_i(t-\tau_i) \cdot \cos(\omega_0 t + \theta_i) + \sum_{i=K+1}^{(J+1)K} A_i R_i \beta_i d_i(t-\tau_i) \cdot PN_i(t-\tau_i) \cos(\omega_0 t + \theta_i) + n_w(t) \quad (1)$$

where $PN_i(t)$ is the spreading sequence of the i-th user, $d_i(t)$ is the binary data waveform of the i-th user, the sets $\{\tau_i\}$ and $\{\theta_i\}$ represent independent time delays and rf phases, respectively, and the $\{R_i\}$ correspond to independent flat fading on each user. The parameters $\{\beta_i\}$ represent the discrimination due to spot beam antenna patterns. Note that, for simplicity, it is assumed that all users in the spot beam of interest are illuminated with a gain of unity. Finally, $n_w(t)$ is additive white Gaussian noise of two-sided power spectral density $N_0/2$.

Due to the small multipath delay spread, the land mobile satellite channel is essentially frequency-nonselective [1]. It can be characterized by Rician fading in nonshadowed conditions. When shadowing is present, the received signal is characterized by Rayleigh/lognormal statistics [2]. That is, the slow shadowing process results in a time-varying mean received power which has a lognormal distribution, whereas the short term fading has a Rayleigh probability density function. As in [1], we assume an open loop power control mechanism which can efficiently neutralize the effect of slow fading. Then, the primary cause of performance degradation is due to the short term fading statistics.

The channel is assumed to be Rayleigh a fraction B of the time, corresponding to when the signal is shadowed, and Rician a fraction $1 - B$ of the time. That is, the probability density function of the fading amplitude, R, is given by the mixture density

$$f_R(R) = B\, 2\, c\, R\, e^{-cR^2} + (1-B) \cdot 2\, c\, R\, e^{\left[-c\left(R^2+1\right)\right]} I_0(2\, c\, R) \qquad R \geq 0 \quad (2)$$

where c represents the ratio of specular power to diffuse power and $I_0(x)$ is the modified Bessel function of the 1-st kind and 0-th order. In both coded and diversity performance calculations, the sum of squared signal amplitudes with independent fades enters the decision statistic. Hence, we define

$$U(d) = \sum_{i=1}^{d} R_i^2 \quad (3)$$

where, in the shadowed case, U is a central chi-squared distributed random variable with $2d$ degrees of freedom and probability density function (pdf) given by

$$f_U(u) = \frac{c^d\, u^{d-1}\, e^{-cu}}{(d-1)!} \qquad u \geq 0 \quad (4)$$

In the nonshadowed state, $U(d)$ in (3) has the following p.d.f. [3]:

$$f_U(u) = c \left(\frac{u}{d}\right)^{\frac{d-1}{2}} e^{-c(u+d)} I_{d-1}\left(2\, c \sqrt{d\, u}\right) \qquad u \geq 0 \quad (5)$$

where $I_{d-1}(x)$ is the modified Bessel function of 1-st kind and $(d-1)$-st order.

Even with open loop power control, some error will result due to a finite measurement window and shadowing dynamics. In the absence of measurement results on the open loop power control error for a mobile satellite channel, we assume an uniform p.d.f. of the amplitude variations due to the power control imperfection. That is, the i-th signal amplitude is $A_i = \lambda_i A$, where A is a constant and λ_i represents the power control error of the i-th user; for simplicity, for any user, λ is assumed uniformly distributed according to the following p.d.f.:

$$f_\Lambda(\lambda) = \frac{1}{2\gamma} \qquad 1-\gamma \leq \lambda \leq 1+\gamma \quad (6)$$

In general, it would be reasonable to assume different values of γ for shadowed and nonshadowed states [1]. Also, all the $\{\lambda_i\}$ are statistically independent.

3. PROBABILITY OF OUTAGE DERIVATION

There is no unique way to define outage. For non-coded signals and flat fading, where the probability of error for each symbol depends on the carrier-to-noise ratio, it is conventional to define the probability of outage as $P_r(R < R_t)$, where R_t is the threshold value on the fade statistic. To define the outage probability for a digital communication system which employs forward error correction, we start with a more general definition of outage probability, P_{out}, given by

$$P_{out} = \Pr\left(BER > BER_{th}\right) \tag{7}$$

where *BER* denotes the instantaneous probability of decoded bit error over a block of bits of length n, and BER_{th} corresponds to some specified maximum acceptable *BER*. This outage definition is analogous to the outage definition in either uncoded digital or analog communications, where signal-to-noise ratio (*SNR*) is used as a measure of performance degradation.

The outage probability will be different in the shadowed and the nonshadowed state, and will be dominated by the probability of outage in the shadowed state characterized by Rayleigh fading and denoted by $P_{out}(Rayleigh)$, so that

$$P_{out} \approx B\, P_{out}\left(Rayleigh\right) \tag{8}$$

Consequently, in this section, we concentrate on the outage performance in the shadowed state and, for simplicity, denote $P_{out}(Rayleigh)$ by P_{out}. For the sake of completeness, the outage probability in Rician fading, corresponding to the nonshadowed state, is derived in Appendix A.

Our intention is to establish an one-to-one relationship between the *SNR* and the corresponding *BER* performance, which will be used to obtain an estimate of P_{out}. In order to accomplish this, we use the well known union bound on the *BER* for a convolutionally coded binary phase shift keyed (BPSK) system, which is exponentially tight at low error rates and is given by [4]

$$BER \le \sum_{d=d_{min}}^{d_{max}(n)} a\,(d)\, P_2\,(d) \tag{9}$$

where $P_2(d)$ represents the pairwise error probability and $a(d)$ is the number of bit errors in all adversaries at distance d from the correct code word/sequence. The parameter $d_{max}(n)$ corresponds to the maximum distance between coded sequences of length n for a terminated convolutional code. For soft decision decoding in an additive white Gaussian noise channel, $P_2(d)$ is given by [5]

$$P_2\,(d) = Q\left(\sqrt{\frac{d}{\sigma_{tot}^2}}\right) \tag{10}$$

where σ_{tot}^2 is defined below and

$$Q\,(x) = \frac{1}{\sqrt{2\,\pi}} \int_x^{\infty} e^{-\frac{y^2}{2}}\, \mathrm{d}\, y \tag{11}$$

From (9) and (10), we can establish a relationship between the BER_{th} and the corresponding threshold *SNR*. More precisely, we define

$$X_t = \left(\frac{1}{\sigma_{tot}^2}\right)_t = F\left(BER_{th}\right) \tag{12}$$

where the function $F(\cdot)$ accounts for inverting (9) and (10).

Assuming that a power compensation factor p [5] is used to compensate for shadowing and fading ($p \ge c$) the conditional pairwise error probability under fading conditions is given by [1]

$$P_2\left(d \mid U\right) = Q\left(\sqrt{\frac{p\,\lambda^2\,U}{\sigma_{tot}^2}}\right) \tag{13}$$

where σ_{tot}^2 is given by [1]

$$\sigma_{tot}^2 = \frac{N_0}{2\,E_c} + \frac{I_0\,K}{3\,L}\left[(1-B)\left(1+\frac{1}{c}\right) + B\frac{p}{c}\left(1+\frac{\gamma^2}{3}\right)\right] \tag{14}$$

In (14), rectangular chips (in the time domain) are used, L is the processing gain per coded symbol, K is the number of simultaneous users per cell, I_0 is the ratio of the total multiple access interference to the multiple access interference within the cell of interest, B is the probability that a user is shadowed and E_c/N_0 is the ratio of energy per coded symbol to the noise power spectral density. We define the pairwise outage probability as the probability that the decoder will produce a pairwise error probability larger than P_{2t}, where P_{2t} corresponds to BER_{th}, according to (10). Now the pairwise probability of outage for two code words/sequences at distance d is given by

$$P_{2out}\left(d \mid \lambda\right) = \Pr\left(U \le \frac{2\,d\,X_t\,\sigma_{tot}^2}{p\,\lambda^2}\right) \tag{15}$$

which evaluates to

$$P_{2out}\left(d \mid \lambda\right) = 1 - e^{-\frac{a}{\lambda^2}} \sum_{k=0}^{d-1} \frac{1}{k!}\left(\frac{a}{\lambda}\right)^k \tag{16}$$

where

$$a = \frac{2\,c\,d\,X_t\,\sigma_{tot}^2}{p} \tag{17}$$

The unconditional pairwise outage probability, aver-

aged over the power control error, is found as

$$P_{2\text{out}}(d) = \frac{1}{2\gamma}\int_{1-\gamma}^{1+\gamma} P_{2out}(d \mid \lambda) f_{\Lambda}(\lambda)\, \mathrm{d}\lambda \tag{18}$$

which, after some algebra, reduces to

$$P_{2\text{out}}(d) = 1 - \frac{\sqrt{a}}{4\gamma}\sum_{k=0}^{d-1}\frac{1}{k!} I(a,k) \tag{19}$$

where

$$I(a,k) = \sum_{i=1}^{k-1}\left[a_1^{2\left(k-i-\frac{1}{2}\right)} e^{-a_1^2} - a_2^{2\left(k-i-\frac{1}{2}\right)} e^{-a_2^2}\right]\times$$

$$\prod_{j-1}^{i-1}\left(k-j-\frac{1}{2}\right) + \sqrt{\pi}\left[Q\left(\sqrt{2\,a_1^2}\right) - Q\left(\sqrt{2\,a_2^2}\right)\right]\times$$

$$\prod_{j-1}^{k-2}\left(k-j-\frac{1}{2}\right) \tag{20}$$

$$a_1 = \sqrt{a}/(1+\gamma), \quad a_2 = \sqrt{a}/(1-\gamma)$$

$$\text{and} \prod_{j=1}^{0}\left(k-j-\frac{1}{2}\right) = 1$$

A lower bound on the outage probability is simply

$$P_{\text{out}}^{l} = P_{2\text{out}}(d_{\min}) \tag{21}$$

To derive an upper bound on outage probability, we define *Out* as the outage event and define

$$A(i) = Q\left(\sqrt{\frac{p\lambda^2 U}{\sigma_{\text{tot}}^2}}\right) - Q\left(\sqrt{2\,i\,X_t}\right) \tag{22}$$

Define also events $E_i : A(i) > 0$, $i = d_{\min},\ldots, d_{\max}(n)$. Due to the monotonicity of $Q(x)$, the event E_i can be redefined as $E_i : U(i) < 2iX_t\sigma_{\text{tot}}^2/(p\lambda^2)$, $i = d_{\min},\ldots, d_{\max}(n)$, where $U(i)$ is defined by (3). A necessary condition for the event *Out* to occur is that at least one of the events E_i occurs. That is, the probability of outage can be upper bounded by the probability of the union of events E_i, $i = d_{\min},\ldots, d_{\max}(n)$. This can be expressed mathematically as

$$\Pr[Out] \le \Pr\left[\bigcup_{i=d_{\min}}^{d_{\max}(n)} E_i\right] \le \sum_{i=d_{\min}}^{d_{\max}(n)} \Pr[E_i] \tag{23}$$

Finally, since $\Pr[E_i] = P_{2\text{out}}(i)$, the upper bound on the outage probability can be written as

$$P_{\text{out}}^{u} = \sum_{d=d_{\min}}^{d_{\max}(n)} P_{2\text{out}}(d) \tag{24}$$

4. NUMERICAL RESULT

To get specific results, we will consider a rate 1/3 convolutional code with constraint length 8, which has $d_{\min}$ = 16 and $a(16)$ = 1; $a(18)$ = 24; $a(20)$ = 113; $a(22)$ = 287... [6]. To compare outage performance with average probability of error performance presented in [1], it is assumed that nonshadowed users operate in an AWGN channel and average power control is considered ($p = c$). The outage probability for a DS-CDMA system, versus the number of users, is shown in Figs. 1-3 for E_b/N_0 = 7 dB and the threshold *BER* of 0.05, 0.01 and 0.005, respectively. The corresponding set of curves for E_b/N_0 = 10 dB is given in Figs. 4-6. In Figs. 7-9 and 10-12, the outage probability versus the standard deviation of the power control error is shown for the three chosen values of the performance threshold, for 10 and 20 simultaneous users, respectively. Finally, some of the average probability of error results from [1] are repeated here for comparison. Specifically, the probability of error results in Fig. 13 correspond to the scenarios of Figs. 1-6, and the probability of error results in Fig. 14 can be compared with the outage results in Figs. 7-12. It can be seen that both outage and probability of error performance exhibit similar qualitative behavior. However, it should be noted that the outage behavior depends upon the chosen performance threshold. Specifically, by comparing the upper bounds on the probability of error in Fig. 13 with the upper bounds on the outage probability in Figs. 1-6, it can be seen that the capacity at *BER* = 10^{-3} corresponds to the outage probability of about 2% when the threshold probability of error is set to 0.01. The outage probabilities cor-

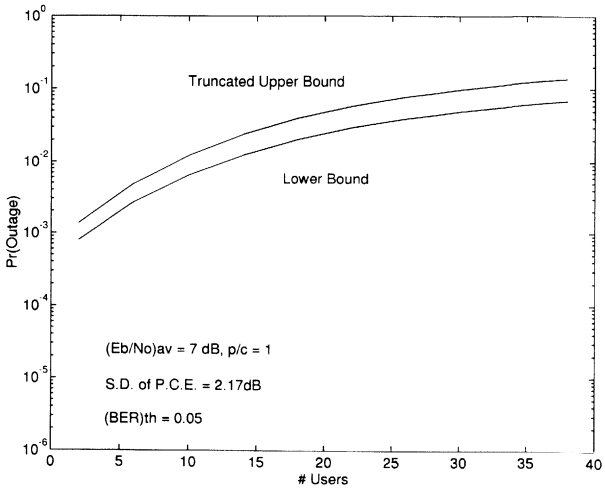

Fig. 1 - Outage probability versus number of users; average E_b/N_0 = 7 dB, $(BER)_{th}$ = 0.05.

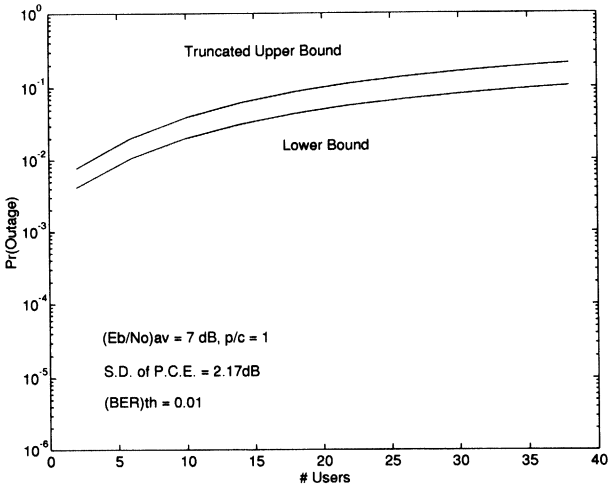

Fig. 2 - Outage probability versus number of users; average E_b/N_0 = 7 dB, $(BER)_{th}$ = 0.01.

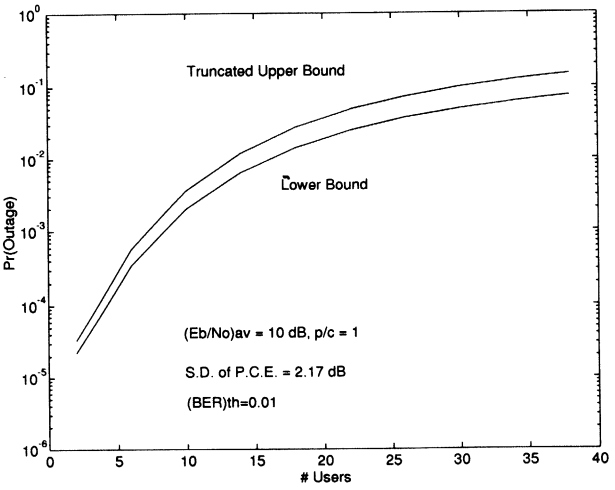

Fig. 5 - Outage probability versus number of users; average E_b/N_0 = 10 dB, $(BER)_{th}$ = 0.01.

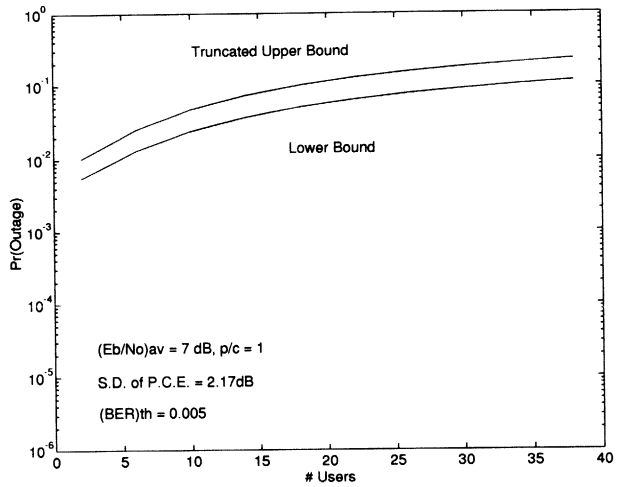

Fig. 3 - Outage probability versus number of users; average E_b/N_0 = 7 dB, $(BER)_{th}$ = 0.005.

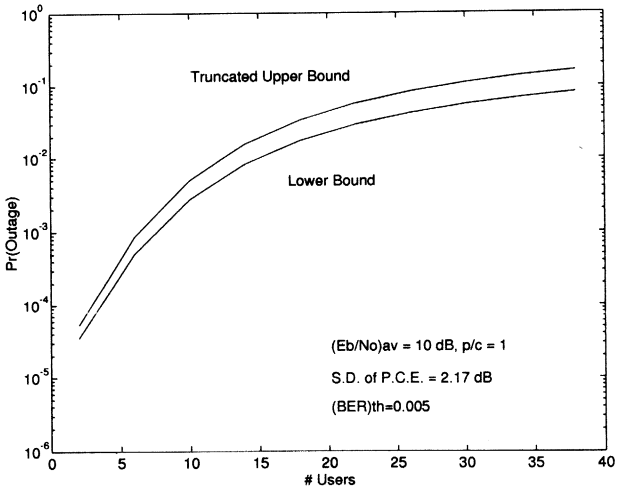

Fig. 6 - Outage probability versus number of users; average E_b/N_0 = 10 dB, $(BER)_{th}$ = 0.005.

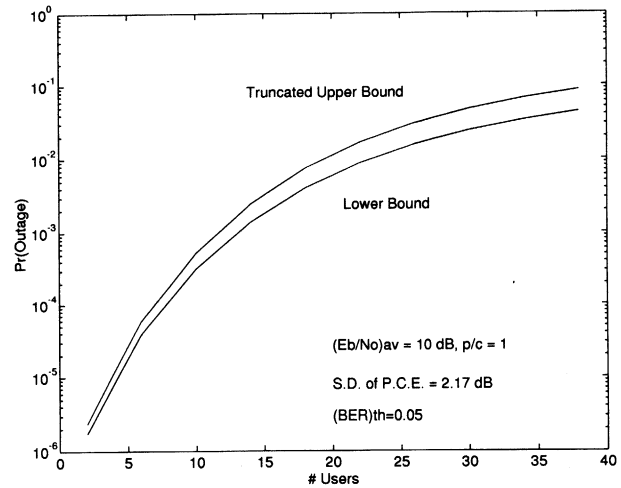

Fig. 4 - Outage probability versus number of users; average E_b/N_0 = 10 dB, $(BER)_{th}$ = 0.05.

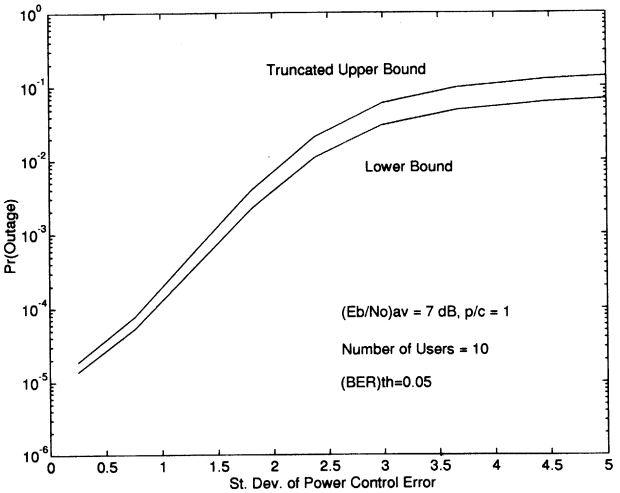

Fig. 7 - Effect of power control error on the probability of outage with 10 users, $(BER)_{th}$ = 0.05.

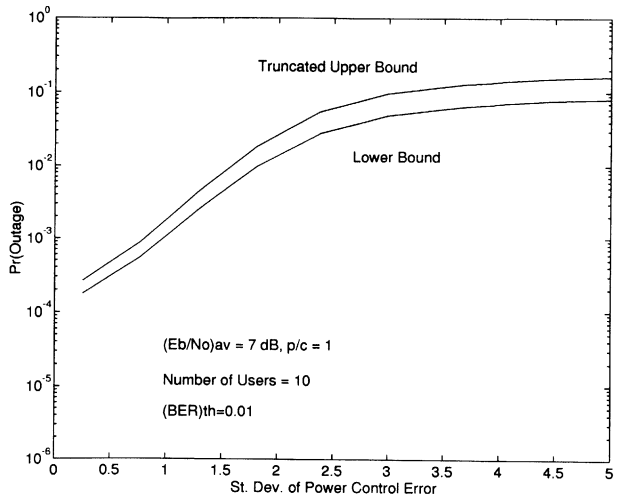

Fig. 8 - Effect of power control error on the probability of outage with 10 users, $(BER)_{th} = 0.01$.

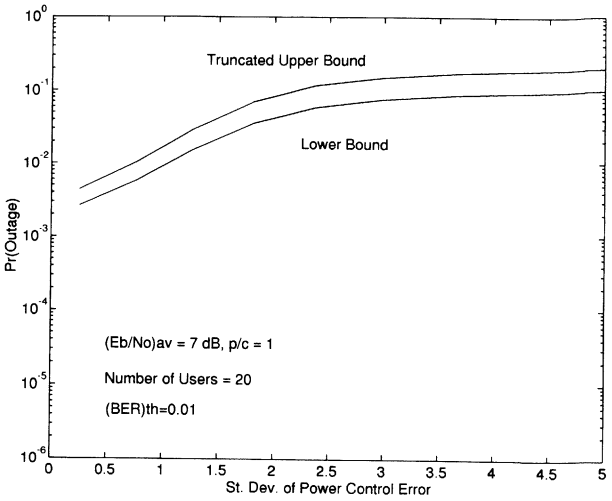

Fig. 11 - Effect of power control error on the probability of outage with 20 users, $(BER)_{th} = 0.01$.

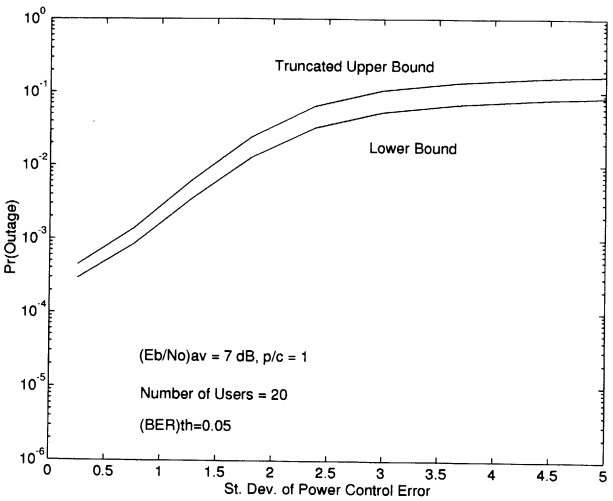

Fig. 9 - Effect of power control error on the probability of outage with 10 users, $(BER)_{th} = 0.005$.

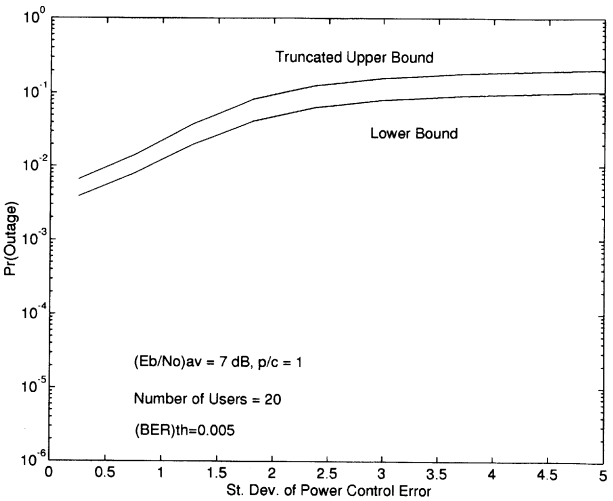

Fig. 12 - Effect of power control error on the probability of outage with 20 users, $(BER)_{th} = 0.005$.

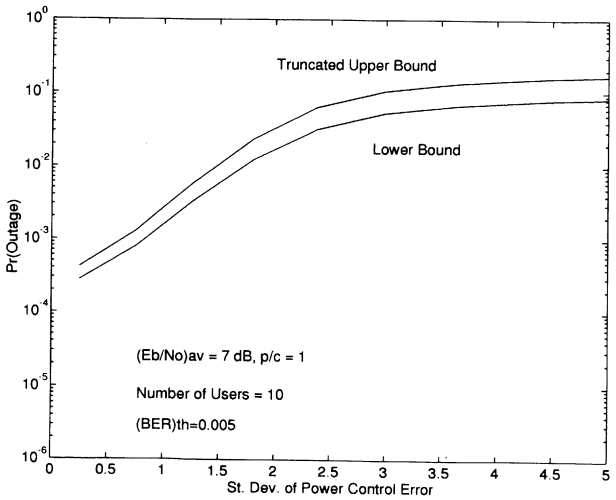

Fig. 10 - Effect of power control error on the probability of outage with 20 users, $(BER)_{th} = 0.05$.

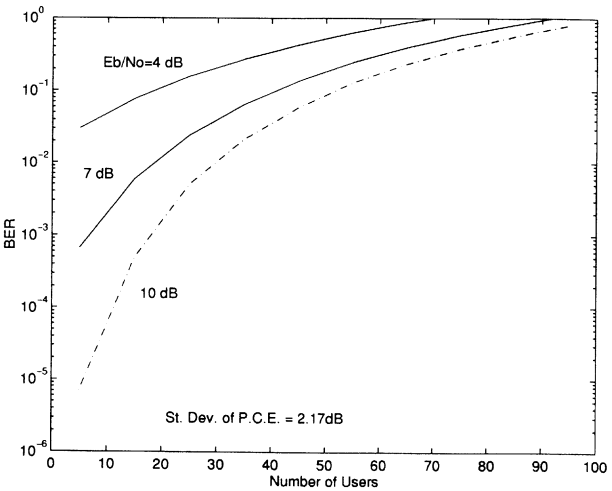

Fig. 13 - Average probability of error versus number of users.

responding to the threshold probability of error of 0.05 and 0.005 are slightly better and worse, respectively. Similar conclusions can be drawn up by comparing curves in Figs. 7 - 12 and those of Fig. 14, which demonstrate the sensitivity to the power control error.

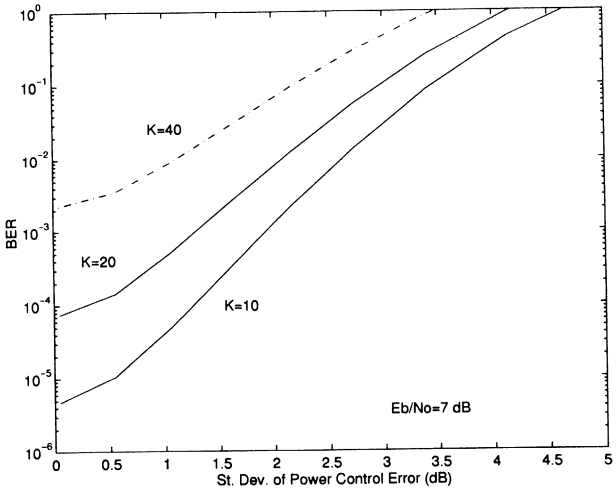

Fig. 14 - Average probability of error versus power control error.

5. CONCLUSIONS

In this paper, we examined the question of defining the probability of outage for a coded, fading signal. Specifically, we considered the uplink of a DS CDMA mobile satellite system. A relationship between the probability of *BER* exceeding an acceptable threshold, and the probability that the combined fade statistic (over an epoch) is less than a corresponding threshold, is established. The work demonstrates that reasonably good upper and lower bounds can be obtained. These bounds are available in closed form for both Rayleigh and Rician fading, although in the Rician case the pairwise outage probability is obtained in terms of infinite series. The outage probability exhibits the same qualitative behavior as does the average probability of error in a fading channel.

APPENDIX A
Outage Probability for Rician Fading

In this appendix, we derive the pairwise outage probability for the case of Rician fading. The cumulative probability distribution function of $U(d)$ is given by

$$F_U(u) = 1 - Q_d\left(\sqrt{2\,c\,d}, \sqrt{2\,c\,u}\right) \tag{25}$$

where $Q_d(u, v)$ is the Marcum Q-function of the d-th order, defined by

$$Q_d(u, v) = \int_v^\infty x\left(\frac{x}{u}\right)^{d-1} e^{-\frac{u^2+v^2}{2}} I_{d-1}(u\,x)\,\mathrm{d}\,x \tag{26}$$

and can be expressed as

$$Q_d(u, v) = Q_1(u, v) + e^{-\frac{u^2+v^2}{2}} \sum_{k-1}^{d-1} \left(\frac{v}{u}\right)^k I_k(u\,v) \tag{27}$$

where

$$Q_1(u, v) = e^{-\frac{u^2+v^2}{2}} \sum_{k=0}^{\infty} \left(\frac{u}{v}\right)^k I_k(u\,v) \quad v > u > 0 \tag{28}$$

and

$$I_k(x) = \sum_{i=0}^{\infty} \frac{(x/2)^{k+2i}}{i!(i+k)!} \tag{29}$$

Now, the conditional P_{2out} is given by

$$P_{\text{out}}(d \mid \lambda) = 1 - Q_d\left(\sqrt{2\,c\,d}, \sqrt{\frac{4\,c\,d\,X_t\,\sigma_{\text{tot}}^2}{\lambda^2}}\right) \tag{30}$$

which after some tedious algebra reduces to

$$P_{2\text{out}}(d \mid \lambda) = e^{-cd\left(1+\frac{a}{\lambda^2}\right)} \sum_{k=d}^{\infty} \sum_{i=0}^{\infty} \frac{(c\,d)^i}{i!(i+k)!} \cdot \left(c\,d\,\frac{a}{\lambda^2}\right)^{i+k} \tag{31}$$

where a is defined in (17). From (18) and (31),one can obtain

$$P_{2\text{out}}(d) = \frac{\sqrt{a_0}\,e^{-cd}}{4\gamma} \sum_{k=d}^{\infty} \sum_{i=0}^{\infty} \frac{(c\,d)^i}{i!(i+k)!}\, I(a_0, i+k) \tag{32}$$

where $a_0 = cda$ and $I(a_0, n)$ is defined by (20).

Acknowledgements

We would like to acknowledge the help and motivation provided to us by Dr. Ray Leopold and Dr. Carrie Devieux of Motorola Satellite Communications.

Manuscript received on May 5, 1994.

REFERENCES

[1] B. R. Vojcic, R. L. Pickholtz, L. B. Milstein: *Performance of DS-CDMA with imperfect power control operating over a low earth orbiting satellite link.* "IEEE Jour. on Sel. Areas in Communications", Vol. 12, No. 4, 1994, p. 560-567.

[2] E. Lutz et al.: *The land mobile satellite channel - recording, sta-*

tistics and channel model. "IEEE Trans. on Veh. Technology", Vol. 40, 1991, p. 375-386.

[3] J. G. Proakis: *Digital communications.* McGraw-Hill, New York, 1989.

[4] A. J. Viterbi, J. K. Omura: *Principles of digital communications.* McGraw-Hill, New York, 1979.

[5] B. R. Vojcic, L. B. Milstein, R. L. Pickholtz: *Power control versus capacity of a CDMA system operating over a low earth orbiting satellite link.* Proceedings of the Communication Theory Mini-Conference held in conjunction with Globecom'93, Houston (USA), November 1993, p. 40-44.

[6] J. P. Odenwalder: *Optimal decoding of convolutional codes.* Ph.D. Thesis, UCLA, 1979.

Performance Evaluation of Multi-Cell Direct-Sequence Microcellular Systems (1)

Chung-Ming Sun
Chung Shan Institute of Science and Technology
Lung Tang PO BOX 90008-16-27, Taiwan, R.O.C.
Andreas Polydoros
Communication Sciences Institute, Dept. of El. Eng.-Systems
University of Southern California, Electrical Engineering
Building 502, Los Angeles, CA 90089-2565 - U.S.A

Abstract. The performance of an asynchronous multi-cell Direct-Sequence Spread Spectrum Multiple-Access (DS/SSMA) system is evaluated in lineal microcells with flat Rician fading and shadowing. Both the Bit Error Rate (*BER*) of the uplink (i.e., the user to the base station) and the downlink (i.e., the base station to the user) are evaluated. We develop a new analytical model to evaluate the uplink performance which accounts for the user's spatial distribution, the chip waveform, the power control, and macro-selection diversity. On the downlink, since no power control is used, the desired signal follows a composite log-normal noncentral chi-square distribution. We propose an approximation method to reduce the computational complexity while still providing satisfactory precision. The analysis results show that the macro-selection diversity can reduce the other-cell interference effectively even for a channel with heavy shadowing. The Rician factor, the standard deviation of the shadowing, and the chip waveform have significant influence on the performance.

1. INTRODUCTION

The microcellular structure has been proposed for efficient spectrum utilization in cellular mobile and future Personal Communication Services (PCS). In microcellular systems, the antenna height of the Base Station (BS) is generally low (e.g., lamp post height), the cell size is small (from 0.2 to 1 km), and the transmitting power is typically a few tens of mW. Due to the short range of the communication link, a microcellular system may operate in Rician fading channel which has much less multipath fading effects than Rayleigh fading channel does in macrocells. Due to the low antenna height, the delay spread is shorter [1].

Because of its inherent anti-multipath and multiple access capabilities, spread spectrum technique, such as DS/SSMA, has been considered as a candidate for high capacity radio cellular systems. The performance of DS/SSMA systems in macrocells has been extensively evaluated in the literature, e.g., [2, 3, 6]. However, their performance in microcells requires further consideration because of the unique propagation characteristics of a microcellular environment. In [10], the Standard Gaussian Approximation (SGA) method [11] was used to compute the *BER* for Binary Phase-Shift-Keying (BPSK) signals with co-channel interference in two-dimensional (*area*) microcells.

In this paper, we study both the uplink and the downlink performance of multi-cell DS/SSMA systems in one-dimensional (*lineal*) microcells with shadowed Rician fading. On the uplink, we develop a new analytical model to evaluate the system performance. The basic approach is to evaluate the average *BER* for both BPSK and Differential Phase-Shift-Keying (DPSK) modulation schemes by employing the Improved Gaussian Approximation (IGA) method [11]. This model can take into account the user's spatial distribution, the chip waveform, the power control, and macro-selection diversity. We also analyze the downlink performance which usually receives less attention than that of the uplink. On the downlink, broadcast operation mode is assumed; a common message or several distinct messages are transmitted simultaneously from BS to different users. Thus, all signals from the same BS will undergo channel fading in common with respect to each specific

(1) This work was supported by Caltrans through the California PATH (Partners for Advanced Transit and Highways) of the University of California, under Agreement MOU#97 between the University of California and the University of Sout hern California.

user and they are different at different places within the cell. This is distinct from that on the uplink where each user experiences independent channel fading. Since no power control is used, the desired signal follows a composite log-normal noncentral chi-square distribution which has not been discussed in the literature. We propose an approximation method to reduce the computational complexity while providing satisfactory precision. The effect of macro-selection diversity on the performance is also investigated through the measure of relative other-cell interference.

The remainder of this paper is organized as follows. In section 2, we study the uplink performance. The analytical model is established. The effect of using the macro-selection diversity to reduce the Multiple-Access Interference (MAI) is investigated. The influence of the Rician factor, the standard deviation of the shadowing, and the chip waveform on the performance is also addressed. In section 3, we study the downlink performance. The proposed approximation method is described. The relative other-cell interference is defined as the performance measure. Finally, we conclude in section 4.

2. UPLINK PERFORMANCE ANALYSIS

In this section, we will evaluate the uplink *BER* performance by considering other-cell interference. We begin with descriptions of the radio channel, the transmitter, and the receiver models. Following that, we find the *BER* performance by using both IGA and SGA methods.

2.1. *System model*

A typical lineal microcellular layout for dense urban streets ([1]) and highways is shown in Fig. 1. The service area is segmented into sections and every section is called a cell. We assume that the BS is at the center of the cell, the cell length is $\mathcal{D}$, and the cell width is $\mathcal{H}$. The BS can distinguish individual users by assigning a unique spreading code to each of them. We assume that omni-directional antennas are employed and there are separate frequency bands for the uplink and the downlink (i.e., frequency division duplex). Furthermore, the frequency band on each link is reused in each cell. These assumptions imply that a given BS will experience interference from all users in the system, but not from other BS's. Similarly, any user in the system will experience interference from all BS's, but it does not experience interference from the transmissions of other users.

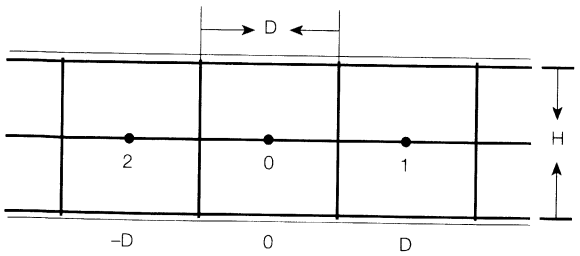

Fig. 1 - Lineal microcellular layout.

([1]) Based on the measurement results [7], the co-channel interference from parallel streets would be generally quite small compared to that from cells along the same street and thus can be ignored.

2.1.1. Channel model

The land mobile radio channel can be statistically characterized by three independent, multiplicative propagation mechanisms, namely, multipath fading, shadowing, and UHF groundwave propagation. Hence, the lowpass equivalent complex impulse response of the microcellular mobile radio channel, $h(t)$, is expressed as

$$h(t) = \sqrt{L_p(r)10^{X/10}}\,\gamma\, e^{j\phi}\,\delta(t-\tau) \tag{1}$$

where $L_p(r)$ is the propagation loss due to the groundwave propagation, with r denoting distance from the BS; $10^{X/10}$ represents the shadowing, with zero-mean random variable X accounting for the fluctuations of the received power around the propagation loss; γ is the Rician fading; and ϕ, τ are the random phase and propagation delay, respectively. The second moment of γ is normalized to be 1. In this model, the channel is assumed to be non-frequency selective for the following reasons. First, various studies have indicated that the delay spread of microcellular systems in an urban street environment is less than a few microseconds [1] and may be much less in a highway environment [4]. Thus, the returned signals from all paths cannot be resolved unless the system bandwidth is sufficiently large. Second, using this assumption may be interpreted as going after a worst-case analysis, since a frequency selective channel will not undergo the broad deep fades that the flat channel will [2]. The propagation loss can be described by [9]

$$L_p(r) = C_p\, r^{-a}\,(1 + r/g)^{-b} \tag{2}$$

where C_p is a constant, a and b are the propagation loss exponents, and g is the Fresnel break point of the attenuation curve.

The probability density function (pdf) of γ is

$$f_\gamma(y) = \frac{y}{\sigma_s^2}\exp\left(-\frac{y^2+\alpha^2}{2\sigma_s^2}\right) I_0\left(\frac{\alpha y}{\sigma_s^2}\right) U(y) \tag{3}$$

where $U(y)$ is a unit step function and $I_0(x)$ is the modified zero-order Bessel function. The Rician factor K (a model constant) is defined as the ratio of the specular component power to the Rayleigh scattered component power, i.e., $K = \alpha^2/(2\sigma_s^2)$. Since $E(\gamma^2) = \alpha^2 + 2\sigma_s^2 = 1$, it follows that $\alpha^2 = K/(K+1)$ and $\sigma_s^2 = 1/[2(K+1)]$, respectively.

2.1.2. Transmitted signal

Let $b_{kn}(t)$ be the data waveform of the n-th user in cell k. For BPSK modulation, $b_{kn}(t)$ is the information sequence, whereas for DPSK modulation, $b_{kn}(t)$ is the differentially encoded version of the n-th user's information sequence. The data signal, $b_{kn}(t)$, can be expressed as $b_{kn}(t) = \sum_{j=-\infty}^{\infty} b_j^{(kn)}\, p\,(t - jT)$, where T is the bit interval, $b_j^{(kn)}$ is the j-th data bit in the binary information sequence, and $p(t)$ ([1]) is a rectangular pulse whose value is equal to unity in $0 \le t \le T$ and zero elsewhere. The information sequence $b_j^{(kn)}$ is modeled as an i.i.d. sequence, taking on the values ± 1 with equal probability.

The spreading waveform, $a_{kn}(t)$, can be written as $a_{kn}(t) = \sum_{j=-\infty}^{\infty} a_j^{(kn)}\, \psi\,(t - jT_c)$, where $a_j^{(kn)}$ is the j-th chip of the kn-th user's signature sequence and $\psi(t)$ represents a chip pulse with arbitrary shape. We assume that each bit is encoded with η chips, i.e., $T = \eta T_c$ with η the familiar spreading ratio, and that perfect alignment exists between bits and chips. To make the computations independent of the choice of employed spreading sequences, the spreading code is assumed to be a sequence of i.i.d. random variables taking on the values ± 1 with equal probability. For an asynchronous DS/SSMA system, on the average, the random sequence code gives approximately the same analytical result as that of a deterministic code [6].

In this analysis, we assume that the power control employed by the system can only compensate for the propagation loss and the shadowing, but not for the fast-varying multipath fading. We also investigate the effect of macro-selection diversity on reducing the MAI. This macro-selection diversity is a technique in which the user is power controlled by the BS with the least attenuation. Therefore, its transmitted power will be proportional to this minimum attenuation and hence will produce the least interference to all other cell BS's [12]. Suppose that the set of BS's that the user can select is limited to the N_c nearest. Hence, the transmitted signal, $S_{kn}(t)$, of the n-th user in cell k can be expressed as

$$S_{kn}(t) = \sqrt{2P_0 \cdot \min_{j \in S_c}\left[\frac{1}{\Lambda_{kn}^{(j)}}\right]}\; a_{kn}(t)\, b_{kn}(t) \cos\left(w_c t + \theta_{kn}\right) \tag{4}$$

where $w_c = 2\pi f_c$ in which f_c is the common carrier frequency, P_0 is the nominal power set by the BS for the desired performance, θ_{kn} is the random phase of the modulator, $\Lambda_{kn}^{(j)}$ represents the propagation loss and the shadowing encountered by the user n in cell k communicating with the BS j, and S_c is the set containing the user's N_c nearest BS's.

([1]) This is modeled so for analytical convenience; note that the actual spectrum of the transmitted waveform (of a typically bandwidth-efficient type) is determined by the shape of the spreading waveform.

2.1.3. Received signal

The received signal, $r(t)$, of the BS at the tagged cell, denoted by cell 0, can be expressed as

$$r(t) = \sum_{k=0}^{K_c} \sum_{n=1}^{N_k} \sqrt{2P_0\, \chi_{kn}}\, \gamma_{kn}\, a_{kn}\left(t - \tau_{kn}\right) \cdot b_{kn}\left(t - \tau_{kn}\right) \cos\left(w_c t + \Phi_{kn}\right) + n(t) \tag{5}$$

where N_k is the number of active users in cell k; K_c is the number of interfering cells under consideration; τ_{kn} and $\Phi_{kn} = (\theta_{kn} - w_c\, \tau_{kn} + \phi_{kn})$ represent the time delay and the random phase, respectively; $n(t)$ is the channel noise process which is assumed to be an AWGN with two-sided power spectral density $\mathcal{N}_0/2$; and χ_{kn} is defined as

$$\chi_{kn} = \min_{j \in S_c}\left[\frac{\Lambda_{kn}^{(0)}}{\Lambda_{kn}^{(j)}}\right] \qquad 1 \le n \le N_k \quad 0 \le k \le K_c \tag{6}$$

For the analysis of the MAI effects on the performance, we are only concerned with the relative phase shifts (modulo 2π) and relative time delays (modulo T) [8]. Hence, we assume that τ_{kn} and Φ_{kn} are uniformly distributed over $[0, T)$ and $[0, 2\pi)$. We also assume that $\{\tau_{kn}\}$, $\{\Phi_{kn}\}$, $\{\chi_{kn}\}$, $\{\gamma_{kn}\}$, $\{a_j^{(kn)}\}$, and $\{b_j^{(kn)}\}$ are mutually independent and the active users are uniformly distributed in cells.

2.2. *BER performance analysis*

2.2.1. BER for BPSK

A correlator receiver is used for the coherent detection of the received signal [4]. We assume that the receiver in BS 0 can perfectly track the phase and the time delay of the desired user which is power controlled by BS 0. Note that this desired user may be in the region of $-(N_c\, \mathcal{D})/2$ to $(N_c\, \mathcal{D})/2$. Due to power control, the statistics of the received signal of this user is independent of its location in the above mentioned region. For notation simplicity, we assume that this user is in the tagged cell, denoted by user "$0i$", without loss of generality. Since only the relative delays and phases are important, we can set $\tau_{0i} = \Phi_{0i} = 0$. Thus, τ_{kn} and Φ_{kn} are the time delay and the phase angle of user kn relative to the desired user. The correlator output ξ_{0i} is

$$\begin{aligned}\xi_{0i} &= \frac{1}{\sqrt{2P_0\, T}} \int_0^T r(t)\, 2\, a_{0i}(t) \cos\left(w_c t\right) \mathrm{d}t \\ &= \gamma_{0i}\, b_0^{(0i)} + \sum_{k=0}^{K_c} \sum_{n=1}^{N_k} \sqrt{\chi_{kn}}\, \gamma_{kn} \cos\left(\Phi_{kn}\right) \mathcal{W}_{kn} + n^* \qquad (k,n) \ne (0,i) \\ &= \gamma_{0i}\, b_0^{(0i)} + I_{\mathrm{MAI}} + n^* = \gamma_{0i}\, b_0^{(0i)} + I_T\end{aligned} \tag{7}$$

where n^* is zero-mean Gaussian with variance $\mathcal{N}_0/(2P_0 T) = \mathcal{N}_0/2E_b$, E_b is the bit energy, I_T is the total interference, and $\mathcal{W}_{kn}$ can be expressed as

$$\mathcal{W}_{kn} = \frac{1}{T}\int_0^T a_{kn}(t-\tau_{kn})\,b_{kn}(t-\tau_{kn})\,a_{0i}(t)\,\mathrm{d}t \tag{8}$$

For more detail anallysis of $\mathcal{W}_{kn}$, the reader can refer to [5, 11].

Since I_T is symmetric, the conditional *BER* given $b_0^{(0i)}$ does not depend on the value of $b_0^{(0i)}$, so we take it to be 1. Let us define the random vectors $\underline{\chi}$, $\underline{\gamma}$, $\underline{\Phi}$, and $\underline{\tau}$ as $(\sum_{k=0}^{K_c} N_k - 1)$-component vectors of the form $\underline{\chi} = (\chi_{01},\ldots, \chi_{0,i-1}\ \chi_{0,i+1},\ldots, \chi_{K_c,N_{K_c}})$ and similarly for the rest. If all the signature sequences are completely random, the spreading ratio is sufficiently large, and $\underline{\chi}$, $\underline{\gamma}$, $\underline{\Phi}$, and $\underline{\tau}$ are fixed, I_{MAI} can be accurately modeled by a Gaussian random variable [11]. This is called the IGA method. We define the conditional variance Ψ of I_T as

$$\Psi = \mathbf{Var}\left(I_T \middle| \underline{\chi},\underline{\gamma},\underline{\Phi},\underline{\tau}\right) = \frac{\mathcal{N}_0}{2E_b} + \sum_{k=0}^{K_c}\sum_{n=1}^{N_k} \chi_{kn}\,\gamma_{kn}^2\,Z_{kn} \quad (k,n)\neq(0,i) \tag{9}$$

where Z_{kn} can be found to be [5]

$$Z_{kn} = \cos^2(\Phi_{kn})\frac{\eta}{T^2}\left[R_\psi^2(\tau_{kn}) + \hat{R}_\psi^2(\tau_{kn})\right] \tag{10}$$

From (7), the conditional *BER*, $P_b(\Psi, \gamma_{0i})$, is

$$P_b(\Psi,\gamma_{0i}) = P_r(\gamma_{0i} + I_T < 0) = \boldsymbol{Q}\left[\frac{\gamma_{0i}}{\sqrt{\Psi}}\right] \tag{11}$$

where $\boldsymbol{Q}(x)$ is the complementary error function defined as $1/\sqrt{2\pi}\int_x^\infty \exp(-y^2/2)\,\mathrm{d}y$. Using the result from [13], we can write

$$P_b(\Psi) = \boldsymbol{E}_{\gamma_{0i}}\left[P_b(\Psi,\gamma_{0i})\middle|\Psi\right] = \boldsymbol{Q}(u,w) - \frac{1}{2}\cdot\left(1+\sqrt{\frac{d}{1+d}}\right)\cdot\exp\left(-\frac{u^2+w^2}{2}\right)I_0(uw) \tag{12}$$

where $\boldsymbol{Q}(u, w)$ is the Marcum Q-function defined by $\int_w^\infty z \exp[-(z^2+u^2)/2]\,I_0(uz)\,\mathrm{d}z$ and

$$d = \frac{1}{2(K+1)\Psi}$$

$$u = \sqrt{K\left[1+2d-2\sqrt{d(1+d)}\right]/2(1+d)}$$

$$w = \sqrt{K\left[1+2d+2\sqrt{d(1+d)}\right]/2(1+d)}$$

Hence, the average *BER* of the desired user can be found by

$$P_b = \boldsymbol{E}_\Psi\left[P_b(\Psi)\right] = \int_0^\infty P_b(\psi)\,f_\Psi(\psi)\,\mathrm{d}\psi \tag{13}$$

It is nontrivial to derive the closed form of the pdf of the conditional variance Ψ, which is a complicated function of the random vectors $\underline{\chi}$, $\underline{\gamma}$, $\underline{\Phi}$, and $\underline{\tau}$. Monte Carlo integration is one possible approach to remove the conditioning on all random vectors. That is

$$P_b = \lim_{M\to\infty}\frac{1}{M}\sum_{j=1}^{M} P_b\left(\Psi_j\right) \tag{14}$$

Another approximation method which has been commonly used is the SGA method [2, 10] where I_T is assumed to be unconditional zero-mean Gaussian. This implies I_T can be completely described by its variance. Thus, the average *BER*, P_b^G, computed by this method is $P_b^G = P_b[\boldsymbol{E}(\Psi)] = P_b(\mu_\psi)$, where μ_ψ is given by

$$\begin{aligned}\mu_\psi &= \boldsymbol{E}(\Psi)\\ &= \frac{\mathcal{N}_0}{2E_b} + \sum_{k=0}^{K_c}\sum_{n=1}^{N_k}\boldsymbol{E}(\chi_{kn})\,\boldsymbol{E}\left(\gamma_{kn}^2\right)\boldsymbol{E}\left(\boldsymbol{Z_{kn}}\right) \quad (k,n)\neq(0,i)\\ &= \frac{\mathcal{N}_0}{2E_b} + \frac{\boldsymbol{m}_\psi\,M_\chi}{\eta}\end{aligned} \tag{15}$$

and $m_\psi = \boldsymbol{E}[\hat{R}_\psi^2(\tau)]/T_c^2 = \boldsymbol{E}[R_\psi^2(\tau)]/T_c^2$. For a rectangular chip pulse shape, $m_\psi = 1/3$. For a half-sine chip pulse shape of the form $\psi(t) = \sqrt{2}\sin(\pi t/T_c)$, $m_\psi = (15 + 2\pi^2)/(12\pi^2)$. For a raised-cosine chip pulse shape of the form $\psi(t) = \sqrt{2/3}\,[1-\cos(2\pi t/T_c)]$, $m_\psi = 1/6 + 35/(48\pi^2)$ [4]. Furthermore, M_χ is given by

$$M_\chi = \sum_{k=0}^{K_c}\sum_{n=1}^{N_k}\boldsymbol{E}(\chi_{kn}) \quad (k,n)\neq(0,i) \tag{16}$$

which can be interpreted as the average interference power from other users without considering the effect of relative delays and phases between the desired user and the interfering users. It is noted that M_χ is mainly determined by the propagation law, the shadowing, the cell geometry, and auxiliary functions, e.g., power control and macro-diversity. For details on the derivation of M_χ, see Appendix A.

2.2.2. BER for DPSK

A possible implementation of the DPSK demodulation is a differentially-coherent matched filter. For this kind of receiver, the conditional BER for the desired user can be written as $P_b(\Psi, \gamma_{0i}) = 1/2\exp(-\gamma_{0i}^2/2\Psi)$. By averaging over γ_{0i}, we get [5]

$$P_b(\Psi) = \frac{\Psi}{2\Psi + 1/(K+1)}\exp\left[-\frac{K}{2(K+1)\Psi+1}\right] \tag{17}$$

Similarly, the average *BER* for DPSK modulation signal can be computed by Monte Carlo integration. Meanwhile, the average *BER* evaluated by the SGA method is

$$P_b^G = \frac{\mu_\psi}{2\mu_\psi + 1/(K+1)} \exp\left[-\frac{K}{2(K+1)\mu_\psi + 1}\right] \quad (18)$$

Unless otherwise noted, we assume that each cell has the same number of active users N, the spreading ratio η equals 511, the cell length $\mathcal{D}$ is 1 km, the cell width $\mathcal{H}$ is 36 m (a typical highway environment), the Fresnel break point g is 200 m, and the propagation exponents a and b are both equal to 2. Also, the rectangular chip waveform is employed and log-normally distributed shadowing is assumed with the standard deviation σ being 6 dB. The interference outside the six adjacent cells can be ignored. Furthermore, due to the relatively short propagation distances, we assume that the AWGN is negligible when compared to the MAI.

Note that when the system reaches the steady state, the average number of active users power controlled by each BS is identical and is equal to N. To account for the effect of other-cell interference, the relative other-cell interference [12], f_I, is defined as $f_I = [M_\chi - (N-1)]/N$. Therefore, my in (15) can be rewritten as

$$\mu_\psi = \frac{\mathcal{N}_0}{2E_b} + \frac{m_\psi (N-1)}{\eta}\left[1 + \frac{N}{N-1} f_I\right] \quad (19)$$

Compared with that of a single-cell DS system, the effective number of interfering users in a multiple-cell system increases by a factor $[1 + (N/N - 1) f_I]$ which will reduce the frequency reuse efficiency. In Table 1, we show f_I as a function of σ for $N_c = 1$, 2, and 3. From this Table, we observe that the significant improvement in f_I is obtained by using $N_c = 2$ instead of $N_c = 1$, but only a small improvement is obtained when we go from $N_c = 2$ to 3.

Figs. 2 and 3 plot the average *BER* of DPSK as a function of N for $N_c = 1$ and 2, respectively. These results show that for this range of N, the average *BER* evaluated by the SGA is smaller than that evaluated by the IGA. For $N_c = 1$, the results from the SGA method are very optimistic when the number of active users is small and the Rician factor K is large. Also, the Rician factor K has a great impact on the average *BER* for $N_c = 2$, but a little impact on that for $N_c = 1$. Furthermore, when $N_c = 2$, the *BER* calculated by the SGA method is close to that by the IGA method.

Table 1 - f_I *as a function of* σ for $N_c = 1$, 2 *and* 3 *with* $a = 2.0$ *and* $b = 2.0$.

σ (dB)	$N_c = 1$	$N_c = 2$	$N_c = 3$
0	0.1525	0.1525	0.1525
2	0.1886	0.1534	0.1534
4	0.3563	0.1580	0.1579
6	1.0288	0.1764	0.1730
8	4.5398	0.2514	0.2113

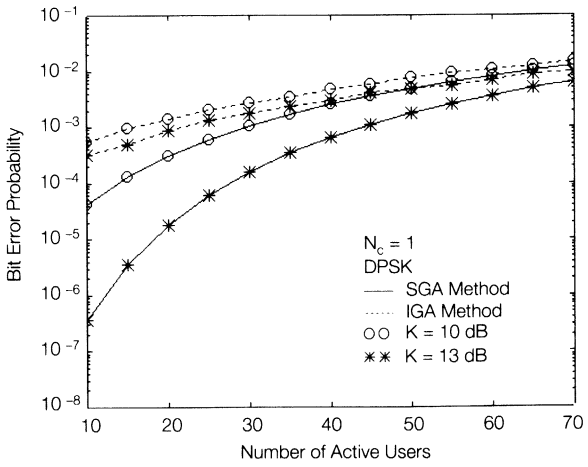

Fig. 2 - *BER* versus N of DPSK for $N_c = 1$.

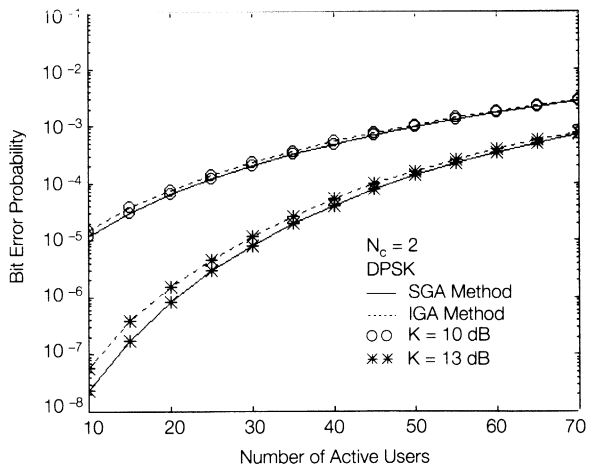

Fig. 3 - *BER* versus N of DPSK for $N_c = 2$.

To further investigate the effect of K on the average *BER*, we illustrate the average *BER* of DPSK as a function of K in Fig. 4 for $N = 35$. It is seen that the larger the Rician factor, the smaller the average *BER*. Although the desired user and the interfering users both have less multipath fading as K becomes large, the Rician factor K has positive effect on the average *BER* performance. Thus, a system operating in a Rician fading channel can be expected to have better performance than that operating in a Rayleigh fading channel.

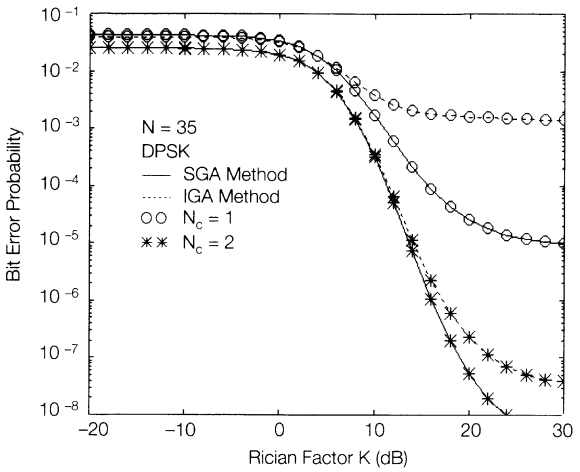

Fig. 4 - *BER* versus K of DPSK for $N_c = 1$ and $N_c = 2$.

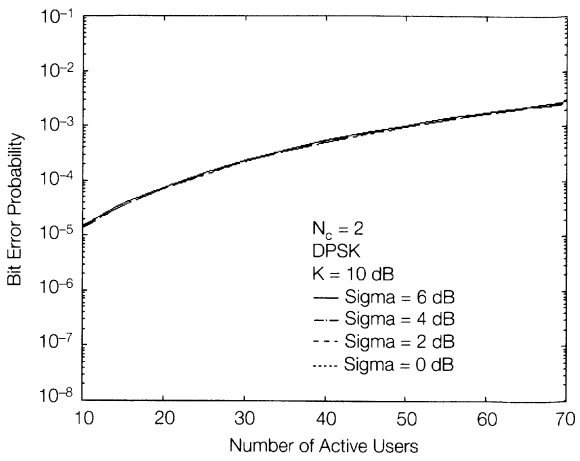

Fig. 6 - *BER* versus N of DPSK using the IGA method for $N_c = 2$ with $\sigma = 0$, 2, 4, and 6 dB.

It is interesting to study the effect of σ on the *BER* performance. We illustrate the average *BER* as a function of N with parameter σ in Fig. 5 for $N_c = 1$ and in Fig. 6 for $N_c = 2$, respectively. For $N_c = 1$, we find that the average *BER* increases very quickly when the value of σ becomes large. However, for $N_c = 2$, the average *BER* increases only slightly with σ. Thus, the macro-selection diversity can reduce the MAI from other cells effectively even for heavy shadowing. This observation matches the results shown in Tables 1.

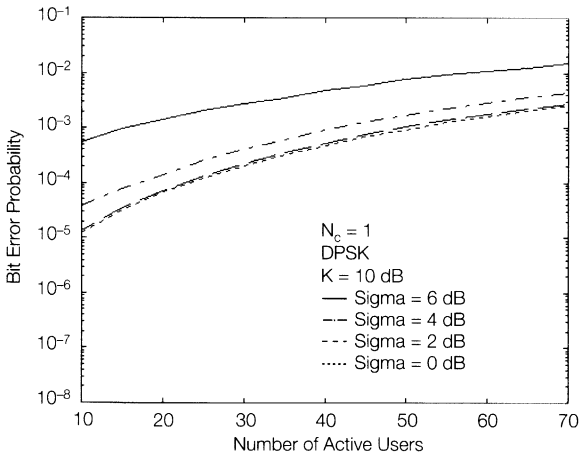

Fig. 5 - *BER* versus N of DPSK using the IGA method for $N_c = 1$ with $\sigma = 0$, 2, 4, and 6 dB.

To compare the average *BER* of DPSK with that of BPSK, we define the effective signal-to-noise ratio as $SNR_{\text{eff}} = \boldsymbol{E}(\gamma_{0i}^2)/\boldsymbol{E}(\boldsymbol{\Psi}) = 1/\mu_{\psi}$. Fig. 7 shows the average *BER* of DPSK and BPSK versus the SNR_{eff} for $K = 10$ dB. When the average *BER* equals 10^{-3}, the SNR_{eff} of BPSK is approximately 3 dB better than that of DPSK for $N_c = 1$. When the average *BER* is 10^{-4}, the SNR_{eff} of BPSK is about 2 dB better than that of DPSK for $N_c = 2$.

In Fig. 8, *BER* versus N is depicted for DPSK signals with rectangular, half-sine, and raised-cosine chip waveforms, respectively, for $N_c = 2$. As expected, the

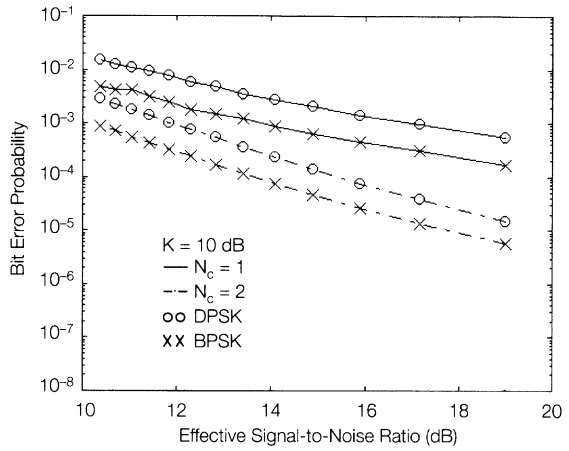

Fig. 7 - *BER* versus SNR_{eff} of DPSK and BPSK using the IGA method for $N_c = 1$ and $N_c = 2$ with $K = 10$ dB.

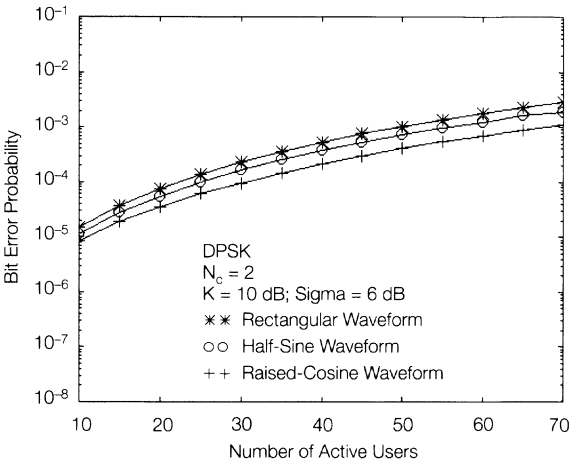

Fig. 8 - *BER* versus N of DPSK using the IGA method for rectangular, half-sine, and raised-cosine chip waveforms with $K = 10$ dB for $N_c = 2$.

raised-cosine waveform provides the best *BER* performance because it possesses the least MAI interference (m_{ψ} is the least). For $P_e = 10^{-4}$, the system can accommodate 30 users with the raised-cosine waveform, but

only 22 users with the rectangular waveform.

3. DOWNLINK PERFORMANCE ANALYSIS

3.1. *System model*

In this section, we will evaluate the downlink performance which has been usually neglected in the literature. The performance measure of interest is the average *BER*. On the downlink, the broadcast operation mode is assumed; a common message or several distinct messages are transmitted simultaneously from a BS to different mobiles. The system and channel models are similar with those described on the uplink. We assume that all signals from the same BS will undergo shadowed Rician fading in common with respect to each specific user and they are different at different places within the cell. However, the composite received signal from each BS is assumed to fade independently. On the downlink, we assume no power control is used. The received signal of the desired user in the tagged cell can be expressed as

$$r_{0i}(t) = \sum_{k=0}^{K_c}\sum_{n=1}^{N_k}\sqrt{2P_0\,L_p(r_{ki})l_k}\;\gamma_k\,a_{kn}(t-\tau_{kn})\cdot b_{kn}(t-\tau_{kn})\cos(2\pi f_c t+\Phi_{kn}) + n(t) \tag{20}$$

where r_{ki} the distance between the BS of cell k and the desired user in cell 0.

3.2. *BER performance analysis*

The normalized sample signal at the output of the correlator which is matched to the desired user is of the form

$$\begin{aligned}\xi_{0i} &= \frac{1}{\sqrt{2P_0}\,T\,L_p(r_{ki})}\int_0^T r_{0i}(t)\,2a_{0i}(t)\cos(2\pi f_c t)\,dt \\ &= \sqrt{l_0\tilde{\gamma}_0} + \sqrt{l_0\tilde{\gamma}_0}\left[\sum_{n=1,n\neq i}^{N_0}\cos(\Phi_{on})\mathcal{W}_{on}\right] + \\ &\quad \sum_{k=1}^{K_c}\sqrt{\frac{L_p(r_{ki})l_k\tilde{\gamma}_k}{L_p(r_{0i})}}\left[\sum_{n=1}^{N_0}\cos(\Phi_{kn})\mathcal{W}_{kn}\right] + n^*\end{aligned} \tag{21}$$

where $l_k = 10^{X_k/10}$, $k = 0,\ldots, K_c$, with X_k being a zero-mean Gaussian random variable with variance σ_k^2; $\tilde{\gamma}_k = \gamma_k^2$ follows a noncentral chi-square distribution; n^* is an AWGN with variance $\sigma_{th}^2 = \mathcal{N}_0/[2E_b\,L_p(r_{0i})]$. To make the notation simple, we define

$$\Upsilon_k = \frac{L_p(r_{ki})}{L_p(r_{0i})} \quad \text{and} \quad \mathcal{L}_k = \Upsilon_k\,l_k\,\tilde{\gamma}_k \tag{22}$$

where $\Upsilon_0 = 1$. Therefore, the correlator output, ξ_{0i}, can be simplified to the form

$$\begin{aligned}\xi_{0i} &= \sqrt{\mathcal{L}_0} + \sum_{k=0}^{K_c}\sqrt{\mathcal{L}_k}\cdot \left[\sum_{n=1}^{N_k}\cos(\Phi_{kn})\mathcal{W}_{kn}\right] + n^* \quad (k,n)\neq(0,i) \\ &= \sqrt{\mathcal{L}_0} + I_T\end{aligned} \tag{23}$$

where the total interference, I_T, consists of the AWGN and the MAI from users in the same cell as well as from those in other cells. Let us define the random vector $\underline{\mathcal{L}} = (\mathcal{L}_0,\ldots,\mathcal{L}_{K_c})$. In order to employ the IGA method to calculate the *BER*, we need to find the conditional variance Ψ of I_T which is given by

$$\begin{aligned}\Psi &= \mathbf{Var}\left(I_T \mid \underline{\mathcal{L}},\underline{\Phi},\underline{\tau}\right) \\ &= \sigma_{th}^2 + \mathcal{L}_0\,Z_0 + \sum_{k=1}^{K_c}\mathcal{L}_k\,Z_k \\ &= \sigma_{th}^2 + \mathcal{L}_0\,Z_0 + \Psi_{oth}\end{aligned} \tag{24}$$

in which the random variables, Z_k, $k = 0,\ldots, K_c$, and the conditional variance of the other-cell interference Ψ_{oth} are given by

$$Z_0 = \sum_{n=1,n\neq i}^{N_0} Z_{on}$$

$$Z_k = \sum_{n=1}^{N_k} Z_{kn} \qquad k = 1,\cdots,K_c$$

$$\Psi_{oth} = \sum_{k=1}^{K_c}\mathcal{L}_k\,Z_k$$

where Z_{kn} is defined in (10). Note that the term $(\mathcal{L}_0\,Z_0)$ represents the MAI from the tagged cell. Since the composite received signal fades *in unison* from a given BS, the faded amplitude of the desired signal, $\sqrt{\mathcal{L}_0}$, and the total interference, I_T, are dependent. This situation is quite different from that on the uplink. In addition, since no power control is used on the downlink, $\mathcal{L}_0$ follows a composite log-normal noncentral chi-square distribution which has not been discussed in the literature. Hence, a approach different from that used ow the uplink is required to evaluate the *BER* performance.

As mentioned before, given the random vectors $\underline{\mathcal{L}}$, $\underline{\Phi}$, and $\underline{\tau}$, I_T can be accurately modeled as a Gaussian random variable. Hence, for the system employing BPSK modulation scheme, the conditional *BER* can be written as

$$P_b(\mathcal{L}_0,Z_0,\Psi_{oth}) = \boldsymbol{Q}\left(\sqrt{\frac{\mathcal{L}_0}{\sigma_{th}^2 + \mathcal{L}_0\,Z_0 + \Psi_{oth}}}\right) \tag{25}$$

In the following analysis, we assume that the AWGN can be ignored when compared to the MAI, irrespective of user's location within the cell. This results from the

fact that the microcellular environment is usually interference limited [2]. Hence, the conditional *BER* can be approximated by

$$P_b\left(\mathcal{L}_0, Z_0, \Psi_{oth}\right) = \boldsymbol{Q}\left(\sqrt{\frac{\mathcal{L}_0}{\mathcal{L}_0 Z_0 + \Psi_{oth}}}\right) \tag{26}$$

Therefore, we can evaluate the average *BER* by $P_b = \boldsymbol{E}_{\mathcal{L}_0, Z_0, \Psi_{oth}}[P_b(\mathcal{L}_0, Z_0, \Psi_{oth})]$. The pdf of the composite log-normal noncentral chi-square $\mathcal{L}_0$ is of the form [5],

$$f_{L_0}(y) = \frac{(K+1)}{\sqrt{\pi}} \exp(-K) \int_{-\infty}^{\infty} e^{-A_0 x} \exp\left[-(K+1) e^{-A_0 x} y\right] \cdot I_0\left[\sqrt{4K(K+1)\exp(-A_0 x) y}\right] \exp\left(-x^2\right) dx \tag{27}$$

where $A_0 = \sqrt{2}\,\lambda\,\sigma_0$ and $\lambda = \ln 10/10$. Letting $\sigma_0 = 0$, this pdf becomes a non-central chi-square distribution. We can employ the Gauss-Hermit integration [14] to evaluate the pdf of $\mathcal{L}_0$. Gauss-Hermit integration is a kind of Gauss Quadrature Rule (GQR). From (27), it can be seen that the weight function is $\exp(-x^2)$ with Hermit polynomials as its associated set of orthonormal polynomials [14]. Here, we just write down the expression for the pdf of $\mathcal{L}_0$ evaluated by this method as follows

$$f_{\mathcal{L}_0}(y) = \frac{(K+1)}{\sqrt{\pi}} \exp(-K) \cdot \sum_{j=1}^{N_{H1}} w_j\, e^{-A_0 x_j} \exp\left[-(K+1) e^{-A_0 x_j} y\right] \cdot I_0\left[\sqrt{4K(K+1)\exp\left(-A_0 x_j\right) y}\right] + R_m \tag{28}$$

where w_j and x_j, $j = 1, \ldots, N_{H1}$, are the N_{H1} weights and nodes of the Quadrature Rule which can be found in [14]. The remainder R_m can be reduced as small as desired by increasing the value of N_{H1}. In general, $N_{H1} = 25 - 30$ is sufficient.

Averaging the conditional *BER* given in (26) over $\mathcal{L}_0$, we have

$$\begin{aligned} P_b\left(Z_0, \Psi_{oth}\right) &= \boldsymbol{E}_{\mathcal{L}_0}\left[P_b\left(\mathcal{L}_0, Z_0, \Psi_{oth}\right)\right] \\ &= \frac{(K+1)}{\sqrt{\pi}} \exp(-K) \sum_{j=1}^{N_{H1}} w_j \exp\left(-A_0 x_j\right) \cdot \\ &\int_0^{\infty} \boldsymbol{Q}\left(\sqrt{\frac{y}{y Z_0 + \Psi_{oth}}}\right) \exp\left[-(K+1) e^{-A_0 x_j} y\right] \cdot \\ &I_0\left[\sqrt{4K(K+1)\exp\left(-A_0 x_j\right) y}\right] dy \end{aligned} \tag{29}$$

Manipulating the above equation by changing the variable and applying the Gauss-Laguerre integration [14], we approximate $P_b(Z_0, \Psi_{oth})$ by

$$P_b\left(Z_0, \Psi_{oth}\right) \approx \frac{\exp(-K)}{\sqrt{\pi}} \sum_{j=1}^{N_{H1}} w_j \left\{ \sum_{k=1}^{N_L} \tilde{w}_k \cdot \boldsymbol{Q}\left[\sqrt{\frac{\left(\frac{\tilde{x}_k}{K+1}\right)\exp\left(A_0 x_j\right)}{Z_0\left(\frac{\tilde{x}_k}{K+1}\right)\exp\left(A_0 x_j\right) + \Psi_{oth}}}\right] I_0\left(\sqrt{4K\tilde{x}_k}\right) \right\} \tag{30}$$

Thus, we can avoid the original two-order integration by employing a two-layer summation which can substantially reduce the computation complexity and still preserves satisfactory precision. Finally, the average *BER* can be calculated by averaging $P_b(Z_0, \Psi_{oth})$ over random variables Z_0 and Ψ_{oth}. One practical way is to employ Monte Carlo integration method. That is

$$P_b = \lim_{M \to \infty} \frac{1}{M} \sum_{j=1}^{M} P_b\left[(Z_0)_j, (\Psi_{oth})_j\right] \tag{31}$$

We call this approach the IGA-MC method. However, with some approximations, we can analytically evaluate the average *BER*. These approximations are as follows. First, if the number of users N_k is large enough, Z_0 and Z_k can be approximated by their mean values. That is $Z_0 \approx C_0 = \boldsymbol{E}(Z_0) = (N_0 - 1)\, m_\psi/\eta$ and $Z_k \approx C_k = \boldsymbol{E}(Z_k) = N_k\, m_\psi/\eta$. The accuracy of this approximation has been validated in [5], which illustrates that the spatial distribution and the shadowing play the dominant role in the *BER* calculation. Second, [5] also shows that if $\sigma_k \geq 4$ dB and $K \geq 7$ dB or if $\sigma_k \geq 2$ dB and $K \geq 10$ dB, then $\mathcal{L}_k$ in (22) can be well approximated by a log-normally distributed random variable $\tilde{\mathcal{L}}_k$. To maintain accuracy, we still treat the desired signal (i.e., $\mathcal{L}_0$) as a random variable with composite log-normal noncentral chi-square distribution. Third, the sum of a finite number of uncorrelated log-normal random variables can be approximated by another log-normal random variable [15]. Based on these approximations, the conditional *BER* given in (30) becomes

$$P_b\left(Z_0, \Psi_{oth}\right) \approx P_b\left(\mathcal{L}_I\right) = \frac{\exp(-K)}{\sqrt{\pi}} \sum_{j=1}^{N_{H1}} w_j \left\{ \sum_{k=1}^{N_L} \tilde{w}_k \cdot \boldsymbol{Q}\left[\sqrt{\frac{\left(\frac{\tilde{x}_k}{K+1}\right)\exp\left(A_0 x_j\right)}{C_0\left(\frac{\tilde{x}_k}{K+1}\right)\exp\left(A_0 x_j\right) + \mathcal{L}_I}}\right] I_0\left(\sqrt{4K\tilde{x}_k}\right) \right\} \tag{32}$$

which has been simplified to be a function of the conditional other-cell interference power, denoted as $\mathcal{L}_I$, given by

$$\mathcal{L}_I = \sum_{k=1}^{K_c} C_k \tilde{\mathcal{L}}_k \tag{33}$$

and $\mathcal{L}_I$ itself can also be approximated by a log-normally distributed random variable which can be expressed as

$$\mathcal{L}_I = 10^{(m_I + X_I)/10} \tag{34}$$

where X_I is zero-mean Gaussian with variance σ_I^2. The value of m_I and σ_I^2 can be found by applying the recursive technique described in [15]. The pdf of $\mathcal{L}_I$ can be expressed as [3]

$$f_{\mathcal{L}_I}(y) = \frac{1}{\sqrt{2\pi}\,\lambda\sigma_I\, y} \exp\left[-\frac{(\ln y - \lambda m_I)^2}{2\lambda^2\sigma_I^2}\right] U(y) \tag{35}$$

Finally, we can find the average *BER* by applying Gauss-Hermit method again which yields

$$\begin{aligned} P_b &= \boldsymbol{E}_{\mathcal{L}_I}\left[P_b(\mathcal{L}_I)\right] \\ &= \frac{1}{\sqrt{\pi}} \int_{-\infty}^{\infty} P_b\left(\tilde{m}_I e^{A_I x}\right) \exp\left(-x^2\right) \mathrm{d}x \\ &\approx \frac{1}{\sqrt{\pi}} \sum_{i=1}^{N_{H2}} \tilde{w}_i P_b\left(\tilde{m}_I e^{A_I \dot{x}_i}\right) \end{aligned} \tag{36}$$

in which $A_I = \sqrt{2}\ \lambda\ \sigma_I$ and $\tilde{m}_I = 10^{m_I/10}$. We call this approximation method the IGA-AP method. The advantage of this approach is that we can not only avoid the time-consuming Monte Carlo simulation required in the IGA-MC method, but also we can use a three-fold summation instead of a three-fold integration to find the average *BER*. The numerical error can be as small as desired by increasing the numbers of N_{H_1}, N_{H_2}, and N_L.

The above *BER* expressions depend on where the desired user is located. When the user moves, its area-averaged *BER* can be obtained by averaging over all the possible locations when it travels in the cell.

In Fig. 9, *BER* as a function of the transversal distance between the desired user and the BS is illustrated. Both IGA-MC and IGA-AP methods are used. We assume that $\sigma_k = \sigma$, $\forall_k$. Although we have made three approximations in the IGA-AP method, the results are still very close to those generated by the IGA-MC method. Furthermore, as expected, the worst *BER* is seen when the desired user is at the boundary between two cells. In [2], the worst *BER* is employed to assess the user capacity. However, this criterion may yield very pessimistic results. In Fig. 10, we illustrate the worst and the area-averaged *BER* as a function of N for $\sigma = 4$ and 6 dB, respectively. For $\sigma = 4$ dB, if a BER of 10^{-3} is required, the system can support about 50 users by using the area-averaged *BER* as the criterion. However, only 13 users can be accommodated based on the worst *BER* criterion. This is due to the "graceful degradation" feature of the spread-spectrum technique.

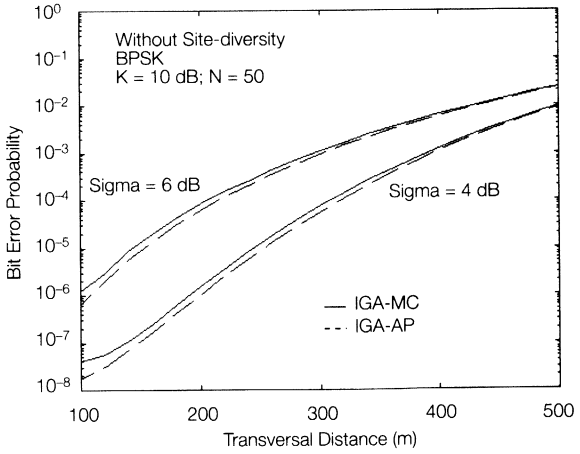

Fig. 9 - *BER* versus transverse distance for $N_c = 1$ on the downlink.

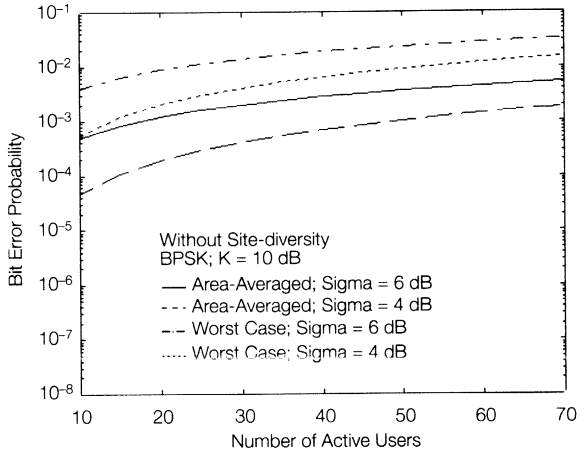

Fig. 10 - Area-averaged and the worst *BER* versus N for $N_c = 1$ on the downlink.

3.3. *The Effect of macro-diversity*

Recall that we have defined the relative other-cell interference f_I on the uplink to assess the effectiveness of the macro-selection diversity. In that part, we reach a conclusion that $N_c = 2$ (i.e., stronger-of-two-nearest-BS processing) is adequate not only to combat the shadowing, but also to keep low system complexity. Based on this measure, it is very simple to examine the impact of the macro-selection diversity on suppressing other-cell interference. We follow the same method to assess the influence of the macro-selection diversity on the downlink performance. On the downlink, the macro-selection diversity means that the user may have access to more than one BS and can select the BS with the best downlink transmission channel. Similarly, we assume the mobile can only access to the nearest N_c BS's.

Without using the macro diversity, it is straightforward to define the relative interference, D_I, on the downlink as

$$D_I = E\left\{\frac{\sum_{k=1}^{K_c} L_p(r_{ki})l_k}{L_p(r_{0i})l_0}\right\} = E\left\{\frac{\sum_{k=1}^{K_c} \Upsilon_k l_k}{l_0}\right\} \quad (37)$$

where we assume that the multipath will not effect the average power level and only K_c adjacent cells are considered. D_I can be interpreted as the average ratio of other-cell interference to the desired signal power.

However, for systems with the macro-selection diversity, D_I should be modified as

$$D_I = E\left\{\frac{\sum_{k=1}^{N_c-1}\Omega_k + \sum_{k=N_c}^{K_c}\alpha_k}{\Omega_0}\right\} = E\left\{\frac{\sum_{k=1}^{N_c-1}\Omega_k}{\Omega_0}\right\} + E\left\{\frac{\sum_{k=N_c}^{K_c}\alpha_k}{\Omega_0}\right\} = D_{I1} + D_{I2} \quad (38)$$

where $\alpha_k = \Upsilon_k l_k$ and $\{\Omega_k\}_{k=0}^{N_c-1}$ is a set of ordered statistics of $\{\alpha_k\}_{k=0}^{N_c-1}$ such that $\Omega_0 \geq \Omega_1 \geq \ldots \geq \Omega_{N_{c-1}}$ and $\Omega_0 = \max\{\alpha_0, \ldots, \alpha_{N_{c-1}}\}$.

The expressions for D_{I1} and D_{I2} as a function of the user's location are derived in Appendix B. Fig. 11 shows D_I versus the transverse distance between the desired user and the BS 0. It is seen that a significant improvement in D_I is obtained by using $N_c = 2$ instead of $N_c = 1$, but little improvement is obtained when we go from $N_c = 2$ to 3. The same conclusion has been reached on the uplink analysis. Furthermore, the relative other-cell interference, D_I, becomes insensitive to the user's location in the cell when the macro-selection diversity is used.

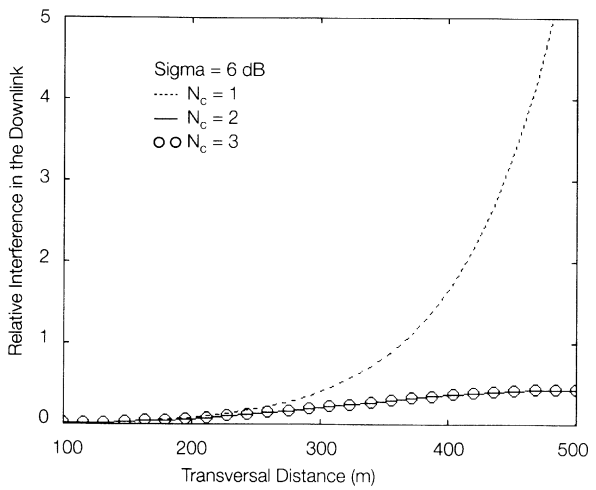

Fig. 11 - Relative other-cell interference, D_I, versus transverse distance on the downlink.

4. CONCLUSIONS

In this paper, we have evaluated the performance of both uplink and downlink of an asynchronous DS/SSMA system in lineal microcells with Rician fading and shadowing. The performance measure of interest is the average *BER*. On the uplink, both BPSK and DPSK modulation schemes are taken into account. Depending on the operation range, the SGA method may yield very optimistic results compared with those obtained by the IGA approach. The macro-selection diversity can reduce the other-cell interference effectively even for a channel with heavy shadowing. Furthermore, the Rician factor has a great impact on the performance for $N_c = 2$ (two nearest BS's), but only little for $N_c = 1$ (nearest BS). Also, raised-cosine chip waveform can significantly improve the user capacity.

On the downlink, we study the *BER* performance for BPSK without macro-diversity. The proposed approximation method can evaluate the *BER* with less computational effort. We use both the area-averaged *BER* and worst *BER* as the criteria to assess the downlink user capacity. It is found that the worst *BER* criterion yields very pessimistic results. We also define a performance measure D_I to investigate the effect of the macro-selection diversity on reducing the other-cell interference. It is shown that the macro-selection diversity can effectively suppress the other-cell interference.

APPENDIX A

From eq. (16), M_χ is defined as

$$M_\chi = \sum_{k=0}^{K_c}\sum_{n=1}^{N_k} E(\chi_{kn}) \quad (k,n) \neq (0,i) \quad (39)$$

Note that χ_{kn} is a function of the user's location in the cell. Its expected value can be evaluated by

$$E_{(\chi_{kn})} = \int_{\mathcal{A}_k} E\left\{\min_{j\in S_c}\left[\frac{\Lambda_{kn}^{(0)}}{\Lambda_{kn}^{(j)}}\right]\right\}\rho\, d\mathcal{A}_k = \int_{\mathcal{A}_k} E\left\{\min_{j\in S_c}\left[\frac{L_p(r_0)10^{X_0/10}}{L_p(r_j)10^{X_j/10}}\right]\right\}\rho\, d\mathcal{A}_k = \int_{\mathcal{A}_k} I_k\,\rho\, d\mathcal{A}_k \quad (40)$$

where $\mathcal{A}_k$ is the area of cell k and ρ is the spatial density of the user in the cell. We assume that the user position is uniformly distributed within the cell. The distance between the kn-th user and the BS j is r_j and the corresponding power fluctuation is X_j. The random variables X_i and X_j are assumed to be independent if $i \neq j$. We have dropped the sub-index kn in r_j and X_j to make the notation simple. Define the relative mean path loss as follows

$$R_j = \frac{L_p(r_0)}{L_p(r_j)} \text{ and } M_j = 10\log_{10} R_j$$

The expected value of χ_{kn} will be computed separately depending on whether or not the BS 0 is one of the N_c nearest BS's of the kn-th user.

Case 1: $0 \notin \mathcal{S}_c$ — We can apply the total probability formula in order to evaluate I_k as follows:

$$I_k = \sum_{j\in S_c} R_j \exp\left(\lambda^2\sigma^2\right) \int_{-\infty}^{\infty} \frac{1}{\sqrt{2\pi}} \exp\left(-\frac{z^2}{2}\right) \mathrm{d}x \cdot \left\{ \prod_{i\in S_c, i\neq j} \left[1 - Q\left(z + \frac{M_i - M_j}{\sigma} - \lambda\sigma\right)\right]\right\} \tag{46}$$

$$I_k = E\left[\min_{j\in S_c} R_j 10^{-\frac{X_j - X_0}{10}}\right] = \sum_{j\in S_c} R_j E\left(10^{\frac{X_0}{10}}\right) E\left[10^{-\frac{X_j}{10}} \,\middle|\, R_j 10^{-\frac{X_j - X_0}{10}} < R_i 10^{-\frac{X_i - X_0}{10}}, \forall i\neq j, i\in S_c\right] P_r\left(A_j\right)$$

$$= \sum_{j\in S_c} R_j E\left(10^{\frac{X_0}{10}}\right) E\left[10^{-\frac{X_j}{10}} \,\middle|\, X_i < X_j + M_i - M_j\right] P_r\left(A_j\right) \tag{41}$$

$$= \sum_{j\in S_c} R_j E\left(10^{\frac{X_0}{10}}\right) \left\{ \int_{-\infty}^{\infty} 10^{-\frac{X_j}{10}} f_{X_j}\left(x_j\right) \mathrm{d}x_j \left[\prod_{i\neq j, i\in S_c} F_{X_i}\left(x_j + M_i - M_j\right)\right]\right\}$$

where A_j is the event given by

$$A_j = \left\{ R_j 10^{-\frac{X_j - X_0}{10}} < R_i 10^{-\frac{X_i - X_0}{10}}, \forall i\neq j, i\in S_c \right\} \tag{42}$$

and $f_{X_j}(x_j)$ and $F_{X_j}(x_j)$are the pdf and the cumulative density function of the random variable X_j, respectively.

Case 2: $0 \in \mathcal{S}_c$ — In this case, the N_c nearest BS's include BS 0. Hence, I_k can be written as

$$I_k = E\left[\min\left(1, \ldots, R_{N_u} 10^{-\frac{X_{N_u} - X_0}{10}}\right)\right] \tag{43}$$

where $N_u = \max_{j\in S_c}\{j\}$. By following the same procedure in (41), eq. (43) can be derived as follows

$$I_k = \sum_{j\in S_c, j\neq 0} R_j E\left[10^{-\frac{X_j - X_0}{10}} \,\middle|\, \hat{A}_j\right] P_r\left(\hat{A}_j\right) + 1 \cdot P_r\left(R_j 10^{-\frac{X_j - X_0}{10}} > 1, \forall j\neq 0, j\in S_c\right) = \sum_{j\in S_c, j\neq 0} R_j E \cdot$$

$$\left[10^{-\frac{X_j - X_0}{10}} \,\middle|\, X_0 < X_j - M_j, X_i < X_j + M_i - M_j, \forall i\neq j\right] P_r\left(\hat{A}_j\right) + P_r\left(X_j < X_0 + M_j, \forall j\neq 0, j\in S_c\right)$$

$$= \sum_{j\in S_c, j\neq 0} R_j \int_{-\infty}^{\infty} 10^{-\frac{x_j}{10}} f_{X_j}\left(x_j\right) \mathrm{d}x_j \left[\int_{-\infty}^{x_j - M_j} 10^{\frac{x_0}{10}} f_{X_0}\left(x_0\right) \mathrm{d}x_0\right] \left[\prod_{i\in S_c, i\neq j, i\neq 0} F_{X_j}\left(x_j + M_i - M_j\right)\right] + \tag{44}$$

$$\int_{-\infty}^{\infty} f_{X_0}\left(x_0\right) \mathrm{d}x_0 \left[\prod_{i\in S_c, i\neq 0} F_{X_j}\left(x_0 + M_j\right)\right]$$

where $\hat{A}_j$ is the given by

$$\hat{A}_j = \left\{ R_j 10^{-\frac{X_j - X_0}{10}} < R_i 10^{-\frac{X_i - X_0}{10}}, \quad \forall\ i\neq j \text{ and } R_j 10^{-\frac{X_j - X_0}{10}} < 1 \right\} \tag{45}$$

If X_j 's are all zero mean Gaussian random variables with equal variance σ^2, Ik for the case of $\{0 \notin \mathcal{S}_c\}$ can be simplified to the form

$$I_k = \sum_{j\in S_c} R_j \exp\left(\lambda^2\sigma^2\right) \int_{-\infty}^{\infty} \frac{1}{\sqrt{2\pi}} \exp\left(-\frac{z^2}{2}\right) \mathrm{d}x \cdot \left\{ \prod_{i\in S_c, i\neq j} \left[1 - Q\left(z + \frac{M_i - M_j}{\sigma} - \lambda\sigma\right)\right]\right\}$$

where $\lambda = \log(10)/10$; I_k for the case of $\{0 \in \mathcal{S}_c\}$ becomes

$$I_k = \sum_{j\in S_c, j\neq 0} R_j \exp\left(\lambda^2\sigma^2\right) \int_{-\infty}^{\infty} \frac{1}{\sqrt{2\pi}} \exp \cdot \left(-\frac{z^2}{2}\right) \mathrm{d}z \left[1 - Q\left(z - \frac{M_j}{\sigma} - 2\lambda\sigma\right)\right] \cdot \left\{ \prod_{j\in S_c, i\neq j, i\neq 0} \left[1 - Q\left(z + \frac{M_i - M_j}{\sigma} - \lambda\sigma\right)\right]\right\} + \tag{47}$$

$$\int_{-\infty}^{\infty} \frac{1}{\sqrt{2\pi}} \exp\left(-\frac{z^2}{2}\right) \mathrm{d}z \left\{ \prod_{j\in S_c, j\neq 0} \left[1 - Q\left(z + \frac{M_j}{\sigma}\right)\right]\right\}$$

Appendix B

In order to evaluate D_{I1}, one direct way is to derive the joint pdf of the ordered statistics $\{\Omega_k\}_{k=0}^{N_c-1}$ and find the numerical results. However, this approach is non-trivial. We will use another approach such that we do not need to find the joint pdf of $\{\Omega_k\}$. In section 3.3, we define D_{I1} as

$$D_{I1} = \boldsymbol{E}\left\{\frac{\sum_{k=1}^{N_c-1}\Omega_k}{\Omega_0}\right\} \tag{48}$$

By using the concept of total probability, D_{I1} can be evaluated by

$$\begin{aligned} D_{I1} &= \sum_{j=0}^{N_c-1}\left\{\sum_{k\in S_c,k\neq j}\boldsymbol{E}\left[\frac{\alpha_k}{\alpha_j}\middle|\alpha_j=\max\{\alpha_i\},\, i\in S_c\right]P_r(A_j)\right\} \\ &= \sum_{j=0}^{N_c-1}\left\{\sum_{k\in S_c,k\neq j}\boldsymbol{E}\left[10^{\frac{m_k-m_j}{10}}10^{\frac{X_k-X_j}{10}}\middle|X_i\le X_j+m_j-m_i,\forall i\in S_c,i\neq j\right]P_r(A_j)\right\} \end{aligned} \tag{49}$$

where $\alpha_i = 10^{(m_i+X_i)/10}$ and X_i is zero-mean Gaussian with variance σ_i^2, $m_i = 10\log_{10}(P_i)$, event $A_j = \{\alpha_j = \max\{\alpha_i\},\, i\in S_c\}$, and S_c is the set of the nearest N_c BS's for the desired user. Define Υ_{kj} as

$$\Upsilon_{kj} = 10^{(m_k-m_j)/10} = \left(\frac{r_{ki}}{r_{kj}}\right)^{-a}\left(\frac{1+r_{ki}/g}{1+r_{kj}/g}\right)^{-b} \tag{50}$$

which is just the ratio of path loss from the BS's k and j to the desired user. Since the random variables X_k and X_j are assused to be independent if $k\neq j$. Thus, D_{I1} becomes

$$\begin{aligned} D_{I1} = \sum_{j=0}^{N_c-1}\sum_{k\in S_c,k\neq j}\Upsilon_{kj}\int_{-\infty}^{\infty}10^{-x_j/10}f_{X_j}(x_j)\mathrm{d}x_j\cdot \\ \left[\int_{-\infty}^{x_j+m_j-m_k}10^{-x_k/10}f_{X_k}(x_k)\mathrm{d}x_k\right]\cdot \\ \left\{\prod_{i\in S_c,i\neq k,j}F_{X_i}(x_j+m_j-m_i)\right\} \end{aligned} \tag{51}$$

In case that $\sigma_k = \sigma$, $\forall\, k\in S_c$ and by some manipulations, D_{I1} can be simplified to the form

$$\begin{aligned} D_{I1} = \sum_{j=0}^{N_c-1}\sum_{k\in S_c,k\neq j}\Upsilon_{kj}\exp(\lambda^2\sigma^2)\int_{-\infty}^{\infty}\frac{1}{\sqrt{2\pi}}\exp\cdot \\ \left(-\frac{z^2}{2}\right)\mathrm{d}z\left[1-\boldsymbol{Q}\left(z+\frac{m_j-m_k}{\sigma}-2\lambda\sigma\right)\right]\cdot \\ \left\{\prod_{i\in S_c,i\neq k,j}\left[1-\boldsymbol{Q}\left(z+\frac{m_j-m_k}{\sigma}-\lambda\sigma\right)\right]\right\} \end{aligned} \tag{52}$$

In the following, we will derive the expression of D_{I2} which is defined as

$$D_{I2} = \boldsymbol{E}\left(\sum_{k=N_c}^{K}\alpha_k\right)\boldsymbol{E}\left(\frac{1}{\Omega_0}\right) = \boldsymbol{E}(\mathcal{L}_R)\boldsymbol{E}\left(\frac{1}{\Omega_0}\right) \tag{53}$$

where $\mathcal{L}_R = \sum_{k=N_c}^{K}\alpha_k$ can be approximated by a log-normally distributed random variable and its statistics can be found by applying the recursive method described in [15]. Therefore, $\boldsymbol{E}(\mathcal{L}_R)$ becomes

$$\boldsymbol{E}(\mathcal{L}_R) = \boldsymbol{E}\left(10^{\frac{m_R+X_R}{10}}\right) = \exp\left(\lambda m_R+\frac{\lambda^2\sigma_R^2}{2}\right) \tag{54}$$

Following the same method used in the derivation of D_{I1}, we can find $\boldsymbol{E}(\Omega_0)$ as follows:

$$\begin{aligned} \boldsymbol{E}\left(\frac{1}{\Omega_0}\right) = \\ \sum_{j=0}^{N_c-1}\boldsymbol{E}\left[10^{-\alpha_j}\middle|\alpha_j\max\{\alpha_i\},\forall i\in S_c\right]P_r(A_j) \\ = \sum_{j=0}^{N_c-1}\boldsymbol{E}\left[10^{-\frac{m_j+X_j}{10}}\middle|X_i\le X_j+m_j-m_i,\right. \\ \left.\forall i\in S_c,\, i\neq j\right]P_r(A_j) \\ = \sum_{j=0}^{N_c-1}e^{-\lambda m_j}\int_{-\infty}^{\infty}e^{-\lambda x_j}f_{X_j}(x_j)\mathrm{d}x_j\cdot \\ \left[\prod_{i\in S_c,i\neq j}F_{X_i}(x_j+m_j-m_i)\right] \end{aligned} \tag{55}$$

Multiplying (54) with (55), D_{I2} becomes

$$\begin{aligned} D_{I2} = \left[\exp\left(\lambda m_R+\frac{\lambda^2\sigma_R^2}{2}\right)\right]\cdot \\ \sum_{j=0}^{N_c-1}\left[\exp\left(-\lambda m_j+\frac{\lambda^2\sigma^2}{2}\right)\right]\cdot \\ \left\{\prod_{i\in S_c,i\neq j}\left[1-\boldsymbol{Q}\left(z+\frac{m_j-m_i}{\sigma}-\lambda\sigma\right)\right]\right\} \end{aligned} \tag{56}$$

Note that the above expressions for D_{I1} and D_{I2} depend on the user's location in the cell. The area-averaged D_I can be evaluated by averaging over the possible locations of the user traversing the cell.

Acknowledgement

The authors would like to thank the anonymous reviewers for their helpful and constructive comments.

Manuscript received on May 15, 1994.

REFERENCES

[1] R. Bultitude, G. Bedal: *Propagation characteristics on microcellular urban mobile radio channels at 910 MHz.* "IEEE Journal on Selected Areas in Commun.", Vol. SAC-7, Jan. 1989, p. 31-39.

[2] L. Milstein, T. Rappaport, R. Barghouti: *Performance evaluation for cellular CDMA.* "IEEE Journal on Selected Areas in Commun.", Vol. SAC-10, May 1992, p. 680-689.

[3] K. Gilhousen, et al.: *On the capacity of a cellular CDMA system.* "IEEE Trans. on Vehicular Technology", Vol. VT-40, May 1991, p.303-312.

[4] A. Polydoros, et al.: *Vehicle to roadside communications study.* Tech. Rep., UCB-ITS-PRR-93-4, Communication Sciences Institute, University of Southern California, Nov. 1993.

[5] C. Sun: *On the performance analysis of microcelluler systems.* Ph.D. Thesis, University of Southern California, Aug. 1994.

[6] W. Yung: *DS/CDMA cellular systems in Rayleigh fading and log-normal shadowing channel.* "ICC'91", 1991, p.28.2.1-6.

[7] N. Amitay, et al.: *Measurements-based estimates of bit-error-ate performance in urban LOS microcells at 900 MHz.* "IEEE Trans. on Vehicular Technology", Vol. VT-41, Nov. 1992, p.414-423.

[8] M. Pursley: *Performance evaluation for phase-coded spread-spectrum multiple-access communications-Part I: system analysis.* "IEEE Trans. on Commun.", Vol. COM-25, Aug. 1977, p.795-799.

[9] P. Harley: *Short distance attenuation measurements at 900 MHz and 1.8 GHz using low antenna heights for microcells.* "IEEE Journal on Selected Areas in Commun.", Vol. SAC-7, Jan. 1989, p.5-11.

[10] H. Misser, R. Prasad: *Bit error probability of microcellular spread-spectrum multiple-access system in a shadowed Rician channel.* Proceedings of the 42nd IEEE Vehicular Technology Conference, 1992, p.439-442.

[11] R. Morrow, J. Lehnert: *Bit-to-bit error dependence in slotted DS/SSMA packet systems with random signature sequences.* "IEEE Trans. on Commun.", Vol. COM-37, Oct. 1989, p. 1052-1061.

[12] A. Viterbi, A. Viterbi, E. Zehavi: *Other-cell interference in cellular power-controlled CDMA.* "IEEE Trans. on Commun.", Vol. COM-42, Feb. 1994, p. 1501-1504.

[13] W. Lindsey: *Error probabilities for Rician fading multichannel reception of binary and N-ary signals.* "IEEE Trans. on Information Theory", Vol. IT-10, Oct. 1964, p.339-350.

[14] M. Abramowitz, I. Stegun: *Handbook of mathematical functions.* (NBS Applied Math. Series, Number 55), Washington, D.C.: U.S. Government Printing Office, 1964.

[15] S. Schwartz, Y. Yeh: *On the distribution function and moments of power sums with log-normal components.* "BSTJ", Vol. 61, Sep. 1982,p.1441-1462.

Chung-Ming Sun, Andreas Polydoros: **Performance Evaluation of Multi-Cell Direct-Sequence Microcellular Systems.**

ETT, Vol. 6 - No. 1 January - February 1995, p. 71 - 83

Dynamic Code Allocation for Integrated Voice and Multi-Priority Data Traffic in CDMA Networks

E. Geraniotis, Y.-W. Chang, W.-B. Yang
Center for Satellite and Hybrid Communication Networks
Institute for Systems Research, University of Maryland
College Park, MD 20742 - USA

Abstract. In the context of deriving schemes for efficient use of the spectrum by multi-media users in direct-sequence code-division multiple-access (DS/CDMA) networks we describe in this paper an optimal policy for CDMA code allocation to voice and multi-priority data traffic We consider CDMA networks with voice traffic and two types of data traffic: high priority data traffic with the same priority as voice traffic that requires real-time delivery and lower priority data traffic that can tolerate delay and thus can be queued. A movable boundary policy in the CDMA code domain is used for the voice and high priority data, whereas a small number of CDMA codes are reserved for the lower priority data which also utilizes any CDMA codes left unused by the other two traffic types. The optimal policy is obtained by minimizing a cost function consisting of the weighted sum of the rejection rates of voice and high priority data traffic subject to performance requirements (bit error rates or *BER*) on all traffic types. The queueing delay of the lower priority data traffic is also evaluated. A semi-Markov decision process (SMDP) with guaranteed *BER*s for voice and data traffic is used for formulating the dynamic code assignment problem. A value-iteration algorithm is applied to this SMDP to derive the optimal policy.

1. INTRODUCTION

Code-division multiple-access (CDMA) techniques find today many commercial applications beyond their traditional use in military communications. Cellular systems, mobile satellite networks, and personal communication networks (PCN) that use CDMA have been proposed and are currently under design, construction, or deployment [1 - 4]. Moreover, networks of LEO (Low Earth Orbit) and MEO (Medium Earth Orbit) satellites for world-wide (global) communications such as Loral/Qualcom's Globalstar and TRW's Odyssey that use CDMA have been proposed and are under design [5 - 6].

Desirable features of CDMA include: increased received signal quality due to protection offered against multipath fading, narrowband in-band interference (other radio signals), and intentional interference (jamming); reduced synchronization requirements (users do need to have a common clock); graceful performance degradation (to gradual addition of users or other interference); flexibility in accommodating multi-media (voice/data) users and users with multiple data rates; privacy is provided; and low-interference coexistence with other CDMA or narrowband systems operating in the same band.

As part of our continuing effort to provide schemes for efficient use of the spectrum in CDMA networks by multi-media users, we derive in this paper an optimal code allocation policy for voice and multi-priority data traffic. This work expands and complements our recent work of [7] where we derived optimal admission policies for a CDMA network with voice and data traffic. In that work, the voice traffic had full priority over the data traffic; the optimal policy pertained to voice traffic only, the data traffic could use only the CDMA codes left unused by the voice traffic, and if there were not a sufficient number of them available, it will be queued. Our work of [7] pertains to a CDMA network offering primarily voice services which also allows the accommodation of some data traffic at lower priority.

In our other recent work of [8] we described and analyzed schemes for voice and data integration in CDMA networks that use for voice traffic a threshold-based admission policy and for data traffic the ALOHA protocol with retransmissions based on feedback about the net-

work state (number of ongoing voice calls and data messages). In [9] we modified and extended the schemes of [8] to a hybrid satellite/terrestrial network using framed ALOHA with reservations on-board the satellite and the CDMA scheme of [8] for the terrestrial network. In both of these schemes voice has priority over data and data traffic is using whatever resources (CDMA codes or slots in framed ALOHA) were left unused by voice traffic. In all our previous work of [7-9] there is no attempt to allocate the resources (CDMA codes) more fairly between voice and data users.

By contrast, in this paper we consider a CDMA network of voice and two types of data users that employ direct-sequence spread-spectrum (DS/SS) signaling. The first type of data traffic has the same priority as the voice users, that is, it requires real-time delivery (thus it can not be queued) and it also requires lower bit error rate (*BER*) than voice. This type of data are considered important by the network and treated with the same level of fairness as voice traffic. The second type of data has a lower priority, it can tolerate delays and thus it can be queued; the required *BER* is larger or equal to that of the high priority data but definitely smaller than the one required for the voice traffic.

We derive an optimal code allocation scheme that determines the number of newly arrived voice calls and data users with high priority that are accepted in the network so that the long-term weighted blocking (rejection) rates of voice calls and data traffic is minimized and the packet error probabilities of these two traffic types are within acceptable limits. Although we refer to our scheme as a code allocation scheme, it is actually an admission policy, since it determines how many voice or data users can be admitted in the system (and allocated CDMA codes) from the total number of users arriving at the system (and requesting services). The activity characteristic of voice traffic is considered for increasing bandwidth efficiency. If the new arrivals are not accepted, they are blocked and there are no CDMA codes assigned to these arrivals.

For the lower priority data we consider two policies. According to the first policy there are no CDMA codes reserved for these data, they get assigned CDMA codes only when the combined voice and high priority data traffic leaves certain codes unused; this is done in a preemptive manner, when voice or high priority data requests arrive the codes are assigned back to them and the low priority data are queued. The second policy operates like the first except that there is also a small number of CDMA codes that are always assigned to low priority traffic; if there is a large demand from low priority data traffic the reserved codes are assigned first and the remaining low priority data packets use the codes left unused by the voice or high priority data traffic or, if there is not a sufficient number of them, they are queued. For both schemes the *BER* requirement for the low priority data traffic is met.

The performance measures are the average blocking rates and average throughputs of the voice calls and all data messages as functions of the offered voice and data traffic loads under the proposed optimal code allocation policy. The queueing delay and the packet loss probability of the low priority data traffic is also evaluated. A semi-Markov decision process (SMDP) with guaranteed BERs for voice and data traffic is used for formulating the system operation as a dynamic code assignment problem. A value-iteration algorithm is applied to this SMDP to derive the optimal policy. The paper is organized as follows. In section 2, the system models are described. The optimal code allocation policy for the voice and high priority data traffic is derived in section 3. In section 4, the performance analyses for voice and high priority data traffic are conducted followed by the performance analysis of the low priority data traffic in section 5. Numerical results and conclusions are presented in sections 6 and 7.

2. SYSTEM MODEL

Let N_v, N_{d_1} and N_{d_2} be the total population of voice and two types of data traffic, respectively, in the CDMA system. From these users a number of them are active at each instant of time according to models described in the next paragraph. Time is divided into slots of duration equal to the transmission time of one packet. In our model, packet transmissions start at common clock instances and packets have constant length of 1000 to few thousand bits. Fig. 1 shows a CDMA system with mobile voice and data user populations. However, our traffic models, the CDMA interference model, the optimal CDMA code allocation protocol, and the accompanying performance analysis of this paper can be applied (with the appropriate modifications) to any CDMA system with voice and data users cellular, mobile satellite, or PCS.

The voice user population is modeled by a three-state (idle, silent, and talkspurt) discrete-time Markov pro-

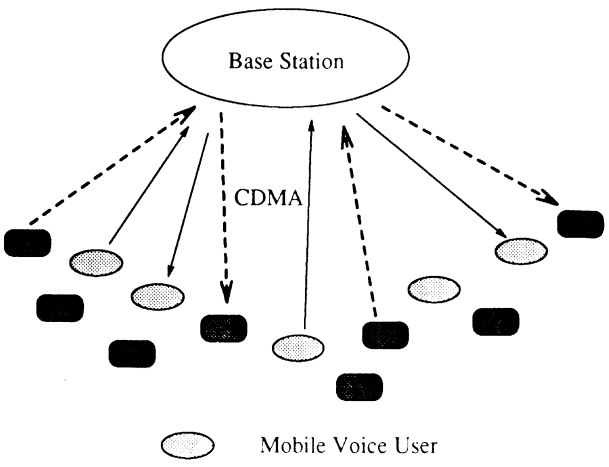

Fig. 1 - Model for mobile CDMA system.

cess each with transition probabilities p_{01}^v, p_{10}^v, p_{12}^v, and p_{21}^v, as shown in Fig. 2. The mean duration of the idle and active periods of voice traffic are $1/p_{01}^v$ and $1/p_{10}^v$. Each data user of high priority is modeled by a two-state (OFF/ON or idle/active) Bernoulli process, shown in Fig. 3 with transition probabilities p_{01}^d and p_{10}^d. Similarly, the mean duration of the idle and active periods of data users are $1/p_{01}^d$ and $1/p_{10}^d$. For the low priority data traffic we assume the number of arriving data packets follows a Poisson distribution with mean rate λ_d. There is some justification for using different models for the high and low priority data users. The high priority data users are treated in the same manner as voice users and the finite population assumption is essential in deriving the optimal allocation strategy. On the other hand the low priority data users are assigned only the codes left unused by all other traffic (voice and data), no optimization takes place, and a Poisson population model simplifies our analysis and admission policy; we could also use a Bernoulli model for the low priority users, but that will complicate matters. Finally, we assume that the data streams of all voice and data users are statistically independent.

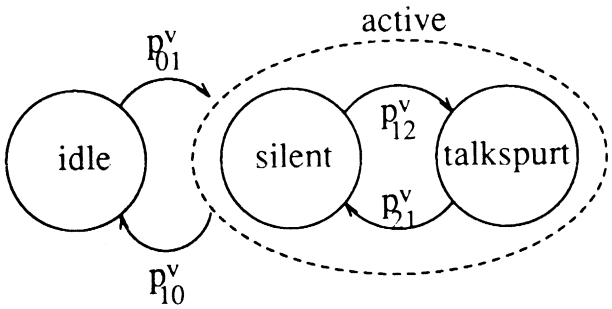

Fig. 2 - Model for voice users.

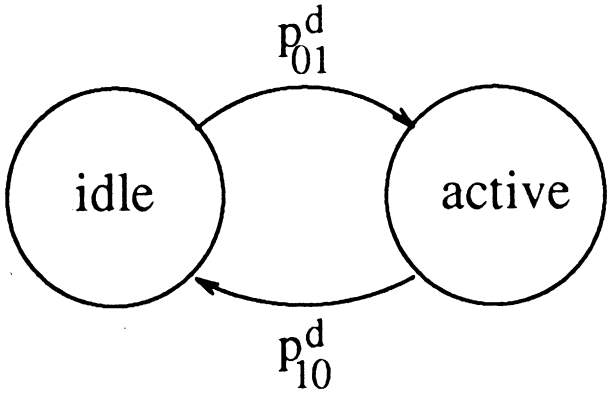

Fig. 3 - Model for data users.

We define the multiple-access capability (MAC) index K_v as the number of voice users that can be accommodated simultaneously, such that the expected packet error probability of voice traffic remains below a specified threshold. Similarly, the MAC index K_{d_1} and K_{d_2} for data users is the number of data users that can transmit simultaneously with a tolerable packet error. Thus we have

$$P_E(k) \le P_E^v, \qquad \forall\, k \le K_v \tag{1}$$

$$P_E(k) \le P_E^{d_1}, \qquad \forall\, k \le K_{d_1} \tag{2}$$

$$P_E(k) \le P_E^{d_2}, \qquad \forall\, k \le K_{d_2} \tag{3}$$

where P_E^v, $P_E^{d_1}$ and $P_E^{d_2}$ are the maximum tolerable voice and data packer error probabilities, respectively, and $P_E(k)$ is the packet error probability in the presence of k simultaneous packet transmissions [10], where k includes both voice users and active data users. In practice, $P_E^v > \max\{P_E^{d_1}, P_E^{d_2}\}$, and, therefore, $K_v > \max\{K_{d_1}, K_{d_2}\}$. Here we also assume $P_E^{d_1} \le P_E^{d_2}$, so that $K_{d_1} \le K_{d_2}$; this assumption can be easily relaxed and any relationship between $P_E^{d_1}$ and $P_E^{d_2}$ can be accommodated. If the total number of simultaneous users is $k \le K_{d_1}$, then all k data or voice packets are received with acceptable error probabilities. If $K_{d_1} < k \le K_{d_2}$, then, among the k packets, the voice packets and the data packets with lower priority are received with acceptable error probabilities, whereas the data packets with higher priority are received with error probabilities higher than the acceptable value $P_E^{d_1}$. If $K_{d_2} < k \le K_v$, then only the voice packets are received with acceptable error probabilities. Finally, if $K_v < k$, then all voice or data packets are received with unacceptable error probabilities. Each active voice or data user accepted into the system employs a distinct code for the transmission of its packets.

If binary phase-shift keying (BPSK) with coherent demodulation and binary convolutional codes with rate 1/2 and constraint length 7 and Viterbi decoding and hard-decisions is used, one can evaluate an upper bound [10] on the packet error probability of a single-receiver system $P_E(k)$. If N is the number of chips per bit and k the number of simultaneous DS/CDMA signals that are both time and phase-synchronous; then the symbol error probability ρ under a Gaussian noise channel from [10]

$$\rho \approx Q\left(\left[\frac{N_0}{E_b} + \frac{(K-1)}{N}\right]^{-1/2}\right) \tag{4}$$

where E_b is the energy per information bit in the received signal, $N_0/2$ is the two-sided spectral density of Gaussian noise, and

$$Q(x) = \frac{1}{\sqrt{2\pi}} \int_x^\infty \exp\left(-\frac{u^2}{2}\right) \mathrm{d}\,u \tag{5}$$

From ρ, we can obtain an upper bound of packet error probability $P_E(k)$ from (3.29) and (4.1) of [10] and Table 1 of [11]. Then the upper bound for $P_E(k)$ is plugged in the inequalities involving P_E^v, $P_E^{d_1}$ and $P_E^{d_2}$ above to obtain the MAC indices K_v, K_{d_1} and K_{d_2},

when the *BER* (and thus the packet error rate) specifications for voice and the two data traffic types are given.

At this point it is important to emphasize that the models and the analysis of this paper are not limited in any manner by the choice of modulation/demodulation or coding/decoding techniques used for DS/CDMA. Actually, the basic traffic models and optimal allocation schemes are in principle and in structure the same for direct-sequence and for frequency-hopped (FH) CDMA systems. The only difference lies in the expressions used for deriving $P_E(k)$ in (1) - (3); the expressions in [10] were used here for DS/CDMA systems. Corresponding expressions in [14] and [15] can be used for FH/CDMA systems. Also notice that the channel impairments assumed present in our system model are limited to i) other-user interference of CDMA and ii) additive white Gaussian noise (-AWGN). We can incorporate of the effects of channel fading (e.g., multipath) and shadowing as well as of power control (for unequal received power levels); however, this work is beyond the scope of this paper; we will report on it in a forthcoming publication. Finally, we assume in this paper that all voice and data users have the same data rate; this assumption can also be relaxed and a true multi-media multi-rate CDMA system can be optimized and analyzed, this is the subject of another forthcoming paper.

Going back to the model of voice traffic, we notice that since each active voice user is in either silent or talkspurt mode, the number of codes which are assigned to active users can be larger than K_v while still guaranteeing the same voice-packet error probability. This is because, even though the number of total active voice users may be larger than K_v, if the number of voice users in talkspurt is less than K_v, the voice packet error probability will still be less than P_E^v.

In this paper, voice and high priority data packets share all but a small number $D2$ (where $D2 < K_{d_2}$) of the available CDMA codes according to the dynamic movable boundary allocation scheme described in detail in section 3. $D2$ codes are always allocated to low priority data users and the remaining low priority data users either use the CDMA codes (if any) left unused by voice and high priority data traffic or their packets are queued.

Given the MAC indices K_v and K_{d_1}, we may compute the maximum number of acceptable voice calls and data users as follows. Let V_t and $D_t^{(1)}$ be the number of active voice and data users at the t-th time-slot. Then the values of V_t and $D_t^{(1)}$ must satisfy the following inequalities

$$\begin{cases} 0 \le D_t^{(1)} \le K_{d_1} - D2 \\ 0 \le V_t \le M_1\left(D_t^{(1)}\right) \end{cases} \tag{6}$$

where $M_1(D_t^{(1)})$ is the maximum number of active voice calls when the number of active data users is $D_t^{(1)}$. The reason that we determine the bound on active voice calls from the current state of high priority data traffic, is that the data have more stringent requirements on *BER* (recall that $P_E^{d_1}$, $P_E^{d_2} < P_E^v$). The value of $M_1(D_t^{(1)})$ is obtained by ensuring that the probability that the number of active calls in talkspurt (out of $M_1(D_t^{(1)})$) is larger than $K_{d_1} - D_t^{(1)} - D2$ remains smaller than a prespecified acceptable value δ, namely,

$$M_1\left(D_t^{(1)}\right) = \arg\max_M \left\{ \sum_{i=K_{d_1}-D_t^{(1)}-D2+1}^{M} \binom{M}{i} \cdot [p_v]^i [1-p_v]^{M-1} < \delta \right\} \tag{7}$$

This is equivalent to stating that under the conditions (6) and (7) the data packet error probability remains smaller than $P_E^{d_1}$ and the voice packet error probability remains smaller than P_E^v with confidence (probability) $1 - \delta$.

In (7) p_v denotes the probability that each active voice user is in talkspurt mode, it turns out that

$$p_v = \frac{p_{12}^v}{p_{12}^v + p_{21}^v} \tag{8}$$

Typical values of the transition probabilities are [12]

$$p_{21} = 0.00833, \quad p_{12} = 0.00556 \tag{9}$$

Therefore, a typical value of p_v is 0.4.

The function $M_1(D_t^{(1)})$ of (7) is non-increasing and the maximum number of active voice calls or active data users is given by $M_1(D_t^{(1)} = 0)$. Thus, the maximum number of CDMA codes to be assigned is $M_1(D_t^{(1)} = 0)$. However, as the value of $D_t^{(1)}$ increases, $M_1(D_t^{(1)})$ decreases dramatically. Consequently, the number of available codes for voice traffic must decrease to meet the performance requirement $P_E^{d_1}$ of data. If $M_1(D_t^{(1)} = 0) = K_v/p_v$, which is generally used for calculating the maximum number of active voice users in the absence of data traffic, then the packet error probability of data exceeds the prespecified value with unacceptably high probability. Among the goals of this paper, is to derive protocols that guarantee the performance of data; thus, the maximum number of voice users is determined so that (7) is satisfied and it takes values between K_v and K_v/p_v (that is, $K_v < M_1(D_t^{(1)}) < K_v/p_v$). Refer to Tables 1a and 1b (for $D_2 = 0$) and Table 1c (for $D_2 = 1$) in section 6 for the values assumed by $M_1(D_t^{(1)})$ for $\delta = 0.01$ (i.e., confidence level 99 %).

3. OPTIMAL CODE ALLOCATION

In this section, we find an optimal policy for code allocation, that is a sequence of allocation functions

$$\begin{cases} F^*\left(V_t, D_t^{(1)}, v_t, d_t^{(1)}, t\right), & t = 0, 1, 2, \ldots, \\ G^*\left(V_t, D_t^{(1)}, v_t, d_t^{(1)}, t\right), & t = 0, 1, 2, \ldots, \end{cases} \tag{10}$$

which minimizes an average cost under the constraints that the mean packet error probabilities of voice and data traffic remain below prespecified values. The average cost is defined as the weighted sum of the rejection (or blocking) rates of voice and high priority data traffic; that is the number of voice calls or high priority data packets from the arrivals that can not be accepted into the system (and assigned CDMA codes) per unit of time. By calibrating the weights in this sum we can assign any desirable priority to voice and data traffic.

The value of an allocation function is called an action. The value of $F^*(.,.,.,.,.)$ is the action a_t^v for voice traffic which represents the number of codes which are assigned to newly active voice calls. Similarly, the value of $G^*(.,.,.,.,.)$ is the action $a_t^{d_1}$ for data traffic which represents the number of codes which are assigned to newly active data users. The newly accepted voice calls and data users should not cause the bounds on the packet error probabilities (for the entire simultaneous system population) to be exceeded.

Let S be the state space of the code allocation problem, then we have

$$\begin{aligned} S = \Big\{ z_t = \left(V_t, D_t^{(1)}, v_t, d_t^{(1)}\right) \Big| \; & 0 \le D_t^{(1)} \le K_{d_1} - D\,2, \\ & 0 \le V_t \le M_1\left(D_t^{(1)}\right), \quad 0 \le v_t \le N_v - V_t, \\ & 0 \le d_t^{(1)} \le N_{d_1} - D_t^{(1)} \Big\} \end{aligned} \tag{11}$$

where v_t and $d_t^{(1)}$ are the number of newly active voice and data users at the t-th time-slot, respectively. For ease of implementation, we consider stationary policies only. A policy is called *stationary* if the actions chosen for voice and data traffic at t-th time-slot merely depend upon the state at time-slot t.

At the beginning of the the t-th time-slot, assume that the state is $z_t = (V_t, D_t^{(1)}, v_t, d_t^{(1)})$ and that the action $a_t = (a_t^v, a_t^{d_1}) \in A(z_t)$ is followed. This incurs a cost

$$C\left(z_t, a_t\right) = w_v\left(v_t - a_t^v\right) + w_d\left(d_t^{(1)} - a_t^{d_1}\right) \tag{12}$$

where w_v and w_d are relative weighting constants and $A(z_t)$ is an action subspace given the system state z_t

$$\begin{aligned} A\left(z_t\right) = \Big\{ \left(a_t^v, a_t^{d_1}\right) \Big| \; & 0 \le a_t^v \le v_t, \; 0 \le a_t^{d_1} \le d_t^{(1)}, \\ & 0 \le D_t^{(1)} + a_t^{d_1} \le K_{d_1} - D\,2, \\ & 0 \le V_t + a_t^v \le M_1\left(D_t^{(1)} + a_t^{d_1}\right) \Big\} \end{aligned} \tag{13}$$

Then the action space is $\boldsymbol{A} = A(z_t) \times S$.

The transition probabilities that at the next epoch the system will be in state $\bar{z}_t$, if action a_t is selected at the present state z_t, are the following:

$$\begin{aligned} P_{z_t \bar{z}_t}\left(a_t\right) = P\Big\{ \bar{z}_t = \left(\bar{V}_t, \bar{D}_t^{(1)}, \bar{v}_t, \bar{d}_t^{(1)}\right) \Big| \; & z_t = \\ & \left(V_t, D_t^{(1)}, v_t, d_t^{(1)}\right), a_t = \left(a_t^v, a_t^{d_1}\right) \Big\} = \\ & b\left(V_t, V_t + a_t^v - \bar{V}_t, p_{10}^v\right) \cdot \\ & b\left(D_t^{(1)}, D_t^{(1)} + a_t^{d_1} - \bar{D}_t^{(1)}, p_{10}^d\right) \cdot \\ & b\left(N_v - V_t - a_t^v, \bar{v}_t, p_{01}^v\right) \cdot \\ & b\left(N_{d_1} - D_t^{(1)} - a_t^{d_1}, \bar{d}_t^{(1)}, p_{01}^d\right) \end{aligned} \tag{14}$$

where $b(M, m, p)$ denotes the binomial distribution with parameters M and p, where $0 \le p \le 1$.

$$b\left(M, m, p\right) = \begin{cases} \binom{M}{m} p^m \left(1-p\right)^{M-m}, & \text{if } 0 \le m \le M \\ 0, & \text{elsewhere} \end{cases} \tag{15}$$

where $b(0, 0, p) = 1$.

In addition, the expected time until the next decision epoch, given that action a_t is followed at the present state z_t, is $\tau(z_t, a_t)$ in packet-slots, where

$$\begin{aligned} \tau\left(z_t, a_t\right) = \Bigg\lceil \Big\{ 1 - & \left(1 - p_{01}^v\right)^{N_v - V_t - a_t^v} \left(1 - p_{10}^v\right)^{V_t + a_t^v} \cdot \\ & \left(1 - p_{01}^d\right)^{N_{d_1} - D_t^{(1)} - a_t^{d_1}} \left(1 - p_{10}^d\right)^{D_t^{(1)} + a_t^{d_1}} \Big\}^{-1} \Bigg\rceil \end{aligned} \tag{16}$$

Here it is assumed that $\tau(z_t, a_t) > 0$, for all states and actions. In the above expression the entity in { } represents the probability of no new arrival to and no new service completion from the current system state (z_t, a_t) in any packet-slot; then $1/\{\ \}$ stands for the mean of the geometrically distributed number of time-slots during which the system remains unchanged (holding time).

The objective of the code allocation problem is to find an optimal stationary policy which minimizes the weighted rejection rates, that is

$$\text{Minimize} \sum_{z_t \in S} \sum_{a_t \in A(z_t)} \left[w_v \frac{v_t - a_t^v}{\tau\left(z_t, a_t\right)} + w_d \frac{d_t^{(1)} - a_t^{d_1}}{\tau\left(z_t, a_t\right)} \right]$$

The optimal allocation problem is formulated as below:

$$\text{Minimize} \sum_{z_t \in S} \sum_{a_t \in A(z_t)} C(z_t, a_t)\, u(z_t, a_t)$$

$$\text{subject to} \sum_{a_t \in A(\bar{z}_t)} u(\bar{z}_t, a_t) = \sum_{z_t \in S} \sum_{a_t \in A(z_t)} P_{z_t \bar{z}_t}(a_t)\, u(z_t, a_t) \cdot \tag{17}$$

$$\sum_{z_t \in S} \sum_{a_t \in A(z_t)} \tau(z_t, a_t)\, u(z_t, a_t) = 1,$$

$$u(z_t, a_t) \geq 0, \quad \bar{z}_t \in S$$

where

$$u(z_t, a_t) = \frac{\pi(z_t, a_t)}{\tau(z_t, a_t)} \tag{18}$$

and $\pi(z_t, a_t)$ is the steady state probability distribution at the state z_t and its action a_t. The *value-iteration algorithm* [13] of a semi-Markov decision model is able to solve the above optimal code allocation problem. The value-iteration algorithm is described as below.

Step 0: Choose $V_0(z_t)$ and τ such that $0 \leq V_0(z_t) \leq \min_{a_t}\{C(z_t, a_t)/\tau(z_t, a_t)\}$, for all z_t and $0 \leq \tau \leq \min_{z_t, a_t} \tau(z_t, a_t)$, for all z_t and a_t. Let $n := 1$.

Step 1: Compute the recursive function of $V_n(z_t)$ for all z_t, from

$$V_n(z_t) = \min_{a_t \in A_t} \left\{ \frac{C(z_t, a_t)}{\tau(z_t, a_t)} + \frac{\tau}{\tau(z_t, a_t)} \cdot \sum_{\bar{z}_t} P_{z_t \bar{z}_t}(a_t)\, V_{n-1}(\bar{z}_t) + \left[1 - \frac{\tau}{\tau(z_t, a_t)}\right] V_{n-1}(z_t) \right\}$$

and determine $\varphi(n)$ as a stationary policy [sequence of actions that minimize the RHS of the above equation].

Step 2: Compute the bounds

$$l_n = \min_{z_t} \{V_n(z_t) - V_{n-1}(z_t)\} \tag{19}$$

and

$$L_n = \max_{z_t} \{V_n(z_t) - V_{n-1}(z_t)\} \tag{20}$$

The algorithm terminates and outputs policy $\varphi(n)$, when $0 \leq (L_n - l_n) \leq \varepsilon l_n$, where ε is a prespecified bound on the relative error (accuracy).

Otherwise, go to *step* 3.

Step 3: $n := n + 1$ and go to *step* 1.

From the above algorithm, we obtain an optimal policy φ for managing the voice and high priority data traffic in the CDMA system. This policy describes the optimal action $a_t = (a_t^v, a_t^{d_1})$ corresponding to the state $z_t = (V_t, D_t^{(1)}, v_t, d_t^{(1)})$, that is, the number of voice calls and high priority data uses out of the new arrivals $(v_t, d_t^{(1)})$ that are allocated CDMA codes and are allowed to transmit together with the continuing users $(V_t, D_t^{(1)})$.

3.1. *Implementation Issues*

The optimal code allocation policy derived in this section is fairly complicated. It appears to lack a simple structure; for example we can not determine the optimal action by comparing the components of the state z_t to proper thresholds and/or to each other. Moreover, the derivation requires multi-dimensional optimization and is rather time-consuming to perform on-line. We are pursuing two solutions to this problem. The first is to construct a look-up table describing the optimal policy; that is, a table listing all possible states $z_t = (V_t, D_t^{(1)}, v_t, d_t^{(1)})$ and the corresponding optimal actions $a_t = (a_t^v, a_t^{d_1})$. This table is constructed by performing the necessary optimization computations off-line for the most likely set of system parameters. Excessive memory size will be the problem here for large systems. The alternative is to derive near-optimal or sub-optimal policies that possess structure and approximate closely the performance of the optimal policy; these will still use some parameters and small-size look-up tables derived off-line but a substantial fraction of the computations for determining the proper action given the network state will take place on-line. We will report this work in a future paper.

4. PERFORMANCE ANALYSIS

In this section we analyze the performance of voice and high priority data traffic under the optimal policy. The performance measures include the rejection rates (number of calls or data messages blocked per unit of time)and the throughputs of voice and high priority data traffic. The performance of low priority data traffic is analyzed in the next section.

To analyze the performance, we have to solve the following set of linear equations

$$\begin{cases} \pi\left(\bar{x}_t = \left(\bar{V}_t, \bar{D}_t^{(1)}\right)\right) = \sum_{V_t} \sum_{D_t^{(1)}} \pi\left(x_t = \left(V_t, D_t^{(1)}\right)\right) P_{\bar{x}_t | x_t} \\ \sum_{V_t} \sum_{D_t^{(1)}} \pi\left(x_t = \left(V_t, D_t^{(1)}\right)\right) = 1 \end{cases} \tag{21}$$

where $\pi = (V_t, D_t^{(1)})$ is the steady state probability distribution at the state $x_t = (V_t, D_t^{(1)})$ and the transition probability $P_{\bar{x}_t | x_t}$ under the optimal action $a_t = (a_t^v, a_t^{d_1})$, under the optimal policy φ, is given by

$$P_{\bar{x}_t|x_t} = P\left\{\bar{x}_t = \left(\bar{V}_t, \bar{D}_t^{(1)}\right) \middle| x_t = \left(V_t, D_t^{(1)}\right),\ a_t = \left(a_t^v, a_t^{d_1}\right)\right\} = \sum_{v_t=0}^{N_v - V_t} \sum_{d_t^{(1)}=0}^{N_{d_1} - D_t^{(1)}} P_\varphi\left\{\bar{x}_t = \left(\bar{V}_t, \bar{D}_t^{(1)}\right) \middle| x_t = \left(V_t, D_t^{(1)}\right),\ a_t = \left(a_t^v, a_t^{d_1}\right), v_t, d_t^{(1)}\right\} P\left\{v_t, d_t^{(1)} \middle| x_t = \left(V_t, D_t^{(1)}\right),\ a_t = \left(a_t^v, a_t^{d_1}\right)\right\} = \sum_{v_t=0}^{N_v - V_t} \sum_{d_t^{(1)}=0}^{N_{d_1} - D_t^{(1)}} P_\varphi\left\{\bar{x}_t = \left(\bar{V}_t, \bar{D}_t^{(1)}\right) \middle| x_t = \left(V_t, D_t^{(1)}\right),\ a_t = \left(a_t^v, a_t^{d_1}\right), v_t, d_t^{(1)}\right\} \cdot P\left\{v_t, d_t^{(1)} \middle| x_t = \left(V_t, D_t^{(1)}\right)\right\} = \sum_{v_t=0}^{N_v - V_t} \sum_{d_t^{(1)}=0}^{N_{d_1} - D_t^{(1)}} b\left(V_t, V_t + a_t^v - \bar{V}_t, p_{10}^v\right) b\left(D_t^{(1)}, D_t^{(1)} + a_t^{d_1} - \bar{D}_t^{(1)}, p_{10}^d\right) \cdot b\left(N_v - V_t, v_t, p_{01}^v\right) b\left(N_{d_1} - D_t^{(1)}, d_t^{(1)}, p_{01}^d\right) \tag{22}$$

Finally, after solving the aforementioned system of linear equations with $P_{\bar{x}_t|x_t}$ obtained from the above equation, we are able to calculate the steady-state probability distribution $\pi(V_t, D_t^{(1)})$ of the state $x_t = (V_t, D_t^{(1)})$. Since all voice and data users are statistically independent each other, the blocking rates of calls and high priority data messages under the optimal allocation policy φ are given by

$$P_B^v = \frac{\sum_{V_t} \sum_{D_t^{(1)}} \sum_{v_t} \sum_{d_t^{(1)}} \left(v_t - a_t^v\right) \pi\left(V_t, D_t^{(1)}, v_t, d_t^{(1)}\right)}{\sum_{V_t} \sum_{D_t^{(1)}} \sum_{v_t} \sum_{d_t^{(1)}} v_t \cdot \pi\left(V_t, D_t^{(1)}, v_t, d_t^{(1)}\right)} \tag{23}$$

$$P_B^{d_1} = \frac{\sum_{V_t} \sum_{D_t^{(1)}} \sum_{v_t} \sum_{d_t^{(1)}} \left(d_t^{(1)} - a_t^{d_1}\right) \pi\left(V_t, D_t^{(1)}, v_t, d_t^{(1)}\right)}{\sum_{V_t} \sum_{D_t^{(1)}} \sum_{v_t} \sum_{d_t^{(1)}} d_t^{(1)}\, \pi\left(V_t, D_t^{(1)}, v_t, d_t^{(1)}\right)} \tag{24}$$

where the joint probability $\pi(V_t, D_t^{(1)}, v_t, d_t^{(1)})$ is evaluated in a sequence of steps described below

$$\pi\left(V_t, D_t^{(1)}, v_t, d_t^{(1)}\right) = P_r\left(v_t, d_t^{(1)} \middle| V_t, D_t^{(1)}\right) \pi\left(V_t, D_t^{(1)}\right) = P_r\left(v_t \middle| V_t\right)\ P_r\left(d_t^{(1)} \middle| D_t^{(1)}\right) \pi\left(V_t, D_t^{(1)}\right) \tag{25}$$

using the facts that

$$P_r\left(v_t \middle| V_t\right) = b\left(N_v - V_t, v_t, p_{01}^v\right) \tag{26}$$

$$P_r\left(d_t^{(1)} \middle| D_t^{(1)}\right) = b\left(N_{d_1} - D_t^{(1)}, d_t^{(1)}, p_{01}^d\right) \tag{27}$$

The throughputs of voice and data traffic are given by

$$\eta_v = \sum_{V_t} \sum_{D_t^{(1)}} V_t \cdot \pi\left(V_t, D_t^{(1)}\right) \tag{28}$$

$$\eta_{d_1} = \sum_{V_t} \sum_{D_t^{(1)}} D_t^{(1)} \cdot \pi\left(V_t, D_t^{(1)}\right) \tag{29}$$

5. DATA TRAFFIC ANALYSIS

According to the code allocation protocol considered in this paper the surplus of low priority data packets is queued, if i) all $D2$ CDMA codes reserved for them are used and ii) there are no codes left unsed by the voice and high priority data. This queueing will be necessary for both the *return link* [from mobile to satellite and gateway station (for satellite networks)] or from mobile to base station (for cellular networks)] as well as for the *forward link* [from gateway to mobile or from base station to mobile] of CDMA networks. For the forward link our analysis and derivation of an efficient code allocation policy is complicated by the fact that the low priority data traffic and the desirable decision (admission) policy must be distributed at the mobile sites. Such a distributed multiple-access protocol will be very complex and its analysis is beyond the scope of this paper. However, for the return link all traffic is concentrated at the gateway or base station and there is a single decision maker: the network controller at that station.

For the scenario described in the previous paragraph there are two approaches that we can follow for modeling and performance evaluation. According to the first approach, the data traffic evolution is modeled by an $M/D/c/B$ queueing model, where B is the buffer size and the number of servers (e.g., CDMA codes) available for the low priority data traffic. We can then obtain the performance measures (throughput, delay, and packet loss probability) for low priority data traffic from an $M/D/c/B$ queueing model with fixed c and then average these performance measures over the probability distribution $q(c)$ of c. Alternatively, we can obtain the transition probability matrix for the states of the system from scratch, without any reference to the $M/D/c/B$ model, and work with the associated Markov chain. In the remaining of this section we follow this second approach.

The probability distribution $q(c)$ of the number of available servers c for low priority data packets at any time-slot is obtained as follows:

$$q(c) = \sum_{\left\{D_t^{(1)} \neq 0,\ M_1\left(D_t^{(1)}+c+1\right) < V_t \le M_1\left(D_t^{(1)}+c\right)\right\}} \pi\left(V_t, D_t^{(1)}\right) + \sum_{\left\{D_t^{(1)} = 0,\ M_2\,(c+1) < V_t \le M_2\,(c)\right\}} \pi\left(V_t, D_t^{(1)}\right) \tag{30}$$

where $M_2(D_t^{(1)})$ is defined similar to $M_1(D_t^{(1)})$ in eq.

(7) with K_{d_1} replaced by K_{d_2}.

Assume that the data buffer at the gateway (for satellite networks) or the base-station (for cellular networks) has size B. Let the number of data packets in the buffer at the t-th time-slot be n_t, where $0 \le n_t \le B$. The number of arriving data packets at each time-slot is Poisson with mean rate λ_{d_2}. Let $\bar{l}_t^{\,d}$ be the number of arrival packets at t-th time-slot, which is independent of n_t; then we have

$$\bar{n}_t = n_t + \bar{l}_t^{\,d} - \bar{d}_t \tag{31}$$

where $\bar{d}_t$ is the number of departing data packets that are transmitted at the beginning of the next time-slot; these depend upon n_t and the number of available channels for data users as $\bar{d}_t = \min\{n_t, c + D2\}$. The states $n_t = 0, 1, \ldots, B$ follow a discrete Markov chain and their steady-state probability distribution π^{d_2} is obtained from the solution of the following set of $B + 1$ linear equations

$$\begin{cases} \pi^{d_2} = \pi^{d_2} \cdot P_{\bar{n}_t \mid n_t} \\ \sum_{k=0}^{B} \pi^{d_2}(k) = 1 \end{cases} \tag{32}$$

where $P_{\bar{n}_t|n_t}$ is the time-slot transition probability matrix for data under the threshold model. The entries of the transition matrix $P_{\bar{n}_t|n_t}$ are obtained from the relationships

$$P_{\bar{n}_t|n_t} = \sum_{\bar{l}_t^{\,d}=0}^{\infty} \sum_{c=0}^{K_{d_2}-D2} P\left(\bar{n}_t \mid n_t, \bar{l}_t^{\,d}, c\right) P\left(\bar{l}_t^{\,d}\right) q(c) \tag{33}$$

where $P(\bar{l}_t^{\,d})$is independent of n_t and is given by

$$P\left(\bar{l}_t^{\,d} = k\right) = \frac{e^{-\lambda_{d_2}} \lambda_{d_2}^{\ k}}{k!}, \quad k = 0, 1, 2, \ldots, \tag{34}$$

for the Poisson model of arriving data traffic (at gateways or base stations). The random variable c only depends on the number of channels used for voice calls and high priority data and is independent of n_t and $\bar{l}_t^{\,d}$. Thus we have

$$P\left(\bar{n}_t \mid n_t, \bar{l}_t^{\,d}, c\right) = \begin{cases} 1, & \text{if } \bar{n}_t = \min\left\{B, n_t + \bar{l}_t^{\,d} - \min\left(n_t, c + D2\right)\right\} \\ 0, & \text{elsewhere.} \end{cases} \tag{35}$$

After obtaining the time-slot transition matrix $P_{\bar{n}_t|n_t}$, we can compute the steady-state probability distribution $\pi^{d_2}(n_t)$, for all $0 \le n_t \le B$. From the latter we can easily obtain the average data delay and the packet loss probability, which is due to the finite buffer size at the gateways or the base stations. First we obtain the average data throughput as

$$\eta_{d_2} = \sum_{c=0}^{K_{d_2}-D2} \sum_{n_t=1}^{B} \min\left(c + D2, n_t\right) \pi^{d_2}\left(n_t\right) q(c) \tag{36}$$

and the average total data delay

$$D_{d_2} = 1 + \frac{1}{2} + \frac{1}{\eta_{d_2}} \sum_{n_t=1}^{B} n_t \, \pi^{d_2}\left(n_t\right) \tag{37}$$

where the value of D_{d_2} is in packets (time-slots), 1 is the service time of one packet, 1/2 is the average waiting time from the arrival time of one packet to the beginning of the next time-slot, and the last term in the right-hand side represents the average data queueing delay. For gateways connecting satellites and mobiles the round trip propagation time between earth stations and satellites may have to be added; the latter delay can be easily computed from the satellite altitude and translated to time-slots by dividing by the packet transmission time. Finally, the packet loss probability is given by

$$P_L = \left(\lambda_{d_2} - \eta_{d_2}\right) / \lambda_{d_2} \tag{38}$$

6. NUMERICAL RESULTS

For our performance results we assume that the DS/CDMA system employs BPSK data modulation with coherent demodulation, binary convolutional codes with rate 1/2 and constraint length 7, and Viterbi decoding with hard-decisions. The parameter values $E_b/N_0 = 9$ dB and $N = 255$ are used in the numerical computations. For the MAC indices $K_v = 15$ and $K_{d_1} = K_{d_2} = 10$ the corresponding packet error probabilities are $P_E^{v} = 3 \times 10^{-3}$ and $P_E^{d_1} = P_E^{d_2} = 1.5 \times 10^{-4}$, respectively. We present the numerical results for $D2 = 0$, that is, there are no CDMA codes reserved for the low priority data, and $D2 = 1$, that is, a single CDMA code is reserved. In eq. (7), we set $\delta = 1\%$; resulting in a probability of 0.99 that the number of active calls in talkspurt is less than and equal to $K_{d_1} - D_t^{(1)}$. Then, if up to $M_1(D_t^{(1)})$ voice calls and $D_t^{(1)}$ data users are in the system, the above voice and data *BER* (and packet error) requirements are met. The values of $M_1(D_t^{(1)})$ as shown in Table 1a when $\delta = 1\%$. For comparison purposes, notice that, if the voice activity characteristic is not taken into account, then the maximum number of active voice users is 9 rather than 13 when there is 1 active data user in the system and 15 rather than 24 when there is no active data user in the system. Table 1b and 1c present similar results for the smaller MAC indices $K_v = 12$, $K_{d_1} = K_{d_2} = 8$ and $D2$ values of $D2 = 0$ (Table 1b) and $D2 = 1$ (Table 1c) which correspond to packet error probabilities of approximately $P_E^{v} =$

Table 1a

$D_t^{(1)}$	0	1	2	3	4	5	6	7	8	9	10
$M_1(D_t^{(1)})$	24	13	11	9	8	6	4	3	2	1	0

Table 1b

$D_t^{(1)}$	0	1	2	3	4	5	6	7	8
$M_1(D_t^{(1)})$	18	9	8	6	4	3	2	1	0

Table 1c

$D_t^{(1)}$	0	1	2	3	4	5	6	7
$M_1(D_t^{(1)})$	13	8	6	4	3	2	1	0

1.3×10^{-3} and $P_E^{d_1} = P_E^{d_2} = 3.5 \times 10^{-5}$. The offered loads of voice and data traffic are defined as the average of the number of active voice calls and the number of active data users, respectively,

$$G_v = N_v \frac{p_{01}^v}{p_{01}^v + p_{10}^v} \quad \text{and} \quad G_{d_1} = N_{d_1} \frac{p_{01}^d}{p_{01}^d + p_{10}^d} \tag{39}$$

In Table 2, we list some of the actions taken under the optimal policy and three different data weighting factors $w_d = 1$, 10, and 100 (for voice $w_v = 1$). With the parameters $G_v = G_{d_1} = 1.43$.

Table 2

Current Users		New Users		$w_d = 1$		$w_d = 10$		$w_d = 100$	
V_t	$D_t^{(1)}$	v_t	$d_t^{(1)}$	a_t^v	$a_t^{d_1}$	a_t^v	$a_t^{d_1}$	a_t^v	$a_t^{d_1}$
3	2	3	0	3	0	3	0	3	0
3	2	3	1	3	1	3	1	1	1
3	2	3	2	3	1	1	2	0	2
3	2	3	3	3	1	0	3	0	3
3	2	3	4	3	1	0	3	0	3
6	0	1	0	1	0	1	0	1	0
6	0	1	1	1	1	1	1	1	1
6	0	1	2	1	2	1	2	0	2
6	0	1	3	1	2	0	3	0	3
6	0	1	4	1	2	0	3	0	3

The performance measures of voice and high priority data traffic are the average blocking rates and the throughputs. For low priority data traffic the performance measures are the average packet loss probability, the throughput, and the queueing and system delays. The results of Figs. 4 to 14 pertain to the system parameters used to generate Table 1b (for $D2 = 0$) and 1c (for $D2 = 1$). In Figs. 4 to 11 we show performance results for voice and high priority data traffic whereas in Figs. 12 to 14 we show performance results for low priority data traffic.

In Figs. 4 and 5 we show the blocking rates of voice and high priority data traffic versus the offered loads of voice traffic (G_v) for an offered high priority data load of $G_{d_1} = 1.43$ and two different data weighting factors ($w_d = 1$, and 100). As expected the blocking rates of voice calls (Fig. 4) and of high priority data traffic (Fig. 5) increase as G_v increases. The blocking rate of voice calls increases and that of high priority data decreases as the weighting factor increases. When $D2$ increases, both the voice and high priority data blocking rates increase.

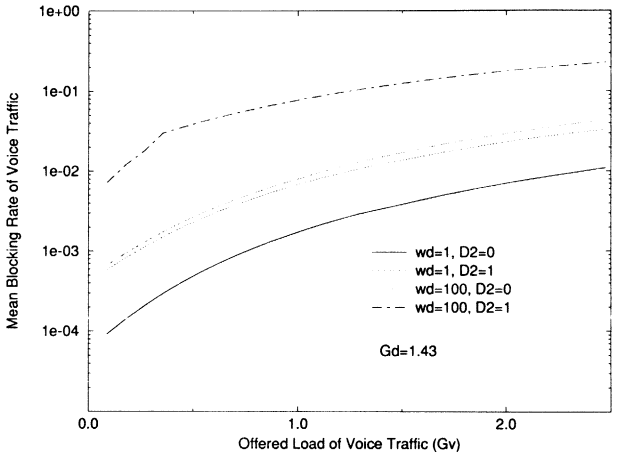

Fig. 4 - Mean blocking rate of voice traffic vs G_v.

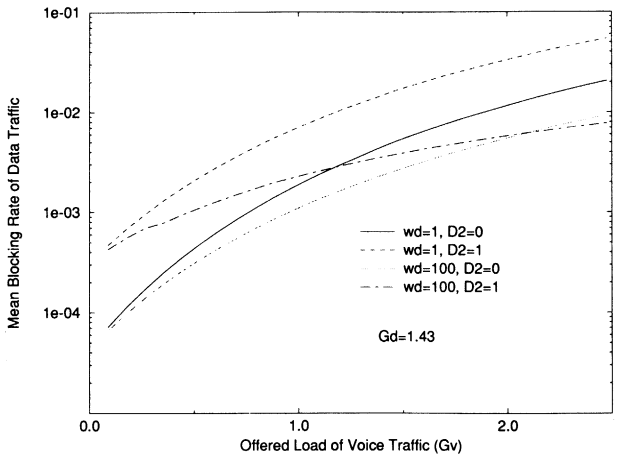

Fig. 5 - Mean blocking rate of data traffic vs G_v.

In Figs. 6 and 7 we show the blocking rates of voice and high priority data traffic versus the offered load of

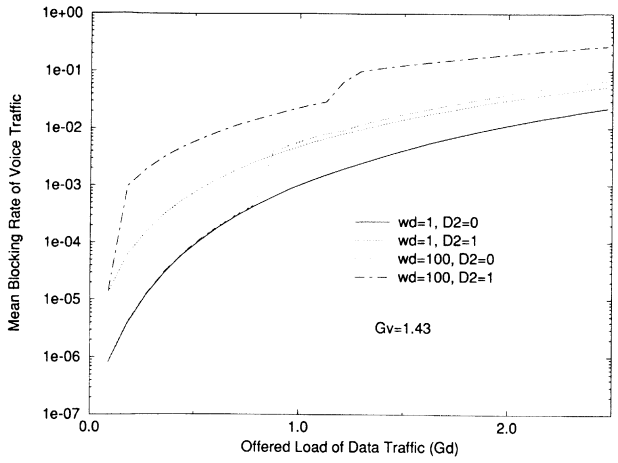

Fig. 6 - Mean blocking rate of voice traffic vs G_{d_1}.

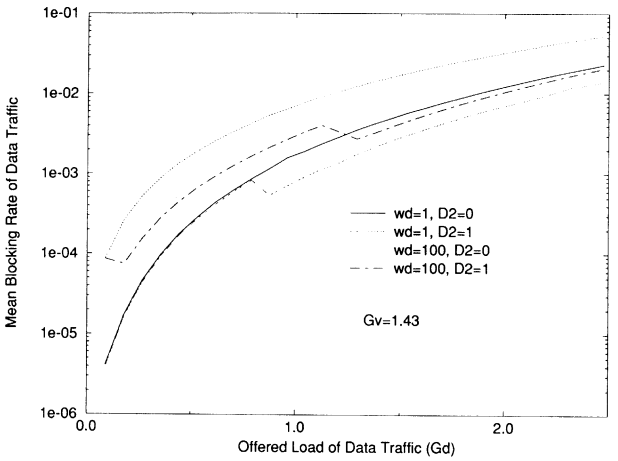

Fig. 7 - Mean blocking rate of data traffic vs G_{d_1}.

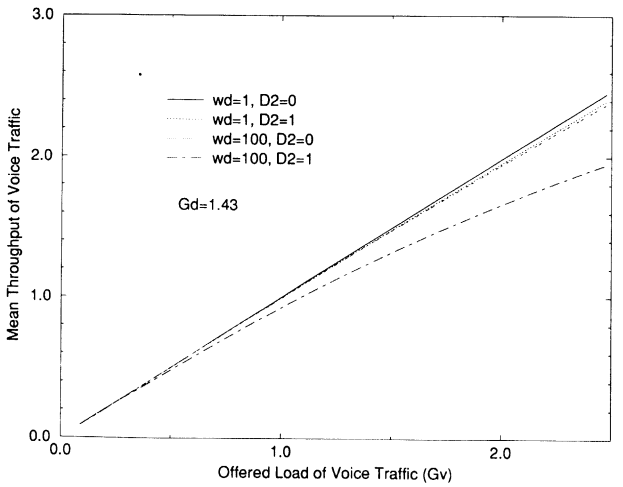

Fig. 8 - Mean throughput of voice traffic vs G_v.

data traffic (G_{d_1}) for an offered voice load of G_v = 1.43 and two different data weighting factors (w_d = 1 and 100). As expected the blocking rates of voice traffic

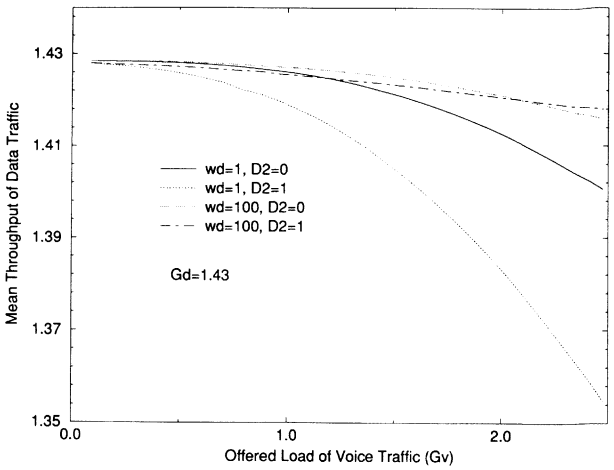

Fig. 9 - Mean throughput of data traffic vs G_v.

(Fig. 6) and of high priority data traffic (Fig. 7) increase as G_{d_1} increases. The effect of increasing w_d and $D2$ is the same as for Figs. 4 and 5.

In Figs. 8 and 9 we show the throughput of voice and high priority data traffic as a function of the voice load G_v and for a data load G_{d_1} = 1.43. As expected the voice throughput increases and the data throughput decreases as G_v increases. Increasing w_d (from 1 to 100) reduces the voice throughput (Fig. 8) more drastically for $D2$ = 1 than for $D2$ = 0. Moreover, increasing $D2$ (from 0 to 1) reduces the data throughput (Fig. 9) more drastically for w_d = 1 than for w_d = 100.

In Figs. 10 and 11 we show the throughput of voice and high priority data traffic as a function of the offered data load G_{d_1} and for a voice load G_v = 1.43. As expected the voice throughput decreases and the data throughput increases as G_{d_1} increases. Moreover, increasing $D2$ (from 0 to 1) reduces the voice throughput (Fig. 10) more drastically for w_d = 100 than for w_d = 1. Increasing $D2$ (from 0 to 1) and/or w_d (from 1 to 100) has little effect on the value of the data throughput (Fig. 11).

In Figs. 12, 13, and 14 we show the average packet

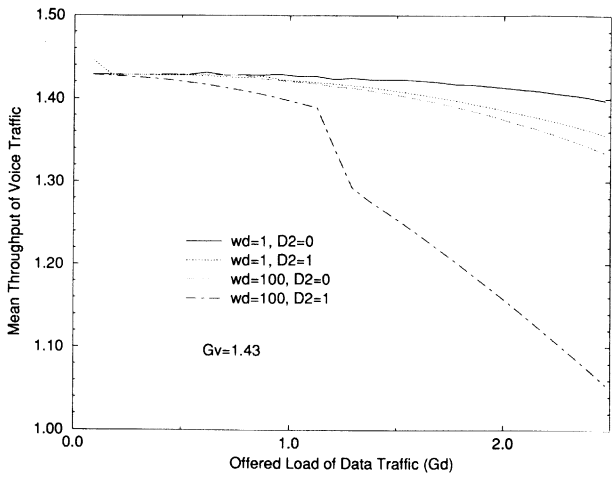

Fig. 10 - Mean throughput of voice traffic vs G_{d_1}.

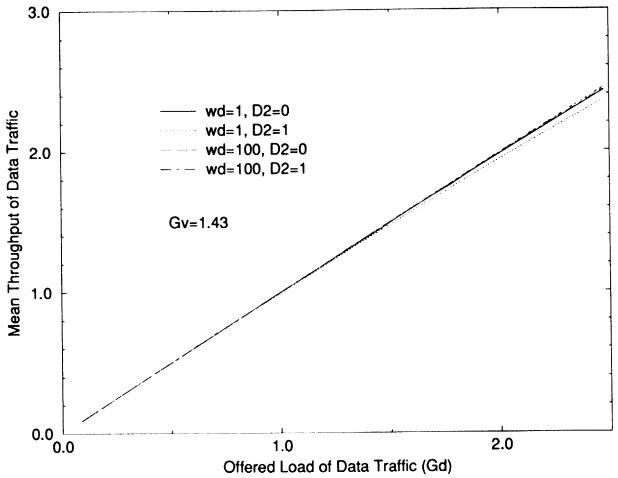

Fig. 11 - Mean throughput of data traffic vs G_{d_1}.

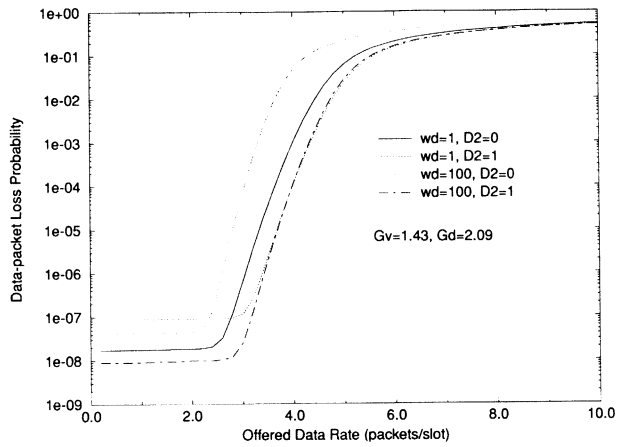

Fig. 12 - Mean packet loss probability vs λ_{d_2}.

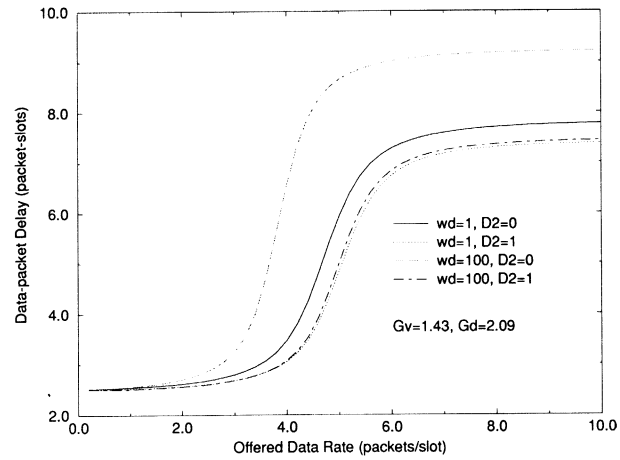

Fig. 13 - Mean packet delay vs λ_{d_2}.

loss probability, the average system delay, and the throughput of low priority data traffic versus the offered low priority data rate (λ_{d_2}), for a voice load $G_v = 1.43$, a high priority data load $G_{d_1} = 2.09$, and two data weighting factors $w_d = 1$ and $w_d = 100$. When a CDMA code is reserved for the low priority data traffic ($D2 = 1$), the data packet loss probability (Fig. 12) and system delay (Fig. 13) decrease whereas the data throughput (Fig. 14) increases; this change is more substantial for larger values of the weighting factor w_d ($w_d = 100$ versus $w_d = 1$).

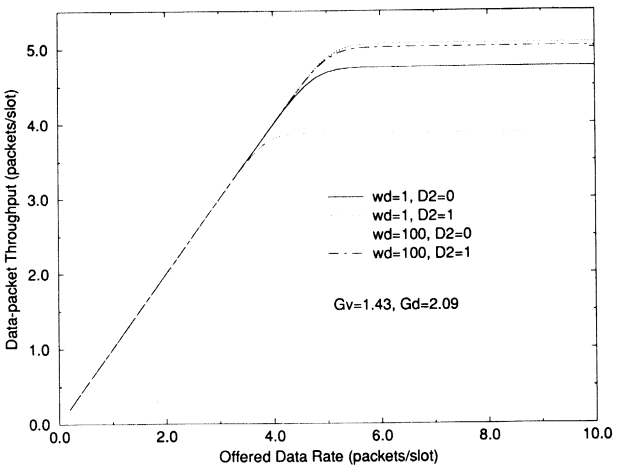

Fig. 14 - Mean packet throughput vs λ_{d_2}.

7. CONCLUSION

In this paper, we have derived and analyzed the performance of an optimal scheme for CDMA code allocation to voice traffic and data traffic with two priorities. Voice calls and high priority data traffic are treated in the same manner and they share the CDMA capacity in a movable boundary fashion; real time delivery is guaranteed for both while their *BER* requirements are met, otherwise blocking occurs. The long-term blocking rates of voice and high priority data traffic are minimized by our scheme. Low priority data users use whatever capacity is left unused by the other two traffic types plus a small fraction of the capacity reserved for them; if sufficient resources are not available, they are queued; delays and packet loss is experienced by these data users.

The performance of the optimal schemes was evaluated for several values of the offered voice and data loads; the tradeoffs involved when the offered voice or data load increase were examined. We showed that the optimal admission policy differs for varying weighting factors w_d ($w_v = 1$) but the performance differs only when w_d becomes much larger than w_v (e.g., $w_d = 100$). The activity characteristic of voice traffic was taken into account and it helped to increase the number of users accommodated. Implementation issues were discussed and directions of our current and future work in this area were outlined. This work together with our work presented in [7] provides some key results about admission policies in CDMA networks with voice and data traffic and we hope it offers some useful insights and guidance for the design of real-life CDMA systems with multi-media traffic.

Manuscript received on May 15, 1994.

REFERENCES

[1] David Jacobson: *Yankee group reports on digital cellular technologies wireless.* "ATT", Vol. 1, No. 1, July 22, 1991, p. 1-8.

[2] K. S. Gilhousen, I. M. Jacobs, R. Padovani, L. A. Weaver, Jr.: *Increased capacity using CDMA for mobile satellite communication.* "IEEE JSAC", May, 1990.

[3] D. C. Cox: *Wireless network access for personal communications.* "IEEE Commun. Magaz.", Vol. 30, No. 12, December 1992, p. 96-115

[4] L. C. Palmer, E. Laborde, A. Stern, P. Y. Sohn: *A personal communications network using a ka-band satellite*, "IEEE JSAC", February, 1992.

[5] Loral/Qualcom Inc.: Globalstar - FCC Filing, 1991.

[6] TRW Inc.: Odyssey - FCC Filing, May, 1991.

[7] W.-B. Yang, E. Geraniotis.: *Admission policies for integrated voice and data traffic in CDMA packet radio networks.* "IEEE JSAC", May 1994, p. 654-664.

[8] M. Soroushnejad, E. Geraniotis.: *Multi-access strategies for an integrated voice/data CDMA packet radio network.* To appear in the "IEEE Trans. on Commun".

[9] E. Geraniotis, M. Soroushnejad, W.-B. Yang: *A multi-access scheme for voice/data integration in hybrid satellite/terrestrial and heterogeneous mixed-media packet radio networks.* To appear in the "IEEE Trans. on Commun".

[10] M. B. Pursley, D. J. Taipale.: *Error probabilities for spread-spectrum packet radio with convolutional codes and viterbi decoding.* "IEEE Trans. on Commun.", Vol. COM-35, January 1987.

[11] J. Conan,: *The weight spectra of some short low-rate convolutional codes.* "IEEE Trans. on Commun.", Sept. 1984.

[12] P. T. Brady: *A statistical analysis of on-off patterns in 16 conversations.* "Bell System Technical Journal", Vol. 47, No. 1, 1968, p.73-91.

[13] H. C. Tijms.: *Stochastic modeling and analysis: a computational approach.* New York: Wiley, 1986.

[14] E. Geraniotis, M. B. Pursley,: *Error probabilities for slow-frequency-hopped spread-spectrum multiple-access communications over fading channels.* "IEEE Trans. on Commun.", May 1982.

[15] M. B. Pursley,: *The role of spread spectrum in packet radio networks.* Proceedings of the IEEE, January 1987.

Telecommunication Systems

Synchronous Digital Hierarchy Byte Pointer Justification Versus VC-12 Payload Bit Justification Effects

Henry L. Owen
School of Electrical and Computer Engineering
Georgia Institute of Technology
Atlanta, Georgia 30332-0250 - USA

Abstract. Four contributors to Synchronous Digital Hierarchy (SDH) network desynchronizer buffer fill variations are the justification bits in the VC-12 payload, the irregular spacing of the data in the VC-12 payload, the irregular spacing of the data in the SDH frame, and the pointer activity which contains byte activity as opposed to the bit activity in the VC-12 itself. These phenomena result in a variation of the rate at which bits arrive at a desynchronizer in a SDH network. Modeling and understanding of these processes is required in order to be able to propose advanced pointer processor algorithms as well as advanced jitter reduction techniques in SDH desynchronizers. This paper examines the relative effects of bit justifications in VC-12 payloads in conjunction with the corresponding byte justifications in SDH networks in order to determine the dynamics of SDH network plesiochronous desynchronizer buffers.

1. INTRODUCTION

The Synchronous Digital Hierarchy (SDH) is an international transmission standard which defines a signal hierarchy in such a manner as to allow compatibility between the European signal hierarchy based on 2.048 Mbit/s and the North American Hierarchy based on 1.544 Mbit/s. The SDH standard [1-3] defines among other things a synchronous frame structure for multiplexed digital traffic. The basic building block for the North American Hierarchy multiplexed digital traffic is the Synchronous Transport Signal Level 1 (STS-1) and is used in the North American equivalent of SDH which is the Synchronous Optical Network (SONET). Multiple STS-1 signals can be interleaved to form higher rate signals. Three STS-1 signals are interleaved to form STS-3 which is the basic building block in Europe. The STS-3 is also defined as the Synchronous Transport Module 1 (STM-1).

A STM-1 signal consists of information payload and section overhead fields organized in a block frame structure which repeats every 125 μs. The information is conditioned for serial transmission on the selected media (i.e. optical fiber) at a rate which is synchronized to the network. A basic STM-1 is defined as 155.520 Mbit/s. At each network node where the signal is demultiplexed, information is required on a byte-wide basis. Thus the network nodal processing done on the signal is byte-wide and all operations are done at 19.44 MHz.

A Virtual Container (VC) is the information structure used in STM-1. It consists of information payload and path overhead information fields organized in a block frame structure which repeats every 125 or 500 µs. Alignment information to identify VC frame start is provided by pointers. A pointer is a value which defines the frame offset of a virtual container with respect to the frame reference. Four VCs are defined by ITU [2] and contain various data rates. A VC-4 contains 139264 kbit/s, a VC-3 contains either 44736 kbit/s or 34368 kbit/s, a VC-2 contains 6312 kbit/s, a VC-12 contains 2048 kbit/s, and a VC-11 contains 1544 kbit/s.

There are two types of VCs, higher order and lower order. The only higher order VC in a STM-1 signal is a VC-4. The VC-4 has associated with it a pointer value which defines the phase relationship between the STM-1 frame and the VC-4 contained within the frame. The combination of the VC-4, the pointer and some additional overhead bytes is named an AU-4. There are several different types of lower order VCs. An example of a lower order VC is a VC-3. The VC-3 has associated with it a second pointer which defines the phase relationship between the VC-3 and the AU-4 in which it is contained. The combination of the VC-3, the pointer

and some additional overhead bytes is named a TU-3. Two more examples of a lower order VCs are the VC-2 and the VC-12. The combination of the VCs, pointers and additional overhead bytes become TU-2 and TU-12 respectively. Both the TU-2 and the TU-12 require four STM-1 frames to contain each of them, their pointers define the phase relationship between the VCs and the four STM-1 frames which contain them.

SDH networks use synchronizers to convert input serial signals into bytes. These bytes are then mapped into the payload positions of a SDH frame. The transmission network then transmits these payloads through the network to their destinations. At the end of the transmission process, the bytes are converted back into a serial bit stream by a desynchronizer with a reconstructed data rate as close to the original data rate as possible. SDH networks are compatible with numerous data rates including but not limited to 139.264 Mbit/s, 34.368 Mbit/s, and 2048 kbit/s. In order to match serial input data rates to the transmission capabilities of SDH, bit justification is used in the synchronization process, while byte justification is used in the transmission process. In certain circumstances, these bit and byte justification processes may introduce undesirable effects in the output of SDH networks in the form of wander and jitter. Wander and jitter are the low frequency and high frequency variations in the output signal relative to an ideal representation of the signal. The minimization of wander and jitter in SDH networks is one objective in SDH network design.

A SDH network transporting a 2048 kbit/s signal is shown in Fig. 1. The entry point for a serial 2048 kbit/s input to the network is the synchronizer. A synchronizer is the network element which must take the incoming 2048 kbit/s serial signal and map it into a SDH floating asynchronous VC-12 payload structure. In addition to path overhead (POH), the floating asynchronous VC-12 payload structure consists of 1023 data bits, six justification control bits, two justification bits *S*1 and *S*2, and eight overhead communications channel bits. The remaining bits are fixed stuff (*R*) bits. The *O* bits are reserved for overhead communications purposes. The VC-12 mapping which this paper exclusively uses is the floating asynchronous mapping, other mappings such as locked and synchronous are defined in G.709 [1] but are not included in this analysis. The VC-12 floating asynchronous mapping used in this paper is shown in Fig. 2 [1]. For a nominal 2048 kbit/s signal, the payload structure is defined such that the *S*2 justification bit must be filled with a payload bit and the *S*1 justification bit is

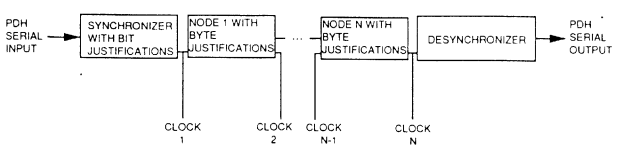

Fig. 1 - SHD network block diagram.

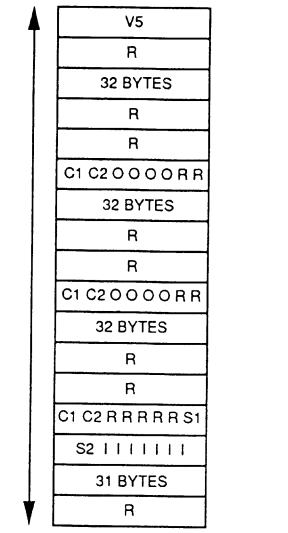

Fig. 2 - Floating asynchronous mapping of 2048 kbit/s tributary into a VC-12.

empty. In the event the synchronizer node reference clock is too fast or the arriving data rate is too slow, *S*2 bit justification opportunities will occasionally not be used. Conversely a slow synchronizer clock or too fast a data rate arrival will result in both *S*2 and also occasionally *S*1 justification bit usage.

After the synchronizer network element block in Fig. 1, the SDH transmission network transports a byte wide representation of the 2048 kbit/s signal. This byte wide transmission requires network nodes to include byte wide FIFOs for storage of a small portion of the payload being transmitted. This storage is required to allow variations between the input clock to a given network node and the output clock for that same node. The clock source for these input and output clocks is different and thus relative variations will occur in network operation. In the event of a variation, the byte wide FIFO in a given node will begin to fill up or empty out. Byte wide justification opportunities are defined in the SDH standards to accommodate such situations [1, 2, 3]. A positive justification opportunity is a byte or group of bytes that are normally filled with payload bytes but may be left empty thus slowing down the rate at which the byte wide FIFO is being emptied. Such use of these positive justification bytes is called a positive pointer action. Similarly, there are negative justification bytes which are normally empty. In the event of a negative pointer action, these justification bytes are filled thus speeding up the emptying of the byte wide FIFO.

There are two levels of pointer activity which correspond to the two types of VCs discussed earlier in this paper. The first is higher order and the second is lower order pointer activity. At the higher level, Administrative Unit (AU) pointer actions may occur. These point-

er actions are associated with network nodes which store a SDH frame in a single FIFO. This single FIFO contains all of the payload bytes for the entire SDH frame. Nodes which operate in this manner are referred to as higher order nodes and may generate AU pointer actions. The second type of pointer activity is that which occurs at lower level in the SDH payload hierarchy. At this lower level, a node breaks a SDH frame down into the lower order payloads and stores these lower order payloads into separate FIFOs. Nodes which operate in this manner are referred to as lower order nodes and may generate Tributary Unit (TU) pointer actions. Lower order nodes are required when lower order payloads are switched in cross-connects or are added/dropped from the network in Add/Drop multiplexer (ADM) equipment. One added complexity to the analysis of SDH pointer activity is that there is some interaction between higher order and lower order pointer activity [6].

The last block in Fig. 1 is the desynchronizer. The desynchronizer portion of the network is the network element that takes the SDH payload mapping and reconstructs the output signal. A nonuniform data arrival rate to the desynchronizer places constraints on the desynchronizer algorithms which are required to minimize the jitter in the output signal. These types of variations in the desynchronizer FIFO bit levels are undesirable [7, 8]. Nonuniform arrival of data at the desynchronizer occurs for several reasons. In the normal operating mode of a SDH network, virtually no pointer activity occurs. Data arrival at the desynchronizer node is dependent upon the byte wide mappings of the transport mechanism. Gaps exist between the data bytes, resulting in an irregularly spaced arrival of the bytes to the desynchronizer bit buffers. These gaps exist in both the VC-12 mapping as defined in Fig. 2, as well as the byte gaps shown between locations which transport a given VC-12 in the STM-1 frame structure shown in Fig. 3 [2, 3].

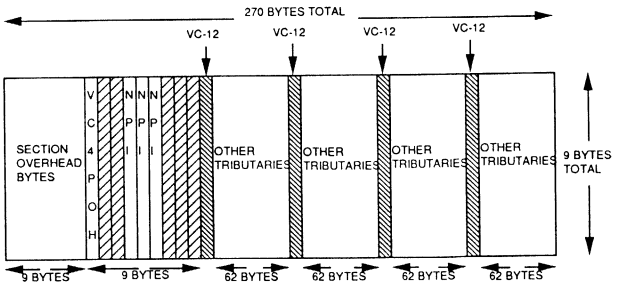

Fig. 3 - STM-1 frame structure.

During "normal" network operation, synchronous clocking throughout the network results in virtually no byte justifications required in any of the byte wide buffers located in each SDH node [4, 5]. In the event of a synchronization failure, a node or several nodes will obtain clocking sources from a clock in holdover or free running mode. This results in relative clock differences between the SDH nodes. Clock differences on the byte wide buffers of SDH networks using fixed thresholds on the FIFOs result in positive or negative pointer activity as shown in Fig. 4 [6]. This figure shows a six node SDH network which has different clocking frequencies at the different nodes in the network. Higher order pointer activity may occur at higher order nodes which are labeled as "LEVEL: AU-4". Lower order pointer activity may occur at lower order nodes which are labeled as "LEVEL: TU-12". At the bottom of Fig. 4, the values of the node clocks are shown relative to an ideal, exactly

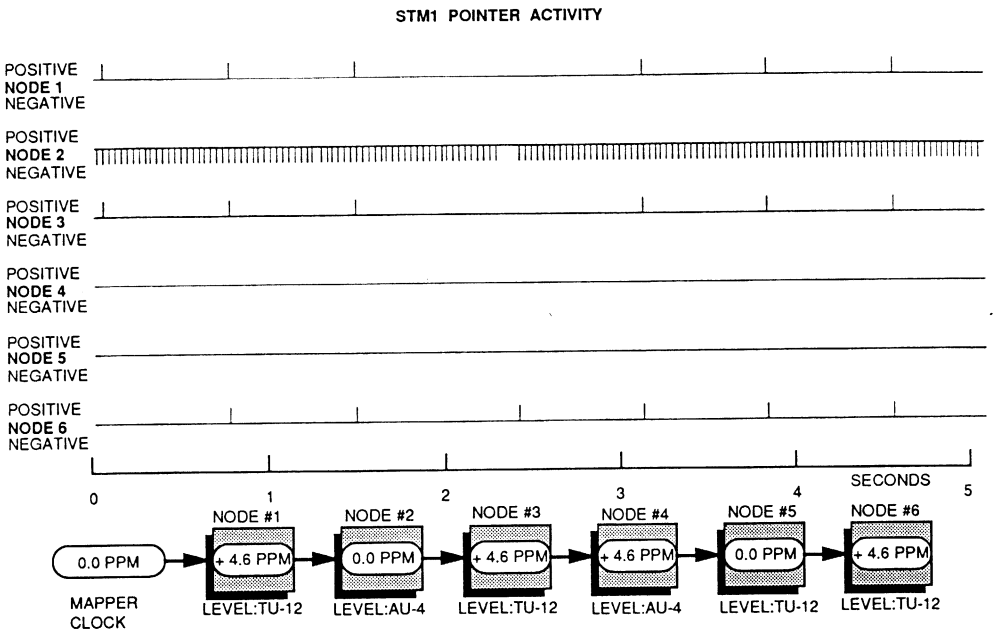

Fig. 4 - Pointer activity in a six node network transporting a TU-12 payload with various relative nodal clocking frequencies.

on frequency, mapper node clocking source. At node 1 in the network, positive pointer activity results from a + 4.6 parts per million (PPM) clock offset frequency. The point in time that the positive pointer occurs at node 1 is shown by placing a tick mark in the upward direction on the node 1 time line which represents five seconds of real time network operation. Similarly, a 0.0 PPM clock offset (i.e. this clock matches the synchronous clocking source exactly) coupled with the different clock source and pointer activity at the previous node resulting in negative pointer activity over time as shown by tick marks in the downward direction on the time line for node 2. Each upward tick mark on an associated node time axis represents the occurrence of a positive pointer activity where one byte is not transmitted during the positive byte justification opportunity. Each downward tick mark represents a negative pointer activity in which an extra byte is placed in the negative byte justification opportunity. The net effect of these pointer activities is that the arrival of data at the desynchronizer is not uniform. For more detailed description of the network shown in Fig. 4, the reader is referred to reference [6].

Modeling of desynchronizer data arrival rates and analysis of these results leads to the information necessary to optimize plesiochronous desynchronizer jitter minimization algorithms and is one of the goals of this work. An early step in this process is to characterize the effects of the bit and byte justification mechanisms which exist in SDH network standards and then to propose techniques which reduce these effects. This paper presents the methodology used and the results obtained in modeling the bit and byte justification effects in a SDH network transporting a 2048 kbit/s payload.

2. SIMULATION MODEL

The simulation model which was used to obtain the results presented in this paper is shown in block diagram form in Figs. 5, 6, and 7. In Fig. 5, the mapping of an asynchronous 2048 kbit/s signal is modeled by generating a byte at the rate required by a network mapper node. For each mapper node byte clock, a byte of the VC-12 structure (shown in Fig. 2) is examined to determine what type of byte is to be placed into the byte wide SDH network. The possible bytes are a normal 8 bit data byte, a byte containing 7 data bits and a *S2* justification byte, a byte containing only one data bit (the byte with the *S1* justification bit opportunity), or an overhead byte which contains 0 data bits. Based upon the fill in the 2048 kbit/s bit wide buffer fill, the justification opportunities are either used or not used so as to keep this bit buffer within acceptable levels. In the simulation model, actual data is not passed through the network. Instead the bytes transmitted through the network simulation model contain values of 8, 7, 1, or 0 representing the number of data bits from the 2048 kbit/s tributary carried in a given STM-1 network byte. This methodology allows the FIFO fill levels to be modeled throughout the network. This also allows detailed analysis of all of the network elements on a clock cycle by clock cycle basis (at the expense of high simulation computational requirements) so as to determine in a very detailed manner the network dynamics.

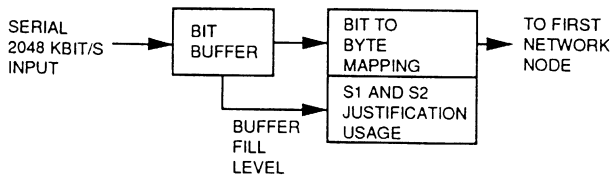

Fig. 5 - Synchronizer model.

2.1. *Network node model*

Fig. 6 shows the next portion of the network simulation model. This portion of the model receives bytes from the synchronizer and places these bytes into the byte locations in the higher level STM-1 frame. Representations of the STM-1 frame are stored in the simulator model so that bytes are requested from the synchronizer only when the first SDH node must transmit a byte throughout the remainder of the SDH network. Each intermediate node in the network contains a byte wide FIFO model as well as an incoming STM-1 frame structure model and an outgoing STM-1 frame structure model. When the byte FIFO in a given SDH network node becomes too full or too empty based upon threshold values, a pointer action will be initiated. The effect of these pointer actions is that one extra or one less byte will be taken from the byte FIFO and used in the positive or negative pointer action byte justification opportunity in either the higher order or the lower order justification location depending upon the network node type. A higher order pointer action results in a STM-1 frame structure model shift relative to other nodes in the network. A lower order pointer action results in a lower order payload shift inside the STM-1 frame structure. The simulator model takes these effects into account so as to represent the new STM-1 frame byte relationships with the other nodes in the network and thus model the effects of pointer activity throughout the SDH network.

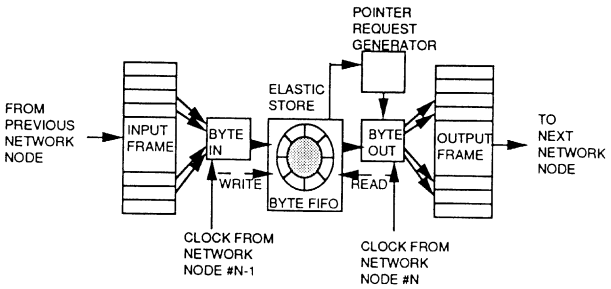

Fig. 6 - Node model.

2.2. *Desynchronizer model*

Fig. 7 shows the terminating point of the transmission of the VC-12 payload, the desynchronizer. The desynchronizer is modeled in the simulator as a simple implementation which either speeds up or slows down by a preset value based upon the fill of the desynchronizer bit FIFO. This is an overly simplified desynchronizer for most applications because of the output jitter which results from such a straight forward approach. A more realistic desynchronizer which minimizes the output jitter requires more complicated algorithms based upon the inputs to the desynchronizer. Additionally, pointer processor algorithms affect this jitter and there are several techniques which have been proposed to reduce this effect [9, 10, 11]. Pointer processor algorithms may be enhanced to reduce the demands placed upon the desynchronizer by modifying the dynamics of pointer activity which is passed down the SDH network. For the purposes of determining the dynamics of SDH networks relative to the desynchronizer, a simplified desynchronizer model is initially used. This meets the present objectives of allowing accurate modeling of the desynchronizer bit FIFO fill in the presence of SDH byte wide network operations.

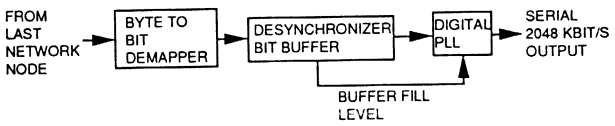

Fig. 7 - Desynchronizer model.

3. SYNCHRONOUS CLOCK OPERATION

During normal synchronous operation of a SDH network, all clocks are of the same frequency. No pointer activity or justification bit temporal activity is required in the transmission of the payloads throughout the network. In this steady state condition, the fill of a desynchronizer bit buffer is dependent upon the irregular arrival times of the bits from the transported STM-1 frame. In normal network steady state operations with the network clocks fully synchronized, the fill of a desynchronizer bit FIFO varies in a regular manner. This fill is determined by the effects of irregular spacings in time of the data inside the VC-12 payload as well as the irregular spacings in time of the VC-12 payload in the STM-1 frame. Fig. 8 shows the number of bits in a desynchronizer bit FIFO versus time in a SDH network with all clocks in fully synchronous operation. The number of bits in the VC-12 desynchronizer bit buffer varies between 19 bits and 50 bits in a periodic manner. This variance occurs in general due to the physical definitions of payload mappings and hierarchies in the SDH standards [1, 2, 3]. The desynchronizer is not required to alter its phase locked loop removal rate of 2048 kbit/s

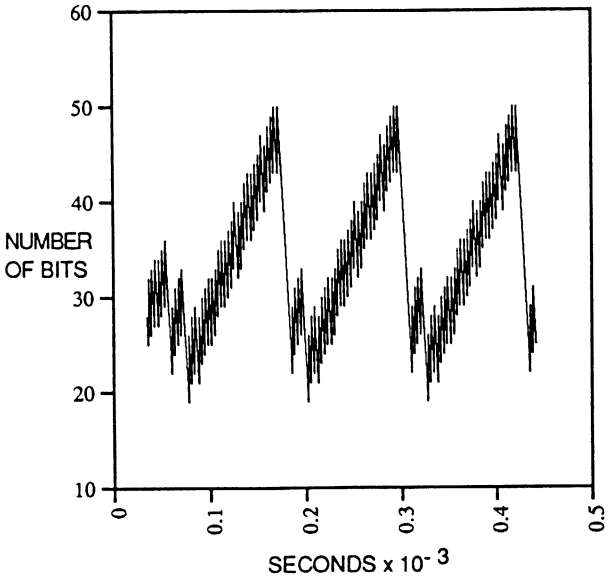

Fig. 8 - Number of bits in the VC-12 desynchronizer bit FIFO buffer with clocks in fully synchronous operation.

since the arrival of the bits over a long term relative to the FIFO threshold levels and the time constant of the phase look loop is equal relative to the desynchronizer data removal rate. The variance of the buffer fill is caused by the spacings between the VC-12 payload bytes as well as the spacing between the STM-1 frame bytes which contain the VC-12 mapping. The major effect is caused by 3 consecutive overhead/fixed stuff bytes in the VC-12 payload arriving sequentially. These 3 bytes contain a large amount of no data, causing a rapid decrease in the desynchronizer bit buffer. The time scale of Fig. 8 is expanded relative to later figures to show the rapid perturbations due to the VC-12 payload mappings.

4. RESULTS OF SIMULATIONS WITH MAPPER NODE IN HOLDOVER MODE

The simulation results presented in the remainder of this paper are obtained from a network model as shown in Figs. 5 -7. A network consisting of a synchronizer, a single node, and a desynchronizer were simulated. In this simple network, only two clocks exist and the value of N shown in Fig. 6 is equal to 1. Thus, the clocks in Fig. 6 may be labeled as "clock from network node #0" and "clock from network node #1". The mapper clock in this simulation which controls the speed at which the VC-12 bytes are constructed is the same clock as the "clock from node #0". The rate at which bytes are delivered to the desynchronizer in Fig. 7 is controlled by the "clock from network node #1". In general the simulation model presented in this paper has the ability model networks consisting of an arbitrary number of nodes. For simplicity, the simulations in the remainder if this paper consists of the simplest network possible. The

simplest network possible is a synchronizer, a single node, and a desynchronizer.

When a VC-12 is formed at the mapper node, justification *S* bits are used to respond to variations in the level of a bit FIFO which holds the incoming asynchronous serial data temporarily. In the event the mapper node clock is slow, the construction of the VC-12 bytes may be too slow and the bit FIFO will become too full. Data must be placed into the VC-12 mapping faster, so *S*1 justification bits will begin to carry data. In the event a mapper node clock is too fast, VC-12 bytes are being constructed too fast for the serial asynchronous bit FIFO. The bit FIFO will begin to empty out and the *S*2 justification byte which normally carries data will begin to not be used. Not putting data into the *S*2 justification bit allows the bit FIFO to begin to fill back up to a normal level. When a SDH network node has a clocking source failure and this node derives its clocking source from a slightly off frequency holdover mode, pointer activity will result. Pointer activity occurs at locations where VC-12 s are stored in byte wide FIFOs. Pointer activity is a result of a byte wide FIFO becoming too full or too empty. Justification *S* bit activity occurs only in synchronizer nodes, where asynchronous mapping takes place.

There are two possible scenarios for the mapper node clock in the simple network in this paper. The first is that the synchronizer clock (mapper node clock) is too fast relative to the remainder of the network (the clock at the desynchronizer side of the network). This situation results in the VC-12 *S*2 justification bit not containing data in some VC-12 bytes as well as negative pointer actions being generated and passed down the SDH network. The VC-12 *S*2 justification bit is only occasionally used by the data in order to keep the synchronizer bit FIFO fill within predefined tolerances. Negative pointer actions are generated because the mapping process will generate too many bytes and the byte FIFO will become too full. The negative pointer justification byte usage will keep the byte FIFO level within acceptable tolerances. Both of these bit and byte justification mechanisms will be active for fixed frequency clock offsets at the mapper node. The second scenario occurs when the synchronizer clock (mapper clock) is too slow, resulting in the VC-12 *S*2 justification bit always containing data while VC-12 *S*1 justification bit will also occasionally contain data. In this case positive pointer actions are generated at the first node and are passed to the desynchronizer node. In this paper the second scenario will be examined where *S*1 justification bit usage occurs as well as positive pointer actions. The first scenario results in similar results and is not specifically presented in this paper.

4.1. *Justification transmission*

The dynamics of justification bit passage down SDH networks are different from the dynamics of pointer byte justification transmission down the networks. The effects of this are significant because of the effects they have on the desynchronizer FIFO fills. Additionally this results in temporary differences in the transmission rate of the VC-12 payload bits, and thus causes undesirable effects at the desynchronizer [9, 10, 11]. These effects were modeled by starting the SDH network model with all clocks synchronized. After 0.1 s of normal synchronous operation, the clock at the mapper was set to a new value with a frequency offset representing network operation with the mapper in holdover mode. The network was then modeled for a total of 1.2 s of real time operation. The results of this for the mapper operating in a holdover mode with an increased clock period by 300 ppm are shown in Figs. 9, 10, and 11.

4.2. *Pointer activity over time*

The amount of STM-1 positive pointer activity over time for this scenario is shown in Fig. 9. This figure shows the resulting positive pointer activity at the node in the SDH network which was simulated. The pointers which are generated result in a byte not being placed in the normally filled STM-1 frame positive byte justification opportunity of the STM-1 frame. When the mapper clock period is larger than normal by 300 ppm, the byte which normally would have appeared in the STM-1 frame positive justification position is one of three types. The first type is that of a normal data byte containing 8 data bits. The second type is that of a data byte containing only one data bit due to use of a *S*1 justification opportunity in the VC-12 payload mapping. The third type is that of a VC-12 over head byte which contains no data. Examples of these overhead bytes are the V5 byte and the *R* bytes in the VC-12 payload. Fig. 9 identifies the type of byte that normally would have appeared at the desynchronizer by placing a mark on the time axis for each positive pointer action. The height of this mark represents the number of data bits which would have been delivered to the desynchronizer had this positive pointer action not occurred. For example, an overhead byte (which contains no data bits) is next in line to be delivered to the desynchronizer bit FIFO. Suppose it is not delivered on time due to a positive pointer action (i.e. nothing is sent in the positive justification byte). In this case a mark with an amplitude representing 0 data bits is placed in the graph at the point in time that corresponds to the positive pointer action.

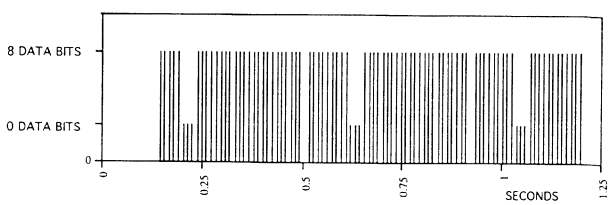

Fig. 9 - Number of data bits that would have been delivered to the desynchronizer bit FIFO had there not been a positive pointer action.

Fig. 9 is plotted for an increased clock period of 300 ppm at the mapper, ie the mapper clock is slower than it should be. Fig. 9 covers a time period of 1.25 s of network real time operation. During this time period, only two of the three possible pointer activity data byte types occurs. One is the positive justification byte had it not occurred would have contained 8 payload (data) bits, and the other is the case where this byte had it not been a pointer justification byte would have contained no payload bits (i.e. an overhead byte). It may be observed that the effects of the overhead bytes in the VC-12 result in no data bits in the positive justification byte for three consecutive STM-1 pointer actions. This can be seen in Fig. 9 by 3 consecutive 0 data bits tick marks just prior to 0.25 s. The desynchronizer bit buffer must be able to handle the variations caused by this.

4.3. *Difference in network justification transmission rates*

The speed at which a SDH network transports justification bits (i.e. *S*1 and *S*2 in the VC-12 itself) and the speed the network transports the byte justifications (i.e. pointers) is very different. To see this effect a running total of the arrival of all justification bits was calculated. This calculation was carried out by adding a one to the running total every time a filled *S*1 justification bit arrived at the desynchronizer node. The effects of the pointer justification bytes were also included in this running total. When a pointer byte arrived at the desynchronizer node in the network, it was examined to see how many data bits would have been contained within it had this byte not been a positive pointer byte (which by definition contains no data when a positive pointer action occurs). After determining the number of data bits (which must be 8, 1, or 0 for this case as discussed in section 4.2) this number of data bits was subtracted from the running total. This running total plotted versus time is shown in Fig. 10. The *y* axis is the running total in bits. When a network is operating with all clocks ideally synchronized, there is no *S*1 bit or pointer byte activity. When a network has one or more nodes operating with clocks that are off frequency, *S* bits and pointer bytes occur. In this example at time 0.1 s, the mapper clock frequency in the network is changed to a value off frequency by +300 ppm, increasing the period of the mapper clock. This results in the mapper clock being too slow relative to the remainder of the network. Since the mapper clock is too slow, the bits of the serial input signal will arrive too fast, resulting in use of the *S*1 bit justification. Since bytes are created too slowly by the mapper node relative to the remainder of the network, positive pointer actions will occur to allow bytes to transported which contain no data. The extra data bits in the *S*1 bit justification and the missing data bits in the positive pointer action cancel each other out over time. However approximately eight *S*1 justification bits are required to cancel out one positive pointer justification byte. Positive pointer activity will not occur immediately throughout the network since byte FIFOs at each node in a network must empty out to a threshold level prior to a given node responding by causing positive pointer actions. This delay of the response of nodes down the network leads to a large effect of *S*1 bits which may be seen in Fig. 10 at 0.1 s. This increase in the running bit total is due to arrival of *S*1 justification bits. The first decrease in the running bit total occurs when a pointer byte finally arrives at the desynchronizer node. The missing data causes a decrease in the running bit total. Other effects in Fig. 10 which cause perturbations in the running bit total are the overhead bytes in the VC-12 (i.e. V1, V2, V3, and V4 bytes) as well as the bytes such as the V5 and the *R* bytes shown in the floating asynchronous mapping shown in Fig. 2. These non-data bytes cause perturbations in the running total and thus cause perturbations in the arrival rates of the data at the desynchronizer. The net result of the mapper clock suddenly changing frequency and becoming slower is the VC-12 *S*1 bit activity being transmitted rapidly through the network, while pointer justification byte activity effects are transmitted through the network in a slower manner. This results in a net increase of bits delivered to the desynchronizer bit FIFO which are not compensated for by the absence of byte arrivals (positive pointer actions) until later in the scenario. The net effect is that the desynchronizer bit FIFO fill is increased. Even when pointer byte effects finally do arrive at the desynchronizer, variations in the desynchronizer bit FIFO fill continue as long as there is a clock offset frequency.

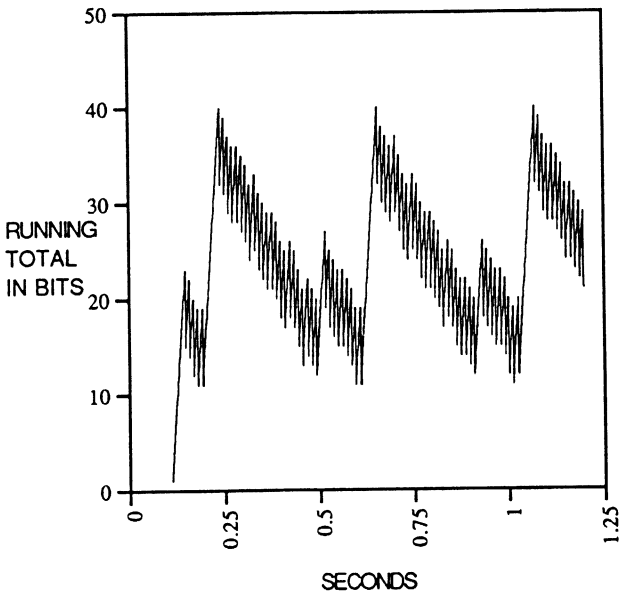

Fig. 10 - Count of VC-12 justification data bits minus count of sdh pointer justification data bytes arriving at desynchronizer.

4.4. *Desynchronizer FIFO levels*

The effects of the different transmission time constants of VC-12 justification bit activity and positive pointer activity on the desynchronizer FIFO fill are

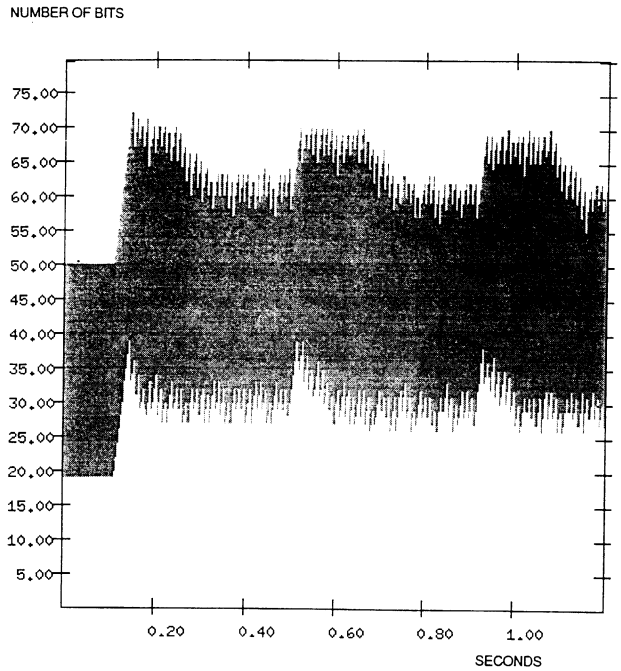

Fig. 11 - Number of data bits in desynchronizer FIFO buffer versus time (large time scale allows only the envelope of the bit FIFO level variations to be seen).

shown in Fig. 11. This figure is essentially a superposition of the effects shown in Fig. 8 (high frequency variations) and the slower effects shown in Fig. 10. Fig. 11 has a large time axis and thus only the envelope of the desynchronizer FIFO bit fill level may be seen. The dark areas of the figure inside the envelope represent rapid high frequency variations that cannot be distinguished in this figure. In determining the magnitude of the variations in the desynchronizer bit FIFO fill, these high frequency variations may be ignore. In Fig. 11, initially the FIFO bit fill is determined only by the effects of VC-12 payload mappings and the STM-1 mappings of the VC-12 into the STM-1 frame. During the first 0.1 s of network operation the FIFO fill varies between 19 and 50 as shown earlier in the expanded time axis of Fig. 8. After the clock for the mapper goes into holdover mode, the result is an additive effect. This additive effect includes the effects of the VC-12 payload mapping, STM-1 mapping of the VC-12 into the STM-1 frame, and the different network transmission time constants for VC-12 justification bits and positive pointer justification byte activity. The net result is that the desynchronizer FIFO fill experiences a perturbation which results in the requirement that the desynchronizer phase locked loop must momentarily increase the speed at which bits are removed from the desynchronizer FIFO [12].

4.5. *Accumulated time error in output*

A concern in SDH networks is the jitter and wander which results in the output signals. Minimization of these effects is one goal of SDH network equipment design. The simple metric of accumulated time error was used in this analysis to indicate the effects of the different arrival rates of bit justification versus byte pointer justification at the desynchronizer. This metric represents the accumulated magnitude of the corrections which the desynchronizer must make in order to keep the desynchronizer bit FIFO level within acceptable tolerances. Any correction made by the desynchronizer introduces undesirable jitter effects since the desired 2048 kbit/s output data rate is instantaneously changed. The accumulated time error resulting in the 2048 kbit/s output data for this network simulation is shown in Fig. 12. The y axis represents the error in nanoseconds introduced into the 2048 kbit/s output signal as a result of the desynchronizer requirement to speed up its output clock due to an increased data arrival rate. This error is defined to be the time difference between the rising edge of a desynchronizer bit output clock for an ideal 2048 kbit/s data rate and the time at which the rising edge of this desynchronizer bit output clock actually occurs. For the purposes of this figure, the desynchronizer clock was increased in speed by reducing its period by a value of 63/64 of its nominal 2048 kHz rate when the desynchronizer bit buffer exceeded 69 bytes. The values in this figure show the accumulated modifications versus time as required by the phase locked loop in steps of 1/64 of a nominal 2048 kbit/s clock period. Fig. 12 would ideally be a flat line in the event that the output signal was not effected by clock inaccuracies throughout a SDH network.

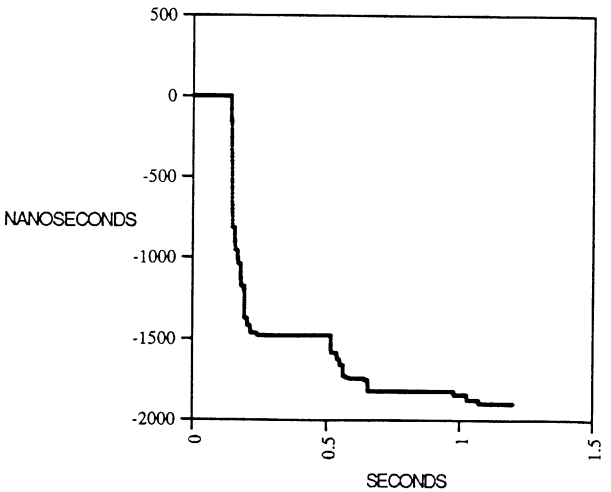

Fig. 12 - Accumulated magnitude of time corrections desynchronizer must make in order to mantain acceptable bit FIFO levels.

5. FUTURE RESEARCH

Using the modeling capabilities and results presented in this paper, future research is required to determine optimal pointer processor algorithms and desynchronizer algorithms which minimize output jitter in the reconstruction of the plesiochronous signal. One possible ap-

proach to minimize jitter at the output is to use pointer processing algorithms that do not just blindly pass pointer activity down the network, but instead react with adaptive thresholds or other threshold modulation techniques. Another approach to minimize jitter is to implement desynchronizer algorithms that treat byte justifications (pointer activity) and bit justifications (*S* bit activity) differently. The effects of these algorithms and methodologies for jitter reduction in SDH desynchronizer reconstruction of plesiochronous signals requires further work.

6. CONCLUSIONS

SDH transmissions of plesiochronous data over synchronous transmission networks places new requirements on desynchronizers. Four contributors to desynchronizer buffer variations are the justification bits in the VC-12, the irregular spacing of the data in the VC-12, the irregular spacing of the VC-12 in the SDH frame, and the pointer activity which results in byte justifications. These are additive in nature and result in variations in desynchronizer buffers. In the event a SDH network is not synchronized due to the first node clock operating in holdover mode, the effects of the gaps in the structures at both the STM-1 frame level and the VC-12 structure level are intensified by the effects of pointer activity. When the pointer justification bytes consecutively contain overhead bytes, variations occur in the desynchronizer bit buffer. VC-12 *S*1 and *S*2 justification bit activity contributes to an uneven arrival of bits to the desynchronizer. In the event a SDH network is operating in synchronous mode and then a clock is switched over to the holdover mode, a transient effect occurs. This effect is cause by a rapid transmission of VC-12 S bits (bit effect) through the network and a relatively slow transmission of pointer effects (byte effect) through the network. The VC-12 *S* bits are transmitted directly as a part of the payload and thus are subject only to the normal network transmission delay. The pointer bytes are delayed at each node in the network by an amount proportional to the distance from the present fill of the STM-1 byte buffers to the threshold which signals the byte buffer level deviation requires a pointer action. A pointer action moves the byte fifo fill level back to an acceptable value by sending out or withholding an extra byte. The net result is that at the desynchronizer, the arrival of VC-12 S bits occurs first and then pointer justification byte effects arrive later.

Acknowledgements

The author would like to acknowledge that Dave Scheer and Thomas Klett wrote portions of the code which was used to obtain the results presented in this paper. This work was supported in part by ALCATEL-SEL.

Manuscript received on December 13, 1993.

REFERENCES

[1] ITU Recommendation G.709: *Synchronous multiplexing structures*. 1990.

[2] ITU Recommendation G.707: *Synchronous digital hierarchy bit rates*. 1990.

[3] ITU Recommendation G.708: *Network node interface for the synchronous digital hierarchy*. 1990.

[4] H. Owen, T. Klett: *Simulation of pointer activity in synchronous digital hierarchy networks*. Proceedings 12-th International Phoenix Conference on Computers and Communication, 1993, p. 409-415.

[5] H. Owen, T. Klett: *Synchronous digital hierarchy network pointer simulation*. "Computer Networks and ISDN Systems", Vol. 26, No. 5, January 1994, p. 481-491.

[6] H. Owen, T. Klett: *Synchronous digital hierarchy statistical simulation of pointer activity*. "Computer Communications", Vol. 16, No. 12, December 1993, p. 759-766.

[7] M. Sexton, A. Reid: *Transmission networking: SONET and the synchronous digital hierarchy*. Artech House, London, 1992, p. 117-145.

[8] SONET Desynchronizers, T1X1.6/89-0-12 (February 1989)

[9] G. Pierobon, R. Valussi: *Jitter analysis of a double modulated threshold pulse stuffing synchronizer*. "IEEE Transactions on Communications", Vol. 39, No. 4, April 1991, p. 594-602.

[10] R. Nawrocki, W. Ehrlich: Waiting time jitter reduction by fill locking. "Electronic Letters", Vol. 26, No. 16, August 1990, p. 1227-1228.

[11] M. Klein, R. Urbansky: *Network synchronization - A challenge for SDH/SONET?*. "IEEE Communications Magazine", Vol. 31, No. 9, p. 42-50.

[12] E. Best: Phase-locked loops : *Theory, design, and applications*. McGraw-Hill, New York 1993.

H. L. Owen: **Synchronous Digital Hierarchy Byte Pointer Justification Versus VC-12 Payload Bit Justification Effects.**

ETT, Vol. 6 - No. 1 January - February 1995, p. 97 - 105

Telecommunication Systems

Fast Computation of Outage Probability for Cellular Mobile Radio Systems

Michele Zorzi
Dipartimento di Elettronica e Informazione, Politecnico di Milano
Piazza Leonardo da Vinci 32, 20133 Milano - Italy

Abstract. In this paper a new approximate method for the computation of outage probabilities in a mobile radio environment is proposed. It allows one to evaluate the performance of a mobile radio system in the presence of fading, in a very fast and accurate way, while maintaining a very good flexibility as to the application to different network environments. Coding is also considered as a possible choice, in order to increase the spectral efficiency of the system, which represents a major concern for the designers of cellular networks.

1. INTRODUCTION

In recent times, mobile radio has been studied with great interest, and very much work has been done in order to evaluate the performance of mobile radio systems, and to provide design criteria for them. The performance measure which is usually considered is the outage probability, i.e., the probability that the Signal-to-Noise plus Interference Ratio at the receiver is not large enough to ensure correct detection.

One major difficulty in evaluating the performance of a mobile communications system is the complexity of the propagation environment, in which various random effects, such as fading and shadowing, must be taken into account, along with the near/far problems. It is not easy to deal with such a model, which leads almost always to complicated expressions.

In the past, various methods for the outage probability evaluation have been proposed. Immovilli and Merani [1] suggested to approximate the interference power by its mean, whereas Prasad and Kegel [2] proposed to model the effect of the superposition of lognormal shadowing and Rayleigh fading by means of an "equivalent" shadowing, whose spread is slightly increased. Linnartz, on the other hand, developed an exact analysis which allows one to obtain formulas for the outage probability, which, however, can only be evaluated numerically [3]. He noticed also that the numerical evaluation can be performed by means of Gauss-Hermite Quadrature Rules, due to the presence of exponentials in the integrands. All these papers consider explicitly only the reverse (i.e., Mobile to Base) channel, even though, for example, the analysis in [3] could be extended to include the forward direction. Conversely, Sowerby and Williamson [4] focused on the forward link, reporting results for only one interfering cell.

In this paper, we develop an approximate approach to the above computation, which enables us to accurately evaluate the outage probabilities with little computational effort. We introduce a technique which can be extended to other environments, and which applies in various conditions; for example, different traffic distributions, number of cells, propagation conditions, etc.. Our computations will show that, under certain conditions (satisfied in most practical systems), the performance in the two directions is the same, as is often conjectured.

It should be noted that, from the system point of view, the above way of looking at the problem is somewhat restrictive. In fact, there are a number of other performance indices which can be considered, and which sometimes are even more relevant than the outage probability. In particular, it seems that the outage probability, rather than being a *performance measure* (as it is from a *link* viewpoint), becomes a *constraint* when a system standpoint is taken. A more significant measure of the system performance can be the *spectral efficiency* (sometimes referred to as *system capacity*, i.e., the number of users which can be accomodated in the system, for a given bandwidth), for a given required outage probability which must be guaranteed to each subscriber in the network. In this view, a discussion about coded performance is briefly presented, in order to gain some valuable in-

sight about the tradeoffs involved. In particular, with reference to the spectral efficiency, it can be clearly shown that the use of coding is not necessarily convenient.

As suggested in [5], a model like the one here considered is good to obtain insight, but is too general to be employed in the design of practical networks. In this latter case, it is very important to take advantage of as many terrain data as possible, and the design process is more complicated. We note that the approach here suggested is very flexible, since it can be employed in the presence of differently distributed classes of users, different cell sizes, or even shapes, irregular layouts, different propagation conditions, and so on. In particular, the approximation here proposed, even though the specific analysis is carried out explicitly for some special cases, is believed to be still applicable to these more general situations. Also, compared to [3], it requires much less computational time; this, of little importance in the evaluation of few outage probability curves, may become valuable when iterative procedures or complicated design processes are to be implemented. Therefore, the approach we propose in the following, combining flexibility, accuracy and little processing requirements, appears to be a valuable tool in supporting network designers.

2. SYSTEM MODEL AND OUTAGE PROBABILITY

In the cellular system we consider, each user in each cell is uniquely assigned a channel; also, to guarantee a tolerable level of interference, the channels available in a cell must not be reused in the neighboring cells. Therefore, a clustered structure is devised [6].

The signals are attenuated due to three factors: the path loss due to the distance r, which is assumed proportional to r^{η}, where η is about 4 for land mobile propagation; the shadowing, modeled as a lognormal random variable (r.v); and the Rayleigh fading, due to multipath, which causes the instantaneous received power to be exponentially distributed [7]. Therefore, the received power from the i-th user at distance r_i can be expressed as

$$S_i = \chi_i \, P_T \, K r_i^{-\eta} \, \alpha_i^2 \, e^{\xi_i} \tag{1}$$

where P_T is the transmitted power, $Kr_i^{-\eta}$ is the path loss due to distance, α_i is a Rayleigh distributed r.v. with unit power, $\chi_i = 1$ if user i is active (with probability p) and 0 otherwise, and e^{ξ_i} accounts for log-normal shadowing. ξ_i is a Gaussian r.v., with zero mean and standard deviation σ. Usually, the shadowing is described in terms of the dB *spread*, σ_{dB}, i.e., decibels are used instead of natural units: of course, $\sigma = (0.1 \log 10)\,\sigma_{\mathrm{dB}}$. In the following, the subscript 0 will refer to the intended user, whereas $i = 1, \ldots, N$ will denote the interferers. Also, we assume that P_T and K are the same for all signals.

The outage probability is defined as in [1], i.e., the probability that the Signal-to-Interference plus Noise Ratio is smaller than a given threshold, denoted by b. Using (1), in the presence of N potential interferers, this probability can be written as:

$$\psi = P\left[S_0 \le b\left(\sum_{i=1}^{N} S_i + W\right)\right] = P\left[\alpha_0^2 \le b\left(\sum_{i=1}^{N} \chi_i \alpha_i^2 e^{\xi_i - \xi_0}\left(\frac{r_i}{r_0}\right)^{-\eta} + \frac{W e^{-\xi_0}}{P_T K r_0^{-\eta}}\right)\right] \tag{2}$$

where W is the power of the thermal noise. When conditioned on $\underline{\xi} = (\xi_0, \xi_1, \ldots, \xi_N)$, $\underline{r} = (r_0, r_1, \ldots, r_N)$, and $\underline{\chi} = (\chi_1, \ldots, \chi_N)$, the outage probability is computed as

$$\psi_1(\underline{\xi}, \underline{r}, \underline{\chi}) = 1 - \int_0^{\infty} \mathrm{d}a_1 \ldots \int_0^{\infty} \mathrm{d}a_N \exp\left(-b\sum_{i=1}^{N} \chi_i e^{\xi_i - \xi_0} \cdot \left(\frac{r_i}{r_0}\right)^{-\eta} a_i - \frac{b W e^{-\xi_0}}{P_T K r_0^{-\eta}}\right) \prod_{i=1}^{N} e^{-a_i} = 1 - e^{-\mu e^{-\xi_0}} \prod_{i=1}^{N} \frac{1}{1 + b\,\chi_i\, e^{\xi_i - \xi_0}\left(\frac{r_i}{r_0}\right)^{-\eta}} \tag{3}$$

where

$$\mu = \frac{b W}{P_T K r_0^{-\eta}} \tag{4}$$

Averaging (3) over r_i, $i = 1, \ldots, N$, and ξ_i, $i = 0, 1, \ldots, N$, we obtain

$$\psi_2(\underline{\chi}) = 1 - \int_{-\infty}^{\infty} d\,\xi_0 \frac{e^{-\frac{\xi_0^2}{2\sigma^2}}}{\sqrt{2\pi}\sigma} e^{-\mu e^{-\xi_0}} \prod_{i=1}^{N} I_i(\xi_0, \chi_i) \tag{5}$$

where

$$I_i(\xi_0, \chi_i) = \int_{-\infty}^{\infty} d\,\xi_i \frac{e^{-\frac{\xi_i^2}{2\sigma^2}}}{\sqrt{2\pi}\sigma} \int_0^{\infty} \frac{f_i(r)\,\mathrm{d}r}{1 + b\,\chi_i\, e^{\xi_i - \xi_0}\left(\frac{r}{r_0}\right)^{-\eta}} \tag{6}$$

and $f_i(r)$ is the pdf of the distance between the i-th interferer and the intended receiver. Last, we average $\psi_2(\underline{\chi})$ over the χ_i's, which are assumed to be independent and identically distributed binary r.v.'s with $P[\chi_i = 1] = p$, to obtain:

$$\psi(\wp) = 1 - \int_{-\infty}^{\infty} \mathrm{d}\xi_0 \frac{e^{-\frac{\xi_0^2}{2\sigma^2}}}{\sqrt{2\pi}\sigma} e^{-\mu e^{-\xi_0}} \prod_{i=1}^{N} \left((1-p) + p \cdot \int_{-\infty}^{\infty} \mathrm{d}\,\xi_i \frac{e^{-\frac{\xi_i^2}{2\sigma^2}}}{\sqrt{2\pi}\sigma} \int_0^{\infty} \frac{f_i(r)\,\mathrm{d}r}{1 + b\, e^{\xi_i - \xi_0}\left(\frac{r}{r_0}\right)^{-\eta}}\right) = 1 - \int_{-\infty}^{\infty} \mathrm{d}\,\xi_0 \frac{e^{-\frac{\xi_0^2}{2\sigma^2}}}{\sqrt{2\pi}\sigma} e^{-\mu e^{-\xi_0}} \prod_{i=1}^{N} \left(1 - p\, J_i(\xi_0, \wp)\right) \tag{7}$$

where

$$J_i(\xi_0, \wp) = \int_{-\infty}^{\infty} d\,\xi_i \frac{e^{-\frac{\xi_i^2}{2\sigma^2}}}{\sqrt{2\pi}\sigma} \int_0^{\infty} \frac{f_i(r)\,dr}{1 + b^{-1} e^{\xi_0 - \xi_i} \left(\frac{r}{r_0}\right)^{\eta}} \quad (8)$$

$$i = 1, \ldots, N$$

Only the dependence on the location of the mobile user, $\wp$, (through both r_0 and $f_i(r)$) is explicit in the notation, even though ψ is actually a function of a number of other parameters as well. In the following, for ease of notation, we will consider only the situation in the absence of noise ($\mu = 0$), as is often done in the literature. From the following analysis, however, it will be clear that this is by no means a critical assumption, and the extension to the case in the presence of noise is straightforward.

2.1. *Reverse link*

On the reverse link, because of the symmetry of the system, all the interferers are statistically equal, and therefore $f_i(r) = f_r(r)$ and $J_i(\xi_0, \wp) = J_r(\xi_0, r_0)$, $i = 1, 2, \ldots, N$. The position of the mobile, $\wp$, is present in the computation only through its radial component, r_0, whereas, because of the circular symmetry, the angle is irrelevant. Therefore, we can write, for the outage probability on the reverse link,

$$\psi_r(r_0) = 1 - \int_{-\infty}^{\infty} d\,\xi_0 \frac{e^{-\frac{\xi_0^2}{2\sigma^2}}}{\sqrt{2\pi}\sigma} \left(1 - p\,J_r(\xi_0, r_0)\right)^N \quad (9)$$

Different expressions of $J_r(\xi_0, r_0)$ are obtained, according to the distribution of the interferers, $f_r(r)$. In this paper, we will consider two examples, namely uniform and deterministic. For a uniform distribution in a circular ring with radii R_1 and R_2, we have

$$f_u(r) = \frac{2r}{R_2^2 - R_1^2}, \qquad r \in [R_1, R_2] \quad (10)$$

whereas, for deterministic position, we have

$$f_d(r) = \delta(r - R_I) \quad (11)$$

where δ is the Dirac delta-function, and R_I is the deterministic distance of the interferers from the receiving base station (BS). Note that this latter model can be used to approximate the former, by taking, $R_I = R_u$, with R_u the reuse distance [5], or to study it in a worst-case situation, by taking $R_I = R_1$ [1]. These considerations will be developed in the following.

2.2. *Forward link*

On the forward link, given the location $\wp$ of the mobile user (which, in this case, is the receiver), the propagation path lengths of the signals are deterministic, since the BSs, i.e., the interfering transmitters, are in fixed positions. On the other hand, these lengths are not all equal, in general. Also, note that, unlike on the reverse link, the situation on the forward link is not symmetric, and two coordinates are needed to adequately describe the location, $\wp$. Let r_i, which depends on $\wp$, be the distance from the i-th BS to the mobile receiving unit. The pdfs $f_i(r)$ are given, in this case, by

$$f_i(r) = \delta(r - r_i), \quad i = 1, 2, \ldots, N \quad (12)$$

and the outage probability is

$$\psi_f(\wp) = 1 - \int_{-\infty}^{\infty} d\,\xi_0 \frac{e^{-\frac{\xi_0^2}{2\sigma^2}}}{\sqrt{2\pi}\sigma} \prod_{i=1}^{N} \left(1 - p\,J_{fi}(\xi_0, \wp)\right) \quad (13)$$

where

$$J_{fi}(\xi_0, \wp) = \int_{-\infty}^{\infty} d\,\xi_i \frac{e^{-\frac{\xi_i^2}{2\sigma^2}}}{\sqrt{2\pi}\sigma} \frac{1}{1 + b^{-1} e^{\xi_0 - \xi_i} \left(\frac{r_i}{r_0}\right)^{\eta}} \quad (14)$$

which depends on $\wp$ through the ratio r_i / r_0.

3. RATIONAL APPROXIMATION

From the above analysis, note that the exact computation of the outage probability involves many integrals, which are to be evaluated in order to obtain numerical values. In the recent literature, several methods have been proposed to overcome this difficulty. In [2], it is suggested to approximate the effect of the superposition of Rayleigh fading and log-normal shadowing by means of an "equivalent" log-normal shadowing, whose spread is slightly increased. As observed in [3], this approach leads to slightly pessimistic results, and involves a recursive procedure which is potentially both time consuming and not very accurate. Another approximation, proposed in [1], consists in replacing the random power of the interfering signals by its mean value: this leads to good results in a certain range of values of the parameters, but its accuracy is not very good for small reuse distances and for heavy shadowing (e.g., for σ = 12 dB), as observed in [8]. Third, Linnartz [3] proposed to directly evaluate the integrals via numerical methods, i.e., the Gauss-Hermite quadrature formulas. He noted that this method may be even more efficient than the log-normal ap-

proximation in [2], and has the advantage of being exact (as long as the numerical procedures have sufficient accuracy).

In this paper, we propose a new method for evaluating the outage probability, which enables us to approximate $J_i(\xi_0, \wp)$, as defined in (8), by means of a simple rational function. The result of this procedure is that the outage probability can be computed by means of a single Gauss-Hermite integration, which is fast and accurate; also, the effect of the rational approximation, as discussed in the following, is an error on the final value of the probability which is less than 5%, for all values of the parameters of practical interest. We note that, for probability evaluations, this method is therefore very accurate.

Let us consider (8) (the subscript i is dropped for ease of notation): note that the inner integration (over r) is from 0 to ∞. In reality, in the cellular environment we are considering, there is no intracell interference (i.e., interference from within the cell in which the intended user is located), so that the pdf $f(r)$ is identically zero up to a positive distance, say R_m, from the BS. Therefore, (8) can be rewritten, without loss of generality, as

$$J(\xi_0, \wp) = \int_{-\infty}^{\infty} \mathrm{d}\,\xi \frac{e^{-\frac{\xi^2}{2\sigma^2}}}{\sqrt{2\pi}\sigma} \int_{R_m}^{R_M} \frac{f(r)\,\mathrm{d}\,r}{1 + b^{-1} e^{\xi_0 - \xi} \left(\frac{r}{r_0}\right)^{\eta}} = \int_{-\infty}^{\infty} \mathrm{d}\,\xi \frac{e^{-\frac{\xi^2}{2\sigma^2}}}{\sqrt{2\pi}\sigma} \int_{R_m}^{R_M} \frac{f(r)\,\mathrm{d}\,r}{1 + A e^{-\xi} \left(\frac{r}{R_m}\right)^{\eta}} \triangleq F(A) \tag{15}$$

where R_M may be infinite, and where we defined

$$A \triangleq \frac{e^{\xi_0}}{b} \left(\frac{R_m}{r_0}\right)^{\eta} \tag{16}$$

With the above notation, it is rather easy to verify that

$$\lim_{A \to 0} F(A) = 1 \tag{17}$$

$$\lim_{A \to \infty} F(A) = 0 \tag{18}$$

$$\lim_{A \to \infty} A\,F(A) = e^{\sigma^2/2} \int_{R_m}^{R_M} \frac{f(r)\,\mathrm{d}\,r}{\left(\frac{r}{R_m}\right)^{\eta}} \triangleq L \tag{19}$$

Given the pdf $f(r)$, the limit in (19) can be explicitly evaluated. In the following, for ease of notation, we will consider the case $\eta = 4$, even though the entire analysis can be developed for any η. For the uniform pdf (10), we have

$$L_u = e^{\sigma^2/2} \int_{R_1}^{R_2} \frac{2\,r\,\mathrm{d}\,r}{\left(R_2^2 - R_1^2\right)\left(\frac{r}{R_i}\right)^4} = e^{\sigma^2/2}\,\frac{R_1^2}{R_2^2} \tag{20}$$

In the presence of deterministic positions, as in (11) (or in (12)), we can take (20) in the limit as $R_1, R_2 \to R_I$ (or r_i), to obtain

$$L_d = e^{\sigma^2/2} \tag{21}$$

Eqs. (17) to (19) suggest to approximate $F(A)$ by means of a rational function of the form:

$$\varphi(A) = \frac{1}{1 + c_1 A^{1/n} + \ldots + c_n A} \tag{22}$$

for an appropriate choice of the order, n, and of the set of coefficients, c_i, $i = 1, \ldots, n$. Note that $c_n = 1/L$.

The choice (22) deserves some comments. First, it can be proven that any minimax rational approximation problem defines a convex function with the property that a best approximation (if one exists) is a minimum of that function ([9] for the details). In this context, this means that the maximum relative error in approximating $F(A)$ with $\varphi(A)$ is a convex function of the coefficients, c_i, $i = 1, \ldots, n$. Therefore, the optimal choice of the c_i's can be obtained numerically by any search method, since any local minimum must also be a global minimum. Moreover, the choice of the c_i's is independent of the variables summarized in A, and this optimization, once the system parameters are chosen (i.e., $f_i(r)$, the cellular layout and η), depends only on the shadowing spread, σ. In particular, the same $\varphi(A)$ can be used for any ξ_0 (the variable of integration), any distance r_0, and any value of the capture ratio, b. Note that, for the uniform distribution (10), $\varphi(A)$ is the same for all users. We also note that, for interferers in fixed locations, the approximation does not depend on the locations themselves, as can be seen from (15) with $f(r) = f_d(r)$ and $R_m = R_I$. Finally, numerical evaluations show that the suggested approximation is very good, in a broad range of parameters, even for $n = 2$. Therefore, in the following, we will consider $\varphi(A) = 1/(1 + c_1\sqrt{A} + c_2 A)$, so that the optimization problem is reduced to one dimension (recall that $c_2 = 1/L$ is known from (19)).

If ε is the minimax relative error in the approximation, the following bounds hold:

$$1 - \prod_{i=1}^{N} \left(1 - p\,(1-\varepsilon)\,\varphi(A_i)\right) \le 1 - \prod_{i=1}^{N} \left(1 - p\,J_i(\xi_0, \wp)\right) \le 1 - \prod_{i=1}^{N} \left(1 - p\,(1+\varepsilon)\,\varphi(A_i)\right) \tag{23}$$

where it is highlighted that A, as defined in (16), may be

a function of i: this happens, for example, on the forward link, where the factors in the product are not equal, because they contain the positions of the interferers, r_i ((16), with $R_m = r_i$). On the other hand, the function φ does not depend on i, i.e., the coefficients c_1 and c_2 are the same for all terms. For a wide range of values of the parameters, covering almost all practical applications, typical values of ε are less than 5%, and the relative error on the approximation (23), i.e., on the outage probability, turns out to be of the same order.

The outage probability, ψ, is therefore obtained from (23) by a single numerical integration, e.g., via Gaussian quadrature, which is very fast and accurate, due to the presence of the exponential in the integrand. We remark that, in the deterministic situations, the direct computation of the integral (14) via the Gauss-Hermite quadrature formulas (as proposed in [5]), requires N_{GH} evaluations of the integrand, if N_{GH} is the number of points (a typical value is $N_{GH} = 20$). In our approach, (14) is approximated by means of a rational function, and therefore its computation requires a single evaluation (there is no integration involved). Moreover, if we were to evaluate (8) on the reverse link, where the random distribution of the interferers must, in general, be taken into account, a double integration is involved: the method in [5] would require $N_{GH}N_{GL}$ evaluations of the integrand, with N_{GL} the number of points for a Gauss-Legendre quadrature (a typical value can be $N_{GL} = 40$). On the other hand, our approximation still requires just a single evaluation, because the complexity lies in finding the coefficients c_i, and this problem is solved only once. In this latter case, i.e., randomly distributed interferers, with the values of N_{GH} and N_{GL} indicated in the above, the exact approach in [5] involves a number of operations which is roughly 800 times as large as in the approximate approach here proposed. We can therefore maintain that this approach, among the methods for the outage probability evaluations in mobile radio proposed in the literature [1, 2, 3], is certainly the most efficient, while guaranteeing, for all values of practical interest, a very good accuracy as well. As a last remark, however, we observe that the different approaches are all valuable, especially because they can potentially be employed in different environments and situations. In particular, the approximate solutions of [1, 2] can be used in Ricean channels as well, whereas the present analysis, along with that in [5], can be easily extended to study the adjacent channel interference or the effect of considering more tiers of cochannel cells (necessary when the activity, p, is small).

4. NUMERICAL RESULTS

In this section, we present some results obtained from the analysis in the above. The reference model will be a layout of hexagonal cells. Most results will be given for a reuse distance $R_u = \sqrt{21}$ (cluster of 7 cells, which is the commonly adopted value). Note, however, that the above analysis applies to any value of R_u.

In Fig. 1, the outage probability, ψ, is plotted vs. r_0, for some values of b and σ, and $p = 1$, whereas, in Fig. 2, different values of the activity, p, are considered. We note the great sensitivity of ψ to the dB spread, σ, as shown in Fig. 1 a). Note, also, that reducing the activity, p, has much the same effect as reducing the outage threshold, b. Figs. 1 and 2 also report some simulation points (obtained via Monte-Carlo evaluation), which show that our approximation is indeed very good.

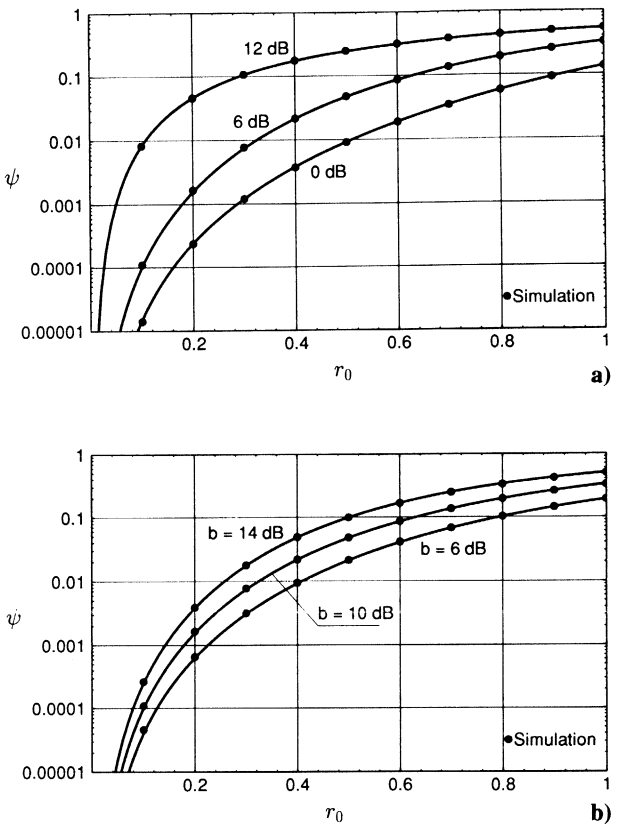

Fig. 1 - Outage probability, ψ, on the reverse link, vs. the normalized distance, r_0, for various values of the outage threshold, b, and of the shadowing spread, σ; $p = 1$, $\eta = 4$, uniform distribution of the interferers as in eq. (10), with $R_1 = \sqrt{13}$ and $R_2 = \sqrt{31}$; $b = 10$ dB, $\sigma = 0$, 6, 12 dB (a); $\sigma = 6$ dB, $b = 6$, 10, 14 dB (b).

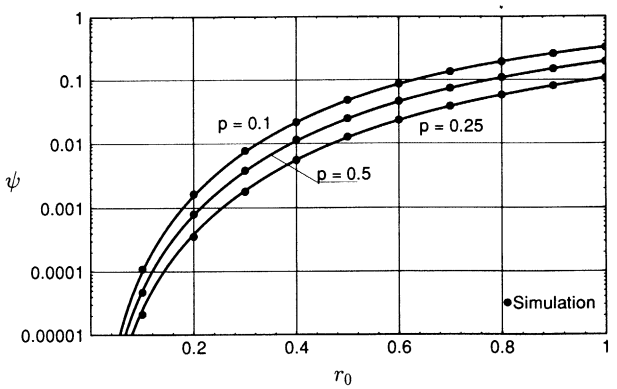

Fig. 2 - Outage probability, ψ, on the reverse link, vs. the normalized distance, r_0, for various values of activity, p; $b = 10$ dB, $\eta = 4$, $\sigma = 6$ dB uniform distribution of the interferees as in eq. (10), with $R_1 = \sqrt{13}$ and $R_2 = \sqrt{31}$, $p = 0.25, 0.5, 1$.

In Fig. 3, three models are compared: exact evaluation (random distribution for the interferers as in (10)), approximate approach (deterministic situation with $R_I = R_u$, as suggested in [5]), and worst-case approach (deterministic situation with $R_I = R_1$, as in [1]). It can be seen that the worst case yields in fact pessimistic results whereas, interestingly, the approximation of considering all interferers located at the center of their cells is remarkably good (the curves are hardly distinguishable), even for $R_u = \sqrt{21}$ (cluster of 7 cells). Of course, this is even better verified as the reuse distance is further increased, whereas the approximation becomes less and less accurate as R_u gets small.

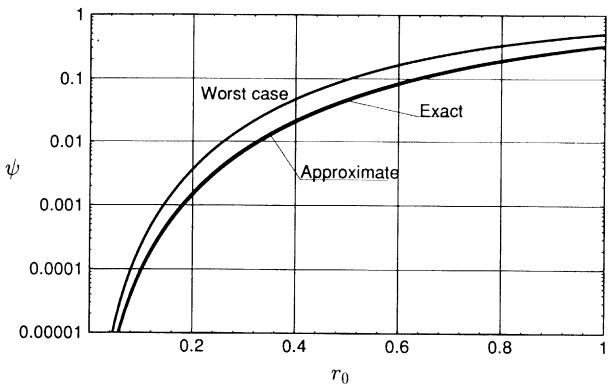

Fig. 3 - Outage probability, ψ, on the reverse link, vs. the normalized distance, r_0, for three models for the distribution of the interferers: worst-case ($r_i \equiv R_1 = \sqrt{13}$), approximate ($r_i \equiv R_u = \sqrt{21}$), exact (uniform distribution of the interferees as in eq. (10), with $R_1 = \sqrt{13}$ and $R_2 = \sqrt{31}$); $p = 1$, $b = 10$ dB, $\eta = 4$, $\sigma = 6$ dB.

Let us assume to be in the situation in which the interferers, although randomly distributed, can be approximated as fixed. In this case, note that the value of the outage probability, for fixed σ and p, depends only on the parameter

$$B = b\left(\frac{r_0}{R_u}\right)^{\eta} \tag{24}$$

In particular, for the worst-case position of the intended user, $r_0 = 1$, the relevant parameter is

$$B_1 = \frac{b}{R_u^{\eta}} \tag{25}$$

Let us consider using coding to improve the performance. The better performance allows a smaller reuse distance, R_u, but the required bandwidth is increased, due to the introduced redundancy. The spectrum efficiency, therefore, can be roughly expressed as:

$$S_E = C\frac{\rho}{R_u^2} \tag{26}$$

where $\rho \le 1$ is the rate of the code, and C is a constant whose value is irrelevant as far as this discussion is concerned (for a more complete definition, [2]). Let us consider two systems, in which the outage threshold, reuse distance and rate are b_1, R_{u1}, ρ_1 and b_2, R_{u2}, ρ_2, respectively. To have the same outage performance, we require, from (25), that

$$\frac{b_1}{R_{u1}^{\eta}} = \frac{b_2}{R_{u2}^{\eta}} \tag{27}$$

and the ratio between the spectrum efficiencies is given by

$$\frac{S_{E2}}{S_{E1}} = \frac{\rho_2}{\rho_1}\frac{R_{u1}^2}{R_{u2}^2} = \frac{\rho_2}{\rho_1}\left(\frac{b_1}{b_2}\right)^{2/\eta} \tag{28}$$

For example, let us consider the case $\rho_1 = 1$, i.e., no coding is used in system number 1, and $\eta = 4$. For system 2 to have a greater spectrum efficiency, it must be

$$\frac{b_1}{b_2} \ge \rho_2^{-2} \tag{29}$$

To have a rough idea of the trade-off involved in eq. (28), let us consider an "equivalent" E_b/N_0, i.e., the ratio of the energy per information bit to the interference spectral density. If P_s is the power of the intended signal, and P_I is the power of the interference, we have $E_b = P_s T_b$ and $N_0 = P_I T_s$, where T_b is the bit duration, and $T_s = T_b\rho$ is the symbol duration. With this notation, we have

$$\left(\frac{E_b}{N_0}\right)_{eq} = \frac{P_s}{P_I\rho} \tag{30}$$

Therefore, if G is the gain of the code in terms of E_b/N_0 (as usually expressed in the literature), the corresponding gain in terms of P_s/P_I (i.e., of the outage threshold, b) is G/ρ. In this case, (29) reduces to

$$G \ge \frac{1}{\rho} \tag{31}$$

In other words, the use of coding is convenient only if the coding gain is at least equal to the inverse of the code rate. For example, for the Golay code (23, 12), with $\rho \simeq 0.52$, we should have a code gain of at least 2.8 dB. In Table 1, the values of the required code gain vs. the code rate for some convolutional codes are reported, along with the coding gains (in dB) achieved by the same codes for an average *BER* of 10^{-3} and 10^{-5}, as given in [10].

As we can see, the coding gains achievable at *BER* 10^{-3} (the reference value for voice) are not very high and, as the code rate decreases, the gain obtained can be even smaller than ρ^{-1}. For these codes the spectral efficiency turns out to be worse than that of the uncoded system. Therefore, it seems that an optimal choice can be made, as to the coding scheme to be used. We remark that the above values of the coding gains are com-

puted for the case of AWGN, which may be a bad approximation of the present situation, where the statistics of the interference, in general, is not Gaussian. These values are taken as a reference, whereas the evaluation of the actual code gains achievable in this environment is still being investigated. On the other hand, although we are aware that these results are not precise quantitatively, we believe that the above discussion raises an important issue about the use of coding: the transmission link point of view, often taken in measuring the performance of coded systems, may become misleading if a system perspective is not taken at the same time. Therefore, it seems that further research should be devoted to the study of this trade-off.

Table 1 - *Comparison of the required code gain for a better spectral efficiency and the code gains at BER = 10^{-3} and 10^{-5} (in AWGN), for some convolutional codes ([10]).*

Code rate, ρ	Required code gain (dB)	Code gain at 10^{-3} (dB)	Code gain at 10^{-5} (dB)
3/4	1.2	2.6	4.2
2/3	1.8	3.1	4.6
1/2	3.0	3.8	5.1
1/3	4.8	4.4	5.9

Note that, in the above, we implicitly assumed $p = 1$. If $p < 1$, the performance is better but the spectrum efficiency is decreased. In fact, p plays a role that, qualitatively, is the same as that of ρ in the above discussion. From Figs. 1 b) and 2, we can see that, again, decreasing p may not be the most efficient choice: what is lost because of the decrease in the spectral efficiency may overweigh what is gained because of the performance enhancement. In this case, if everything is kept the same, increasing the reuse distance may be a more convenient solution.

On the forward link, as stated in section 2.2, the outage probability is a function of two variables, i.e., the distance, r_0, and the angle, θ. We computed $\psi(r_0)$ along some fixed directions, and the results we obtained (for $R_u = \sqrt{21}$, as before) were almost the same for any direction. Therefore, even though, in theory, both variables must be considered, in practice only the distance, r_0, is needed. However, this is true only when the reuse distance is large enough: in fact, for $R_u = \sqrt{3}$ (i.e., the frequency spectrum is reused in every cell), the dependence on θ cannot be neglected (on the other hand, we must observe that in order to achieve acceptable performance, a large R_u is required). Another approximation, which is very good for practical values of the reuse distance, is to take $r_i = R_u$, $i = 1, \ldots, 6$ (recall that r_i are actually functions of $\wp$). When this approximation can be made (and, for clusters of 7 cells or more, this is the case), the performance of the two links turns out to be equal, as often conjectured in the literature [5]. In this case, the above discussion about coding and spectrum efficiency applies on the forward link as well.

5. CONCLUSIONS

In this paper, we consider an analytical framework and an approximation method, which enable us to efficiently compute the outage probability in a mobile macrocellular environment. The proposed approximate approach is shown to be very accurate and to greatly reduce the computation time, compared to other methods presented in the recent literature. Also, the range of values of the parameters where our approach is accurate is broader than, for example, those in [1, 2]. The possibility of using coding to improve the spectral efficiency is also investigated, even though a correct analysis would require considering the actual statistics of the interference. Our current research is following this direction.

Manuscript received on December 16, 1993.

REFERENCES

[1] G. Immovilli, M. L. Merani: *Simplified evaluation of outage probability for cellular mobile radio systems.* "Electronics Letters", Vol. 27, Jul. 1991, p. 1365-1367.

[2] R. Prasad, A. Kegel: *Improved assessment of interference limits in cellular radio performance.* "IEEE Trans. on Veh. Tech.", Vol. VT-41, May 1992, p. 412-419.

[3] J. P. M. Linnartz: *Exact analysis of the outage probability in multiple-user mobile radio.* "IEEE Trans. on Commun.", Vol. COM-40, Jan. 1992, p. 20-23.

[4] K. W. Sowerby, A.G. Williamson: *Outage probabilities in mobile radio systems suffering cochannel interference.* "IEEE J. on Selected Areas in Commun.", Vol. SAC-10, Apr. 1992, p. 516-522.

[5] J.P.M. Linnartz: *Narrowband land-mobile radio networks.* Artech House, 1993.

[6] V.H. McDonald: *The cellular concept.* "Bell System Technical Journal", Vol. 58, No. 1, Jan. 1979, p. 15-41.

[7] M. Zorzi, S. Pupolin: *Outage probability in multiple access packet radio networks in the presence of fading.* "IEEE Trans. on Veh. Tech.", Vol. VT-43, Aug. 1994, p. 604-610.

[8] C. Caini, G. Immovilli, M.L. Merani: *Outage probability for cellular mobile radio systems - simplified analytical evaluation and simulation results.* "Electronics Letters", Vol. 28, Mar. 1992, p. 669-671.

[9] I. Barrodale: *Best rational approximation and strict quasi-convexity.* "SIAM J. Numer. Anal.", Vol. 10, Mar. 1973, p. 8-12.

[10] J.G. Proakis, *Digital communications.* New York, McGraw-Hill, 1989.

M. Zorzi: **Fast Computation of Outage Probability for Cellular Mobile Radio Systems.**

ETT, Vol. 6 - No. 1 January - February 1995, p. 107 - 113

Telecommunication Systems

Letter

The Pairwise Error Probability for Decoding a Convolutionally Encoded Sequence Using Integer Metrics

Haim Goldman
TADIRAN, Communications and Systems Group
26 Hashoftim Str., Holon, Israel

Abstract. The performance of a communication system that operates over a binary-input, output-symmetric memoryless channel and employs a convolutional error correcting code is usually evaluated by applying the union bound to the node error and the bit error probabilities. These bounds depend on the probability that an incorrect path on the code trellis accumulates a larger metric than the correct path. The paper presents an easy method to compute this pairwise error probability that is applicable to the significant case of a Viterbi decoder that uses a finite set of integer branch metrics.

1. INTRODUCTION

The performance of a communication system that operates over a binary-input, output-symmetric memoryless channel and employs a convolutional error correcting code is usually evaluated by applying the union upper bound to the error probability at node n, $P_e(j)$ and to the bit error probability, P_b [1, chapter 4]. The former is the probability that the maximum-likelihood decoder chooses an incorrect path that diverges from the correct path at node j on the code trellis and converges with the correct path at a later node. The latter is the probability of an erroneously decoded bit. For the discussed channel, the correct path can be assumed to be the all-zeros data path with no loss of generality.

By applying the union bound, the above probabilities can be upper bounded by [1, Chapter 4]:

$$P_e(n) \le \sum_{d=d_f}^{\infty} a(d)P(d)$$
$$P_b \le \frac{1}{K}\sum_{i=1}^{\infty}\sum_{d=d_f}^{\infty} i\,a(d,i)P(d) \qquad (1)$$

where

- d - The Hamming distance between the correct path and the incorrect path,
- d_f - The free distance of the convolutional code,
- K - The number of information bits transmitted over a single branch of the code trellis,
- $a(d)$ - The number of incorrect paths at Hamming distance d from the correct path over the unmerged segment on the code trellis,
- $a(d, i)$ - The number of paths at Hamming distance d from the correct path and with i "+1" bits in the data sequence over the unmerged segment,
- $P(d)$ - The pairwise error probability, i.e., the probability that an incorrect path on the code trellis, located at a Hamming distance d from the correct path, accumulates a larger metric than the correct path.

Note that $a(d)$ and $a(d, i)$ depend only on the convolutional code while the pairwise error probability is independent of the code and depends only on the channel and on the metrics used by the decoder.

If the exact pairwise error probabilities cannot be computed, they are often bounded by applying the Bhattacharyya upper bound [1]. A case in which pairwise error probabilities are employed and that is most significant for practical applications is the case of a Viterbi decoder that decodes a convolutionally encoded sequence using a finite set of integer metrics. This is characteristic of digitally implemented decoders.

Let denote the set of $2M$ integer metrics used by the decoder by S_1:

$$S_1 = \{\pm m_1, \ \pm m_2, \ \ldots \ \pm m_M\} \qquad (2)$$

The binary-input, output-symmetric memoryless

channel is characterized by the set of transition probabilities associated with the set of metrics:

$$\begin{cases} P_{tr}(j) = \Pr\{\text{metric } j \text{ is assigned} / \text{"+1" was transmitted}\} \\ Q_{tr}(j) = \Pr\{\text{metric } j \text{ is assigned} / \text{"-1" was transmitted}\} \end{cases}, j \in S_1 \quad (3)$$

Since the channel is output-symmetric, we have $Q_{tr}(j) = P_{tr}(-j)$ and we also assume that $P_{tr}(j) \geq P_{tr}(-j)$.

The pairwise error probability for the this case is given in [1, p. 292] as:

$$P(d) = G\left\{\left[\prod(z)\right]^d\right\} \quad (4)$$

where

$$\prod(z) = \sum_{j=-m_M}^{m_M} P_{tr}(j) z^j$$

$$A(z) = \sum_{k=-N}^{N} a_k z^k \quad (5)$$

$$G\{A(z)\} = \frac{1}{2} a_0 + \sum_{k=-N}^{-1} a_k$$

Direct application of eq. (4) is quite difficult because it requires to raise the polynomial $\prod(z)$ to the d-th power and then to derive a set of coefficients $\{a_k\}$ so that $[\prod(z)]^d$ can be expressed as a polynomial $A(z)$. For computing the probabilities in eq. (1), this procedure should be repeated independently for a sequence of increasing distances starting with the free distance of the convolutional code d_f. Note that for most practical codes $d_f \geq 10$.

A method to compute $P(d)$ was presented in [3]. This method is quite difficult to use because it requires to determine, separately for every value of distance d, the set of all the possible combinations of integers that satisfy a certain pair of non-trivial conditions.

In the next Section we present a simple method for computing the pairwise error probability that can be easily programmed and used in a straightforward manner for the evaluation of the node error and the bit error probabilities. The method does not involve any complex procedures as those required for either direct application of eq. (4) or for use of the method suggested in [3].

2. ANALYSIS

The pairwise error probability is next evaluated using a set of metrics and a set of transition probabilities that are equivalent to the sets defined in (2), (3). Assume that the integer metrics of the set defined in (2) satisfy

$$m_j > m_{j-1} \qquad M \geq j \geq 2 \quad (6)$$

This assumption implies that all the metrics in S_1 are distinct. There is no loss in generality because if there were two identical metrics $m_k = m_{k+1}$, then one could replace $P_{tr}(k)$ by $P_{tr}(k) + P_{tr}(k+1)$, delete metrics $\pm m_{k+1}$ from S_1 and use a reduced metrics set with only $(2M - 2)$ entries. Special attention should be paid to the case of $m_1 = 0$; in this case, the zero metric appears twice in S_1. We then use only one zero metric with an associated transition probability $P_{tr}(0) + P_{tr}(-0)$.

Define a set of $2M$ non-negative metrics S_2 by increasing each metric in S_1 by m_M, the largest metric in S_1:

$$S_2 = \{0, -m_{M-1} + m_M, -m_{M-2} + m_M, \ldots 2m_M\} \quad (7)$$

Define a set of corresponding transition probabilities $\{R(i), 0 \leq i \leq 2m_M\}$

$$R(i) = \begin{cases} P_{tr}(i - m_M) & i \in S_2 \\ 0 & \text{otherwise} \end{cases} \quad (8)$$

Hence

$$R(0) = P_{tr}(-m_M) \qquad R(2m_M) = P_{tr}(m_M) \quad (9)$$

With the above assumptions, all $2M$ entries of S_2 (or $2M - 1$ entries, if $m_1 = 0$ in S_1) are distinct. Since only metric differences matter at the Viterbi decoder, the performance of a decoder operating with the set S_2 and transition probabilities $\{R(i)\}$ is identical with the performance of a decoder operating with the set S_1 and transition probabilities $\{P_{tr}(j)\}$.

Using the definitions in (5) and (8) we obtain:

$$B(z,d) = \left[\prod(z)\right]^d = \left[\sum_{j=-m_M}^{m_M} P_{tr}(j) z^j\right]^d = z^{-m_M d}\left[\sum_{j=0}^{2m_M} R(j) z^j\right]^d \quad (10)$$

Note that the index j in the first sum in (10) runs over the entries of S_1 while the index in the second sum runs over the entries of set S_2.

By applying to eq. (10) the formula given in [2, p. 14, formula 0.314] for a power of a series, we obtain:

$$B(z,d) = \sum_{j=-N}^{N} c_{j+N} z^j \quad (11)$$

where

$$c_0 = R(0)^d$$
$$N = m_M d \quad (12)$$

and

$$c_j = \frac{1}{j\,R(0)} \sum_{i=1}^{j} \left[i(d+1) - j \right] R(i)\, c_{j-i} \tag{13}$$

In eq. (13), it is assumed that $R(0) \neq 0$. However, If $R(0) = R(1) = ... = R(k-1) = 0$ but $R(k) \neq 0$ then eq. (10) should be modified to

$$B(z,d) = z^{d(k-m_M)} \left[\sum_{j=0}^{2m_M - k} U(j)\, z^j \right]^d \tag{14}$$

where $U(j) = R(j+k)$ and eqs. (11)-(13) should be redefined in terms of $U(j)$.

By inserting the result of eq. (11) into eq. (4), we obtain the formula for the pairwise error probability as

$$P(d) = G\{B(z,d)\} = \frac{1}{2} c_N + \sum_{j=0}^{N-1} c_j \tag{15}$$

Note:

1) The summation in (13) is over $1 \leq i \leq j$ and, since $j \leq N = m_M d$, j can be quite large when a pairwise error probability is computed for a large distance d, as might be required for calculating a tight bound on $P_e(n)$ or on P_b at low signal-to-noise ratio. However, there are no more than $(2M-1)$ non-zero terms in the sum.
2) There are at most $2N+1$ non-zero coefficients $c_j(c_0, c_1, ... c_{2N})$ defined by eq. (13), but only the first $N+1$ coefficients $(c_0, c_1, ... c_N)$ are required for computing $P(d)$.
3) If the set of metrics S_1 is comprised of only even or only odd metrics, then both $R(j)$ and c_j are zero for odd indices j.

3. CONCLUSIONS

The analysis presented in the previous section facilitates an easily programmable, straightforward procedure for computation of the pairwise error probability $P(d)$ for any required value of d:

1) Use eq. (8) to define a set of $2M$ transition probabilities for the metrics set S_2.
2) Use eqs. (12)-(13) to compute the $(N+1)$ coefficients $c_j, j = 0, 1, ...N$.
3) Use eq. (15) to compute $P(d)$.

It can be verified that for the special case of $M = 1$, the result in eq. (15) indeed degenerates to the result given in [1, p. 247, eq. 4.5.3] for a binary symmetric channel.

Manuscript received on February 16, 1993.

REFERENCES

[1] A. J. Viterbi, J. K. Omura: *Principles of digital communications and coding*. McGraw-Hill, 1979.

[2] I. S. Gradshteyn, I. M. Ryzhik: *Tables of integrals, series and products*. Academic Press, 1980.

[3] Y. Yasuda, K. Kashiki, H. Yasuo: *High-rate punctured convolutional codes for soft decision Viterbi decoder*. "IEEE Trans. on Communications", Vol. COM-32, 1984, p. 315-319.

Haim Goldman: **the Pairwise Error Probability for Decoding a Convolutionally Encoded Sequence Using Integer Metrics.**

ETT, Vol. 6 - No. 1 January - February 1995, p. 115 - 117

Contributors

Yu-Wen Chang received the B.S. degree in Electrical Enginering from the National Taiwan University, Taiwan, in 1985, the M.S. degree in Electrical Engineering from the University of Maryland, College Park, in 1991, and is currently working toward the Ph.D. degree in Electrical Engineering at the same institution. Mr Chang is a research assistant of the Institute for Systems Research at the University of Maryland since 1992. His interests include admission control, handoff and power control problems in CDMA networks.

Rolands E. Ezers received the B.A.Sc. degree in Engineering Science from the University of Toronto, Ontario, Canada in 1987 and the M. Eng. and Ph. D. degrees in Electrical Engineering from Carelton University in 1989 and 1993.
He worked at Bell-Northern Research in Ottawa, Ontario, Canada from 1993 to 1994 in the area of optical-fibre communications. Currently, he is working at Shape Tecnical Centre in The Hague, The Netherlands in the area of satellite communications.

Barry Felstead was born in Medince Hat, Alberta in 1940. He received a BSc in Engineering Physics in 1962, and a MSc in EE in 1964, both from the University of Saskatchewan. From 1964 through 1966 he worked at Canadian General Electric, Toronto, on the application of optical signal processing to radar. He received a PhD in EE in 1970 from Queen's University, Kingston, Ontario. He has been at the Communications Research Centre, Ottawa since 1969. Since 1980, he has worked on military satellite communications with emphasis on spread spectrum techniques.

Evaggelos Geraniotis (S'76-M'82-SM'88) received the Diploma (with highest honors) in Electrical Engineering from the National Technical University of Athens, Greece, in 1978, and the M.S. and Ph.D. degrees in Electrical Engineering from the University of Illinois at Urbana-Champaign in 1980 and 1983, respectively. From September 1982 to August 1985 he was with the Department of Electrical and Computer Engineering at the University of Massachussetts, Amherst. Since September 1985 he has been with the University of Maryland, College Park, where he is presently a Professor of Electrical Engineering and a member of the Institute for Systems Research. Dr. Geraniotis's recent research has been in communication systems and networks with emphasis on the channel and traffic modelling, performance evaluation, and system design of: multi-access protocols for mobile, satellite, cellular, PCS, and optical networks; and multi-media (video, image, voice, and data) integration schemes for wireless networks, optical networks, high-speed ATM networks, and hybrid satellite/terrestrial networks.For the past fifteen years he has been conducting research on spread - spectrum and anti-jam communication systems; on schemes for interception, feature-detection, and classification of signals; on radar detection and discrimination; and on distributed detection, estimation, multi-sensor correlation, and data fusion. He is the author of over 140 technical papers in journals and conference proceedings. He serves regularly as a consultant in the above areas for governmental and industrial clients. Dr. Geraniotis has received several awards including the Ministry of Education of Greece First National Prize in 1973 and an Alan Berman Naval Research Laboratory Pubblication Award in 1990.
In the past three years, has served as officer of the Washington D.C./Northern Virginia Chapter of the Information Theory Society and as its Chairman, for 1989-1990. From February 1989 to October 1992 he was Editor for Spread-Spectrum of the IEEE Transactions on Communications.

Dennis Goeckel grew up in Indianapolis, IN, USA and split time between Purdue University and Sundstrand Corporation from 1987-1992, receiving his BSEE from Purdue in 1992. Since 1992, he has been at the University of Michigan where he received his MSEE in 1993 and is currently working on his Ph.D. in Electrical Engineering as a National Science Foundation Graduate Fellow. His current research interests are analysis and receiver design for coded digital communication systems.

Haim Goldman was born in 1954. He received the B.Sc. degree (Cum Laude) in Electrical Engineering in 1976 and the M.Sc. degree (Summa Cum Laude) in Electrical Engineering in 1981, both from the Tel-Aviv University, Tel-Aviv, Israel. From 1976 to 1981 he served with the Israeli Defence Forces. During 1982-1983 he was with the Israel Aircraft Industries. He has joined TADIRAN in 1983. Since 1993 he is the Scientist of the Communications and Systems Group and works on applied research and development of advanced communications systems.

T. Aaron Gulliver received the B.SC. and M.Sc. degrees in Electrical Engineering from the University of New Brunswick, Fredericton, NB, in 1982 and 1984, respectively, and the Ph.D. degree in Electrical and Computer Engineering from the University of Victoria, Victoria, BC, in 1989.
From 1989 to 1991 he was employed as a Defence Scientist at Defence Research Establishment Ottawa, Ottawa, ON, where he was primarily involved in research for secure frequency hop satellite communications.
From 1990 to 1991 he was an Adjunct Research Professor, and since 1991 an Assistant Professor in the Department of Systems and Computer Engineering, Carleton University.
His current research interests include spread spectrum communications, algebraic coding theory and the implementation of error control coding.

Hideki Imai was born in Shimane, Japan on May 31, 1943. He received the B.E., M.E. and Ph.D. degrees in Electrical Engineering from the University of Tokyo in 1966, 1968, 1971, respectively. Since 1971 he has been on the faculty of Yokohama National University (Lecturer 1971; Associate Professor 1972; Full Professor 1984), where he is presently a part-time Professor in the Division of Electrical and Computer Engineering.
In 1992 he joined the faculty of the University of Tokyo, where he is currently a Full Professor in the Institute of Industrial Science.
His current research interests include information theory, coding theory, cryptography, spread spectrum systems and their applications. He is the author of three books, the editor of four books, and coauthor of seven books. He received Excellent Book Awards from the Institute of Electronics, Information and Communication engineers (IEICE) of Japan in 1976 and 1991. He also received the Best Paper Award (Yonezawa Memorial Award) from IEICE in 1992.
He chaired several committees of scientific societies such as the IEICE Professional Group on Information Theory and the IEICE Professional Group on Information Security. He served as the editor of several scientific journal such as IEICE Transactions on Engineering Science. He chaired the 8th International Conference on Applied Algebra, Algebraic Algorithms and Error-Correction Codes (AAECC-8) in 1990, and the Program Committees of the International Symposium on Information Theory and Its Applications (ISITA'90) and of the Asiacrypt'91; He will chair the IEEE Information Theory Workshop in 1993.
Dr. Imai is on the board of IEEE IT Society, IEICE, International Association for Cryptologic Research (IACR) and Japan Society of Security Management (JSSM). He is also a member of IEE of Japan, IPS of Japan, and ITE of Japan.

Srinivas Kandala was born in Guntur, India on October 26, 1965. He received the B.E. degree in Electronics and Communications Engineering from Osmania University, Hyderabad, India in 1986, M.Tech in Electrical Engineering from Indian Institute of Technology, Kanpur, India in 1988 and Ph.d from University of Toronto, Toronto, Ontario, Canada in 1994.
He is currently a research associate at Institute National de la Recherche Scientifique-Telecom in Montreal, Canada. His research interests include tranceivers, power control, and mobile computing.

Ryuji Kohno was born in Kyoto, Japan on March 30, 1956. He received the B.E. and M.E. degrees in Computer Engineering from Yokoham National University in 1979 and 1981, respectively, and the Ph.D. degree in electrical engineering from the University of Tokyo in 1984.
He joined in the Department of Electrical Engineering, Tokyo University in 1984 and became an Associate Professor in 1986. Since 1988 he has been an Associate Professor in the Division of Electrical and Computer Engineering, Yokohama National University. During 1984-1985 he was a Visiting Scientist in the Department of Electrical Engineering, the University of Toronto.
At the present, he is the Vice-Chairman of the Society of Spread-Spectrum Technology of the IEICE (Institute of Electronics, Information, Communications Engineers). He was the Chairman of the Technical Program Committee of 1992 IEEE International Symposium on Spread-Spectrum Techniques and Applications (ISSSTA'92), the Vice-Chairman of the Technical Program Committee of 1993 International Symposium on Personal Indoor and Mobile Radio Communications (PIMRC'93) and so on.
His current research interests lie in the areas of adaptive signal processing, coding theory, spread spectrum systems, and their applications to various kinds of pratical communication systems. He is a member of IEEE, EURASIP, IEICE, IEE of Japan, IPS of Japan.
He wrote technical books entitled *"Spread Spectrum Techniques and Applications", "Digital Signal Processing", "Data Communications Systems"* and is currently writing the book entitled *"Advanced Spread Spectrum Techniques and Applications"*.

Laurence B. Milstein (S'66-M'68-SM'77-F'85) received the B.E.E., degree from the City College of New York, New York, NY, in 1964, and the M.S. and Ph.D. degrees in Electrical Engineering from the Polytechnic Institute of Brooklyn, N.Y., in 1966 and 1968, recpectively.
From 1968 to 1974 he was employed by the Space and Communications Group of Houghes Aircraft Company, and from 1974 to 1976 he was a member of the Department of Electrical and Systems Engineering, Rensselaer Polytechnic Institute, Troy, NY. Since 1976 he has been with the Department of Electrical and Computer Engineering, University of California at San Diego, La Jolla, CA, where he is a Professor and former Department Chairman, working in the area of digital communication theory with special emphasis on spread-spectrum communication systems. He has also been a consultant to both government and industry in the areas of radar and communications.
Dr. Milstein was an Associate Editor for Communication Theory for the *IEEE Transactions on Communications*, an Associate Editor for Book Reviews for the *IEEE Transactins on Information Theory*, and an Associate Technical Editor for the *IEEE Communications Magazine*, and is currently a Senior Editor for the *IEEE Journal on Selected Areas in Communications Society*, and is currently a member of the Board of Governors of both the IEEE Communications Society and the IEEE Information Theory Society. He is also a member of Eta Kappa Nu and Tan Beta Pi.

Henry L. Owen received his BSEE in 1979, MSEE in 1983 and his Ph.D. in 1989 from the Georgia Institute of Technology. Between 1979 and 1989 he worked for the Georgia Tech Research Institute. Since 1989 he has been an assistant professor in the School of Electrical and Computer Engineering, Georgia Institute of Technology. During 1991 and 1992 he was a research consultant for ALCATEL Standard Elektrik Lorenz. His research interests include computer aided design tools and algorithms for Synchronous Digital Hierarchy network performance and analysis, pointer activity effects on plesiochronous network boundaries, distributed cros connect restoration algoritms, and routing and protection algorithms for networking consisting of self healing rings and meshed topologies.

Subbarayan Pasupathy was born in Madras, Tamilnadu, India, on September 21, 1940. He received the B.E. degree in Telecommunications from the University of Madras in 1963, the M. Tech. degree in Electrical Engineering from the Indian Institute of Technology, Madras, in 1966, and the M.Phil. and Ph.D. degree in engineering and applied science from Yale University in 1970 and 1972, respectively.
He joined the faculty of the University of Toronto in 1973 and became a Professor of Electrical Engineering in 1983.
He was the Associate Chairman of the Electrical Engineering Department from 1979 to 1982. At present, he is the Chairman of the Communications Group.
His research interests lie in the areas of communication theory, digital communications, and statistical signal processing.
Dr. S. Pasupathy is a registered Professional Engineer in the province of Ontario. During 1982-1989 he was an Editor for *Data Communications and Modulation* for the IEEE TRANSACTIONS ON COMMUNICATIONS. He has also served as a Technical Associate Editor for the IEEE COMMUNICATIONS MAGAZINE (1979-1982) and as an Associate Editor for the *Canadian Electrical Engineering Journal* (1980-1983). Since 1984, he has been writing a regular column entitled "Light Traffic" for the IEE COMMUNICATION MAGAZINE. He was elected as a Fellow of the IEEE in 1991 " for contributions to bandwidth efficient coding and modulation schemes in digital communication."

Raymond L. Pickholtz, professor in and former chairman of the Department of Electrical Engineering and Computer Science at The George Washington University received his Ph.D. Electrical Engineering from the Polytechnic Institute of Brooklyn in 1966. He was a researcher at RCA Laboratories and at ITT Laboratories. He was on the faculty of the Polytechnic Institute of Brooklyn and of Brooklyn College. He was a visiting professor at the Université du Quebec and the University of California. He is a fellow of the Institute of Electrical and Electronic Engineers (IEEE) and of the American Association for the Advancement of Science (AAAS). He was an editor of the *IEEE Transactions on Communications*, and guest editor for special issues on Computer Communications, Military Communications and Spread Spectrum Systems. He is editor of the Telecommunication Series for Computer Science Press. He has published scores of papers and holds six United States patents.
Dr. Pickholtz is President of Telecommunications Associates, a research and consulting firm specializing in Communication System disciplines. He was elected a member of the Cosmos Club and a fellow of the Washington Academy of Sciences in 1986. In 1984, Dr. Pickholtz received the IEEE centennial medal. In 1987, he was elected as Vice President, and in 1990 and 1991 as President of the IEEE Communications Society.

Andreas Polydoros, Ph.D., was born in Athens, Greece, in 1954. He was educated at the National Technical University of Athens, Greece (Diploma in EE, 1977), State University of New York at Buffalo (MSEE, 1979) and the University of Southern California (Ph.D., EE, 1982). He has been a faculty member in the Electrical Engineering Department/Systems and the Communication Sciences Institute at USC since 1982, becoming a Professor in 1992.
His general area of scientific interest is statistical communication theory with applications to spread-spectrum systems, signal detection and classification, data demodulation in uncertain environments, and multi-user radionetworks. He has over fifteen years of teaching, research, and extensive consulting experience on these topics, both for the government and industry.
Prof. Polydoros is the recipient of a 1986 NSF Presidential Young Investigator Award. He has served as the Associated Editor for Communications of the *IEEE Transactions on Information Theory* (1987-88), the Guest Editor of the July 1993 Special Issue on "Digital Signal Processing in Communications" for *Digital Signal Processing: A Review Journal* and a designated Area Editor for the International Journal *Wireless Personal Communications*.

Pedrag Rapajic received his B.Sc. degree in Electrical Engineering from the University of Banjaluka in 1982, M.E. in Communication Engineering from the University of Belgrade in 1988 and PhD in electrical Engineering from the University of Sydney in 1994.
He is currently with the University of Sydney. His present research interests are related to the wideband communications, adaptive signal processing and error control.

Ahmed Saifuddin received the B.Sc. and M.Sc. degree in Electrical Engineering form Bangladesh University of Engineering and Technology, B.U.E.T., in 1988 and 1990 respectively. He came to Japan in 1990 under Monbusho (Ministry of Education) scholarship and received the M.S. degree from Fukui University in 1993.
He is currently attending the Ph.D. programme at Yokohama National University. His research interests are in the areas of spread spectrum, coding and information theories. He is a student member of IEEE.

Elvino S. Sousa was born in Graciosa, Azores, (Portugal) on December 28, 1956. He received the B.A.Sc. degree in Engineering Science, and the M.A.Sc. degree in Electrical Engineering from the University of Toronto in 1980 and 1982 respectively, and the Ph.D. degree in Electrical Engineering from the University of Southern California in 1985. Since 1986 he has been with the department of Electrical and Computer Engineering at the University of Toronto where he is presently an Associate Professor.
Since 1986 he has been a Natural Sciences and Engineering Research Council of Canada (NSERC) University Research Fellow.
He has performed research in the areas of packet ratio networks, spread spectrum systems, mobile communications, and indoor wireless communications.
At the University of Toronto he has taught graduate courses in error-correcting codes and mobile communications.
He has given various lectures and short courses in mobile communications throughout the world.
He is the Technical Program Chairman for the Sixth International Symposium on Personal Indoor and Mobile Radio Communications (PIMRC95).

Wayne Stark received the B.S. (with highest honors), M.S., and Ph.D. degrees in Electrical Engineering from the University of Illinois, Urbana in 1978, 1979, and 1982 respectively. Since September 1982 he has been a faculty member in the Department of Electrical Engineering and Computer Science at the University of Michigan, Ann Arbor. From 1984-1989 he was Editor for Communication Theory of the IEEE Transactions on Communication in the area of Spread-Spectrum Communications. He was involved in the planning and organization of the 1986 International Symposium on Information Theory which was held in Ann Arbor, Michigan. He was selected by the National Science Foundation as a 1985 Presidential Young Investigator. His research interests are in the areas of coding and communication theory, especially for spread-spectrum and wireless communication networks. Dr. Stark is a member of Eta Kappa Nu, Phi Kappa Phi and Tau Beta Pi.

Chung-Ming Sun was born in Taiwan, Republic of China, in 1960. He received the B.S. (with the highest honor) and the M.S. degrees in Communication Engineering in 1982 and 1984, respectively, from the National Chiao Tung University of Taiwan, Republic of China, and the Ph.D. degree in Electrical Engineering in 1994 from the University of Southern California, Los Angeles, U.S.A.
Since 1986, he has been with the Chung Shan Institute of Shience and Technology, Republic of China, where he is involved in several advanced radar system studies.
His research interests include digital signal processing, image processing, radar systems, spread-spectrum communications, personal communication networks, and cellular communications.
Dr. Sun is a member of Phi Tau Phi.

Branimir R. Vojcic received the Diploma in Electrical Engineering, and the M.S. and D.Sc. degrees in 1980, 1986 and 1989, respectively, from the Faculty of Electrical Engineering, University of Belgrade, Yugoslavia. In 1986/87 he was a graduate student at the George Washington University. Since 1991 he has been at the George Washington University, where he is an Assistant Professor in the Department of Electrical Engineering and Computer Science. He teaches courses in digital communications, communication theory and computer networks. His current research interests include the performance evaluation and modelling of terrestrial and satellite mobile communications, spread spectrum, multiuser detection, equalization and wireless data networks.

Branka Vucetic received the Ph.D. degree in Electrical Engineering for the University of Belgrade, Belgrade in 1982.
From 1977 to 1985 she was a faculty member at the University of Belgrade. In 1986 she joined the University of Sydney where she is currently Associate Professor at the Communications Science & Engineering Laboratory.
Her research interests include digital communications, coding, modulation and channel modelling.

Jim S. Wight (S'72-M'76-SM'85) received the B.Sc. (1972) degree from the University of Calgary and the M. Eng. (1973) and Ph.D. (1976) degrees from Carleton University, Ottawa.
He is presently Professor and Chairman of the Department of Electronics, Charleton University. His research interests focus on microstrip patch antennas and arrays, monolithic microwave integrated circuits, and code synchronizers for wireless and satellite systems.
Dr. Wight has acted for fourteen years as consultant to CAL Corporation, SPAR Aerospace, Info Magnetic Technologies and Vistar; and has conducted many joint research programs with the Communications Research Centre and the Defence Research Establishlent Ottawa over the past twenty years.

Wen-Bin Yang (S'89-M'94) received the B.S. degree from Feng-Chia University, Taiwan, in 1978, the M.S. degree from Tsing-Hua University, Taiwan, in 1980, and the Ph.D. degree from the University of Maryland, in 1993, all in Electrical Engineering.
From 1982 to 1988, he was an instructor of Electrical Engineering Department at Feng-Chia University, Taiwan. In September of 1993, he joined LCC Incorporated, Virginia. His interests include PCS, LEO satellite systems, CDMA, BISDN, and broadband satellite networks.

Michele Zorzi was born in Venice, Italy, in 1966. In 1990, he received the Laurea Degree in Electrical Engineering from the University of Padova, Italy, where he is completing his Ph.D. program in Communications Engineering. During the Academic Year 1992/93, he was on leave at the University of California, San Diego, attending graduate courses and doing research on multiple access in mobile radio networks. In 1993, he joined the Dipartimento di Electronica e Informazione, Politecnico di Milano, Italy, where he currently holds a Research position. His present research interests involve performance evaluation in mobile communications systems, and random access in mobile radio networks. Mr. Zorzi is a Student Member of the IEEE and of the AEI.

Information for ETT Authors

European Transactions on Telecommunications and Related Technologies (ETT) welcomes submission of manuscripts for publication as papers or letters. Letters are subjected to an editorial examination faster then papers. Manuscripts already published in other journals or submitted to other journals cannot be presented to ETT (except papers published in proceedings of limited circualtion. In the affirmative, the data about first publication are required).

1. FORMAL PREPARATION OF MANUSCRIPTS

1.1 Texts

1.1.1 Texts to be submitted to ETT must be written in English and typed double spacing.

1.1.2 Use of wordprocessing with text formatters based on MS DOS (such as Microsoft word, Wordstar) APPLE/MAC (such as Microsoft word) is strongly recommended. In any case the text formatter must be specified on the diskette.

1.1.3 Each text should be preceded by a sheet (title page) with: paper title; name (in full) and surname of the Author/s, their Affiliations and relevant addresses.

1.1.4 All text pages should be numbered (title page is not numbered).

1.1.5 Invited papers should have indicatively a length of no more than 40 pages of about 1800 characters/page (10 pages in print).

1.1.6 Regular papers should have a length of no more than 24 pages of about 1800 characters/page (6 pages in print).

1.1.7 Letters should have a length of no more than 8 pages of about 1800 characters/page (2 pages in print).

1.2 Printing types and symbols

1.2.1 For literal symbols, units and graphical symbols, the recommendations of IEE (International Electrotechnical Commission) and ISO (International Organization of Standardization) must be followed.

1.2.2 In case of typewritten manuscripts letters to be printed in italic should be underlined; letters to be printed in bold should be double underlined.

1.3 Formulae and footnotes

1.3.1 Formulae and footnotes should be numbered in accordance with the quotation order followed in the text.

1.3.2 The serial number of each formula should be written at right side, between round brackets (i.e. (1), (2), etc.).

1.3.3 The serial number of footnotes should be written between round brackets and upper (i.e. $(^1)$, $(^2)$, etc.).

1.4 References

1.4.1 References are usually gathered at the end of the text and numbered according to the order of quotation in the text. The serial numbers should be written between square brackets (i.e. [1], [2], etc.).

1.4.2 References must be completed in ETT style as follows:

Papers: Author(s), first initials followed by last name, title in quotation marks, periodical, volume, inclusive page numbers, month and year.
Books: Author(s), first initials followed by last name, title, location, publisher, year, chapter, page numbers.

Papers in periodical publications:
F. Valdoni, M. Ruggieri, F. Vatalaro, A. Paraboni: *A new millimetre wave satellite system for land mobile communications.* «ETT» Vol. 1, No. 5, 1990, p. 533.

Papers in non periodical publications:
K. Sallberg, I. Andersen, B. Stavenow: *A resource allocation framework in B-ISDN. XIII International Switching Symposium.* Stockolm (Sweden). May, June 1990, paper A2.4.

Papers in joint works:
O. Gonzales Soto: *On traffic modeling and characterization of ISDN users.* In: *Data communication in the ISDN era.* (Y. Perry, Ed.), North Holland, IFIP 1985.

Books:
Y.P. Tsividis: *Operation and modeling of the MOS Transistors.* McGraw-Hill, New York 1987, p. 141-148.

1.5 Illustrations

1.5.1 The originals of illustrations can be either drawings (in black ink) or photographs.

1.5.2 Illustrations must report besides the Author(s)' name, their order numbers (All illustrations should be numbered following the order of quotation in the text, irrespective of photographs and drawings.

1.5.3 Since most illustrations will be reduced in size to 8 cm width, alphanumeric characters must be written so to be legible after reduction.

1.5.4 Graphs should be contained into rectangles with four sides quoted. (The use of graph paper or similar should be avoided, except for graphing recorders).

1.5.5 Photographs (if possible in black and white) must not exceed 10×15 cm.

1.5.6. Include a separate list of figure captions with the manuscript.

1.6 Submission of a manuscript

1.6.1 Five copies of manuscript are requested for examination and processing.

1.6.2 Each copy should include a complete set of illustrations. (One of the five sets should containt the originals: drawings in black ink and/or photographs).

1.6.3 Besides the manuscript, Authors are invited to send their own biographies and photos for publication in the section «Contributors». (In case of absence of biography and/or photo of an Author the publication of the paper is not hindered).

1.6.3.1 Authors' biographies, in English, must be concise (not more than a half page).

1.6.3.2 Authors' photos must report on the back the Authors' name in capital letters.

1.6.4 The five copies must be sent to the Editor-in-Chief: Prof. Maurizio Decina, Viale Monza 259, I-20126 Milano. Fax: +39.2.27002395. E-mail: antola@mailer.cefriel.it

1.7 Free copies and Reprints

1.7.1 The Author(s) will receive, on the whole, 6 free copies of ETT where the paper has been published.
These copies are sent to the Reference Author's address with the kind request to provide for the forwarding to the co-authors.

1.7.2 Reprints are supplied *on payment* only.
The estimated charge for reprints may be requested, at receipt of the final acceptance letter, by.letter or Fax.
In order to assure the reprints delivery the relevant request should reach ETT Secretariat in due time.

2. GUIDELINES FOR ORGANIZING A SCIENTIFIC PAPER

A scientific paper should be organized in five parts: title, abstract, introduction, body, conclusions. Additional parts, such as a glossary of symbols and/or appendixes may be included.

2.1 The title should indicate the subject of the manuscript as briefly as possible. (Since any scientific paper is indexed by significant words in the title, this should be chosen with a particular care).

2.2. The abstract (from 100 to 150 words) should state the contents of the paper on a self-explanatory manner, so that it may be published in abstracts journals, separately from the paper.

2.3 The introduction should delineate the subject in a way intelligible also to non-specialists. It should point-out: the nature of the problem in the back-ground of referenced previous works, the purpose and significance of the paper and the approach to the problem, if applicable. The introduction is, as a rule, the first paragraph in the text.

2.4 The body of the paper should shown the primary message of the paper in detail. Usually it is divided in paragraphs (with explanatory titles) and, where the case, paragraphs may be divided in sub-paragraphs.

2.5 The conclusions should summarize the significance of the results shown in the paper, emphasizing limitations and advantages, possible applications, recommendations for further works (if any). Conclusions are, usually, the last paragraph of the text and they are followed be the references.

2.6 Mathematical details, ancillary to the main discussion of the paper, may be included in one or more appendixes, that are printed after conclusions and before references.

2.7 In manuscripts containing lot of symbols, a glossary may be included after introduction.

PAPERS TO BE PUBLISHED NEXT ISSUE

ETT, Vol. 6, No. 1, 1995

Focus on Economics of Telecommunications
Postponement to Issue 4, 1995

The ETT Editorial Board has postponed the pubblication of the Focus on Economics of Telecommunications to Issue 4 in 1995 in order to accommodate the substantial response to the Call for Papers. The Editors apologise to readers for any disappointment or inconvenience which this postponement may cause.